MULTISCALE MODELING OF DAMAGE
IN
MULTIDIRECTIONAL COMPOSITE LAMINATES

A Dissertation

by

CHANDRA VEER SINGH

Submitted to the Office of Graduate Studies of
Texas A&M University
in partial fulfillment of the requirements for the degree of

DOCTOR OF PHILOSOPHY

December 2008

Major Subject: Aerospace Engineering

MULTISCALE MODELING OF DAMAGE

IN

MULTIDIRECTIONAL COMPOSITE LAMINATES

A Dissertation

by

CHANDRA VEER SINGH

Submitted to the Office of Graduate Studies of
Texas A&M University
in partial fulfillment of the requirements for the degree of

DOCTOR OF PHILOSOPHY

Approved by:

Chair of Committee,	Ramesh Talreja
Committee Members,	Junuthula N. Reddy
	Vikram Kinra
	Anastasia Muliana
Head of Department,	Helen Reed

December 2008

Major Subject: Aerospace Engineering

ABSTRACT

Multiscale Modeling of Damage in Multidirectional Composite Laminates.

(December 2008)

Chandra Veer Singh, B.En., Dayalbagh Educational Institute, Agra, India;

M.Tech., Indian Institute of Science, Bangalore, India

Chair of Advisory Committee: Dr. Ramesh Talreja

The problem of damage accumulation in laminated composite materials has received much attention due to their widespread application in the aerospace, automotive, civil, and sports industries. In the aerospace industry, composites are used to make light weight and efficient structural components. In the Boeing 787, for example, more than 50% of the structure is made of composite materials. Although there have been significant developments in analyzing cross-ply laminates, none of the present approaches provides reasonable predictions for multidirectional laminates in which intralaminar cracks may form in multiple orientations. Nevertheless, the prediction of damage accumulation and its effect on structural performance is a very difficult problem due to complexity of the cracking processes.

This study presents a synergistic damage mechanics (SDM) methodology to analyze damage behavior in multidirectional composite laminates with intralaminar cracks in plies of multiple orientations. SDM combines the strengths of micro-damage mechanics (MDM) and continuum damage mechanics (CDM) in predicting the stiffness degradation due to these cracks. The micromechanics is performed on a representative unit cell using a three-dimensional finite element analysis to calculate the crack opening displacement accounting for the influence of the surrounding plies, the so-called constraint effect. This information is then incorporated in the CDM formulation dealing with laminates containing cracks in different ply orientations through a

'constraint parameter'. Following CDM, a separate damage mode is defined for each type of crack and the expressions for engineering moduli of the damaged laminate are then derived in terms of crack density and the constraint parameter. The SDM methodology is implemented for $[0_m/\pm\theta_n/0_{m/2}]_s$ laminates containing cracks in $\pm\theta$ plies. It is then extended to $[0_m/\pm\theta_n/90_r]_s$ and $[0_m/90_r/\pm\theta_n]_s$ laminates with cracks additionally in the 90°-plies. The predictions agree well with published experimental data as well as independent FE computations. Limited parametric studies are performed to show usability of SDM for more general laminates.

To predict the initiation and growth of intralaminar cracks, an energy based model is proposed in which these cracks initiate and multiply when the work required to form new set of cracks exceeds a laminate dependent critical energy release rate. The approach requires determination of average crack opening and sliding displacements at varying crack spacing. This task is performed through a suitable 3-D FE analysis. In case of off-axis ply cracking, a mixed mode fracture criterion is utilized, where the critical energy release rates in normal and shear modes are determined by fitting the damage model with the experimental data for a reference laminate. The predictions from the model for $[0/\pm\theta_4/0_{1/2}]_s$ and $[0/90/\mp 45]_s$ laminates show remarkable agreement with the experimental results.

The methodology and the results covered in this dissertation will be of interest to mechanics of materials researchers as well as to engineers in industry where composite materials for structural applications are of interest.

To my parents

ACKNOWLEDGMENTS

Man is not made by himself, but by the collective efforts of his parents, teachers, friends and the society. This is one of those rare opportunities to thank all of them from the bottom of my heart. I thank my parents, siblings and family to take me from a toddler to the person that I am today.

My foremost thanks go to all the researchers who sought answers to nature's puzzles, and laid the foundations to my work. I am pleased to thank my adviser Prof. Ramesh Talreja, who guided me through the thick and thin of my Ph.D. research. I have tremendous respect for him, not only for the sincere advice and guidance he provided, but also for how nice a person he is. I would also like to express my sincere thanks and gratitude to the members of my thesis committee, Prof. J.N. Reddy, Prof. Vikram Kinra, and Dr. A. Muliana, for their suggestions and support. My heartfelt thanks go to Dr. Amine Benzerga, Dr. Zubeida Ounaies, Prof. Dimitris Lagoudas, and other professors who helped me build my knowledge in the materials and mechanics area, and aerospace engineering, in general.

My special thanks go to my professors at Indian Institute of Science, Profs. Dattaguru, Raghunandan, Gopalakrishnan, Ganguli and Harursampath.

I would like to thank all my friends, particularly, Shantanu, Sachin, Adhir, Arvind, Pradeep, Guru, Piyush, Amnaya, Shyam, Krishnendu, Aditya, Gary, Deepak, Darren, Shreyas, Prateek and many more. I also thank the members of the 'TAMU Roadrunners club', and the marathon training group, who helped me develop running as my hobby, for the wonderful times we had during running and traveling together, especially Cheryl, Jose, Alissa, Michael, Katherine, Annie, Megan, and Hana.

My final thanks go to Ms. Karen Knabe for helping me with many of the official formalities.

TABLE OF CONTENTS

CHAPTER Page

CHAPTER Page

LIST OF TABLES

LIST OF FIGURES

FIGURE Page

FIGURE Page

FIGURE Page

FIGURE Page

FIGURE Page

FIGURE Page

CHAPTER I

INTRODUCTION

"Materials science underpins every product and process on which our modern society depends."

Senator P. Domenici, US senator for the state of New Mexico, keynote lecture

Heterogeneous materials combining the best aspects of dissimilar constituents have been present in nature for millions of years. Composites are heterogeneous engineering materials made from two or more constituents with significantly different mechanical properties and which remain separate and distinct within the finished structure. Although, they have been in use from the primitive times, e.g., ancient societies like Romans, extensively used mortars and concrete for building purposes [1], the technological developments in past few decades have made them the materials of choice over metals and alloys for many engineering applications.

Polymer Matrix Composites (PMCs) are a class of composites in which a polymer matrix is reinforced with glass or carbon fibers. Advanced PMCs depict the leading edge of materials technology with applications ranging from golf clubs and tennis rackets to jet skis, aircrafts, missiles and spacecrafts. The fibers used in modern composites far surpass traditional bulk materials in terms of specific strengths and stiffnesses. The high strength of fibers is a consequence of less internal or surface flaws than a bulk material. To protect the fibers from abrasion and environmental attack and enable proper load transfer, the fibers are usually impregnated by a matrix material. This dilutes properties to some degree, but they are still far superior than those of the bulk material. While composites are often stronger, stiffer and lighter

---

The journal model is *IEEE Transactions on Industry Applications*.

than the monolithic materials, they lack ductility and fracture toughness of metals making them sensitive to the presence of cracks and notches. However, there has been significant progress in increasing toughness of fiber composites through stitching [2–5], Z-pinning [6] or adding whiskers [7, 8] or using braided composites. These advances have made PMCs increasingly attractive materials, with processing difficulties and predictive capabilities being their major limitations.

In past few decades, the composites are fast replacing their metallic counterparts. In particular, carbon fiber reinforced composites have shown tremendous potential. Fig. 1, taken from [9], shows the market expansion of carbon fibers in recent decades. It highlights how advances in materials, technologies and customer awareness are creating new opportunities for the carbon fiber in a variety of applications [9]. Also the price of carbon fiber has come down substantially in recent decades. In aerospace industry composites usage has increased mostly in the past decade, as exemplified by Boeing 787. Fig. 2, reproduced from [10], depicts the increase in percentage of components made from composites for commercial airplanes. Nearly all the exterior surfaces of the Boeing 787 are composites (blue in Fig. 3, source: [11]), except the leading edges of the wings, the stabilizers and the engine pylons. For future airplanes, the composites would yield better fatigue and corrosion resistance and higher strength-to-weight ratios, provide for a more integrated structure, and increase the useful life and residual value of each aircraft. Further, composite resistance to condensation would allow engineers to increase cabin humidity to enhance passenger comfort.

However, usage of new advanced materials entails development of new predictive methodologies. Engineered structures are exposed to a series of events that can involve loading, environment, and damage threats. These events, either individually or in combination, can cause structural degradation, which, in turn, can affect the ability of the structure to perform its function. The degradation of performance in

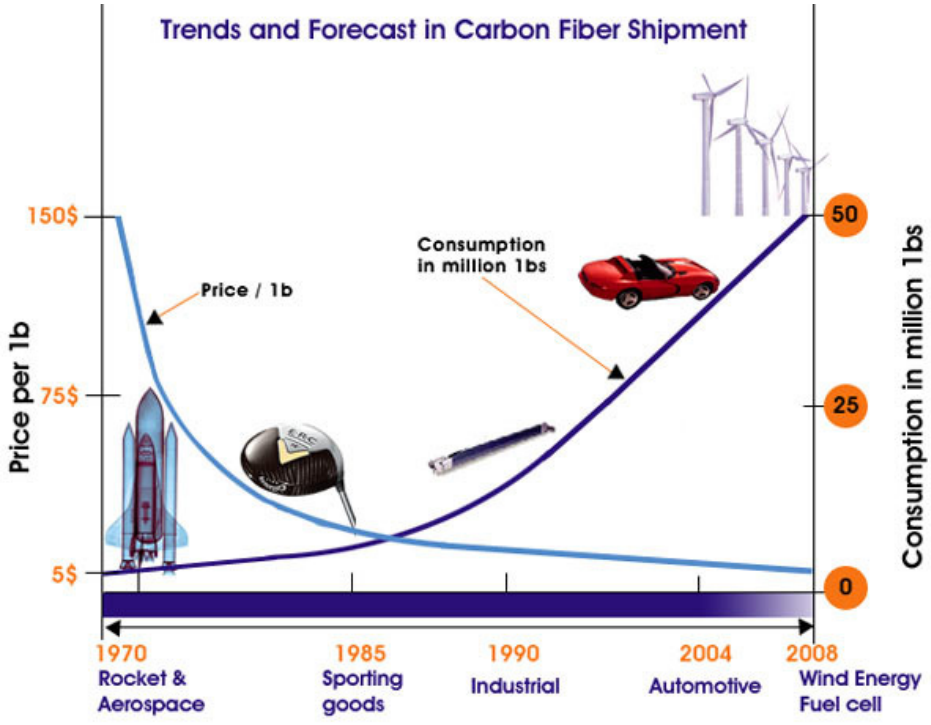

Fig. 1. Market expansion of carbon fibers in the past few decades (source: [9]).

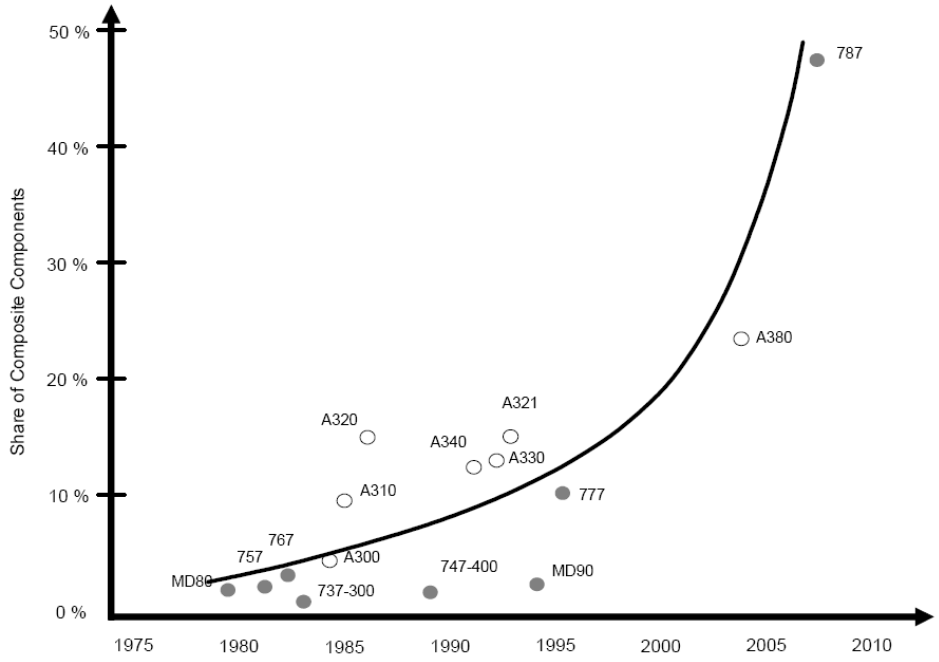

Fig. 2. Percentage of composite components in commercial aircrafts (source: [10]).

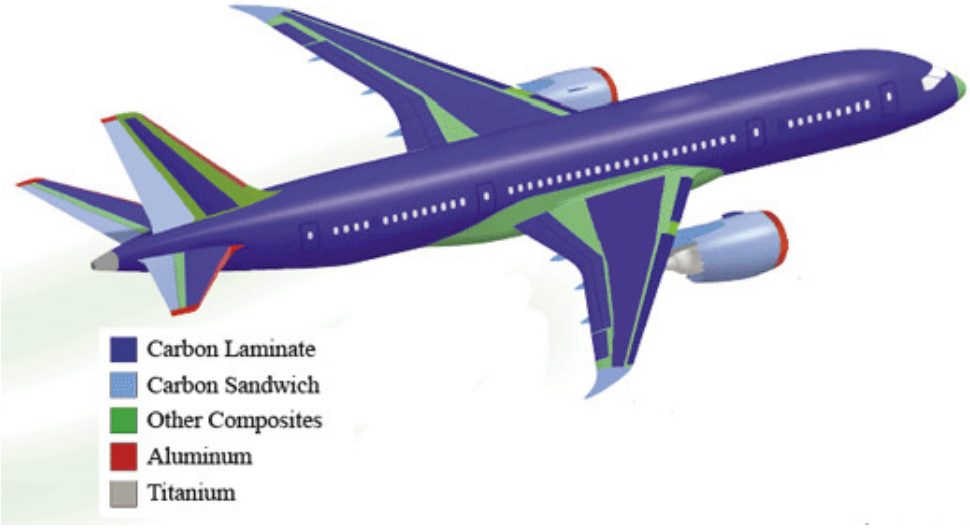

Fig. 3. Materials usage in Boeing 787. Composites constitute more than 50% by volume of the airplane (source: [11]).

composite structures is different than metallic components because composites do not have a uniquely defined failure. Instead, due to extreme levels of anisotropy and inhomogeneity of constituents, a multiplicity of damage mechanisms can degrade the material. For PMCs, these include transverse cracking of the matrix (Fig. 4a), separation of fibers from the matrix (debonding) (Fig. 4b), fiber breaks Fig. (4c), or separation of lamina from each other (delamination) (Fig. 4d).

Amongst these, matrix cracking is mostly the first observed mode of damage. Although, usually not critical from failure aspect, matrix cracks may degrade material stiffness significantly, thereby affecting its overall structural integrity. Moreover, they may initiate and assist other damage mechanisms in complex ways. Since matrix cracks generally develop long before final failure of a structure they should be taken into account in the design in order to fully utilize the load bearing capacity of a composite structure. The National Research Council has recognized that "the inability to predict the long-term durability of PMCs–and the consequent overdesign of struc-

tures necessitated by this uncertainty has limited their use" [11]. Thus, development of an accurate predictive methodology for microcrack initiation and progression is paramount to the potential of composite structures.

The design of structures made of composites often involves layup optimization. The stacking sequence of plies affects the overall stiffness and failure properties of the designed structure. The simplest layup configuration is that of the cross-ply laminates where the plies are oriented along 0° and 90° directions. But more complex loadings necessitate more elaborate layup configurations. Often, the coupling between extension, bending and twisting can be a useful tool for achieving specific aerodynamic and structural capability in the airplanes. This is exemplified by Grumman X-29 aircraft where the laminate layup is chosen such that bending induces twist to counteract aerodynamic forces. Thus laminates with layers in various orientations with respect to the principal loading are quite useful in aerospace industry. Examples of layup sequences are cross-ply, angle ply or multidirectional.

For cross-ply laminates, a wealth of analytical and numerical tools exist to predict microcracking initiation, progression and their effects on material stiffness. However, damage modeling in multidirectional laminates is little understood and no accurate model exists at present to analyze effects of matrix induced damage in multidirectional composite laminates. This study caters to the development of such a predictive methodology.

The overall approach is to combine the knowledge base available from experimental, analytical and computational techniques to yield a more effective and general methodology, which can be used to analyze damage in multidirectional composite laminates. The required analytical expressions are developed in the framework of continuum damage mechanics (CDM). This is aided by suitable micromechanical computations carried out through finite element calculations. The methodology is

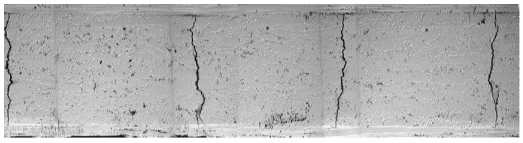

(a) Matrix Cracking

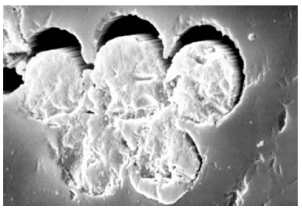

(c) Fiber/Matrix Debonding

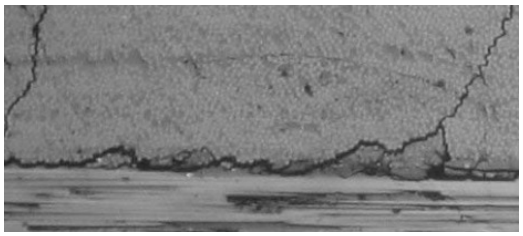

(b) Delamination

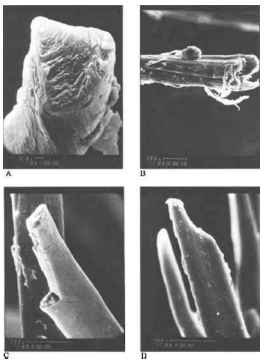

(d) Fiber Fracture

Fig. 4. Various mechanisms of damage in composite laminates.

applied to a variety of laminate layups and the predictions are compared with experiments and independent FE simulations wherever applicable.

A. Background and Motivation

Damage in composite materials usually initiates with matrix cracking. Fig. 5, reproduced from [12] depicts the stress-strain response of a glass without fibers and fiber-reinforced glass in tension loading. The striking difference in the behavior is due to non-linearity shown by the reinforced specimen. This non-linearity is a type of ductility which occurs due to multiple matrix cracking [12]. In case of laminated composites, this phenomenon is called transverse ply cracking. Ply cracking does not cause laminate failure, but reduces its stiffness properties, and thus is considered as

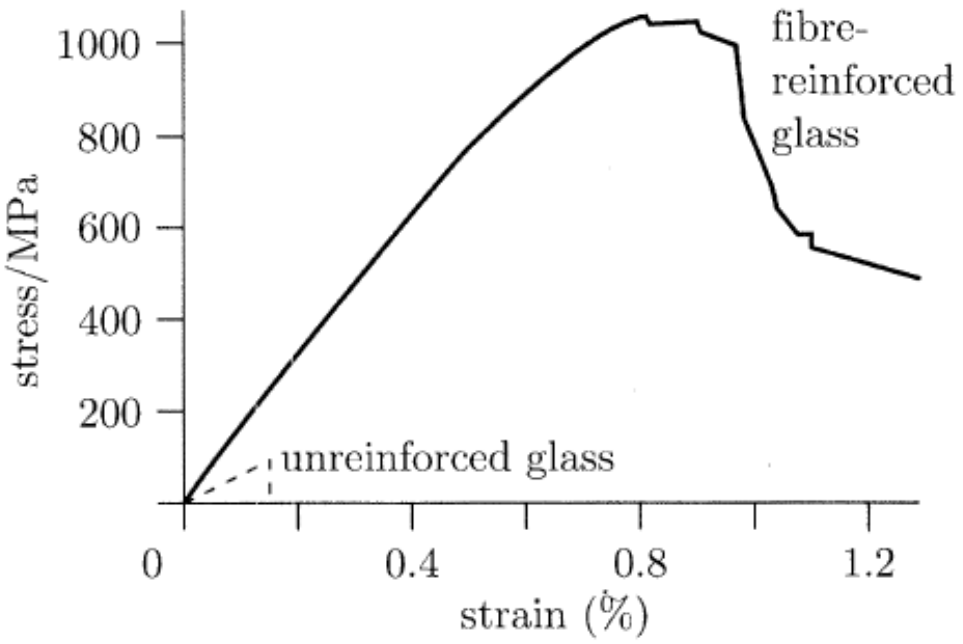

Fig. 5. The stress strain curves for borosilicate glass alone (dotted line) and reinforced with aligned carbon fibers (source: [12]).

'sub-critical' from the viewpoint of failure analysis. The subject of 'damage mechanics' caters to characterization of the initiation of sub-critical damage, its growth, and its effects on overall laminate behavior.

The phenomenon of multiple fracture occurs due to difference in failure strains of constituent materials. As argued by Aveston et al. [13], if one of the two constituents of a fibrous composite breaks at a much lower elongation than the other and if the non-broken constituent is able to bear the load, a tensile specimen will show multiple fracture of the more brittle phase until the specimen finally breaks when the ultimate strength of the stronger phase is reached. For a unidirectional lamina with strong, stiff fibers in a weak matrix, the matrix phase will undergo multiple fractures if

$$\sigma_{fu} V_f > \sigma_{mu} V_m + \sigma_f^{'} V_f \tag{1.1}$$

where, σ_{fu} and σ_{mu} are failure strengths and V_f, V_m are the volume fractions of fiber and matrix, respectively; and $\sigma_f^{'}$ is the stress carried by the fiber after matrix failure.

In the following paragraphs, we will review the progress in damage of composite materials over the past three decades. Due to the vast literature available, the following review is divided into sub-sections. First, we cover the initial studies in the light of experimental evidence. Then, we briefly describe modeling approaches for stiffness degradation and damage evolution. Finally the recent progress focusing on damage in off-axis laminates is summarized.

1. Initial Research Investigations

Initial studies of microcracking were done in the 1970s. These studies concentrated on the initiation of microcracking glass-reinforced polyester [14, 15] and glass-reinforced epoxy [16–21] cross-ply laminates. The effect of 90° ply thickness was investigated. For thick 90° plies, transverse microcracks initiated at the edge of the specimen and propagated instantaneously through the width of entire cross-section. Thin plies also developed cracks at the edges. However, cracks propagated under load control. Fig. 6 shows that as thickness of 90° plies decreases, the strain to transverse crack initiation increases [22]. For very thin plies ($< 0.1\ mm$), cracks are suppressed and the laminate fails before initiation of transverse cracks. Talreja [23] later explained this thickness effect in terms of *constraint* posed by un-cracked plies over cracked plies. As thickness of 90° plies increases, the constraint from 0° plies decreases and microcracking initiates at lower applied strain and vice-versa. A microscopy study into the origin of microcracks [17] has revealed that they are associated with the processing flaws, voids and regions of higher fiber volume fraction; and usually initiate with debonding at the fiber-matrix interface.

Hahn and Tsai [24] put forward the *first-ply failure* theory to predict the strain

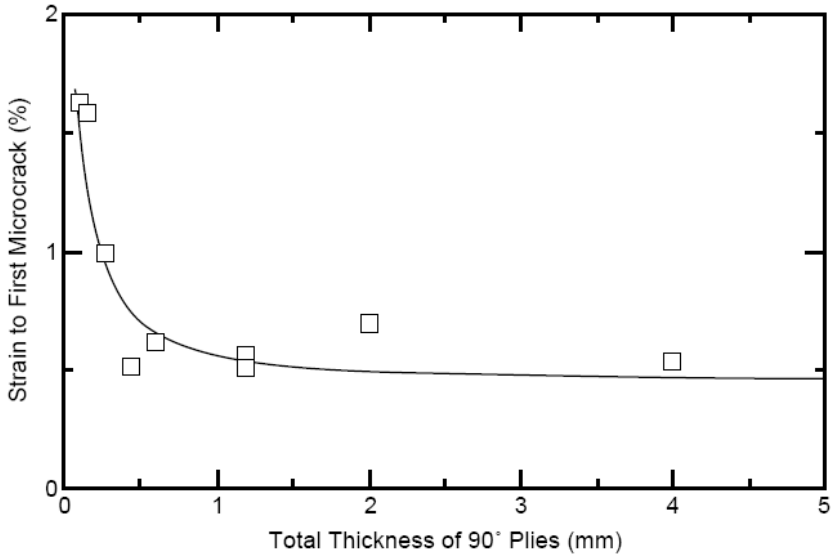

Fig. 6. Strain to initiate transverse cracks in $[0/90_n]$ laminate for different thickness of 90° layer (from [22]).

to first microcrack assuming that the first crack develops when the strain in the plies reaches the strain to failure. However, the predictions did not match with the experimental observations because it predicts initiation strain to be independent of the ply-thickness, which obviously is contrary to the experimental observations. More advanced ply-failure criteria [25, 26] that included all stress components were also inaccurate. Modification of first-ply failure theory by using *in situ* failure properties have also been tried [26] with little success. Statistical strength arguments have also been put forward to account for the variations in microcrack initiation strain [27–31]. These statistical strength models also use *in situ* statistical parameters to fit experimental results [30, 31] and fail to distinguish between $[0_m/90_n]_s$ and $[90_n/0_m]_s$ laminates. The strain to initiate microcracking is lower for surface 90° plies than for central 90° plies. It is because central 90° plies are supported from both sides, whereas surface 90° plies are free to crack on the outer side. Thus, microcracking

initiates more readily in $[90_n/0_m]_s$ laminates [19, 32–35].

The first transverse crack has almost no effect on the laminate behavior. However, continued loading causes formation of more matrix cracks thereby causing a significant degradation in thermo-elastic properties of the structure. Numerous experimental investigations [30,32,36–44] have focused on counting the number of transverse cracks in cross-ply laminates during quasi-static loading. Qualitatively, all offer similar insights: microcracks form very quickly just after first crack initiates. This initial rapid rise in microcrack density is followed by a slowing down, eventually reaching a saturation level. Reifsnider [45, 46] described this micro-crack saturation as a material state called *characteristic damage state* (CDS). They observed that CDS is a well defined laminate property and does not depend on load history, environment or residual or moisture stresses. However, later investigations by Akshantala and Talreja [47] refuted this because CDS depended upon strain rate during fatigue loading.

At high loading levels, other damage modes start to occur. Frictional sliding at the fiber/matrix interface becomes significant and delaminations can form from the tip of a transverse microcrack at the interface. Once delaminations begin to form, they propagate on continued loading while additional microcracking slows down or stops. If the applied strain is high enough, the Poisson's effect can lead to microcracking (splits) in the 0°-ply. On very high strains, progressive fiber breakage takes place leading to localization of damage and subsequent failure of the composite structure.

Failure theories can be used to predict the final event of failure. Hinton et al. [48] compared five well-known failure criteria against leakage and fracture stresses for filament wound tubes of $\pm\theta$ fiber orientations and found the failure criteria were generally deficient in predicting failure because of the lack of account for progressive damage. A World Wide Failure Exercise (WWFE) carried out a careful investigation

into applicability of failure theories against experimental evidence. Models by Puck [49], Zinoviev [50] and Tsai [51] were found to exhibit good predictive capability and have only minor weaknesses. However, some issues, such as the effect of thermal residual stresses on failure prediction, use of *in-situ* strength by some models, and failure modeling of leakage in tubes under internal pressure loading, still remain open due to lack of evidence [52].

2. Modeling Thermoelastic Properties of Damaged Laminates

Analysis of material degradation as a result of damage or defect mechanisms is an important consideration in materials design. A broad classification of models used to address material degradation in polymer matrix composites was documented in a report by the 'National Research Council' [11]. Table I, reproduced from [53], compares the broad modeling approaches to model material degradation.

In the present context of analyzing mechanical behavior of composite laminates subsequent to the development of transverse matrix cracking, the basic theme of nearly all studies has been to predict the stiffness degradation as a function of transverse crack density. The major attempts to model thermo-elastic constants of damaged laminates are described below.

a. Ply discount method

The simplest way to model transverse matrix cracks in composite laminates is to completely neglect the transverse stiffness of cracked plies [54]. This method underestimates the stiffness of cracked laminates since the cracked plies in reality can support a substantial portion of applied loading. The modified ply-discount model where only the transverse stiffness of a cracked layer is put to zero, does not help either. Also, these models do not characterize stiffness as a function of the crack

Table I. Comparison of various approaches to model material degradation in composite materials (reproduced from [53], based on [11]).

Approach	Principle	Strength	Weakness
Phenomenological	Correlate operating conditions with tabulated life-data	Experimental basis	Empirical
Continuum mechanics	Balance of forces, mass, momentum, energy etc.	Physical basis	Can't solve complex practical problems
Strength of materials	Employ traditional yield based failure criteria	Easy to use	No microstructural information
Micromechanics	Model matrix, fibers and damage at microstructural level, homogenize to yield continuum level description	Microstructural details	Not versatile, complex
Damage Mechanics	Characterize damage as an internal thermodynamics variable	Strong Physical, and experimental basis	Needs evaluation of material constants
Chemical	Represent degradation processes as rate equation, e.g., Arhenius equation	Simple, explicit temperature dependence	Empirical, not physics based
Atomistic	Describe the structure as an array of atoms and molecules	Atomistic level details	Huge computational time, not practical

density and therefore are more suitable at high crack densities. Although being simple, they are based on a crude estimate of the effect of transverse cracking and, often unreliable for design and failure analysis [55].

b. Shear lag method

The most common approach to include the effects of load transfer between micro cracked plies and their neighbors is by so called *shear lag analysis* [14, 37]. In this model, the load transfer between plies is assumed to take place in shear layers between neighboring plies and the normal stress in external load direction is assumed to be constant over ply thickness. The unknowns are the thickness and stiffness of these shear layers. The shear lag theory neglects variations in the stresses and strain through ply thickness. Moreover, being a one dimensional theory, its application to layup configurations other than cross plies is doubtful. The shear lag theory has however successfully been applied to cross-ply laminates [14,37,56–58]. Crack interaction has also been included in some shear lag models [27, 34].

All shear lag analyses are based on the concept that in the plane of transverse crack the transverse ply carries no load, while away from the crack a part of this load is transferred back to the transverse ply by shear. For a cross-ply laminate, the shear lag analysis assumes that

$$\tau_i = G\frac{u_{90} - u_0}{t} \tag{1.2}$$

where τ_i is the shear stress at the 0°/90°-interface, G is a proportionality constant, similar to the shear modulus, u_{90}, u_0 are the longitudinal displacements in 90°, and 0° plies, respectively, and t is a thickness parameter. In some initial shear lag models, e.g., [14, 59], t is taken to be equal to thickness of the 90° layer (t_{90}), whereas in others [27, 60], it is taken as the thickness of resin-rich layers about the 0°/90°-

interface. Following [14, 59], the use of equilibrium and constitutive equations results in the following ordinary differential equation (ODE) for the longitudinal stress in 90° layer, σ_{xx}^{90},

$$\frac{\mathrm{d}^2\sigma_{xx}^{90}}{\mathrm{d}x^2} - \frac{\beta^2}{t_{90}^2}\sigma_{xx}^{90} = -\frac{\beta^2}{t_{90}^2}\frac{E_{x0}^{90}}{E_c}\sigma_c \tag{1.3}$$

where x denotes the laminate longitude, β is a material parameter known as 'shear lag parameter', E_{x0}^{90}, E_c are longitudinal moduli for 90° layer and the whole laminate in the undamaged form, respectively, and σ_c is the longitudinal stress applied to the laminate. The solution of the above ODE gives 1-D stress field in the laminate. Averaging stress and strain fields over a typical unit cell of the cracked laminate gives the effective longitudinal modulus for a fixed state of damage (prescribed crack spacing, $2l$) as [32]

$$\frac{1}{E_x} = \frac{1}{E_c}\left(1 + \frac{E_{x0}^{90}}{\lambda E_{x0}^{0}}\frac{\tanh\beta\rho}{\beta\rho}\right) \tag{1.4}$$

where $\lambda = \frac{t_0}{t_{90}}$, and $\rho = \frac{l}{t_{90}}$ with t_0 being the thickness of 0° layer.

Good reviews of shear lag methods for damage analysis of composite materials can be found in [61–63].

c. Variational approach

By application of the principle of minimum complementary potential energy, Hashin [64, 65] derived estimates for stiffness, ply stresses and thermal expansion coefficients of cross-ply laminates with regularly spaced ply cracks. This approach attempts to solve a two-dimensional boundary value problem, and thus yields much better results than 1-D shear lag models. The predictions are in reasonably good agreement with the experimental data. It is important to note that Hashin's method essentially yields a lower bound for the stiffness. Varna and Berglund [66–68] have improved Hashin's model by using a better stress analysis. A disadvantage of the variational approach

is that the stress analysis problem is extremely complex for laminate layups other than cross plies and currently no variational solution exists for off-axis laminates. Other significant works on Hashin's variational analysis involved inclusion of thermal residual stresses [69], stress solutions for orthogonally cracked cross-ply laminates [70], comparison of stress fields and stiffness reductions in $[0/90]_s$ and $[90/0]_s$ laminates [35], and analysis of delaminations induced by matrix cracking [71].

For cracked cross-ply laminates, the basic unit cell for the resulting 2-D boundary value problem is as sketched in Fig. 7 (adapted from [63]). Hashin [64] constructed admissible stress field for the problem assuming that the normal stresses in the loading direction are constant over the ply thickness. The admissible stress field satisfied equilibrium and boundary and interface conditions. The stresses and reduced stiffness coefficients for the damaged laminate were then obtained using minimization of complementary energy. Hashin's variational problem results into the following ODE

$$\frac{d^4\phi}{d\xi^4} + p\frac{d^2\phi}{d\xi^2} + q\phi = 0 \tag{1.5}$$

where ϕ is an unknown function representing stress perturbation due to cracking, $\xi = \frac{x}{t_{90}}$, and p, q are laminate parameters. The longitudinal stress in 90° layer is related to ϕ as

$$\sigma_{xx}^{90} = \sigma_{xx0}^{90}\left[1 - \phi\left(x\right)\right] \tag{1.6}$$

where σ_{xx0}^{90} is the 90° ply stress in un-damaged state. For details on complete stress field, the reader is referred to the original study [64].

McCartney [72] used a generalized plain strain formulation to derive governing equations similar to Hashin's model. His main assumption was that the in-plane normal stress dependence on the two in-plane coordinates is given by two independent functions. This approach is actually equivalent to the minimization of Reissner's

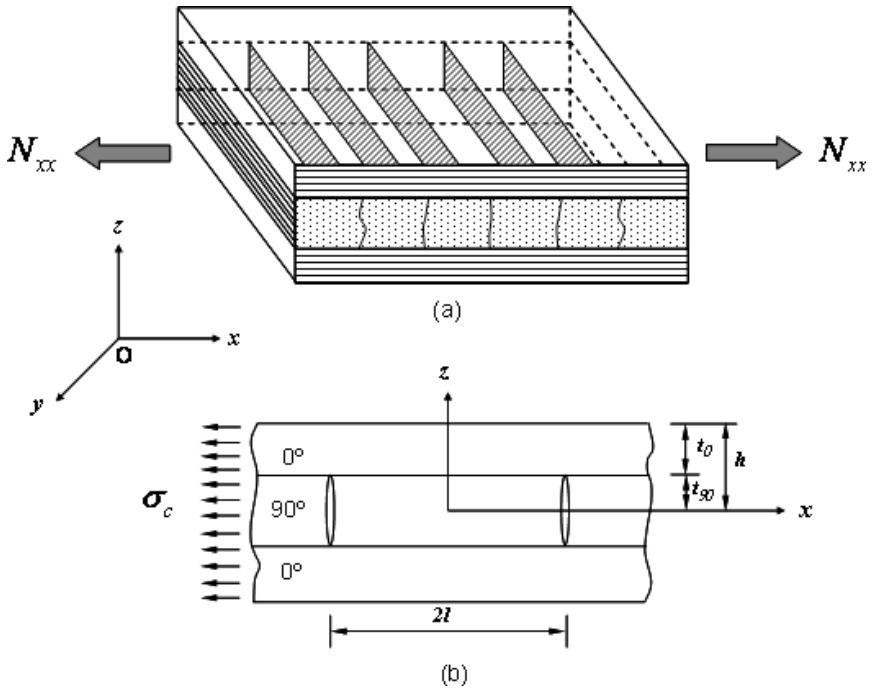

Fig. 7. Boundary value problem for a cracked cross-ply laminate (adapted from [63]).

energy function [73]. To have a better representation of stress variation across ply thickness, a ply is sub-divided into thin layers and equilibrium equations are applied using average stress fields for each layer. This results into a series of recursive equations. For this reason, McCartney's model is semi-analytical and requires numerical calculations for complete damage characterization [73–75].

d. Self consistent method

Laws and Dvorak [76, 77] have estimated stiffness and thermal expansion coefficients of matrix cracked composite plies by use of self consistent approximations. In their model, each crack was modeled as the limit of an elliptic cylinder when the aspect ratio tends to zero, thus leading to a three-phase model for cracked fibrous composites (fibers, matrix and cracks). The self consistent stiffness matrix was then derived for an infinite, homogeneous, matrix cracked material. The predicted results, however,

are not consistent with experimental data.

A similar micromechanics approach for cross-ply laminates has recently been developed by Hoiseth and Qu [78, 79]. Following the differential self-consistent method, they have derived an incremental differential equation describing the effective longitudinal modulus for the cracked laminate by representing the change in strain energy due to increase in terms of number of cracks in a lamina.

e. 3-Dimensional laminate theory

Gudmundson and co-workers [80,81] considered laminates with general layup and used the homogenization technique to derive expressions for average stiffness and thermal expansion coefficient of laminates with cracks in layers of 3-D laminates. These expressions in an exact form correlate damaged laminate thermo-elastic properties with parameters characterizing crack behavior: the average crack opening displacement (COD) and average crack face sliding. However, these parameters follow from the solution of the local boundary value problem and their determination is a very complex task. Gudmundson and co-workers suggested to neglect the effect of neighboring layers on crack face displacements and to determine them using the known solution for a periodic system of cracks in an infinite homogeneous transversely isotropic medium (90°-layer). As will be shown later, this assumption is actually not valid due to constraint effects on cracked ply surface displacements from the supporting plies. The application of their methodology by other researchers has been rather limited due to the fairly complex form of the presented solutions and use of approximate COD and CSD parameters. Further developments on this methodology can be found in [41, 82–86].

f. Continuum damage mechanics (CDM)

An alternative way to describe the mechanical behavior of matrix cracked laminates is to apply concepts of damage mechanics. Talreja [23, 87–89] and Allen et al. [90, 91] have derived models for laminate stiffness in terms of internal damage state parameters. In order to apply the models, it is necessary to fit certain parameters to experimental or numerical data. For a matrix cracked cross-ply laminate Lee and Allen [92] have derived approximate relations between the internal damage state parameter and laminate stiffness. They determined approximate solutions for local stresses and strains by use of the principle of minimum potential energy. In this way upper bounds for laminate stiffness could be derived.

We will use this methodology as our basis in formulation of effective stiffness properties of a cracked laminate. Further details will be given in the subsequent chapters.

g. Numerical methods

Several numerical solutions to cracked cross-ply and quasi-isotropic laminates have also been obtained. Most of the analyses have tried to solve the 2-D boundary value problem similar to that of Hashin's variational analysis (see Fig. 7) assuming a plane stress or generalized plane strain condition [93, 94], while few have attempted a full 3-D stress analysis [84, 95]. The chief computational methods used are: the finite element method (FEM) [84, 93–95], finite difference method, boundary element method (BEM), and finite strip method [96]. Some have attempted Fourier and other series expansions to describe the stress and displacement fields [97] in cracked cross-ply laminates. Modifications of laminated plate theories, such as the 'layerwise laminate theory' [98], are some other numerical tools to analyze transverse cracking.

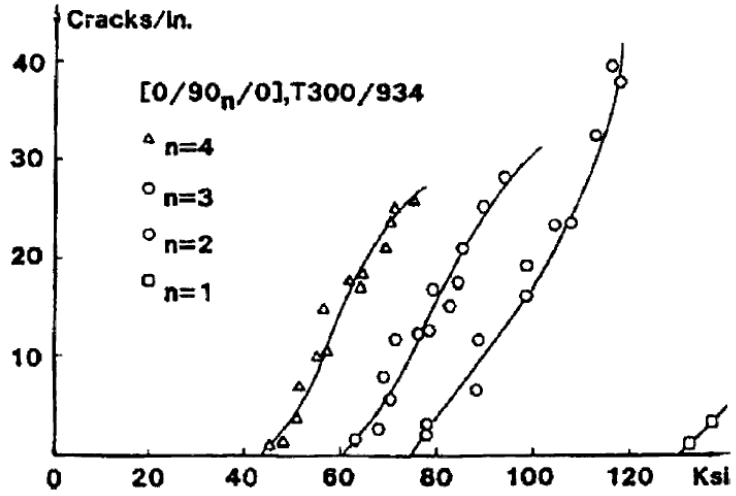

Fig. 8. Damage evolution in $[0_m/90_n]_s$ laminates (source: [99]).

The benefit of these approaches is that they provide more accurate stress solutions, thereby providing important insights. However, they need to be performed every time laminate layup, material or crack density changes, and thus can not be used in practice. Often computational tools have also been used to verify, compare or validate existing or proposed analytical methods. Additionally, some semi-analytical methods, e.g., [73, 74], use numerical tools to reinforce or improve their solutions to stress and displacement fields in cracked laminates.

3. Damage Evolution

If the applied load is increased beyond the stress at the initiation of cracking in a transverse ply, new cracks form in the cracked ply in between existing cracks. Initially these cracks are far apart and do not interact with each other. However, quickly they form a roughly periodic array of parallel cracks. Fig. 8 (source: [99]) shows the increase in density of transverse cracks for typical configurations of cross-ply laminates [43]. The figure distinctly marks three stages in cracking: initial rapid

rise, slowing down and saturation. Usually, the damage evolution is measured or predicted in terms of the number of cracks per mm (crack density) as a function of applied strain or stress. The approaches to model crack initiation and damage evolution can be divided into two categories:

1. *Strength Based Models:* According to these models, microcracks form when the stress reaches the transverse strength of the ply material or some multi-axial stress state criterion is met [14–17, 24, 27–29, 31, 59, 100]. Since, the stress state at the onset of transverse cracking is not constant for different laminates [26], these models fail to account for difference in crack initiation and progression for specimens of different ply thicknesses. Moreover, detailed stress analysis is a necessary step in prediction, thereby limiting their usage to cross-ply laminates. Still, their main drawback is lack of agreement with the experimental predictions. Even statistical strength models [27–31] do not help because they use *in situ* strength properties requiring additional measurements for each stacking sequence.

2. *Energy Based Models:* These models predict a microcrack when the total energy released by the formation of that microcrack reaches the critical energy release rate for microcracking. Highly similar in concept and nature to fracture mechanics, it has also been termed as *finite fracture mechanics* [101]. In contrast to the conventional fracture mechanics, transverse cracking comprises events that involve *finite* amount of new fracture area. When complemented with an accurate stress analysis approach, this methodology has proved to be highly successful. For example, in case of cross-ply laminates, finite fracture mechanics coupled with variational analysis predicts accurate damage evolution for a wide variety of laminates [35, 44, 102].

For microcracking in $[0/\pm\theta]_s$ laminates, as θ is made smaller than 90°, 3-D stress analysis shows that the principal stress trajectories in the off-axis plies is no longer straight [103] and may account for the observation of curved microcracks at low crack density. Moreover, the microcracks initiate on the edge but only propagate part way into the laminate. Such curved and angled edge cracks typically cause edge delaminations.

Nairn et al. [43] carried out the most comprehensive experimental study of damage evolution in cross-ply laminates by comparing 18 different laminate layups of same material. It was found that the energy release rate criterion when combined with an accurate stress analysis, such as the variational approach, only gave consistent results. Clearly, all strength models are bound to fail to predict damage evolution in off-axis laminates. Energy based models using average *crack opening displacement* (COD) for damage evolution do not require a detailed stress analysis of the cracked solid [104–106] and are suited irrespective of laminate layup.

4. Studies on Off-axis Laminates and Recent Progress

Experimental studies on off-axis laminates [45, 60, 107–110] show that the matrix crack pattern is more complex than cross-ply laminates and majority of cracks form at the edges of the test coupons and may or may not grow across the thickness and the width of the specimen immediately. Johnson and Chang [111] carried out extensive experiments on a variety of off-axis laminate configurations and found that for laminates having ply angle greater than 45°, significant ply cracking is a dominant damage mode, although edge effects can lead to delaminations. The approaches proposed for analyzing off-axis laminates include 2-D finite element method (FEM) [94, 110, 112], first order shear deformation laminated plate theory (FSDT) [113], equivalent constraint model (ECM) [114], and modified shear lag models [115–120].

But these models provide approximate solutions whose accuracy cannot be verified as no exact analytical solutions currently exist. Moreover, these authors do not verify their stiffness predictions with experimental data.

It should be pointed out that the damaged laminate material may contain a large number of tiny internal and partially grown cracks. On increase in loading, these cracks may grow and coalesce to form fully developed matrix cracks. The usual experimental methods such as X-ray, The common techniques for nondestructive detection of transverse matrix cracks in laminated composites, such as edge replication, penetrant-enhanced X-ray radiography, acoustic emission and ultrasonic C-scan imaging etc. do not provide accurate information on the formation, number, size and progression of these internal cracks. A through-transmission ultrasonic C-scan imaging with inclined focusing transducers in confocal configuration has been suggested for the detection of partial and internal cracks in composite laminates [121, 122].

Recently, use of CFRP laminates for the cryogenic propellant tanks to the develop light-weight future reusable/expendable launch vehicles has thrown a new light into matrix cracking because they may cause unallowable propellant leakage [123]. Experimental studies on such laminates consisting multiple off-axis plies, a high density form of matrix microcracking, called stitch cracking, can form in plies adjacent to a cracked ply [124]. Yokozeki et al. [125, 126] have clarified the effect of ply angle on stitch cracking. They have carried out experimental investigations on $[0/\theta/90]_s$ laminate to study development of microcracks in θ-ply subsequent to formation of fully grown ply cracks in contiguous 90° plies.

Crocker et al. [127] studied the intra-laminar fracture in angle ply laminates and found that cracks in an angle ply do not grow fully through the coupon width, in contrast to 90°-ply, and are significantly affected by the ply orientation. Below a ply orientation of 45°, delamination started just after the formation of off-axis ply cracks.

For generally symmetric laminated systems, McCartney [74, 128] has developed a semi-analytical approach that is capable of predicting the stress and displacement distributions in cross-ply and general symmetric laminates containing arrays of ply cracks having a single orientation. McCartney and Shoeppner [129] also studied the effect of non-uniform matrix cracking on laminate properties in cross-ply laminates. On the experimental side, 'Raman Spectroscopy' has also been used to study off-axis ply cracking [130–133].

Approximate variational solutions for stress fields in cracked cross-ply laminates in bending have been reported in [134], wherein the predictions are compared with FE calculations. The stress results for the $[0/90]_s$ and $[90/0]_s$ laminates show that the transverse normal stress can be tensile or compressive, depending on the laminate lay-up and location of the cracked layer; and this complicates the damage analysis. Kim and Nairn [135,136] have also performed a similar study for analyzing the crack formation in coating/substrate systems under bending loads.

For prediction of crack formation and damage evolution, energy based methods are gaining popularity and wide acceptance. Some such models are proposed by McCartney [79,128,137]. Other issues have also been addressed lately. For example, the randomness and non-uniformity of the microcracking process is accounted by using statistical distribution of matrix fracture toughness [102,129,137–139]. The non-uniformity of fiber distribution in ceramic-matrix composites has also been analyzed [140].

B. Problem Statement

Consider a generally symmetric composite laminate loaded in axial tension (Fig. 9). Depending upon the ply layup and material properties, different plies will have dif-

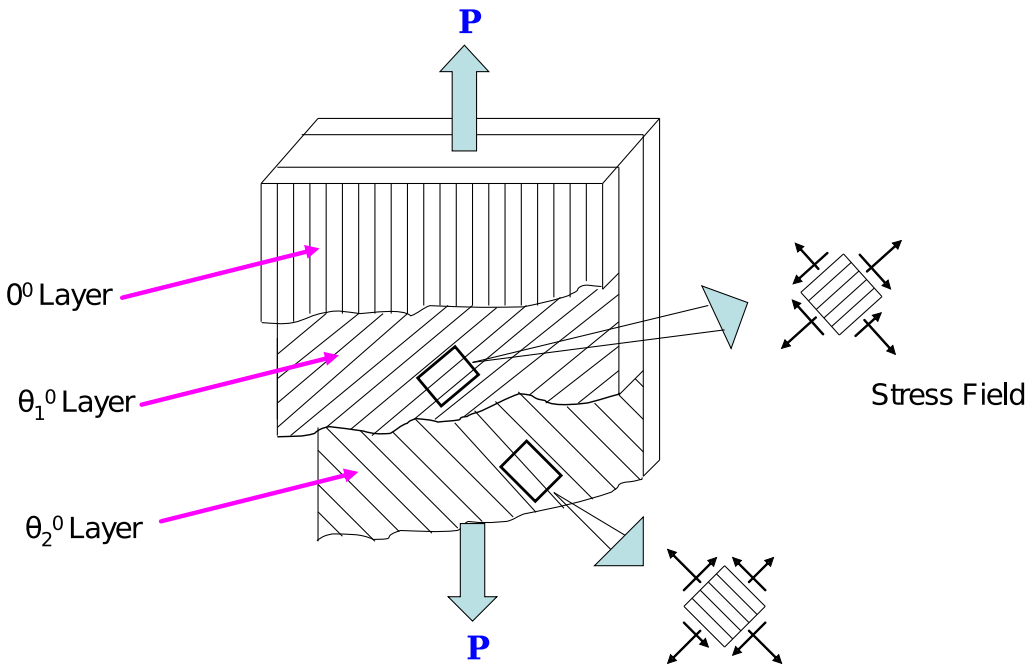

Fig. 9. A representative volume element (RVE) illustrating intralaminar multiple cracking in a general off-axis ply of a composite laminate.

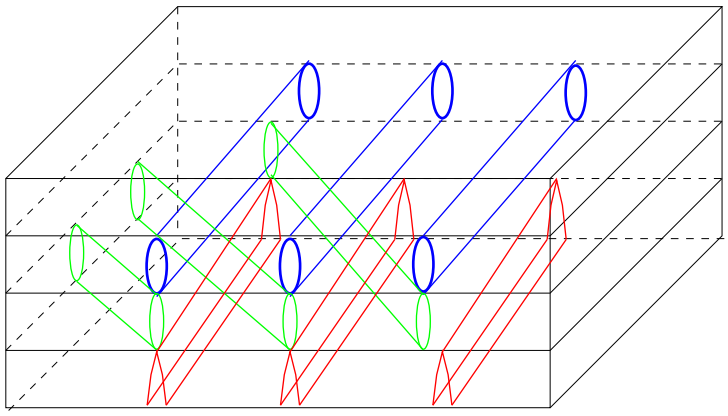

Fig. 10. An illustration of multiple cracking systems in a $[0/90/\theta_1/\theta_2]$ laminate.

ferent stress states. On sufficient tensile loads, some of these plies will develop matrix cracks in direction preferably transverse to the loading direction. So, the cracks will first appear in a ply with 90° orientation to the loading direction. Subsequently, other off-axis plies with orientations close to 90° will also develop matrix cracks. Currently we have many analytical and numerical models, e.g., Shear lag, variational, 3-D laminate and continuum damage mechanics, which can analyze damage due to matrix cracking in cross-ply laminates to a good accuracy. However, one faces an uphill task while analyzing damage in multidirectional composite laminates due to following modeling challenges:

- The resulting boundary value problem accounting for an array of matrix cracks in a layer of an arbitrary direction with respect to the laminate loading direction is very complex and can not be solved even with the variational approach.

- Depending on the laminate layup, the transverse cracks may appear in multiple layers. Since these cracks tend to follow the fiber direction in a particular layer, we may have different crack patterns in different layers. See, e.g., Fig. 10 for an illustration of multiple cracking systems in a $[0/90/\theta_1/\theta_2]$ laminate.

- The crack patterns in different cracked layers will influence the stress and displacement profile in other layers.

- There is no clear cut way of determining the constraint of the undamaged layers on opening of the cracked surfaces.

The above issues necessitate an analysis method which can consider a truly multimode damage scenario while predicting stiffness changes. Although there have been some efforts in damage analysis of multidirectional composites, there is no acceptable approach. The following issues highlight the limitations of available approaches:

- Some of the researchers claim to have developed models for generally symmetric off-axis laminates. However, they always verify their results with cross-ply ($[0_m/90_n]_s$) or $[\pm\theta_m/90_n]_s$ laminates thereby considering cracks in 90° layer only [84, 119, 141].

- Modified or two dimensional shear lag models [113, 116, 125] use questionable assumptions related to the shear layer properties and stiffness transformation.

- Gudmundson's approach [41, 81] assumes approximate crack opening displacement for infinite solid and hence neglects effects of constraint of neighboring layers on opening of cracked surfaces.

- McCartney [74] has developed an analytical model for general symmetric laminates. However, this approach involves a system of recurrent relations and a fourth order differential equation, thus requiring substantial numerical computations. Moreover, the case of damage in multiple orientations requires homogenization [75] and is still not fully developed.

- Continuum damage mechanics can provide predictions for almost any laminate layup. However, it needs determination of certain phenomenological constants for every configuration limiting its practical application [87, 142].

- The aspects pertaining to non-stationary length scale during damage evolution and multiple damage modes are not treated in most models.

- Many approaches are unable to treat stiffness degradation and damage evolution in a common framework.

- Some of the existing models can provide predictions for stiffness changes only (e.g., semi-analytical methods), and do not treat damage evolution explicitly.

- Some of the recently developed analytical models for general symmetric laminates use coordinate transformation [84,125,126] of damage effects in an off-axis ply to an equivalent 90° ply. This is an inaccurate description of the actual damage and do not conform to the experimental observations.

These issues are taken up in some further detail in the chapter II. In essence, the above issues suggest that it is incredibly difficult to obtain solutions to stress fields in a cracked multidirectional laminate. CDM, which rather focuses on predicting effective stiffness properties, is quite general and can be used for variety of laminate layups. It however requires determination of phenomenological constants, which may change with laminate configuration. To eliminate the limitation of CDM, Talreja [142] proposed a *synergistic damage mechanics* (SDM) methodology and applied it for $[\pm\theta/90_2]_s$ layup. This approach combines micromechanics and continuum damage mechanics judiciously to produce a versatile methodology. The micromechanical damage mechanics, or briefly, micro-damage mechanics (MDM) performs analysis of local stress-redistributions due to cracking, incorporating the micro-level geometry. On the other hand, CDM, as formulated by [88,143], allows a specific output of MDM (average crack surface displacements) to be used within a representative volume element (RVE), i.e., at meso level. In this way, the synergism between micromechanics and CDM effectively treats the multi-scale nature of damage. More recently, the SDM approach has also been extended to analyze viscoelastic behavior of composites with damage [144].

In the present work, we advance the SDM technique for multidirectional laminates. Although the basic framework of CDM is retained, the damage stiffness relations are derived with multiple damage modes with each damage mode corresponding to the family of transverse cracks in ply of a particular orientation. SDM will be ap-

plied for the cases with cracks in two and three different orientations. The framework is quite general and can be extended to more complex laminate configurations. Moreover, SDM effectively treats the multiscale nature of damage mechanisms and their evolution. Finally, the approach can be complemented easily with an energy based damage evolution model, thereby enabling a complete description of damage analysis problem for multidirectional composites in a common framework.

C. Overall Objective and Scope

The SDM methodology proposed above will be developed and applied for the following tasks:

1. *Stiffness Degradation in Multidirectional Laminates:* This part will aim at deriving stiffness relations for damaged off-axis laminates in terms of matrix crack spacing.

    - Two Damage Modes: First we will develop SDM formulation for damage in off-axis laminates due to transverse cracking in 2 damage modes, i.e., $+\theta$ and $-\theta$ plies. Our major objective here will be to develop numerical micromechanics for evaluation of CODs for $[0/\pm\theta_4/0_{1/2}]_s$ laminate configuration and compare them with published experimental data [109]. In addition, the SDM predictions for stiffness degradation will be compared against the experimental results [109]. Additionally, to enable predictions for a more general configuration $[0_m/\pm\theta_n/0_{m/2}]_s$, parametric studies will be carried out to evaluate COD as a function of important geometry and material parameters.

    - Three Damage Modes: This task will involve extending SDM approach to a more complex laminate configuration, specifically $[0_m/\pm\theta_n/90_p]_s$ system.

SDM predictions will be compared with independent computational (FE) simulations. We will also verify SDM results against experimental data for quasi-isotropic laminates.

2. *Damage Evolution in Off-axis Plies of Multidirectional Laminates:* This section will target the problem of how matrix crack density evolves with applied loading. A fracture mechanics based energy criterion will be developed for prediction of crack initiation and progression. The analysis will be done for the case with two damage modes as well as for three damage modes.

3. *Stress-strain Response of Multidirectional Laminates:* This task will combine the SDM predictions for stiffness changes with evolution of crack density to arrive at the overall stress-strain response of the composite structure subjected to tensile loading along the longitudinal direction.

The approach and predictions covered in this study can be applied to treat behavior of laminated structures containing sub-critical damage in the form of matrix cracking. Many of present designs treat initiation of ply cracking as structural failure, making them too conservative. Some other approaches only consider more severe damage modes, e.g., delaminations in their models. Design of composites based on progressive damage analysis can improve the design life of the structures, reducing our dependence on using arbitrary "knock-down" factors. Proper treatment of progressive damage can also assist in predicting laminate failure more accurately, thus helping us to get away from empirical failure theories. The constitutive relations derived in this work can be easily incorporated in a multiscale FE model, thereby enabling complete structural analysis of composite structures.

The scope of the study is limited to:

1. Laminated composite materials made from polymer reinforced plastics.

2. Multiple matrix cracking: Other forms of damage are not considered.

3. Quasi-static loading: No fatigue or time dependent aspects are considered.

4. Uni-axial loading.

D. Outline of Dissertation

In the present chapter, we have introduced the issues in damage analysis of multidirectional laminates citing the relevant literature. In chapter II, we will discuss them in some more detail, present the available approaches, and make a case for a synergistic approach which addresses these issues. Chapter III will describe the 3D FE modeling and its limited verification with experimental data. In the next two chapters, SDM approach will be implemented and illustrated for two and three damage modes, respectively. Chapter VI will cover modeling of damage evolution in multidirectional laminates. We will then discuss the results obtained in this study in the light of the "big" picture and end with some concluding remarks.

CHAPTER II

DAMAGE MECHANICS OF COMPOSITE MATERIALS

From the chapter I, it is clear that all the existing analytical models are inadequate for an accurate analysis of damage in multidirectional laminates. In this chapter, we will focus on developing a coherent strategy for damage analysis of such laminates. We will highlight the main issues and complexities in the analysis of multidirectional laminates, and formulate a multiscale damage mechanics methodology to address them. The approach, its implementation and validation will be the main focus of the successive chapters.

A. Damage Development in Composite Materials

Property tailoring is one of the main objective in the design of composite materials by which a designer can assure desirable stiffness properties in desired directions. Polymer matrix composites (PMCs) use strong, stiff fibers embedded in a compliant polymer matrix to make up a unidirectional lamina (UDL), which provides the necessary strength in the direction along fiber longitude. When a UDL (also known as a ply) is loaded in tension along the fiber direction, it fails by the rupture of fibers. Since the failure strain of fibers is quite large, a UDL can support sufficiently large tensile loads. Usually, the failed UDL specimen will show fiber ruptures at random locations due to variation in fiber strength because of inherent defects, and this can be accounted for by using a suitable statistical distribution for fiber strength [139, 145–149]. If, on the other hand, the usual thin UDL is loaded transversely, normal to the fiber direction, it fails abruptly by a single crack lying in matrix between fibers or at the fiber/matrix interface, without a prior discernible development of damage. Thus, the strength and stiffness of a UDL are very high in the fiber direction, but very low transverse

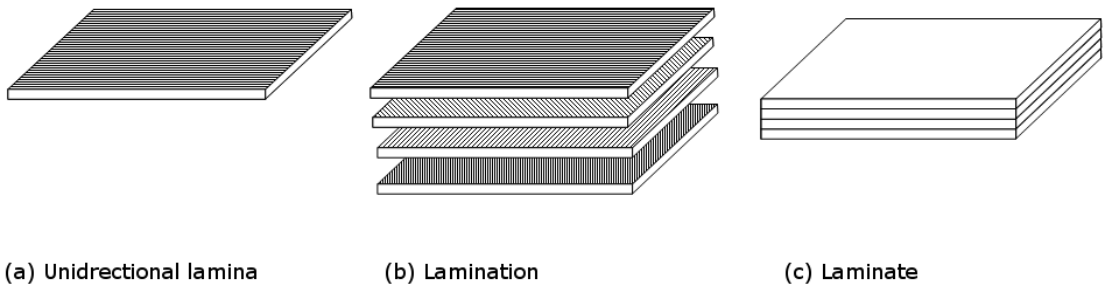

Fig. 11. Lamination scheme for property tailoring in the design of composite materials.

to fibers. To meet the necessary strength and stiffness requirements in transverse direction, two or more laminae having different fiber directions are stacked together to make a 'composite laminate' (see Fig. 11). The sequence of fiber orientations for laminae from top to the bottom is known as 'layup configuration', and its choice and optimization is an important step in achieving desired directional properties for the composite structure. For an undamaged laminate, the stress state in each lamina is constant and plane stress except at the free edges where it is three dimensional. The stresses, strains and effective stiffness properties in the laminate can be obtained by the so called 'classical laminated plate theory' (CLPT) [147].

A schematic description of damage development in composite laminates in tension is depicted in Fig. 12 (based on [46, 87]), where the five identifiable damage mechanisms are indicated in the order of their occurrence. Although the figure is developed on the basis of fatigue experiments, it provides the basic details for quasi-static loading.

In the early stage of damage accumulation, multiple matrix cracking dominates in the layers which have fibers aligned transverse to the applied load direction. Static tensile tests on cross-ply laminates have shown that the transverse matrix cracks can initiate as early as at about 0.4-0.5% applied strain depending upon the laminate

configuration. They initiate from the locations of defects such as voids, or areas of high fiber volume fraction or resin rich areas. Ply cracks grow unstably through width direction and quickly span the specimen width. As the applied load is increased (or the specimen is cyclically loaded), more and more cracks appear. The accumulation of ply cracks in a cracked ply is depicted in Fig. 13 (redrawn from [55], based on X-ray radiographs reported in [99]). Initially these cracks are irregularly spaced and isolated from each other, i.e., have no interaction among themselves. However, as cracks become closer they start interacting, i.e., the in-between tensile stresses diminish and can no longer build up to earlier levels. Thus further increase in load is required to produce new cracks. This is well illustrated in Fig. 14, reproduced from [46], by plots of diminishing crack spacing versus load or number of cycles. The state at which crack density saturates, often reached only under fatigue loading, is termed as 'Critical Damage State' (CDS) [46]. This state seems to mark the termination of the intralaminar cracking.

Subsequent loading causes initiation of cracks transverse to the primary (intralaminar) cracks lying in plies adjacent to the ones with those primary cracks (see Fig. 12). These cracks, known as secondary cracks, are small in size and they can cause interfacial debonding, thereby initiating interlaminar cracks. The interlaminar cracks are also initially small, isolated and distributed in the interlaminar planes. Subsequently, some interlaminar cracks merge into strip-like zones leading to large scale delaminations. This results into the loss of the integrity of the laminate in those regions. Further development of damage is highly localized, increasing unstably and involving large scale fiber breakage. The final failure event is manifested by the formation of a failure path through the locally failed regions and is therefore highly stochastic.

Our focus here is to analyze sub-critical damage related to the intralaminar

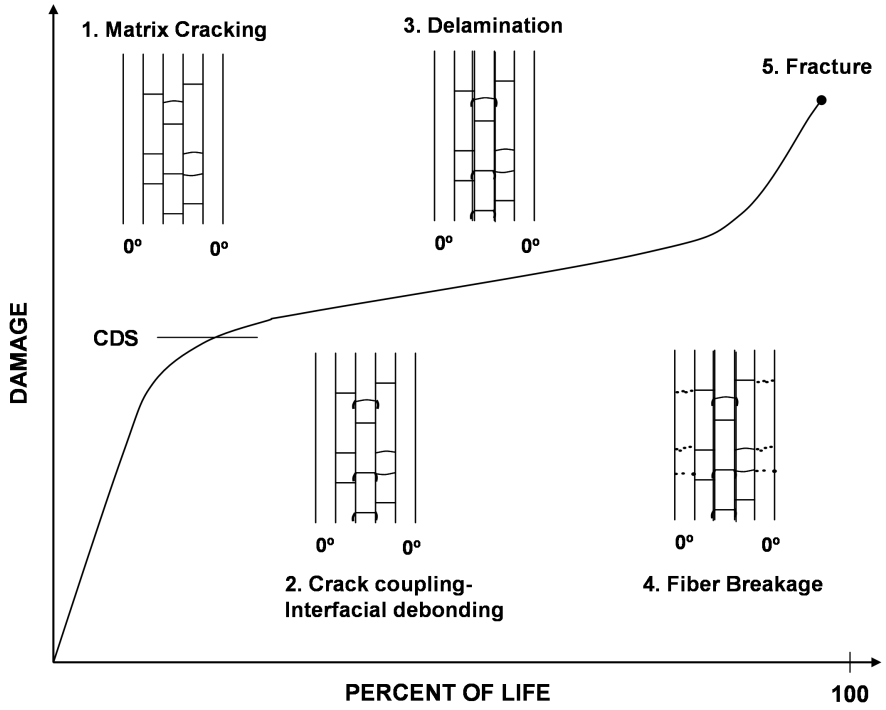

Fig. 12. Damage development in composite laminates (based on [46,87]).

cracking. Intralaminar or transverse ply cracking causes loss of stiffness properties in the laminate. The field of 'damage mechanics' caters to the development of methods to predict the initiation, and growth of intralaminar cracks, and their effect on the overall stiffness properties of the laminate.

B. Complexity of Analyzing Ply Cracking in Multidirectional Laminates

The major issues in analyzing damage in a multidirectional laminate are given below:

1. Anisotropy & heterogeneity: All the laminate analysis in the literature is based on the assumption that the plies are homogeneous and orthotropic. This is a valid assumption for undamaged laminates for general membrane force and moment loading. Here, the resulting laminate stresses are either constant or

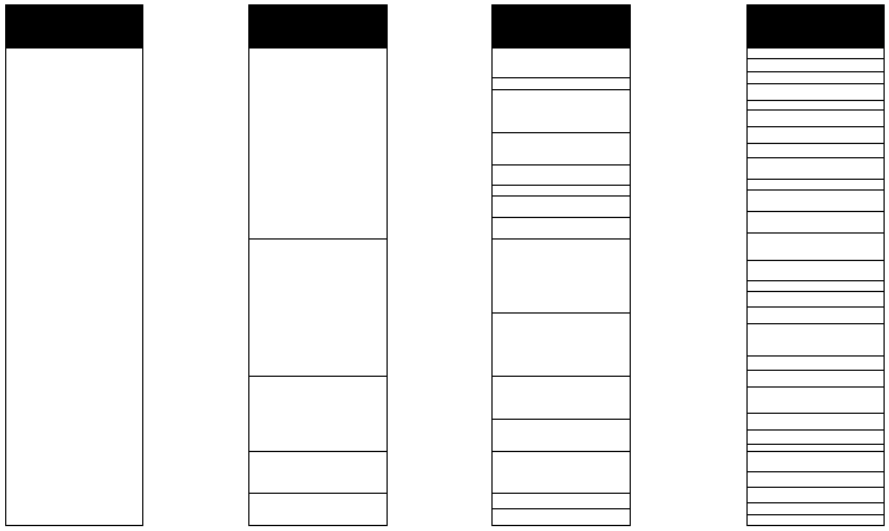

Fig. 13. Accumulation of intralaminar cracks in an off-axis ply of a composite laminate. The figure is redrawn from [55], based on X-ray radiographs reported in [99].

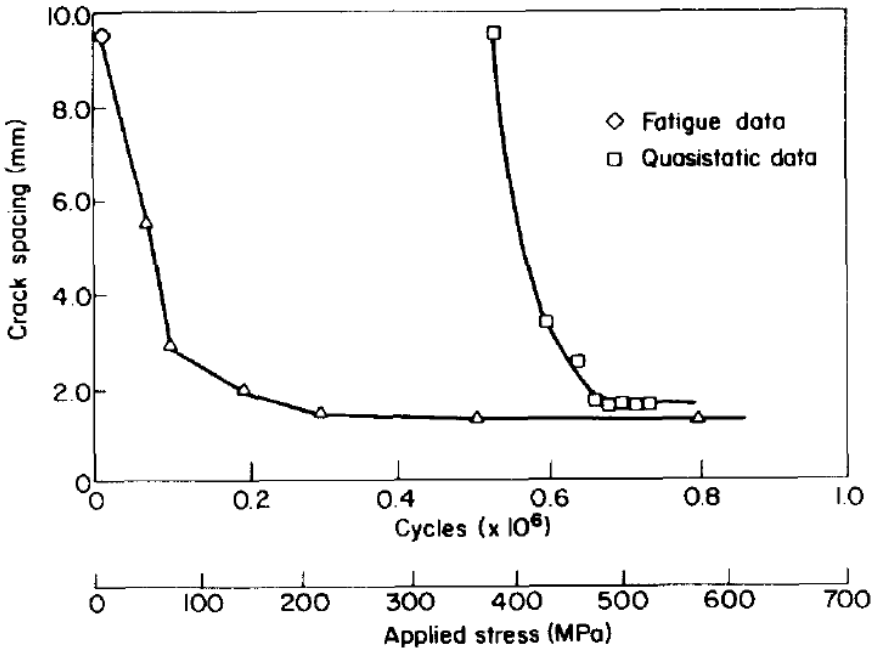

Fig. 14. Spacing of cracks in $-45°$ plies of $[0/90/\pm 45]_s$ graphite/epoxy laminates as a function of quasi-static and fatigue loading (source: [46]).

linearly varying across ply thickness. The presence of intralaminar cracks however, may invalidate this assumption because the cracking may lead to high stress gradients through very thin plies [55].

2. Stress singularity: Theoretically, there is a stress singularity at the crack tip, which leads to a very high transverse shear and normal stresses near the crack tip. In reality, however, the crack tips are blunted due to the finitely sized fibers near to the inter-ply interface, and other nonlinear (plastic) processes. Hence, the actual stress field in the vicinity of the crack tip is very complex, and the usual damage procedures can not be expected to describe it accurately. Numerical approaches, such as [150], can only accurately model stress gradients at the crack tip.

3. Interaction between cracks: At sufficient crack densities, the stress fields around two adjacent cracks in a ply start interacting, thereby relaxing the region in between those two cracks. This crack interaction affects the crack surface displacements as well as the overall stress fields. Accurate modeling of crack interaction is a complex task.

4. Three dimensionality of the boundary value problem: Following all the previous points, and realizing that in a real scenario the cracks may be curved, irregularly spaced, or not fully grown through the laminate width, we get the full picture of a complex 3D boundary value problem (BVP) arising out of intralaminar cracking. In a cracked cross-ply laminate, along with the assumption that all cracks are periodic, straight and fully grown, the resulting BVP can be reduced to a generalized plane strain problem. The off-axis ply cracking can however result into a truly 3D BVP, and any generalization to a 2D scenario cannot provide accurate predictions.

5. Difficulty in RVE definition: To apply elasticity theory to a composite material body, it is important that the RVE size is sufficiently large enough to contain many micro-entities, and that the whole composite structure is itself much larger than RVE, i.e., $L_{micro} << L_{RVE} << L_{macro}$. It is difficult to meet this definition while choosing an RVE for a cracked laminate. A typical ply may have thickness of the order of 0.2 mm, while typical fiber diameter is of the order of 0.01 mm. At typical fiber volume fraction 0.60, a ply can accommodate about 15 fibers. A typical 2D RVE for damage analysis may be about 10×10 fibers size. This is not fully consistent with the definition of effective media, because crack tip uncertainty regions may not be very small compared to crack size (i.e., ply thickness) and RVE size is of the same order as of the macrosize [55].

6. Multiscale effects: Reinforcing the previous point, there are multiple scales involved in damage analysis. Transverse cracks initiate from material defects, which can be of much smaller scale than the laminate. Additionally, the structure made of the laminate, e.g., an aircraft wing, may involve analysis at a much larger scale. Thus the damage analysis procedure should be easily integrable with the structural integrity analysis module.

7. Constraint effects: In a cracked laminate, stress perturbations are caused by the surface displacements of the ply cracks in response to the applied loading. These surface displacements do not occur freely, as they would if the cracks were to lie in a homogeneous ply of infinite thickness, but are affected by constraint from the neighboring plies. Understanding these constraint effects is the key in determining the effective properties of cracked laminate. Following Talreja [87, 145], they can be classified in four categories: A-no constraint; B-low constraint; C-high constraint, and D-full constraint. Considering $[0_m/90_n]_s$ laminate, for

example, the constraint of 0° plies on 90° cracks will decrease as 'n' increases, or if 'm' decreases, or if the 0° ply is somehow made less stiffer (by using a different material). This will force the surface displacements of cracks in 90° plies to increase in magnitude, thereby affecting the overall stiffness properties to a greater degree. The stress-strain response in the four categories, illustrated in Fig. 15 (source: [145]), clearly shows widely different characteristics, resembling an elastic-plastic behavior for constraint type A at one extreme, and linear elastic behavior for constraint type D at the other extreme. The constraint effect in a real scenario is usually somewhere in between the two and has to be determined/modeled accurately in a damage analysis.

8. Complexity of off-axis ply cracking: Unlike in cross-ply laminates, transverse cracking in off-axis plies of orientations other than 90° can be extremely complex. Morphological observations suggest that these cracks may be partially grown, erratic in shape, size, and distribution [60, 108]. Raman Spectroscopy experiments on $[0/45]_s$ laminates showed that a crack developing in the 45° ply behaves differently from a similar crack in the 90° ply of a cross-ply laminate [133], which seemed to suggest that the initiation and propagation strains for 45° were different. For the laminates containing a 90° ply, the cracks usually initiate in that ply, while cracks in other off-axis plies initiate at higher loading. The observations on multidirectional laminates indicate that intersecting angle between the two plies may have significant effects on damage initiation and progression. When the intersecting angle is small, micro-formed cracks are observed before propagation in the fiber direction. However, developed cracks mainly form in the cases of large intersecting angles [126]. The damage development in the 60° ply of a $[0/60_2/90]_s$ is shown in Fig. 16, taken from [126].

Moreover, shear-extension coupling may introduce some additional complexity in analysis of off-axis laminates [119, 120].

9. Multiple damage modes: Multidirectional laminates, having plies in different orientations may develop ply cracks in multiple plies with different orientations because cracks grow parallel to the fibers in a cracked ply. This means there could be crack systems in a number of orientations, with each family of cracks constituting a particular cracking mode, which can interact and perturb stress fields. Obviously, analyzing such a cracked laminate is extremely complex, and even numerical methods may not fully cope with the situation, as defining a representative unit cell for analysis can be too demanding, and may sometimes be impossible.

10. Randomness in cracking process: In general, all damage models assume a uniform longitudinal distribution of transverse cracks, i.e., they are assumed to be periodic and self-similar. This neglects the effect of variations in crack spacing that are considerable in some cases. Recently, there have been some developments to account for the influence of the spatial scatter of matrix cracking on the stress transfer and the effective mechanical properties of cracked cross-ply laminates [129, 138, 139].

11. Multiple damage mechanisms: Since damage in composites may occur due to multiple processes, they need to be characterized appropriately to fully analyze the laminated structure. Here, our focus is on transverse cracking, which usually occurs much before other damage mechanisms such as delaminations, fiber fracture etc. may occur. Influence or interaction from manufacturing induced defects like voids, fiber clusters may further complicate the analysis. They may become important for failure analysis of 'Short Fiber Composites' (SFC), and

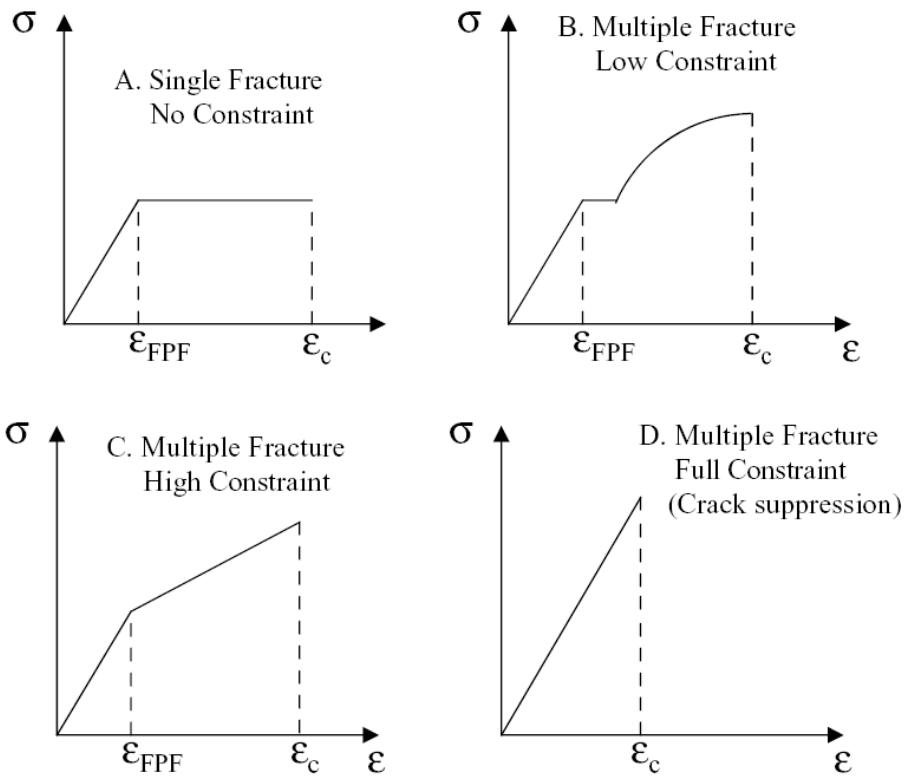

Fig. 15. Schematic stress-strain response of cross-ply laminates at different constraint to transverse cracking, reproduced from [145].

are dealt in [151–156].

The above list of complex issues governing analysis of cracked laminates, even for simple configurations, may overwhelm any analyst. It is obvious that accurate stress analysis for a cracked laminate with a general layup is extremely demanding, and can be obtained only through computational means. There is still a silver-lining. The effects of the crack tip are highly localized, and cannot induce appreciable consequences on the overall stiffness properties. This is the major motivation for the CDM approaches, which do not worry too much about the complexity of stress field inside a cracked laminate, but focus on the prediction of effective properties. It is highly unlikely to address all the above issues, and we will simplify the development as and

when necessary. Our main focus will be to formulate a methodology which can be applied to many practical laminate sequences, while preserving the essential aspects of off-axis ply cracking.

C. Modeling of Ply Cracking in Multidirectional Composite Laminates

Consider a laminate consisting of plies of various fiber orientations loaded in tension along the longitudinal direction. Each lamina within the laminate will develop a state of plane stress, which can be different for different plies depending upon their orientation, thickness and material properties. When the stress exceeds the threshold for initiation of matrix cracking, one or more off-axis plies may develop cracks along fibers. We shall call these plies as *cracked plies*, and the remaining plies as *constraining plies*. Also, for a given cracked ply, all the surrounding plies, whether cracked (in orientation different than the current ply) or uncracked, will constrain the motion of cracked surfaces.

An example of an multidirectional laminate undergoing transverse cracking in multiple off-axis plies is shown in Fig. 17 (adapted from [91]). All the developed methods to meet the objectives mentioned above can be broadly categorized in two approaches: Micro Damage Mechanics and Continuum Damage Mechanics.

1. Micro Damage Mechanics

Micro damage mechanics (MDM) basically tries to solve the boundary value problem arising out of damaged microstructure and evaluate the resulting stress and displacement fields in the vicinity of damage entities. It would appear at first that MDM must be an obvious choice because it provides more insight into the mechanics of damage processes and their effects on modifying the stress and strain fields in the

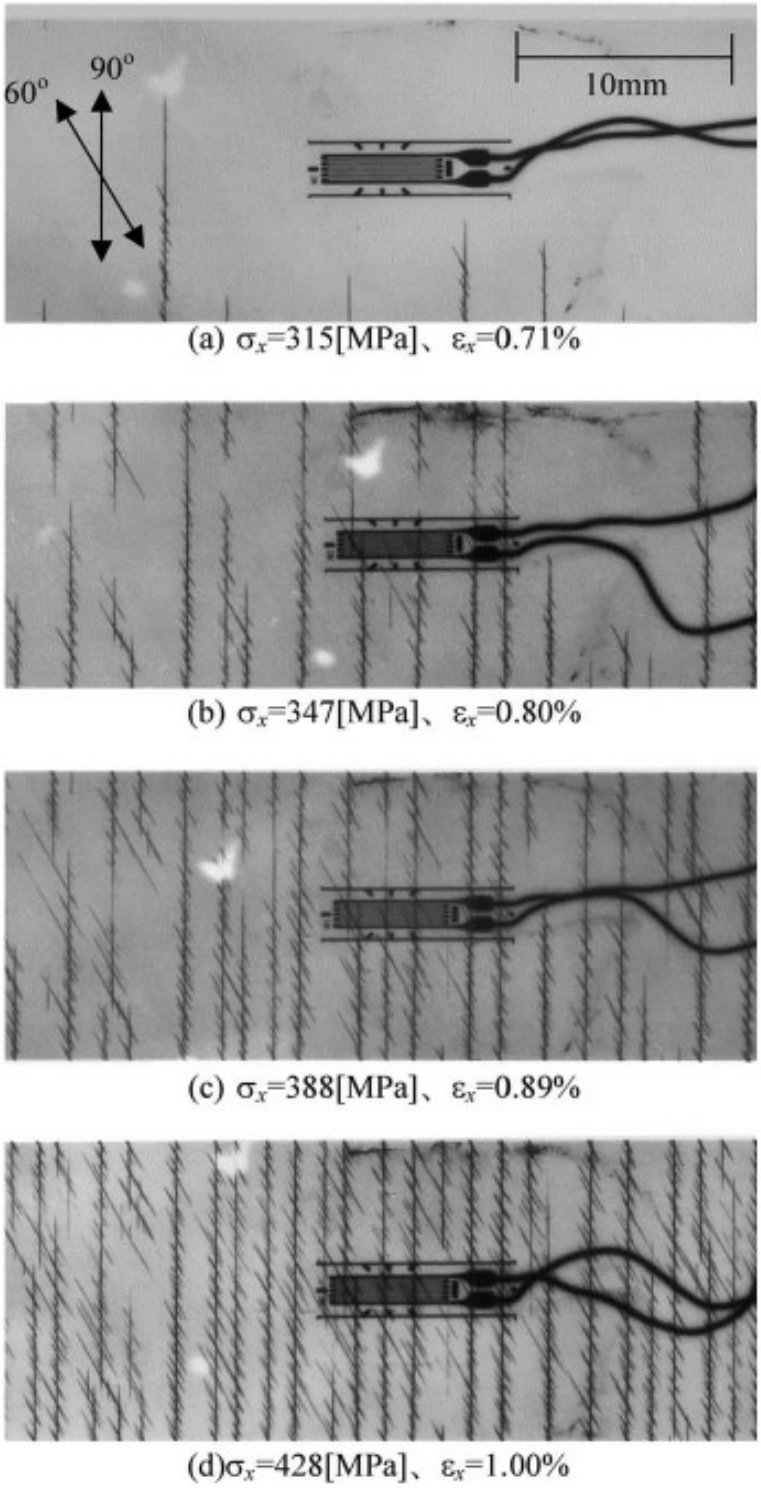

Fig. 16. Consecutive matrix cracking behavior in contiguous plies in a $[0/60_2/90]_s$ laminate (source: [126]).

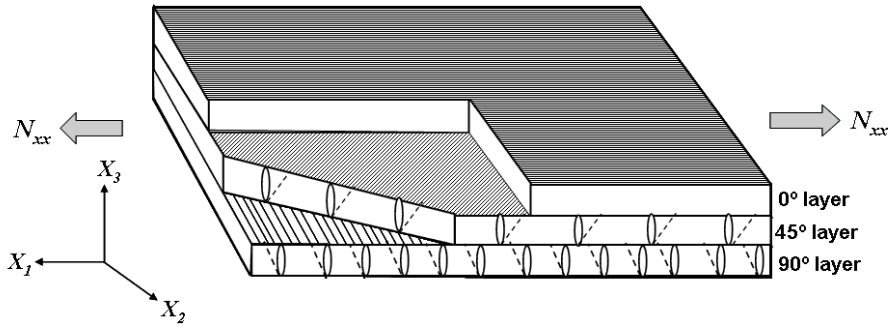

Fig. 17. A schematic representation of an off-axis laminate ($[0/45/90]_s$) laminate undergoing ply cracking in multiple off-axis orientations during tensile loading in longitudinal direction (adapted from [91]). The laminate coordinate system is shown by $X_i, i = 1, 2, 3$.

neighboring volume. Unfortunately, it is also very difficult to carry out, since it requires the determination of stress and displacement fields produced by many interacting damage entities and can therefore be performed only for relatively simple geometries utilizing simplifying assumptions along side. In fact, there is no MDM solution for cracked laminates other than cross-ply ($[0/90]_s$) and similar variations which can yield consistent and accurate results.

1-D Shear lag models [14, 27, 34, 37, 56–58], 2-D variational methods [64–70], self-consistent approximations [76–79], 2-D generalized plane strain models [72–75], 3-D laminate theories [41, 80–86], and numerical methods [93, 94, 96–98] all belong to this category. These have already been described in some detail in the introductory chapter.

2. Continuum Damage Mechanics

Continuum Damage Mechanics (CDM) on the other hand tries to look at the stiffness changes resulting from damage development. In CDM, the material microstructure, e.g., distributed fibers, and the distributed damage, which may be called the mi-

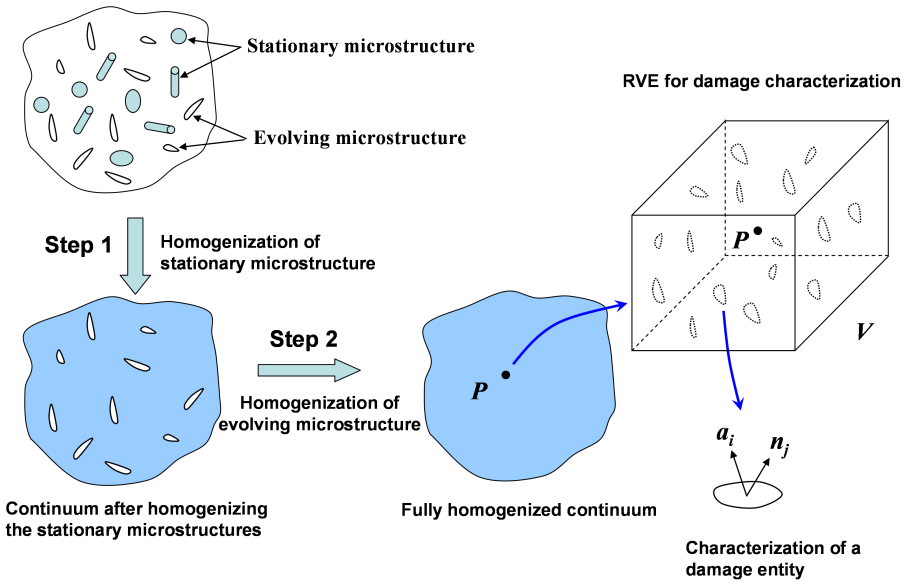

Fig. 18. Illustration of the two-step homogenization process for composites with damage, redrawn from [157].

crodamage structure, are treated as smeared-out fields. For evaluating the effective properties of the continuum body, the continuum is homogenized using a two step homogenization procedure (see Fig. 18 redrawn from [157]), where the material microstructure is viewed as consisting of "stationary" entities, e.g., fibers and plies, and the microdamage structure is considered as a family of "evolving entities", e.g., cracks. In the first step, the stationary microstructure of the composite material (e.g., fibers, plies) are smeared into a homogeneous, anisotropic material. In the next step, the evolving microstructure (damage entities) are smeared into a homogeneous field represented by suitable internal variables. A set of response functions are expressed in terms of the field variables (stress, strain, temperature), and internal variables which represent the smeared-out field of evolving damage entities.

Following Talreja [87,89], the damage is characterized using a second order tensor called the 'damage mode tensor'. Consider an RVE containing a representative sample

of damage entities, around a generic point P in the solid body (Fig. 18). Focusing on a typical damage entity within RVE, let it be bounded by a surface S, and associate two vectors a_i and n_i with a point on the damage surface S, such that the vector a_i represents some pre-specified influence (e.g., displacement, extent of disturbance) of the considered point on the surrounding volume, and n_i is a unit outward normal to the surface as shown in Fig. 18. Let the surface integral of dyadic product $a_i n_j$, described by a second order tensor, be given as

$$d_{ij} = \oint_S a_i n_j \mathrm{d}S \tag{2.1}$$

The total set of damage entities may be divided in subsets of entities having same geometrical characteristics (orientation, shape, etc.) and termed as damage modes. For example, matrix cracks may constitute one damage mode, while fiber/matrix debonds may constitute another. Also, matrix cracks in different orientations may be grouped into different damage modes. Assuming that there are N damage entities of a given mode α in the RVE, the damage mode tensor is defined by

$$D_{ij}^{(\alpha)} = \frac{1}{V} \sum_{k_\alpha}^{N} \left(d_{ij}\right)_{k_\alpha} \tag{2.2}$$

Following the theory of thermodynamics with internal variables developed by Coleman and Gurtin [158], the thermomechanical response of a composite body can be represented by a set of response functions consisting of the Cauchy stress tensor σ_{ij}, the specific Helmholtz free energy ψ, the specific entropy η, the heat flux vector q_i, and a set of damage rate tensors $\dot{D}_{ij}^{\alpha}$. The thermodynamic state of the body is given by the strain tensor ϵ_{ij}, the absolute temperature T, the temperature gradient $g_i = T_{,i}$, and a set of damage tensors D_{ij}^{α}. Assuming the Truesdell's principle of equipresence,

we have

$$\begin{aligned}
\sigma_{ij} &= \sigma_{ij}\left(\epsilon_{kl}, T, g_k, D_{kl}^{(\alpha)}\right) \\
\psi &= \psi\left(\epsilon_{kl}, T, g_k, D_{kl}^{(\alpha)}\right) \\
\eta &= \eta\left(\epsilon_{kl}, T, g_k, D_{kl}^{(\alpha)}\right) \\
q &= q\left(\epsilon_{kl}, T, g_k, D_{kl}^{(\alpha)}\right) \\
\dot{D}_{kl}^{(\alpha)} &= \dot{D}_{kl}^{(\alpha)}\left(\epsilon_{kl}, T, g_k, D_{kl}^{(\beta)}\right)
\end{aligned} \tag{2.3}$$

Invoking the Clausius-Duhem inequality, we obtain [87, 89]

$$\sigma_{ij} = \rho\frac{\partial\psi}{\partial\epsilon_{kl}} \tag{2.4}$$

$$\eta = -\frac{\partial\psi}{\partial T} \tag{2.5}$$

and

$$\frac{\partial\psi}{\partial g_i} = 0 \tag{2.6}$$

This reduces the function dependence of variables in Eq. (2.3). Considering only σ_{ij} for a purely mechanical response (at constant temperature), we get

$$\sigma_{ij} = \rho\frac{\partial\psi}{\partial\epsilon_{kl}} \tag{2.7}$$

where

$$\psi = \psi\left(\epsilon_{kl}, D_{kl}^{(\alpha)}\right) \tag{2.8}$$

Thus, the constitutive relation for a damaged composite body is given by

$$C_{ijkl} = \rho\frac{\partial^2\psi\left(\epsilon_{kl}, D_{kl}^{(\alpha)}\right)}{\partial\epsilon_{ij}\partial\epsilon_{kl}} \tag{2.9}$$

Here it is important to note that the Helmholtz free energy ψ is a function of damage mode tensor. In CDM [87, 89], ψ is written as a polynomial function in strain and

damage mode terms such that the material symmetries present in the solid body are exploited by using the so called integrity bases [159, 160].

D. Synergistic Damage Mechanics (SDM)

Obviously, the CDM approach is quite versatile, and can be used for any laminate configuration. However, it needs determination of certain phenomenological constants, which requires experimentation or computational simulations. Additionally, these constants need to be determined whenever laminate material or layup changes. This is a major limitation which puts a question mark on its practical applicability.

Fortunately, the past experience has shown these phenomenological constants are primarily determined by the constituent ply properties and are negligibly affected by the ply orientations [106]. This assumption was found to hold for $[\pm\theta/90_2]_s$ laminates of carbon/epoxy [142] and of glass/epoxy laminates [161]. For intralaminar cracking in an off-axis lamina with ply orientation θ with respect to the loading direction, the elements of damage mode tensor can be represented as [87]

$$D_{ij}^{(\alpha)} = \frac{\kappa_\theta t_c^2}{st \sin\theta} n_i n_j \tag{2.10}$$

where κ_θ, known as the 'constraint parameter', is a parameter characterizing the displacement of the crack surfaces. The change in κ measures the effect of ply orientation on the crack opening displacement (COD). Since the energy stored in the system changes according to how much these crack surfaces move, average COD is a good measure of change in the overall stiffness properties of a cracked laminate. Also, the average COD in a cracked laminate is less sensitive to the stress singularities, and can be determined through a suitable computational or analytical procedure. The most suitable way to determine is by using micromechanics of the damaged lami-

nate. Hence, *if we assume the phenomenological constants to be independent of the ply orientation, for a given laminate system, and can find the relative change in the constraint parameter, we can characterize stiffness changes in a variety of laminate configurations.* This is the basic idea behind the 'Synergistic Damage Mechanics' (SDM) which combines the strengths of CDM and MDM. MDM can provide an easy solution to the constraint parameter, and by using this parameter into CDM formulation, we can predict stiffness changes in a multidirectional laminate.

In fact, some studies on analysis of stiffness degradation in cross-ply laminates have identified that the stiffness changes can be directly expressed in terms of average COD [162, 163]. For example, Varna et al. [163] demonstrated that the rate of reduction in longitudinal modulus is directly related to average COD. They compared shear lag and variational approaches and recognized that the major difference between these analyses is how they model average COD.

The basic steps in damage analysis using the SDM approach are shown in Fig. 19. As an example consider $[\pm\theta/90_4]_s$ laminates. Suppose, for the given material, we have stiffness degradation results available to us for $[0_2/90_4]_s$ laminate. We call it the reference laminate. Applying the CDM stiffness-damage relationships (see,e.g. [106]), we can obtain the damage constants. For this step, we essentially require E_1, E_2, ν_{12}, and G_{12} for the damaged cross-ply laminate at a fixed crack density. Being a cross-ply, stiffness changes can be easily obtained, either by experiments, numerical simulations, or by an MDM approach, such as the variational approach. In a separate step, we determine average COD for $[\pm\theta/90_4]_s$ laminate as θ varies. Since the average COD carries the constraint effects appropriately, the relative change in average COD as θ varies gives us the relative constraint parameter. Then, the SDM stiffness-damage relationships are utilized to obtain stiffness changes for a $[\pm\theta/90_4]_s$ laminates. If we are concerned in the analysis of a structure made of $[\pm\theta/90_4]_s$ laminates, the SDM

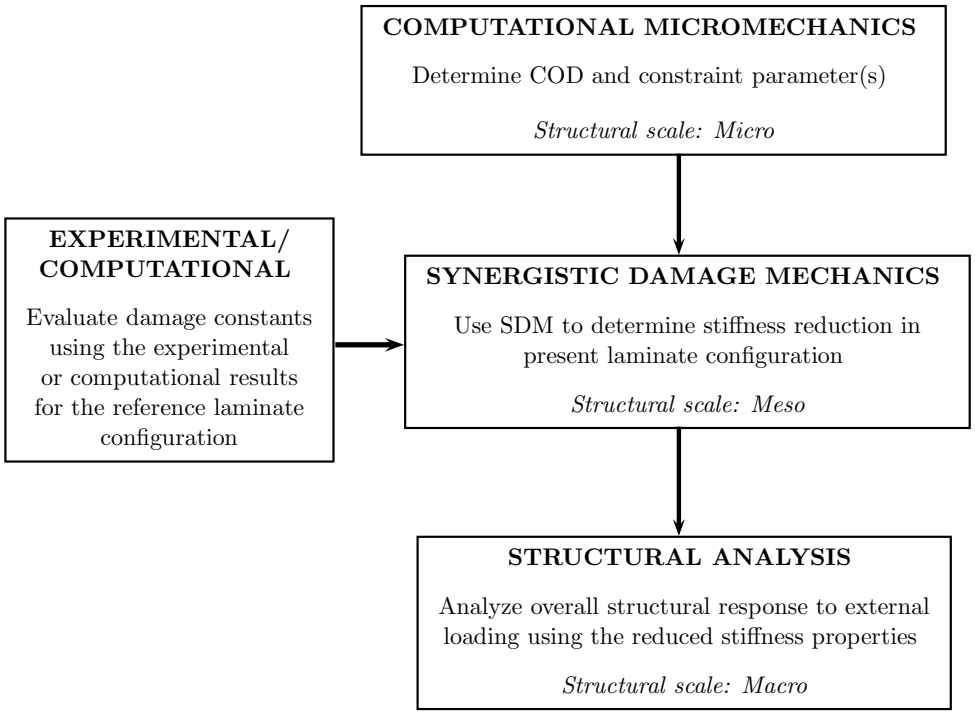

Fig. 19. Flowchart showing the multi-scale synergistic methodology for analyzing damage behavior in a class of symmetric laminates.

approach can be linked in a multiscale framework to update the structural stiffness as and when damage initiates and progresses.

The SDM approach has been successfully verified for $[\pm\theta/90_2]_s$ carbon/epoxy laminates [142], and $[\pm\theta/90_4]_s$ glass/epoxy laminates [104, 106, 161]. The approach has also been extended for damage analysis of viscoelastic cross-ply laminates [144]. In this study, we extend it to the multidirectional laminates with multiple damage modes.

E. Assumptions

Before we proceed to the implementation of SDM methodology, we would like to point out the assumptions made in the present study:

1. A unidirectional ply is considered to be homogeneous and orthotropic. To obtain 3D orthotropic properties, a lamina is assumed to be transversely isotropic. Perfect bonding between fibers and matrix, and a uniform distribution of fibers is assumed.

2. The analysis does not consider any residual stresses, either formed during manufacturing process or by thermal effects.

3. Laminates are considered to be symmetric about the mid-plane.

4. The laminate material is assumed to behave elastically.

5. All the cracks are considered periodic, planar and fully developed. However, a way to account for partial cracks, specially in non-dominant damage modes, is also discussed while modeling damage in quasi-isotropic laminates.

F. Summary

The composite laminates can "perform" satisfactorily in the presence of sub-critical damage to some level. Intralaminar cracking, usually the first mode of damage affects is a complex process which affect the stiffness properties of the laminates. This chapter highlighted some of the issues which mechanics researchers face while modeling transverse cracking in composite laminates. Analysis of off-axis ply cracking is even more complex owing due to multiplicity of crack paths, and hence the two common strategies used presently, continuum damage mechanics and micro damage mechanics, both fail to accurately model this scenario. A practical solution is to combine these two approaches so that they complement each other and such a methodology, termed as the synergistic damage mechanics, is described in the chapter.

CHAPTER III

FINITE ELEMENT MODELING OF CRACKED COMPOSITE LAMINATES

A. Introduction

Computational micromechanics is an essential component of the SDM approach (see Fig. 19). It helps us determine the change in average COD as the laminate configuration is changed. In a general sense, the average COD in a cracked off-axis ply of a composite laminate depends upon the ply material, ply thickness, ply orientation and the constraint effects of the supporting plies. Due to heterogeneity in the composite laminates and constraint effects on crack surfaces from the surrounding uncracked plies makes it is impossible to derive exact analytical solutions. It should be pointed that some researchers, e.g. [81,82,164], use approximate analytical solutions for COD in their damage models. In their models, the crack surface displacements are assumed to be equal to those for a single crack in an infinite, homogeneous transversely isotropic medium. Obviously, this assumption is not accurate for the constrained cracking in a multidirectional composite laminate, because it does not consider the effect of ply orientation and the interaction between cracks in the same and different cracked layers. In fact, these solutions are not even true for a cross-ply laminate. More accurate COD modeling has been performed by Varna and his colleagues [162, 163] using 2D and 3D FE modeling for cross-ply laminates. When the average COD, determined experimentally or numerically, is used in combination with the CDM approach, consistent predictions for stiffness degradation can be obtained [105, 106, 109, 161]. Also, detailed parametric calculations [106], on cross-ply laminates have shown that the average COD can be expressed as a function of material and geometry parameters. For example, for $[S/90]_s$ glass/epoxy laminates, where S represents the sublaminate,

the average COD can be expressed by [84, 85]

$$u_{an} = A + B\left(\frac{E_2}{E_x^s}\right)^n \tag{3.1}$$

where A, B and n are given by

$$\begin{aligned} A &= 0.52, \\ B &= 0.3075 + 0.1652\left(\frac{t_{90} - 2t_s}{2t_s}\right) \\ n &= 0.030667\left(\frac{t_{90}}{2t_s}\right)^2 - 0.0626\left(\frac{t_{90}}{2t_s}\right) + 0.7037 \end{aligned} \tag{3.2}$$

where $u_{an} = u_a \dfrac{E_2}{t_{90}\sigma_{20}}$ is the normalized average COD, with E_2 is the transverse modulus for ply material, t_{90} and t_s are the thicknesses for 90° and sublaminate plies, respectively, E_x^s is the effective longitudinal modulus for uncracked sublaminate, and σ_{20} is the far away stress in the 90° ply in the laminate longitude direction.

In the present chapter, the 3D FE modeling for cracked multidirectional composite laminates will be described. FE analysis carried out in the present study will utilized for the following purposes:

1. Calculation and analysis of average crack surface displacements (COD and CSD), and the constraint parameter(s) derived from them,

2. Calculation of stiffness changes for a fixed state of damage (crack density),

3. Verification of SDM predictions, in cases where experimental data is not available, and

4. Parametric study of stiffness changes due to change in material and geometry parameters for the laminate.

An obvious advantage of FE computations is the accuracy of displacement fields.

B. FE Modeling Strategy

Although some analyses in literature use 2-D generalized FE models even for damage in off-axis plies, e.g. in $[0/90/\mp 45]_s$ laminates [94], the boundary value problem for a multidirectional laminate necessitates a 3-D analysis. It should be noted, however, it is not easy to define a repeating unit cell for a multidirectional laminate undergoing cracking multiple layers. A repeating unit cell can be defined upto a maximum of two off-axis cracking modes, utilizing a skewed RVE in FE modeling (refer [165, 166] for more details). But, the application of periodic boundary conditions in a skewed RVE is a complex task. Fortunately, for our purpose here, we need average surface displacements and stiffness properties, and they are less sensitive to periodicity. Thus, it makes more sense to develop simpler FE models, which carry the essential aspects of the cracking process and the external loading. On the other hand, if one is interested in actual stress fields inside the cracked laminate, it is essential to model the periodic conditions accurately, and we suggest the use of a skewed RVE for such analysis.

The second issue in developing unit cell for multidirectional laminates is that the different crack systems in different cracked plies may have different densities. If a laminate contains a 90° layer, it is expected that for most of the time during the damage development that 90° crack density is the highest. This is true except at very high loads because 90° cracking will start well before other plies start developing cracks, and till sufficient load levels, other plies may not even develop fully grown cracks before the laminate fails by delamination. Hence, for the worst case scenario, we can assume the same crack densities in 90° and other cracked layers.

The interaction between adjacent cracks in a layer can be easily modeled by varying the length of unit cell, i.e., by varying the crack spacing. This requires multiple FE calculations. The present SDM approach, is a linear model with respect

to the crack density variation. Hence, we require COD calculation at one crack spacing only. For the calculation of average COD, to be used in SDM, we choose a very high crack spacing to avoid any interaction between cracks. But, as will be shown later, the prediction of damage progression requires determination of average COD and CSD as a function of crack spacing, and there multiple FE calculations are necessary. Also, for verification of SDM predictions for stiffness changes in cases where experimental data is not available, we carry out FE calculations at varying crack densities.

It is also quite possible that the crack systems in different damage modes may interact and affect average COD. Because the crack spacing in the two crack systems may be different, we simulated two scenarios:

1. Case 1: Maximum interaction between different damage modes - For this, the FE models contained cracks in all possible damage modes.

2. Case 2: No interaction between different damage modes - For this, cracks were assumed to exist only in the layer in consideration. This way if the laminate contained three damage modes, FE analysis were performed three times, with only one active damage mode each time. This was achieved by closing all the nodes on surfaces of inactive cracks.

The above scenarios represent extreme material behavior and the real situation will be somewhere in between. To determine the exact response of a laminate undergoing cracking in multiple damage modes, the information regarding crack densities in different layers is necessary.

The representative geometric model for $[0/\pm\theta_4/0_{1/2}]_s$, as shown in Fig. 20, represents the damage model with two damage modes and contains cracks in $+\theta$ and $-\theta$ plies. The models for $[0_m/\pm\theta_n/90_r]_s$ and $[0_m/90_r/\mp\theta_n]_s$ laminate configurations,

shown in Fig. 21, represent the case with three damage modes, and contain cracks in 90°, $+\theta$ and $-\theta$ plies. The boundary conditions and the local and global coordinate systems are also shown in the figures.

In a periodic unit cell, the periodicity in the displacement and stress fields are represented by

$$\begin{aligned} u_i\left(x_\alpha + \Delta x_\alpha\right) &= u_i\left(x_\alpha\right) + \Delta x_\beta \left\langle \frac{\partial u_i}{\partial x_\beta} \right\rangle \\ \epsilon_{ij}\left(x_\alpha + \Delta x_\alpha\right) &= \epsilon_{ij}\left(x_\alpha\right) \\ \sigma_{ij}\left(x_\alpha + \Delta x_\alpha\right) &= \sigma_{ij}\left(x_\alpha\right) \end{aligned} \tag{3.3}$$

where u_i, $\left\langle \frac{\partial u_i}{\partial x_\beta} \right\rangle$, and Δx_β, $i, \alpha, \beta = 1, 2, 3$, are the displacements, the volume average displacement gradients, and the vector of periodicity, respectively.

Assuming a periodic array of fully developed ply cracks in off-axis plies, the periodicity in the laminate longitude direction (X_1) is automatically satisfied by the present choice of FE models. However, the periodicity in the laminate width direction is not modeled here because the representative unit cells shown in Figs. 20-21 are not repeatable in the X_2 direction. To avoid errors due to free edges of the unit cells, the width of unit cells is chosen large as compared to the ply thicknesses. The exact application of periodic boundary conditions requires a more sophisticated RVE definition, and can be obtained by using a skewed RVE. A recently submitted work [166] on FE modeling of a skewed RVE with cracks in $+\theta$, and $-\theta$ plies in $[0/\pm\theta_4/0_{1/2}]_s$, and $[0/\pm 45/0]_s$ laminates provides the details this issue. For three damage modes, such as $[0_m/\pm\theta_n/90_r]_s$ considered here, definition of a periodic unit cell is not possible, and some simplification is necessary.

The in-plane material properties in the analysis were obtained from the literature. To obtain the remaining properties for use in the 3-D model, the unidirectional ply is assumed transversely isotropic in the cross-sectional plane.

The mid-plane symmetry of the laminate was accounted for in the FE models.

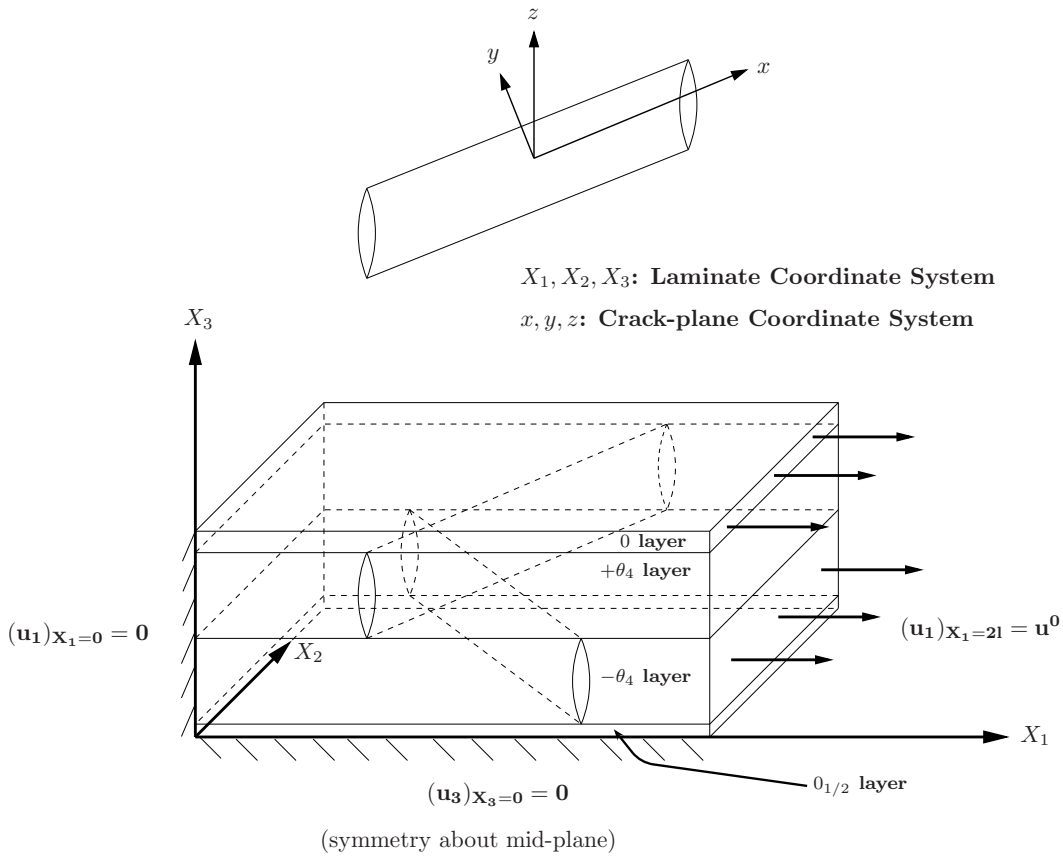

Fig. 20. A representative unit cell for FE analysis of $[0/\pm\theta_4/0_{1/2}]_s$ laminate.

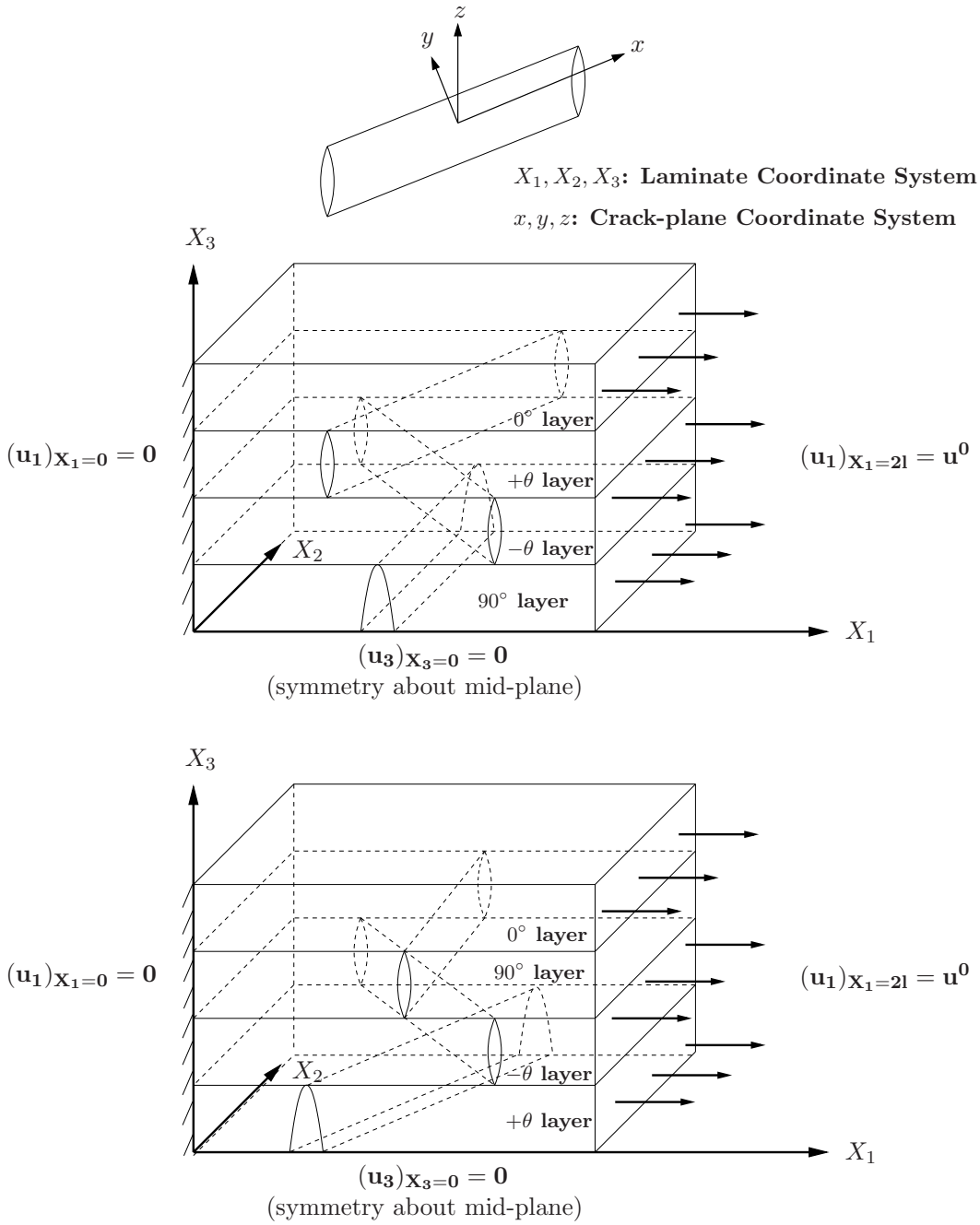

Fig. 21. Representative unit cells for FE analysis of $[0_m/\pm\theta_n/90_r]_s$ and $[0_m/90_r/\mp\theta_n]_s$ laminates.

The matrix cracks were taken to have grown across the entire width of the specimen. ANSYS SOLID45 (eight-noded isoparametric) elements were used. Each FE model contained a large number of elements. Mesh density was varied to arrive at an optimum level of accuracy and complexity of the 3-D FE model. Mapped meshing was utilized to flow the mesh smoothly through the thickness. Aspect ratio of elements near the crack surfaces was kept close to 1.0 for better accuracy. Linear Elastic FE analyses were carried out using ANSYS version 9.0-11.0 at strain levels ranging from 0.1% to 1.0%. Displacement boundary conditions were applied by constraining the left end of the unit cell and providing required displacement at the right end, such that,

$$(u_1)_{X_1=0} = 0; \quad (u_1)_{X_1=2l} = u^0; \quad (u_3)_{X_3=0} = 0 \ \ (symmetry) \tag{3.4}$$

where $\Delta X_1 = 2l$ and u^0 represent the length of unit cell and the applied displacement, respectively, in the laminate longitudinal direction. The ply orientation was modeled using a elemental coordinate transformation.

C. Post-processing

The crack opening displacements are calculated in the lamina coordinate system (x, y, z) by calculating the difference of nodal displacements on the two sides of a crack surface normal to the fiber direction and in the lamina plane, i.e., $\Delta u_y = u_y^+ - u_y^-$, where $+$ and $-$ represent the right and left crack surfaces, respectively. The total relative displacements of the crack surfaces along the laminate longitude was calculated in the laminate global coordinate system $(X_i, i = 1, 2, 3)$, such that, $\Delta u_{X_1} = {u_{X_1}}^+ - {u_{X_1}}^-$. The crack sliding displacement in the lamina coordinate system is then given by $\Delta u_x = \sqrt{(\Delta u_{X_1})^2 - (\Delta u_y)^2}$.

The average COD and CSD are then determined by averaging the surface dis-

placements first along the fiber direction in each cracked ply, then averaging the result across the ply thickness. Thus, they are given as

$$\overline{\Delta u_y} = \frac{1}{t_c}\int_{-t_c/2}^{t_c/2} \Delta u_y(z)\ \mathrm{d}z \tag{3.5}$$

and,

$$\overline{\Delta u_x} = \frac{1}{t_c}\int_{-t_c/2}^{t_c/2} \Delta u_x(z)\ \mathrm{d}z \tag{3.6}$$

where Δu_y, and Δu_x represent the separation of crack planes in the direction normal and parallel to the crack face, respectively.

For the calculations of average stiffness properties at a fixed crack density, the following homogenization relation is utilized:

$$\langle * \rangle = \frac{1}{V_{RVE}}\int_V * \ \mathrm{d}V \tag{3.7}$$

where $\langle * \rangle$ represents the volume average of the variable $*$, and V_{RVE} is the volume of the RVE. Thus, the average longitudinal modulus and the Poisson's ratio of the damaged laminate were obtained using the volume averaging of stresses and strains as given by the following equations

$$E_1 = \frac{\langle \sigma_{11} \rangle}{\langle \epsilon_{11} \rangle} = \frac{\frac{1}{V_{RVE}}\int_V \sigma_{11}\ \mathrm{d}V}{u^0/2l} \tag{3.8}$$

$$\nu_{12} = -\frac{\langle \epsilon_{22} \rangle}{\langle \epsilon_{11} \rangle} = -\frac{\frac{1}{V_{RVE}}\int_V \epsilon_{22}\ \mathrm{d}V}{u^0/2l} \tag{3.9}$$

D. Validation

Since this is possibly the first 3D FE modeling utilized for cracked multidirectional composite laminates, the modeling approach is verified with the published experimental data for both cross-ply and off-axis laminates.

1. Cross-ply Laminates: $[0_m/90_n]_s$

The stiffness degradation in glass/epoxy $[0_m/90_n]_s$ were simulated using the FE modeling approach described above. The models were created to have an equivalent crack density varying from 0.1 to 2.0 cracks/mm, in steps of 0.1 cracks/mm. The variation of the longitudinal modulus and the Poisson's ratio are shown in Fig. 22 for $[0/90_2]_s$ laminate, and in Fig. 23 for $[0_2/90_2]_s$ laminate. The experimental data shown is taken from reference [84]. Clearly the FE predictions are in excellent agreement with the experimental data for both laminate sequences and both for the longitudinal modulus and the Poisson's ratio. It can be observed that the stiffness reductions are of smaller magnitude for $[0_2/90_2]_s$ laminate than $[0/90_2]_s$ laminate. This is due to the higher constraint on the opening of 90° in $[0_2/90_2]_s$ laminate than in the $[0/90_2]_s$ laminate, as the 0° ply is thicker in the former case. Another point to observe is that FE simulations accurately follow the nonlinear shape of the reduction plots. This shows that the interaction between adjacent cracks is being modeled correctly.

2. Off-axis Laminates: $[0/\pm\theta_4/0_{1/2}]_s$

In the above sub-section, we have verified the stiffness degradation modeling using FEM for a cross-ply laminate. For the case of off-axis ply cracking in multidirectional laminates, we considered $[0/\pm\theta_4/0_{1/2}]_s$ glass-epoxy laminates, for which experimental data is reported in [109]. In this case, 3D FE models were constructed for $\theta = 90°, 70°, 55°, 40°$ and 25°, and for varying crack density along X_1 direction. Linear FE analyses using ANSYS 10.0 were conducted for varying crack spacing, $s_\theta = 16, 8, 4, 3, 2, 1.5, 1.25, 1, 0.75, 0.6$ and 0.5 mm. Figs. 24-25 compare FE simulations with the published experimental data [109] for $[0/90_8/0_{1/2}]_s$ and $[0/\pm 70_4/0_{1/2}]_s$ laminate configurations. As can be seen these simulations show excellent agreement

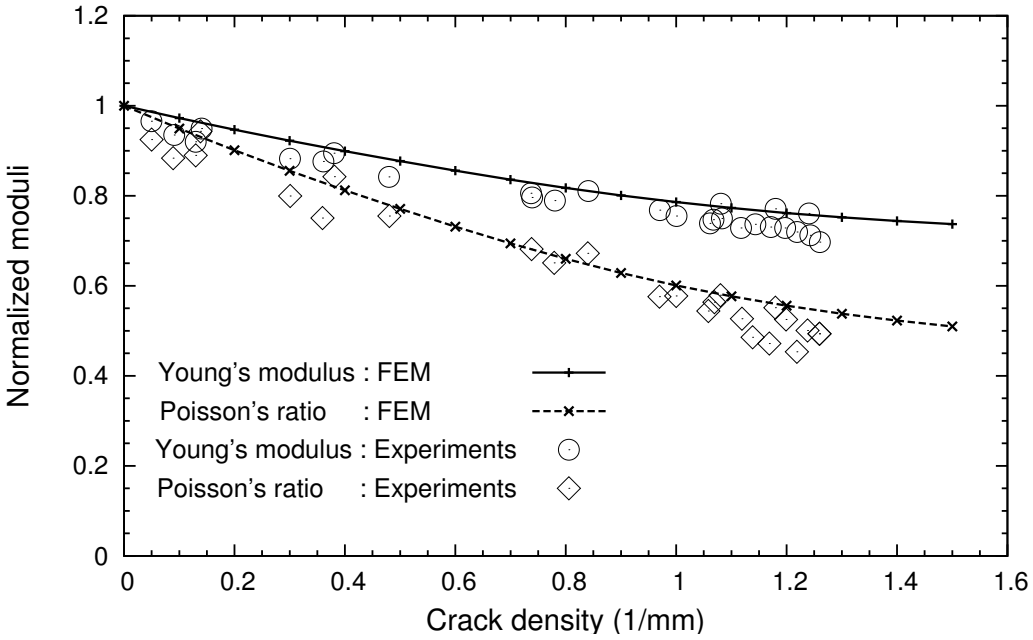

Fig. 22. Comparison of FE simulated stiffness properties for $[0/90_2]_s$ laminates with experiments reported in [84].

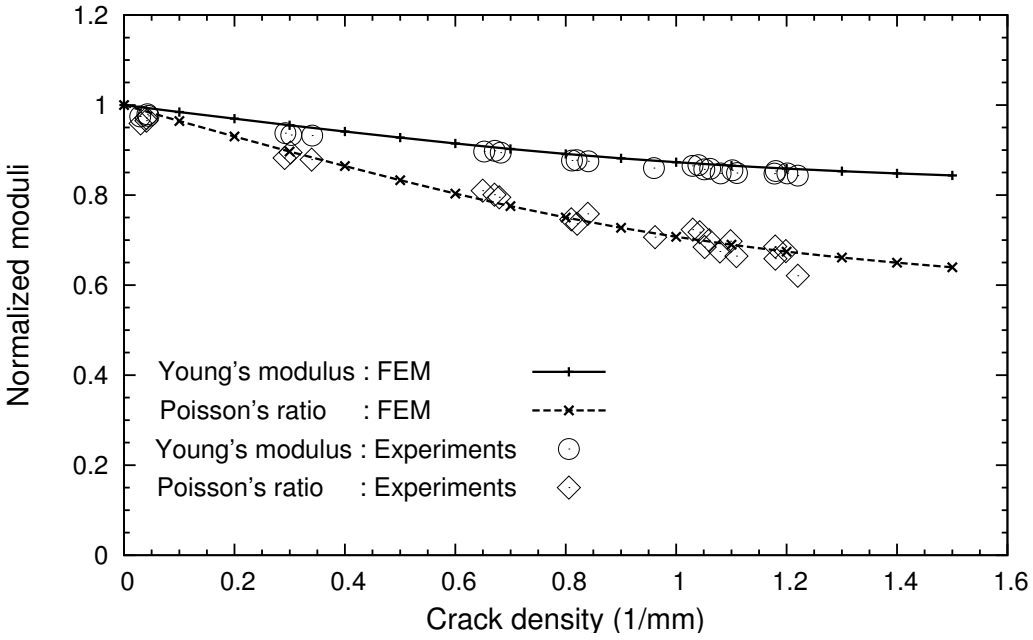

Fig. 23. Comparison of FE simulated stiffness properties for $[0_2/90_2]_s$ laminates with experiments reported in [84].

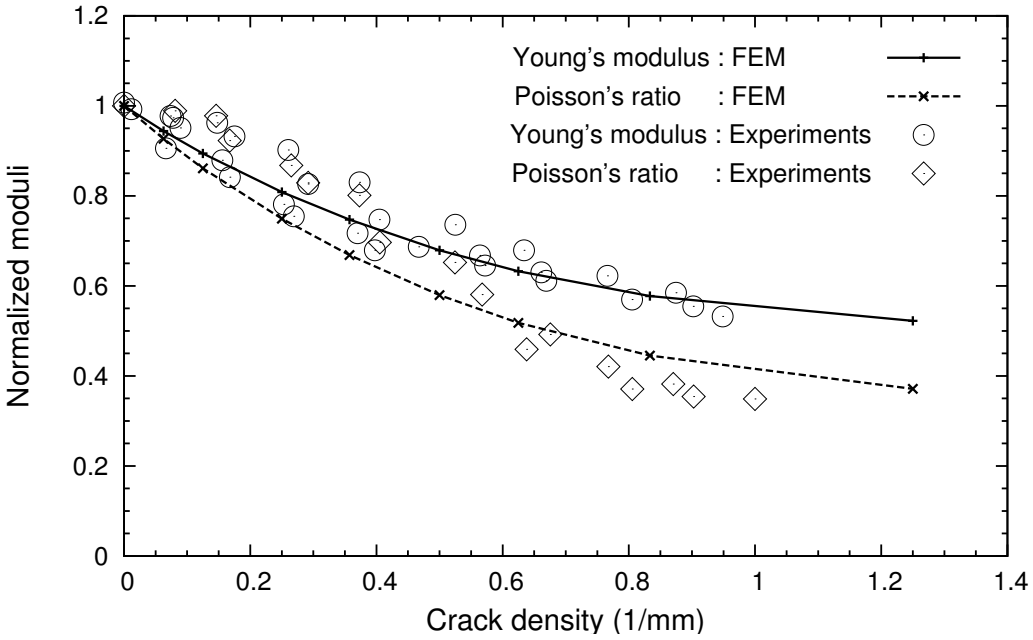

Fig. 24. Comparison of FE simulated stiffness properties for $[0/90_8/0_{1/2}]_s$ laminates with experiments reported in [109].

with the experimental data for $\theta = 90°$, and reasonable agreement for $\theta = 70°$. For $\theta = 70°$, the experimental data for Poisson's ratio shows no change beyond initial cracking. This could be due to average data reported here, the actual experimental measurements showed a large scatter [109]. Also, the experimental measurement of the Poisson's ratio of a cracked laminate is not easy to carry out and may carry some measurement errors.

E. Summary

In this chapter, we described the finite element procedure used in the evaluation of crack surface displacements and stiffness reductions in cracked multidirectional laminates. The strategy for developing three dimensional RVE for damage analysis was described along with the accompanying issues and simplifications. The FE simula-

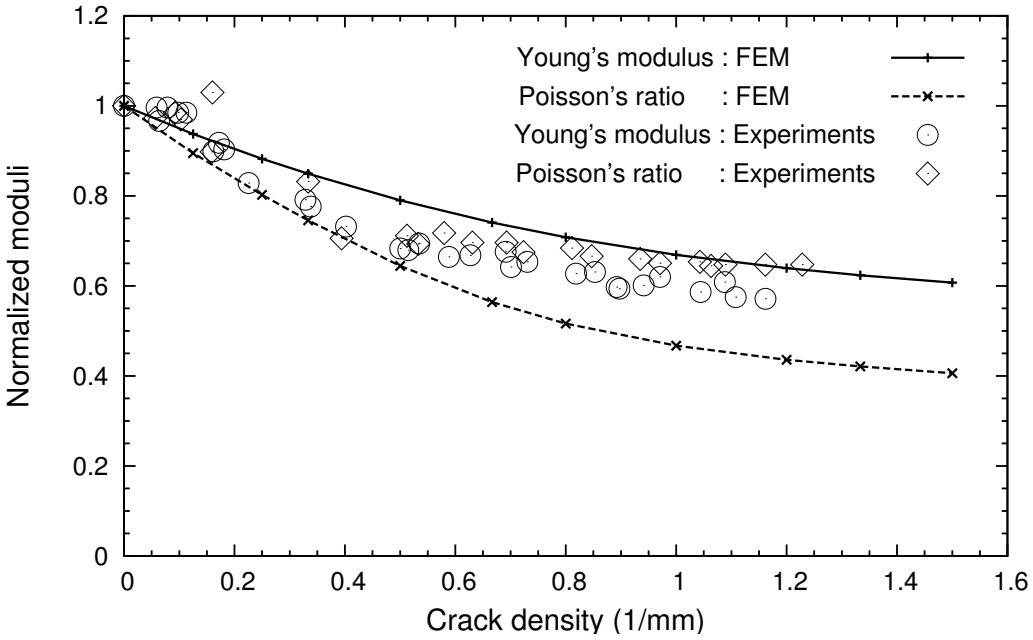

Fig. 25. Comparison of FE simulated stiffness properties for $[0/\pm 70_4/0_{1/2}]_s$ laminates with experiments reported in [109].

tions for stiffness properties were compared with the published experimental data to verify the analysis procedure.

CHAPTER IV

STIFFNESS CHANGES WITH TWO DAMAGE MODES[1]

A. Introduction

In an un-constrained uni-directional composite, such as a ply not bonded to other plies, a uniform tensile stress applied normal to fibers will cause failure from a single crack lying in the matrix between fibers or at the fiber/matrix interface. However, if the composite is constrained, such as a ply within a laminate, then failure does not result from a single crack. Instead, multiple cracks form as the applied load increases. This phenomenon is described as multiple matrix cracking [145]. These matrix cracks usually form first in the ply thickness direction and then grow along fibers spanning the laminate width. Matrix cracks, usually the first mode of damage, are not critical from a final failure point of view but can lead to a significant reduction in individual ply properties as well as in the laminate properties. Modeling of stiffness degradation subsequent to matrix damage has been the topic of extensive research in the recent decades, especially for cross-ply laminates ($[0_m/90_n]_s$). A variety of analytical approaches have been suggested, e.g., ply-discount method, shear lag models [37, 56], variational method [64], self-consistent approximation [77], 3D laminate theory [80] and continuum damage mechanics [88,90]. However, most of the research work is limited to cross-ply laminates, which are easier to analyze but are not used often in practical applications. Analyzing damage in laminates of general layup is quite challenging due to multiplicity of damage modes and the constraints induced on individual ply cracks by the neighboring plies.

---

[1]Reprinted from Int. J. Solids Struct., vol. 45, no. 16, C.V. Singh and R. Talreja, Analysis of multiple off-axis ply cracks in composite laminates, pp. 4574–4589, Copyright (2008), with permission from Elsevier.

Composite laminates with off-axis plies are important for applications where structures undergo loading combinations that necessitate use of multiple fiber orientations to generate required properties. Still, damage in such laminates has not been fully analyzed. Masters and Reifsnider [60] experimentally observed damage development in quasi-isotropic ($[0/\pm 45/90]_s$ and $[0/90/\pm 45]_s$) carbon-epoxy laminates under fatigue loading. Tong et al. [108] conducted experimental investigations of matrix crack growth behavior under quasi-static and fatigue loadings in quasi-isotropic glass-epoxy $[0/90/\mp 45]_s$ laminates and used generalized plane-strain finite element analysis to predict stiffness degradation and ply stress distribution [94]. However, damage in off-axis plies is essentially a 3-D stress analysis problem and a generalized plane strain formulation cannot adequately address it. Other approaches such as equivalent constraint model (ECM), in combination with the first order shear deformation laminated plate theory (FSDT) [113] and with a modified shear lag analysis [116], have also been attempted. Recently, Yokozeki et al. [126, 167, 168] have analyzed laminates with obliquely crossed matrix cracks utilizing a two dimensional shear lag analysis. Considering the complexity of the problem at hand, these works are good starting point but they provide approximate solutions whose accuracy cannot be fully verified as no exact analytical solutions currently exist.

To analyze the deformational response of composite laminates subsequent to matrix cracking, the most direct measure of crack influence over laminate properties is the "coefficient" of crack opening displacement (COD), i.e., average crack surface separation per unit of an applied load quantity. Only a few researchers in the past have focused on surface displacements of ply cracks in an explicit manner. Gudmundson and Ostlund [80] derived analytical expressions for average stiffness properties of cracked symmetric laminates in terms of COD. They assumed that the average COD for matrix cracks in a composite laminate of general layup could be approxi-

mated by the analytical solutions of an array of parallel cracks in an infinite homogeneous medium. However, this completely neglects the constraint effect on COD and evaluating the consequence of such approximation is therefore necessary either by experimental or computational means. To study COD, Varna et al. [162] developed a device to experimentally measure COD in cross-ply laminates. A separate study [163] verified the accuracy of different analytical models for estimating COD in cross-ply laminates. Joffe et al. [104] later used a FE plane stress model to evaluate the average COD dependence on the crack spacing and on the constraint of adjacent sub-laminates.

The classical CDM approach is quite efficient in predicting stiffness degradation if certain phenomenological constants can be evaluated [23]. An experimental evaluation of the constants may not be easy in all cases and to alleviate this limitation, Talreja [142] later proposed a synergistic damage mechanics (SDM) approach and illustrated it to describe the deformational response of $[\pm\theta/90_2]_s$ laminates. This approach combines micromechanics and continuum damage mechanics judiciously to produce a versatile methodology. The micromechanical damage mechanics, or briefly, micro-damage mechanics (MDM) performs analysis of local stress-redistributions due to cracking, incorporating the micro-level geometry. On the other hand, CDM, as formulated by [88, 143], allows a specific output of MDM (COD) to be used within a representative volume element (RVE), i.e., at meso level. In this way, the synergism between micromechanics and CDM effectively treats the multi-scale nature of damage. More recently, the SDM approach has also been extended to analyze viscoelastic behavior of composites with damage [144].

In the present study, we present a synergistic methodology to deal with matrix cracks in plies with multiple off-axis orientations. The continuum damage mechanics formulation of particular relevance to this work is the one presented by [89, 143],

wherein the damage state in the laminate is described by second order tensors. In the present scenario, the damage state can be suitably represented by damage mode tensors regarding ply cracking in each orientation as an individual damage mode. The constraint effects on the cracked plies imposed by the surrounding plies are evaluated in terms of the COD changes in off-axis plies. CODs are determined using 3-D FE analysis and then subsequently used in the CDM model through the constraint parameter to predict the stiffness properties of the degraded laminate. The CODs are evaluated at different applied strains and the variation in these is checked against the experimental values at 0.4% and 0.6% strains. The strength of SDM approach lies in accurate COD calculation using computational micromechanics and an accurate damage description using CDM. Thus, SDM promises to be a pragmatic solution to the damage analysis problem for laminates with complex layups for which analytical results are difficult to derive. In order to make the SDM approach more versatile, detailed parametric studies are conducted to study the variables which may affect the constraint of un-cracked plies over cracked plies. Using these parametric studies, a master equation for CODs in terms of geometry and material variables is proposed. Also, the profile of average crack surface displacements through thickness of the cracked ply is studied for different laminate configurations. Finally, stiffness moduli for $[0_m/\pm\theta_n/0_{m/2}]_s$ laminates are predicted for different stiffness and thicknesses of cracked and supporting plies.

B. Damage Characterization and Elastic Response for Two Damage Modes

Consider a symmetric laminate with a general layup (see Fig. 9 on page 24), e.g. $[0_m/\pm\theta_n/\phi_p]_s$, loaded in axial tension, with ϕ restricted to angles which do not cause cracking. The loading will produce an in-plane stress state in each off-axis ply

consisting of normal stresses along and perpendicular to fibers in that ply and a shear stress in the plane of the ply. Depending on the values of θ, ϕ and ply properties, the stress perpendicular to the fibers could be tensile or compressive. Thus, on loading, an off-axis ply may or may not develop intralaminar cracks. When $\theta = 90°$ the matrix will undergo multiple cracking in the transverse plies. For other cases of off-axis ply orientations, multiple cracking is typically observed to occur for angles from 50° to 90°. However, it has been observed that even in cases where these cracks do not initiate in the off-axis plies, the laminate moduli change with the applied load due to shear stress induced damage within the plies [109].

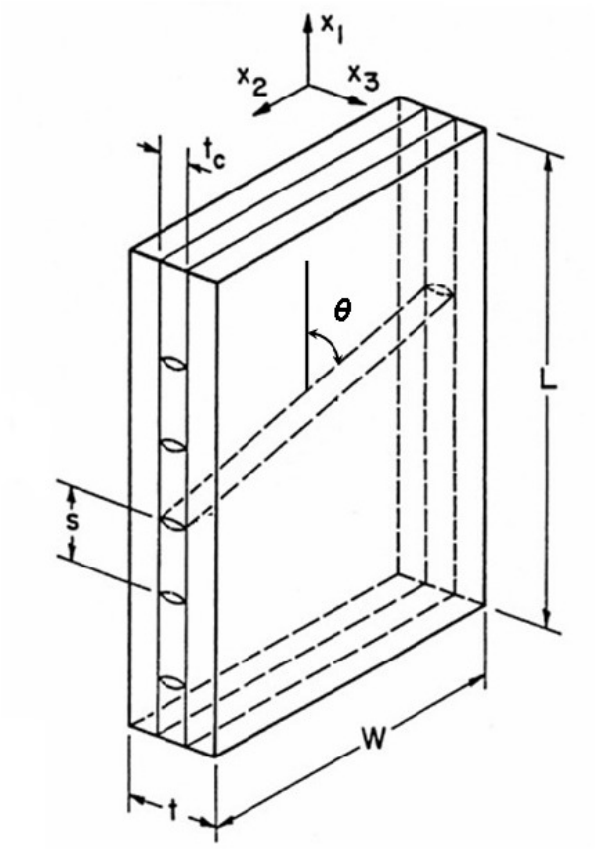

Fig. 26. A representative volume element (RVE) illustrating intralaminar multiple cracking in a general off-axis ply of a composite laminate.

When cracks are formed, the opening and sliding of crack surfaces alter the stress and strain states in the cracked plies, thereby changing the global deformational response of the laminate. The damage state in the laminate representative volume element (RVE) can be described suitably by a set of second order tensors [89, 143]. Fig. 26 shows an RVE of a general laminate with an array of transverse cracks in an off-axis ply. For simplicity in presentation cracks are shown in only one off-axis ply. However, it is understood that transverse cracks may develop in multiple off-axis plies of a general laminate. Assuming these matrix cracks to be fully grown parallel to the fiber direction in each lamina, the family of cracks in a given lamina can be represented by a separate damage modes. In this way a general laminate with cracks in plies of multiple orientations can be characterized suitably using multiple damage modes. At present, it is assumed that the interactions between different damage modes are negligible.

For $[0_m/\pm\theta_n/\phi_p]_s$ laminates with cracks in $+\theta_n$ and $-\theta_n$ plies, the damage state can be represented by two damage mode tensors, one each for matrix cracking in $+\theta_n$ plies and $-\theta_n$ plies. Assuming that there are N damage entities of a given damage mode α in the RVE, the damage tensor is defined as [87, 89]

$$D_{ij}^{(\alpha)} = \frac{1}{V}\sum_{k_\alpha}\left[\oint_S a_i n_j \, \mathrm{d}S\right]_{k_\alpha} \tag{4.1}$$

where $n_i = (\sin\theta, \cos\theta, 0)$ are components of the unit vector normal to a matrix crack plane in the off-axis ply of orientation θ with respect to laminate longitudinal axis, V is volume of RVE and $k_\alpha = 1, 2, ..., N$. The tensor D_{ij} is an asymmetric tensor in general. However, we can represent the vector a_i along the normal and tangential directions at any point on the surface of the damage entity and write

$$d_{ij} = d_{ij}^1 + d_{ij}^2 \tag{4.2}$$

where

$$d_{ij}^{1} = \oint_S a n_i n_j \, \mathrm{d}S \tag{4.3}$$

and

$$d_{ij}^{1} = \oint_S b m_i n_j \, \mathrm{d}S \tag{4.4}$$

Here a and b are the magnitudes of the normal and tangential projections of vector a_i, and vectors n_i, and m_j are unit normal and tangential vectors, respectively. Thus the damage damage mode tensor D_{ij} can be written as

$$D_{ij}^{(\alpha)} = D_{ij}^{1(\alpha)} + D_{ij}^{2(\alpha)} \tag{4.5}$$

where

$$D_{ij}^{1(\alpha)} = \frac{1}{V} \sum_{k_\alpha} \left(d_{ij}^{1}\right)_{k_\alpha} \tag{4.6}$$

and

$$D_{ij}^{2(\alpha)} = \frac{1}{V} \sum_{k_\alpha} \left(d_{ij}^{2}\right)_{k_\alpha} \tag{4.7}$$

Physically, the damage tensor $D_{ij}^{1(\alpha)}$ represents the effects of crack opening on the surrounding medium whereas tensor $D_{ij}^{2(\alpha)}$ represents the effects of sliding between the two crack faces. For intralaminar cracks constrained by stiff plies, the sliding between the crack faces can be negligible, and hence we assume $D_{ij}^{2(\alpha)} \equiv 0$. This implies $D_{ij}^{(\alpha)} = D_{ij}^{1(\alpha)}$ which is a symmetric tensor. For intralaminar cracking in an off-axis ply, the volume of the RVE V, the surface area of a crack, S, and the influence vector magnitude, a, are specified as

$$V = L.W.t \tag{4.8}$$

$$S = \frac{t_c.W}{|\sin\theta|} \tag{4.9}$$

$$a = \kappa.t_c \tag{4.10}$$

where κ, called the constraint parameter, is an unspecified constant of (assumed) proportionality between a and the crack size t_c (also cracked-ply thickness), L is the RVE length, and W is the laminate and width (Fig. 26). Assuming a to be constant over the crack surface, $D_{ij}^{(\alpha)}$ for the case of intralaminar cracking is given by

$$D_{ij}^{(\alpha)} = \frac{\kappa t_c^2}{s_\theta t \sin\theta} n_i n_j \tag{4.11}$$

where $s_\theta = L/N$ is the axial crack spacing in the cracked ply.

Now we derive the stiffness-damage relations for multiple modes of damage. With the damage mode tensors $D_{ij}^{(\alpha)}, \alpha = 1, 2, 3, ..,$ taken as internal variables, the Helmholtz free energy is given by

$$\rho\psi = \rho\psi\left(\epsilon_{ij}, D_{ij}^{(\alpha)}\right) \tag{4.12}$$

where ψ is the specific Helmholtz energy, ρ is the mass density, and ϵ_{ij} is the strain tensor. Using the second law of thermodynamics in the form of the Clausius-Duhem inequality, stress response for a given state of damage is given by [87]

$$\sigma_{ij} = \rho\frac{\partial\psi}{\partial\epsilon_{ij}} \tag{4.13}$$

Utilizing the linear elastic stress-strain relation $\sigma_{ij} = C_{ijkl}\epsilon_{ij}$ for the composite material, its stiffness tensor C_{ijkl} is given by

$$C_{ijkl} = \rho\frac{\partial^2\psi}{\partial\epsilon_{ij}\partial\epsilon_{kl}} \tag{4.14}$$

Composite laminates used in practice are usually symmetric and balanced about the mid-plane. Such stacking introduces an orthotropic symmetry of the laminate in its virgin state. To incorporate this material symmetry, the integrity bases [159,160] are used to express $\rho\psi$ as a polynomial function. Here, we are interested in describing damage in $[0_m/\pm\theta_n/0_{m/2}]$ laminates with the following two damage modes

$$\text{Damage Mode 1} \Rightarrow \alpha = 1, \text{ cracks in } +\theta \text{ plies}$$
$$\text{Damage Mode 2} \Rightarrow \alpha = 2, \text{ cracks in } -\theta \text{ plies}$$

The irreducible integrity bases for a scalar polynomial function of symmetric second rank tensors (strain and two damage mode tensors) for this case ($\alpha = 1, 2$) are given by [159, 160]

$$\begin{aligned}
&\epsilon_{11}, \epsilon_{22}, \epsilon_{33}, \epsilon_{23}^2, \epsilon_{31}^2, \epsilon_{12}^2, \epsilon_{23}\epsilon_{31}\epsilon_{12},\\
&D_{11}^{(1)}, D_{22}^{(1)}, D_{33}^{(1)}, \left(D_{23}^{(1)}\right)^2, \left(D_{31}^{(1)}\right)^2, \left(D_{12}^{(1)}\right)^2, D_{23}^{(1)} D_{31}^{(1)} D_{12}^{(1)},\\
&D_{11}^{(2)}, D_{22}^{(2)}, D_{33}^{(2)}, \left(D_{23}^{(2)}\right)^2, \left(D_{31}^{(2)}\right)^2, \left(D_{12}^{(2)}\right)^2, D_{23}^{(2)} D_{31}^{(2)} D_{12}^{(2)},\\
&\epsilon_{23} D_{23}^{(1)}, \epsilon_{31} D_{31}^{(1)}, \epsilon_{12} D_{12}^{(1)}, \epsilon_{23} D_{23}^{(2)}, \epsilon_{31} D_{31}^{(2)}, \epsilon_{12} D_{12}^{(2)},\\
&\epsilon_{31}\epsilon_{12} D_{23}^{(1)}, \epsilon_{12}\epsilon_{23} D_{31}^{(1)}, \epsilon_{23}\epsilon_{31} D_{12}^{(1)}, \epsilon_{31}\epsilon_{12} D_{23}^{(2)}, \epsilon_{12}\epsilon_{23} D_{31}^{(2)}, \epsilon_{23}\epsilon_{31} D_{12}^{(2)},\\
&\epsilon_{23} D_{31}^{(1)} D_{12}^{(1)}, \epsilon_{31} D_{12}^{(1)} D_{23}^{(1)}, \epsilon_{12} D_{23}^{(1)} D_{31}^{(1)}, \epsilon_{23} D_{31}^{(2)} D_{12}^{(2)}, \epsilon_{31} D_{12}^{(2)} D_{23}^{(2)}, \epsilon_{12} D_{23}^{(2)} D_{31}^{(2)},\\
&\epsilon_{23} D_{31}^{(1)} D_{12}^{(2)}, \epsilon_{31} D_{12}^{(1)} D_{23}^{(2)}, \epsilon_{12} D_{23}^{(1)} D_{31}^{(2)}, \epsilon_{23} D_{31}^{(2)} D_{12}^{(1)}, \epsilon_{31} D_{12}^{(2)} D_{23}^{(1)}, \epsilon_{12} D_{23}^{(2)} D_{31}^{(1)}
\end{aligned} \tag{4.15}$$

If we consider a thin laminate loaded in its plane, this set of integrity bases can be further reduced by considering only the in-plane strain and damage tensor components. Thus, the remaining integrity bases in the Voigt notation, for the case with two damage modes, are given by

$$\begin{aligned}
&\epsilon_1, \epsilon_2, \epsilon_6^2\\
&D_1^{(1)}, D_2^{(1)}, \left(D_6^{(1)}\right)^2, D_1^{(2)}, D_2^{(2)}, \left(D_6^{(2)}\right)^2\\
&\epsilon_6 D_6^{(1)}, \epsilon_6 D_6^{(2)}
\end{aligned} \tag{4.16}$$

where $\epsilon_1 \equiv \epsilon_{11}, \epsilon_2 \equiv \epsilon_{22}, \epsilon_6 \equiv \epsilon_{12}, D_1 \equiv D_{11}, D_2 \equiv D_{22}, D_6 \equiv D_{12}$. Using these integrity bases, the most general polynomial form for $\rho\psi$, restricted to second order terms in the strain components (small strains) and first order terms in damage tensor

components (small volume fraction of damage entities in the RVE), is given by

$$\begin{aligned}\rho\psi = P_0 \;&+\; c_1\epsilon_1^2 + c_2\epsilon_2^2 + c_3\epsilon_6^2 + c_4\epsilon_1\epsilon_2 \\ &+\; \epsilon_1^2\left\{c_5 D_1^{(1)} + c_6 D_2^{(1)} + c_7 D_1^{(2)} + c_8 D_2^{(2)}\right\} \\ &+\; \epsilon_2^2\left\{c_9 D_1^{(1)} + c_{10} D_2^{(1)} + c_{11} D_1^{(2)} + c_{12} D_2^{(2)}\right\} \\ &+\; \epsilon_6^2\left\{c_{13} D_1^{(1)} + c_{14} D_2^{(1)} + c_{15} D_1^{(2)} + c_{16} D_2^{(2)}\right\} \\ &+\; \epsilon_1\epsilon_2\left\{c_{17} D_1^{(1)} + c_{18} D_2^{(1)} + c_{19} D_1^{(2)} + c_{20} D_2^{(2)}\right\} \\ &+\; \epsilon_1\epsilon_6\left\{c_{21} D_6^{(1)} + c_{22} D_6^{(2)}\right\} + \epsilon_2\epsilon_6\left\{c_{23} D_6^{(1)} + c_{24} D_6^{(2)}\right\} \\ &+\; P_1(\epsilon_p, D_q^{(1)}) + P_2(\epsilon_p, D_q^{(2)}) + P_3(D_q^{(1)}) + P_4(D_q^{(2)}) \end{aligned} \tag{4.17}$$

where P_0 and c_i are material constants, P_1 and P_2 are linear functions of strain and damage tensor components, and P_3 and P_4 are linear functions only of the damage tensor components. Setting $\rho\psi = 0$ for unstrained and undamaged material, we have $P_0 = 0$; and assuming the unstrained material of any damaged state to be stress-free, we get $P_1 = P_2 = 0$ on using Eq. (4.13). Considering the virgin material to be orthotropic and proceeding in a similar manner as given in [142], we obtain following relations for stiffness matrix of the damaged laminate

$$C_{pq} = C_{pq}^0 + C_{pq}^{(1)} + C_{pq}^{(2)} \tag{4.18}$$

where $p, q = 1, 2, 6$, C_{pq}^0 is the stiffness coefficient matrix of the virgin laminate and the changes in stiffness brought about by the individual damage modes are represented

by $C_{pq}^{(1)}$ and $C_{pq}^{(2)}$. The three matrices are given by

$$C_{pq}^{0} = \begin{bmatrix} 2c_1 & c_4 & 0 \\ c_4 & 2c_2 & 0 \\ 0 & 0 & 2c_3 \end{bmatrix} = \begin{bmatrix} \frac{E_1^0}{1-\nu_{12}^0\nu_{21}^0} & \frac{\nu_{12}^0 E_2^0}{1-\nu_{12}^0\nu_{21}^0} & 0 \\ \frac{\nu_{12}^0 E_2^0}{1-\nu_{12}^0\nu_{21}^0} & \frac{E_2^0}{1-\nu_{12}^0\nu_{21}^0} & 0 \\ 0 & 0 & G_{12}^0 \end{bmatrix} \tag{4.19}$$

$$C_{pq}^{(1)} = \begin{bmatrix} 2c_5 D_1^{(1)} + 2c_6 D_2^{(1)} & c_{17} D_1^{(1)} + c_{18} D_2^{(1)} & c_{21} D_6^{(1)} \\ & 2c_9 D_1^{(1)} + 2c_{10} D_2^{(1)} & c_{23} D_6^{(1)} \\ Symm & & 2c_{13} D_1^{(1)} + 2c_{14} D_2^{(1)} \end{bmatrix} \tag{4.20}$$

$$C_{pq}^{(2)} = \begin{bmatrix} 2c_7 D_1^{(2)} + 2c_8 D_2^{(2)} & c_{19} D_1^{(2)} + c_{20} D_2^{(2)} & c_{22} D_6^{(2)} \\ & 2c_{11} D_1^{(2)} + 2c_{12} D_2^{(2)} & c_{24} D_6^{(2)} \\ Symm & & 2c_{15} D_1^{(2)} + 2c_{16} D_2^{(2)} \end{bmatrix} \tag{4.21}$$

where E_1^0, E_2^0, ν_{12}^0 and ν_{21}^0 are longitudinal modulus, transverse modulus, and major and minor Poisson's ratios, respectively, for the virgin laminate. Since we are dealing here with off-axis ply cracking, it is more convenient to rewrite the damage mode tensor defined in Eq. (4.11) in terms of normal crack spacing, $s_n^\theta = s_\theta \sin\theta$, where s_θ is the crack spacing in the axial direction (see Fig. 27) for the ply of orientation θ. Accordingly, the damage tensor is given by

$$D_{ij}^{(\alpha)} = \frac{\kappa t_c^2}{s_n^\theta t} n_i n_j \tag{4.22}$$

With reference to Fig. 27(b) where the orientations of the two damage modes are shown and using Eq. (4.11), the damage tensor elements for this scenario are given by

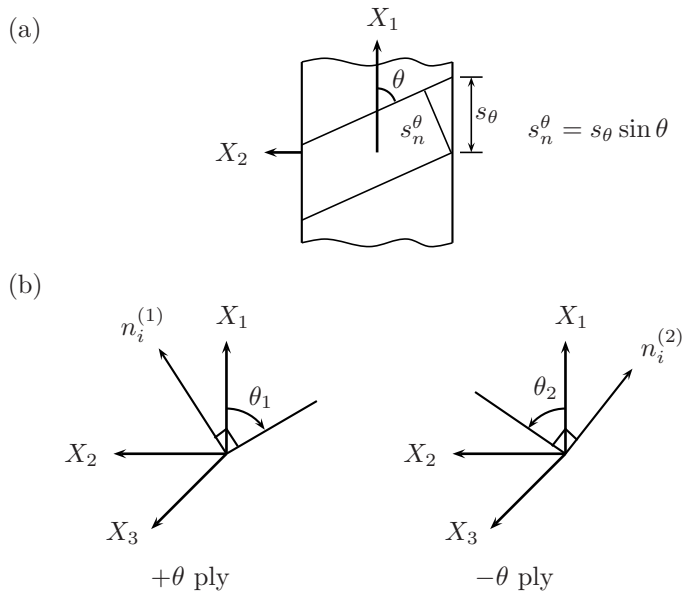

Fig. 27. Characterization of damage in $\pm\theta$ off-axis plies: (a) normal crack spacing s_n^θ, and axial crack spacing s_θ in a cracked ply, and (b) directions of normal vectors for cracks in $+\theta$ and -θ plies, respectively.

$\alpha = 1$: $n_i^{(1)} = (\sin\theta, \cos\theta, 0)$

$$D_1^{(1)} = \frac{\kappa^{\theta^+} t_c^2}{s_n^{\theta^+} t} \sin^2\theta; \quad D_2^{(1)} = \frac{\kappa^{\theta^+} t_c^2}{s_n^{\theta^+} t} \cos^2\theta; \quad D_6^{(1)} = \frac{\kappa^{\theta^+} t_c^2}{s_n^{\theta^+} t} \sin\theta\cos\theta \tag{4.23}$$

$\alpha = 2$: $n_i^{(2)} = (\sin\theta, -\cos\theta, 0)$

$$D_1^{(2)} = \frac{\kappa^{\theta^-} t_c^2}{s_n^{\theta^-} t} \sin\theta; \quad D_2^{(2)} = \frac{\kappa^{\theta^-} t_c^2}{s_n^{\theta^-} t} \cos^2\theta; \quad D_6^{(2)} = -\frac{\kappa^{\theta^-} t_c^2}{s_n^{\theta^-} t} \sin\theta\cos\theta \tag{4.24}$$

where the superscripts θ^+ and θ^- indicate variables for $+\theta$ and $-\theta$ plies, respectively. We now make an assumption that will be evaluated in the main text of the paper: the damage in $+\theta$-plies and $-\theta$-plies occurs at the same intensity of damage and it has the same effect on the laminate behavior. Thus,

$$\kappa^{\theta^+} = \kappa^{\theta^-} = \kappa_\theta, \qquad s_n^{\theta^+} = s_n^{\theta^-} = s_n^\theta \tag{4.25}$$

With this assumption it follows that the laminate will retain its orthotropic symmetry,

implying that the normal stress to shear stress coupling vanishes. Thus, from (4.23)-(4.25) and using (4.18), (4.20) and (4.21), we get

$$\begin{aligned}
C_{11}^{(1)} + C_{11}^{(2)} &= 2\tfrac{\kappa_\theta t_c^2}{s_n^\theta t}\left[(c_5 + c_7)\sin^2\theta + (c_6 + c_8)\cos^2\theta\right] \\
C_{22}^{(1)} + C_{22}^{(2)} &= 2\tfrac{\kappa_\theta t_c^2}{s_n^\theta t}\left[(c_9 + c_{11})\sin\theta + (c_{10} + c_{12})\cos^2\theta\right] \\
C_{66}^{(1)} + C_{66}^{(2)} &= 2\tfrac{\kappa_\theta t_c^2}{s_n^\theta t}\left[(c_{13} + c_{15})\sin^2\theta + (c_{14} + c_{16})\cos^2\theta\right] \\
C_{12}^{(1)} + C_{12}^{(2)} &= \tfrac{\kappa_\theta t_c^2}{s_n^\theta t}\left[(c_{17} + c_{19})\sin^2\theta + (c_{18} + c_{20})\cos^2\theta\right] \\
C_{16}^{(1)} + C_{16}^{(2)} &= \tfrac{\kappa_\theta t_c^2}{s_n^\theta t}\sin\theta\cos\theta\left[-c_{21} + c_{22}\right] = 0 \\
C_{26}^{(1)} + C_{26}^{(2)} &= \tfrac{\kappa_\theta t_c^2}{s_n^\theta t}\sin\theta\cos\theta\left[-c_{23} + c_{24}\right] = 0
\end{aligned} \tag{4.26}$$

Finally,

$$C_{pq}^{(1)} + C_{pq}^{(2)} = \begin{bmatrix} 2a_1D_1 + 2b_1D_2 & a_4D_1 + b_4D_2 & 0 \\ a_4D_1 + b_4D_2 & 2a_2D_1 + 2b_2D_2 & 0 \\ 0 & 0 & 2a_3D_1 + 2b_3D_2 \end{bmatrix} \tag{4.27}$$

where the superscripts for denoting damage mode have been dropped for convenience, and a_i and b_i, $i = 1, 2, 3, 4$ are the two sets of four material constants, given by

$$\begin{aligned}
&a_1 = c_5 + c_7; \quad a_2 = c_9 + c_{11}; \quad a_3 = c_{13} + c_{15}; \quad a_4 = c_{17} + c_{19} \\
&b_1 = c_6 + c_8; \quad b_2 = c_{10} + c_{12}; \quad b_3 = c_{14} + c_{16}; \quad b_4 = c_{18} + c_{20}
\end{aligned} \tag{4.28}$$

Denote

$$\begin{aligned}
a_1(\theta) &= a_1\sin^2\theta + b_1\cos^2\theta \\
a_2(\theta) &= a_2\sin^2\theta + b_2\cos^2\theta \\
a_3(\theta) &= a_3\sin^2\theta + b_3\cos^2\theta \\
a_4(\theta) &= a_4\sin^2\theta + b_4\cos^2\theta
\end{aligned} \tag{4.29}$$

Then,

$$C_{pq}^{(1)} + C_{pq}^{(2)} = D_\theta \begin{bmatrix} 2a_1(\theta) & a_4(\theta) & 0 \\ & 2a_2(\theta) & 0 \\ Symm & & 2a_3(\theta) \end{bmatrix} \tag{4.30}$$

where

$$D_\theta = \frac{\kappa_\theta t_c^2}{s_n^\theta t} \tag{4.31}$$

Rewriting Eq. (4.29), as

$$a_i(\theta) = a_i \sin^2\theta + b_i \cos^2\theta = a_i \sin^2\theta \left(1 + \frac{b_i}{a_i}\cot^2\theta\right) \tag{4.32}$$

We now consider the case when $a_i \geq b_i$. Then,

$$\frac{b_i}{a_i}\cot^2\theta \leq 1 \quad \text{for} \quad \frac{\pi}{4} \leq \theta \leq \frac{\pi}{2} \tag{4.33}$$

Also, it can be expected that

$$\begin{aligned} \frac{b_i}{a_i}\cot^2\theta << 1 \qquad & \text{for} \quad \frac{\pi}{3} \leq \theta \leq \frac{\pi}{2} \\ i.e., \qquad a_i(\theta) \approx a_i \qquad & \text{for} \quad \frac{\pi}{3} \leq \theta \leq \frac{\pi}{2} \end{aligned} \tag{4.34}$$

Thus, finally the elastic stiffness tensor of the damaged laminate for in-plane response can be expressed as

$$C_{pq} = \begin{bmatrix} \frac{E_1^0}{1-\nu_{12}^0\nu_{21}^0} & \frac{\nu_{12}^0 E_2^0}{1-\nu_{12}^0\nu_{21}^0} & 0 \\ \frac{\nu_{12}^0 E_2^0}{1-\nu_{12}^0\nu_{21}^0} & \frac{E_2^0}{1-\nu_{12}^0\nu_{21}^0} & 0 \\ 0 & 0 & G_{12}^0 \end{bmatrix} + \frac{\kappa_\theta t_c^2}{st} sin\theta \begin{bmatrix} 2a_1 & a_4 & 0 \\ & 2a_2 & 0 \\ Symm & & 2a_3 \end{bmatrix} \tag{4.35}$$

In equation (4.35), κ_θ is the constraint parameter and $a_i(\theta)$, i=1,2,3,4 are phenomenological constants for ply of orientation θ. From this equation it is clear that the two symmetric damage modes ($+\theta$ and $-\theta$ cracking) effectively act as a single damage mode. The engineering moduli for the damaged laminate can now be derived from

the following relationships:

$$E_1 = \frac{C_{11}C_{22} - C_{12}^2}{C_{22}}; \;\; E_2 = \frac{C_{11}C_{22} - C_{12}^2}{C_{11}}; \;\; \nu_{12} = \frac{C_{12}}{C_{22}}; \;\; G_{12} = C_{66} \tag{4.36}$$

Thus, using equations (4.35)-(4.36), we get

$$E_1(\theta) = \frac{E_1^0}{1-\nu_{12}^0\nu_{21}^0} + 2\frac{\kappa_\theta t_c^2 sin\theta}{st}a_1(\theta) - \frac{\left[\frac{\nu_{12}^0 E_2^0}{1-\nu_{12}^0\nu_{21}^0} + \frac{\kappa_\theta t_c^2 sin\theta}{st}a_4(\theta)\right]^2}{\frac{E_2^0}{1-\nu_{12}^0\nu_{21}^0} + 2\frac{\kappa_\theta t_c^2 sin\theta}{st}a_2(\theta)} \tag{4.37}$$

$$E_2(\theta) = \frac{E_2^0}{1-\nu_{12}^0\nu_{21}^0} + 2\frac{\kappa_\theta t_c^2 sin\theta}{st}a_2(\theta) - \frac{\left[\frac{\nu_{12}^0 E_2^0}{1-\nu_{12}^0\nu_{21}^0} + \frac{\kappa_\theta t_c^2 sin\theta}{st}a_4(\theta)\right]^2}{\frac{E_1^0}{1-\nu_{12}^0\nu_{21}^0} + 2\frac{\kappa_\theta t_c^2 sin\theta}{st}a_1(\theta)} \tag{4.38}$$

$$\nu_{12}(\theta) = \frac{\frac{\nu_{12}^0 E_2^0}{1-\nu_{12}^0\nu_{21}^0} + \frac{\kappa_\theta t_c^2 sin\theta}{st}a_4(\theta)}{\frac{E_2^0}{1-\nu_{12}^0\nu_{21}^0} + 2\frac{\kappa_\theta t_c^2 sin\theta}{st}a_2(\theta)} \tag{4.39}$$

$$\tag{4.40}$$

$$G_{12}(\theta) = G_{12}^0 + 2\frac{\kappa_\theta t_c^2 sin\theta}{st}a_3(\theta) \tag{4.41}$$

As seen from equations (4.37)-(4.41), the shear modulus is uncoupled from the other three moduli and thus can be treated independently. The three material constants $\kappa_\theta a_1, \kappa_\theta a_2$ and $\kappa_\theta a_4$ are present in the first three coupled equations and can be evaluated for a selected reference laminate, e.g. a cross ply laminate ($\theta = 90°$), by using data generated either experimentally or by an analytical or a computational model. The remaining constant $\kappa_\theta a_3$ associated with the shear modulus change can in principle also be obtained similarly. However, experimental data to determine shear modulus are usually difficult to obtain. The analytical or computational determination of the shear modulus for a cracked cross ply laminate would require setting up

a boundary value problem different from that needed to determine the other moduli. We shall not treat the shear modulus here since the constraint parameter κ_θ can as well be studied by considering the other three elastic moduli.

The stiffness change in a given laminate subsequent to damage depends on how much the matrix cracks "open up" in response to the imposed loading. This opening is affected by the neighboring plies as they apply constraint on the deformation of the cracked plies. Consequently, the stiffness change in a given laminate can be expressed as a function of the constraint effect measured in an appropriate way. Here a reference laminate belonging to the class of laminates considered is selected and the relative constraint effect in the other laminates is expressed with respect to this laminate. The stiffness change as a function of crack density in the reference laminate ($\theta = 90^\circ$) is determined either from experiments or from numerical simulations (FE or micromechanics). Based on notions of fracture mechanics, the relative constraint effect is taken as the ratio of the COD in the off-axis ply to that of the same-sized transverse crack in the reference laminate.

For laminates of the $[0_m/\pm\theta_n/0_{m/2}]_s$ configurations, the material constants a_i are assumed to remain unaffected by the angle θ for a given ply material. From experimental observations on carbon/epoxy [142] and glass/epoxy [161] laminates, this assumption has been found to hold true. This is supposedly because the damage-associated constants are primarily determined by the constituent ply properties and are only weakly dependent on ply orientation. Of course, the influence of the ply orientation on the constraint imposed by surrounding plies over damaged plies is important and is suitably carried by the 'constraint parameter' through changes in COD. The procedure to evaluate a_1, a_2, a_4 and κ_θ will now be described. Using equations (4.37)-(4.41) with $\theta = 90$ and $s = s_0$; we obtain

$$\begin{bmatrix} \frac{E_1^0}{1-\nu_{12}^0\nu_{21}^0} & \frac{\nu_{12}^0 E_2^0}{1-\nu_{12}^0\nu_{21}^0} & 0 \\ & \frac{E_2^0}{1-\nu_{12}^0\nu_{21}^0} & 0 \\ Symm & & G_{12}^0 \end{bmatrix} + \frac{\kappa_{90} t_c^2}{s_0 t} \begin{bmatrix} 2a_1 & a_4 & 0 \\ & 2a_2 & 0 \\ Symm & & 2a_3 \end{bmatrix} = \begin{bmatrix} \frac{E_1}{1-\nu_{12}\nu_{21}} & \frac{\nu_{12}E_2}{1-\nu_{12}\nu_{21}} & 0 \\ & \frac{E_2}{1-\nu_{12}\nu_{21}} & 0 \\ Symm & & G_{12} \end{bmatrix} \tag{4.42}$$

where, the right-hand side of the equation represents the stiffness matrix of the damaged laminate expressed in terms of moduli $E_1, E_2, G_{12}, \nu_{12}$ and ν_{21} evaluated at crack density $s = s_0$. Solving this equation the material constants of interest can be written as

$$a_1\kappa_{90} = \frac{s_0 t}{2t_c^2}\left[\frac{E_1}{1-\nu_{12}\nu_{21}} - \frac{E_1^0}{1-\nu_{12}^0\nu_{21}^0}\right] \tag{4.43}$$

$$a_2\kappa_{90} = \frac{s_0 t}{2t_c^2}\left[\frac{E_2}{1-\nu_{12}\nu_{21}} - \frac{E_2^0}{1-\nu_{12}^0\nu_{21}^0}\right] \tag{4.44}$$

$$a_4\kappa_{90} = \frac{s_0 t}{t_c^2}\left[\frac{\nu_{12}E_1}{1-\nu_{12}\nu_{21}} - \frac{\nu_{12}^0 E_1^0}{1-\nu_{12}^0\nu_{21}^0}\right] \tag{4.45}$$

The procedure for damage analysis in the synergistic damage mechanics approach is sketched in Fig. 28. As illustrated, this procedure combines micromechanics with CDM for complete evaluation of structural response. Micromechanics involves analysis to determine CODs in cracked plies within a RVE (or unit cell, if applicable), from which the constraint effect is evaluated, as we shall explain in the next section. The constraint effect is carried over in the CDM formulation through the constraint parameter. In a separate step, the damage constants $\kappa_{90}a_i$ are determined from data for a reference laminate, which, as mentioned earlier, is chosen here to be $[0/90_8/0_{1/2}]_s$. With the values of the $\kappa_{90}a_i$ constants and $\beta = \frac{\kappa_\theta}{\kappa_{90}}$ known, the CDM based expressions given by equations (4.37)-(4.40) are employed to predict stiffness degradation with crack density. The overall structural behavior is finally analyzed using the reduced stiffness properties for the laminate.

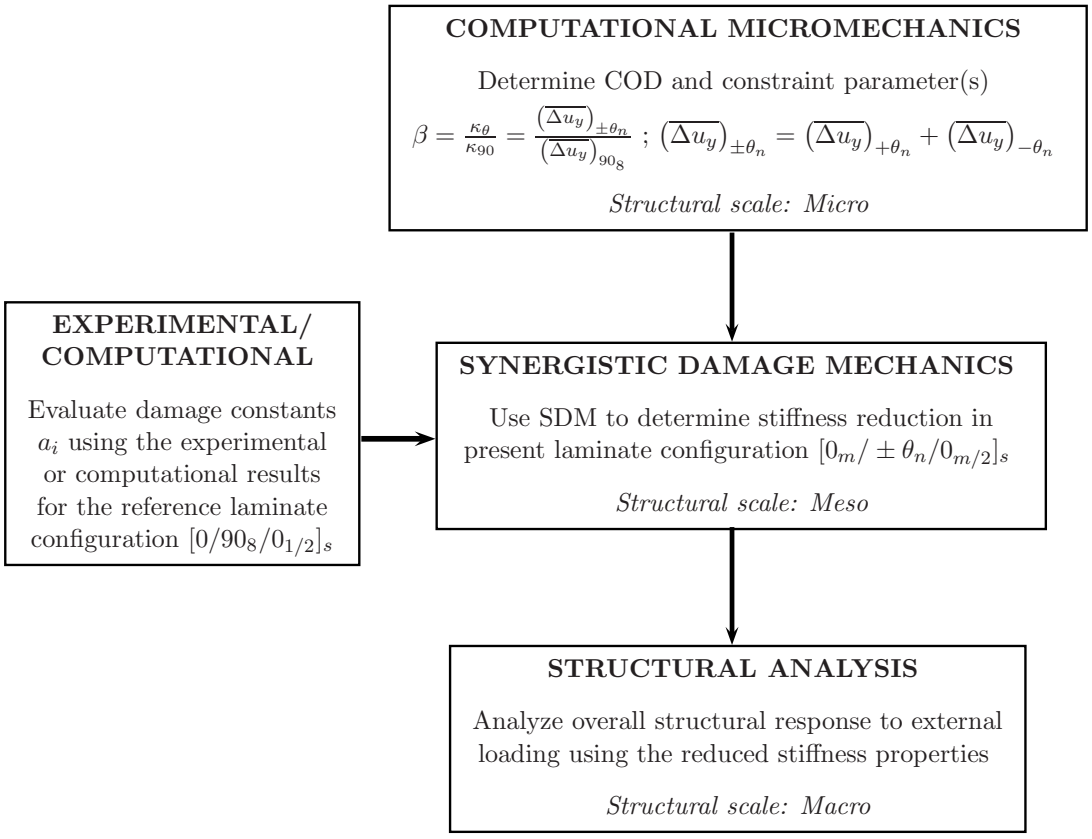

Fig. 28. Flowchart showing the multi-scale synergistic methodology for analyzing damage behavior in a class of symmetric laminates with layup $[0_m/\pm\theta_n/0_{m/2}]_s$ containing transverse cracks in $+\theta$ and $-\theta$ layers.

C. FE Modeling

Three-dimensional FE analysis is performed here as a micromechanical tool to evaluate the constraint effect. It should be noted that although some analyses in literature use 2-D generalized FE modeling even for damage in off-axis plies , e.g. in $[0/90/\mp 45]_s$ laminates [94], the boundary value problem requires a 3-D analysis. A representative geometric model for $[0/\pm\theta_4/0_{1/2}]_s$ laminate configuration along with the boundary conditions is shown in Fig. 20 on page 56. As noted earlier, in this laminate configuration both sets of of-axis plies ($+\theta$ and $-\theta$ plies) experience almost identical constraint from the un-cracked 0-plies and hence the COD values for cracks in both orientations are expected to be nearly equal. The experimental results, which naturally show scatter, seem to support this [109]. We shall compute the CODs here to validate this expectation. Since the experimental data on COD were taken for cracks sufficiently away from neighboring cracks to eliminate the mutual crack interaction effect on CODs, focusing instead on the constraint effect, we shall simulate the experimental condition by choosing a large length of the RVE (unit cell) in the FE analysis conducted here.

For the laminate used in the experimental work, ply thickness and laminate width were equal to 0.125 mm and 3.5 mm, respectively. The ply material is glass-epoxy (HyE 9082Af, Fiberite) with in-plane properties E_{11}=44.7 GPa, E_{22}=12.7 GPa, G_{12}=5.8 GPa and ν_{12}=0.297. To obtain the remaining properties for use in the 3-D model, the unidirectional ply is assumed transversely isotropic in the cross-sectional plane. Thus, $E_{33} = E_{22} = 12.7$ GPa; $G_{13} = G_{12} = 5.8$ GPa; $\nu_{13} = \nu_{12}$=0.297; $G_{23} = \frac{E_{22}}{2(1+\nu_{23})}$=4.885 GPa. The Poisson's ratio in the isotropic cross-sectional plane ν_{23} is taken as 0.3.

Separate 3-D FE models were constructed for $[0/\pm\theta_4/0_{1/2}]_s$ laminate configura-

tion for ply orientations $\theta = 25$, 40, 55, 70 and 90°. The models assumed the matrix cracks to have grown across the entire width of the specimen, as observed in the experimental work. More details on the FE simulations methodology have already been provided in the previous chapter.

D. Results and Discussion

The results obtained by the SDM approach described in section 2 are grouped in four sections below. First, the CODs computed by the FE model are compared with available experimental data to verify their accuracy. Next, the stiffness moduli for $[0/\pm\theta_4/0_{1/2}]_s$ laminates are predicted and compared with the experiments. A detailed parametric study is then conducted to determine the dependency of the COD on the factors that characterize the constraint effect. Finally, the constraint parameter is calculated from the COD results and used in the SDM methodology described above for prediction of stiffness property changes due to off-axis cracking in $[0_m/\pm\theta_n/0_{m/2}]_s$ laminates with varying m, n and stiffness ratio of the cracked plies relative to the constraining plies.

1. Crack Surface Displacements

Fig. 29 shows the variation of nodal displacements in x, y and z directions (see Fig. 20 on page 56 for coordinate system) plotted with respect to x. All the displacements are averaged over thickness of the cracked layers. The average nodal displacements in x (crack longitudinal) and y (normal to crack plane) directions are nearly same in $+\theta$ and $-\theta$ layers in values and show similar trends over x; whereas in z-directions they are just opposite showing that as overall out of plane displacement is nullified. Thus, displacements averaged over the two orientations of cracks result in only sym-

metric components. The canceling of anti-symmetric components retains the overall orthotropic symmetry of the laminate. While the nodal displacements of the crack surfaces in y direction correspond to the opening mode (Mode I), the nodal displacements in x and z directions correspond respectively to the in-plane and out-of-plane sliding modes (Mode II and III). The sliding displacements are observed to be lower than the opening displacements. Especially, the out-of-plane displacements are negligible as compared to the opening displacements. Hence, for prediction of stiffness of the damaged laminate, crack opening displacements are enough. However, the in-plane sliding displacements may release substantial energy during fracture events and must be considered while analyzing the damage progression in off-axis laminates, which will be dealt in a future work.

In a previous work [109], comprehensive experiments were carried out to evaluate CODs in $[0/\pm\theta_4/0_{1/2}]_s$ laminates subjected to tensile loading in axial direction. The full-size specimens (20 mm width) were loaded in an Instron 1272 testing machine to measure residual elastic properties at different states of damage and to characterize damage (density of cracks in the θ-plies) in the laminates at increasing tensile loads. Thin strips (3.5 mm width) were then cut longitudinally from the cracked specimens and were placed in a set-up developed for measuring COD. The set-up consisted of a miniature materials tester (MINIMAT) for loading the thin strip to open cracks, which were observed by an optical microscope equipped with a video camera. The video signal transmitted to a TV monitor displayed the crack profile at sufficient magnification ($\times$2463) to measure the COD. A typical COD of 10 μm was thus magnified to 24.63 mm. The micro-specimens (thin strips) were loaded at two preselected longitudinal strains, 0.4 and 0.6%, for the COD measurements. A specially constructed mini-extensometer was used to measure strains on the micro-specimens. These strains were much below the strains in the macro-specimens at which the

intralaminar cracks were produced, thus generating no further cracking. The CODs for a given crack were recorded at 25 equidistant points along the crack length (i.e. the total thickness of the ply group containing cracks). In a general case, COD in a RVE depends on the crack spacing, the laminate layup parameters, the orientations of the cracked plies, their relative thickness as compared to the longitudinal plies, the imposed loading level and the ratio of stiffnesses of cracked and constraining plies. The average COD is defined as

$$\overline{\Delta u_y} = \frac{1}{t_c} \int_{-t_c/2}^{t_c/2} \Delta u_y(z) \, \mathrm{d}z \tag{4.46}$$

where Δu_y represents the separation of crack planes in the direction normal to the crack face. In experiments, no matrix cracks were observed on the specimen edge for ply orientations below $\theta = 40°$. However, note that FE analysis assumes transverse cracks present for all angles of ply orientations. To estimate $\overline{\Delta u_y}$ numerically, Δu_y is determined from nodal y-direction displacements averaged over the entire crack surface. Furthermore, in keeping with the assumption of equal damage in $+\theta$ and $-\theta$ plies, the average COD values are averaged over the two orientations to eliminate any small differences. The experimental and numerically estimated results are compared in Fig. 30(a) for 0.5% axial strain. The experimental data for this strain is taken by averaging COD measurements for 0.4% and 0.6% axial strains. The variation of CODs with applied axial strain is compared with experimental data in Fig. 30(b).

The profiles of normalized CODs, averaged over $+\theta$ and $-\theta$ plies, through the thickness for different ply orientation are shown in Fig. 31(a). As expected, for cross-ply laminates, the profile is symmetric about mid-plane of the cracked ply and consequently the maximum COD occurs at the mid-plane of the cracked layer. This COD profile is different from an elliptic profile for a single crack in an infinite isotropic elastic medium subjected to a uniform far-field stress due to difference in constraint

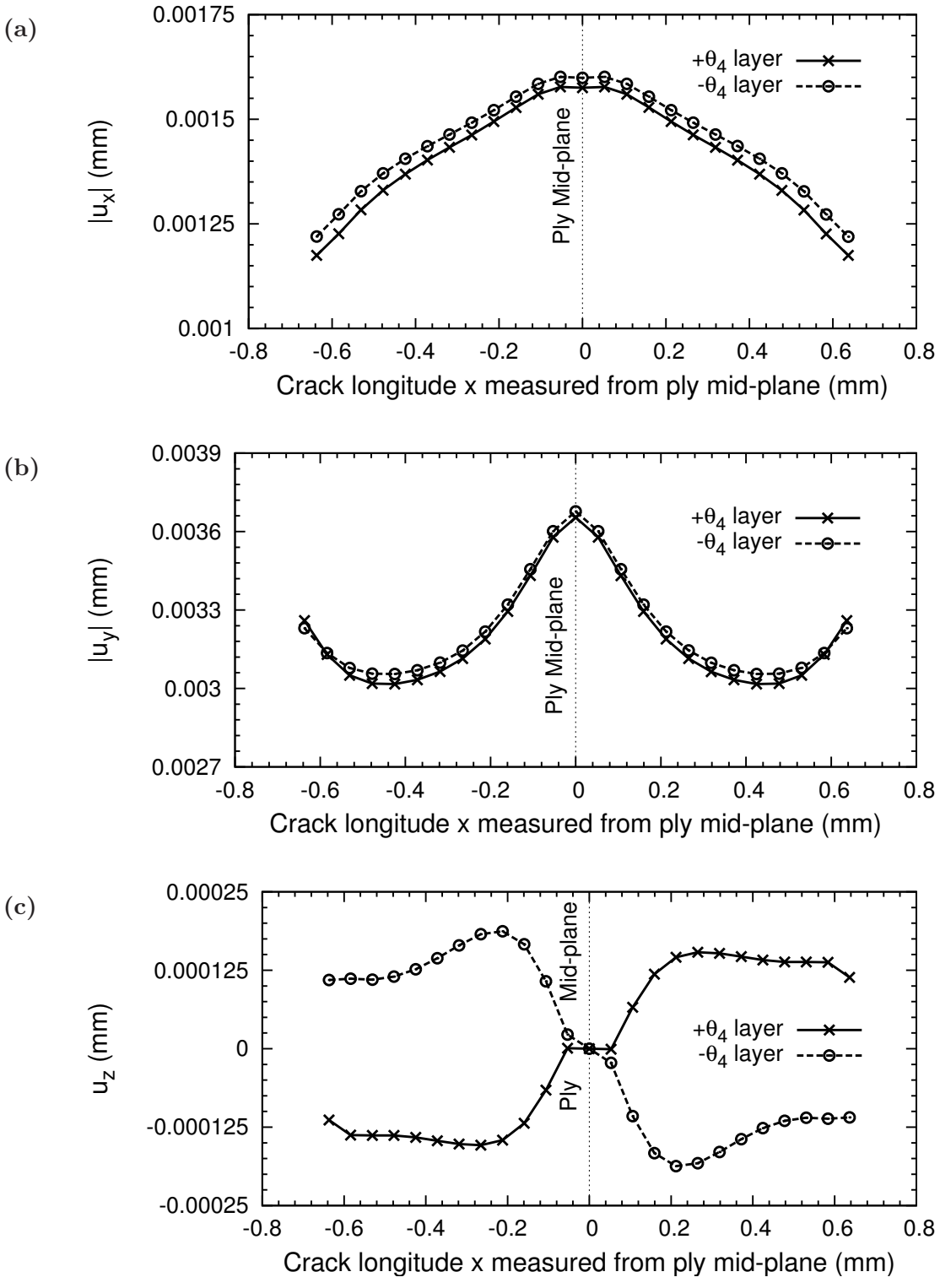

Fig. 29. Variation of average nodal displacements for $[0/\pm 70_4/0_{1/2}]_s$ laminate with respect to crack longitudinal (x) direction. The displacements u_x, u_y and u_z are averaged over cracked ply thickness.

(a)

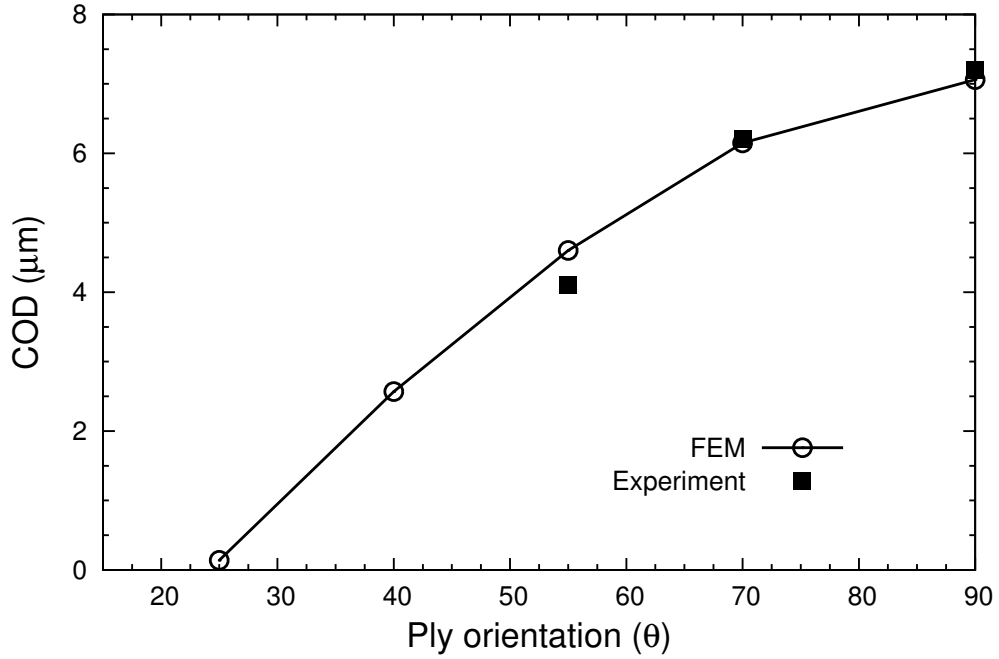

(b)

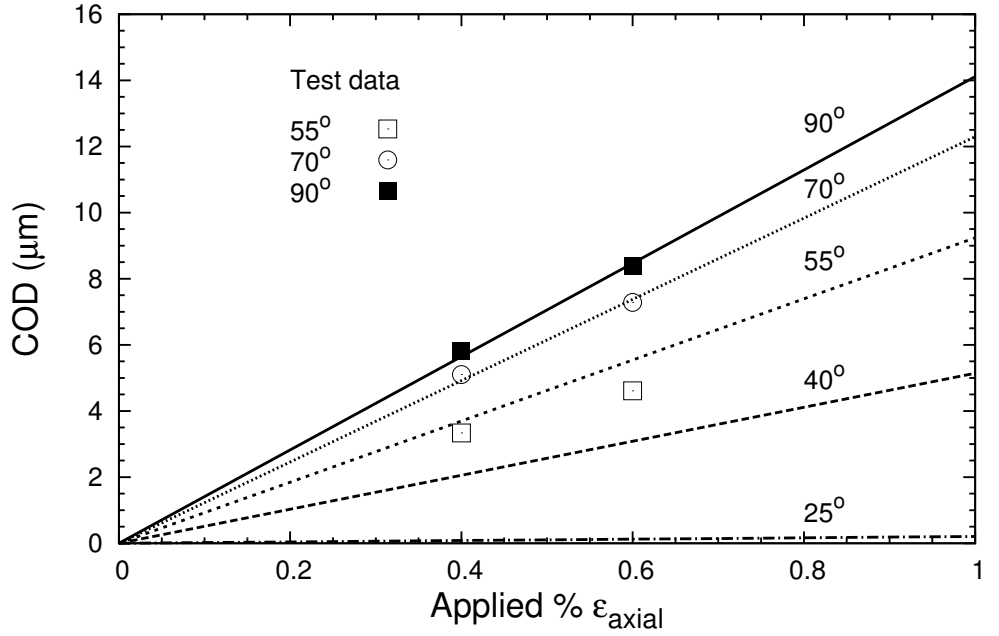

Fig. 30. Comparison of average CODs with experimental results for $[0/\pm\theta_4/0_{1/2}]_s$ laminate for (a) ϵ_{axial}=0.5% (b) varying ϵ_{axial}.

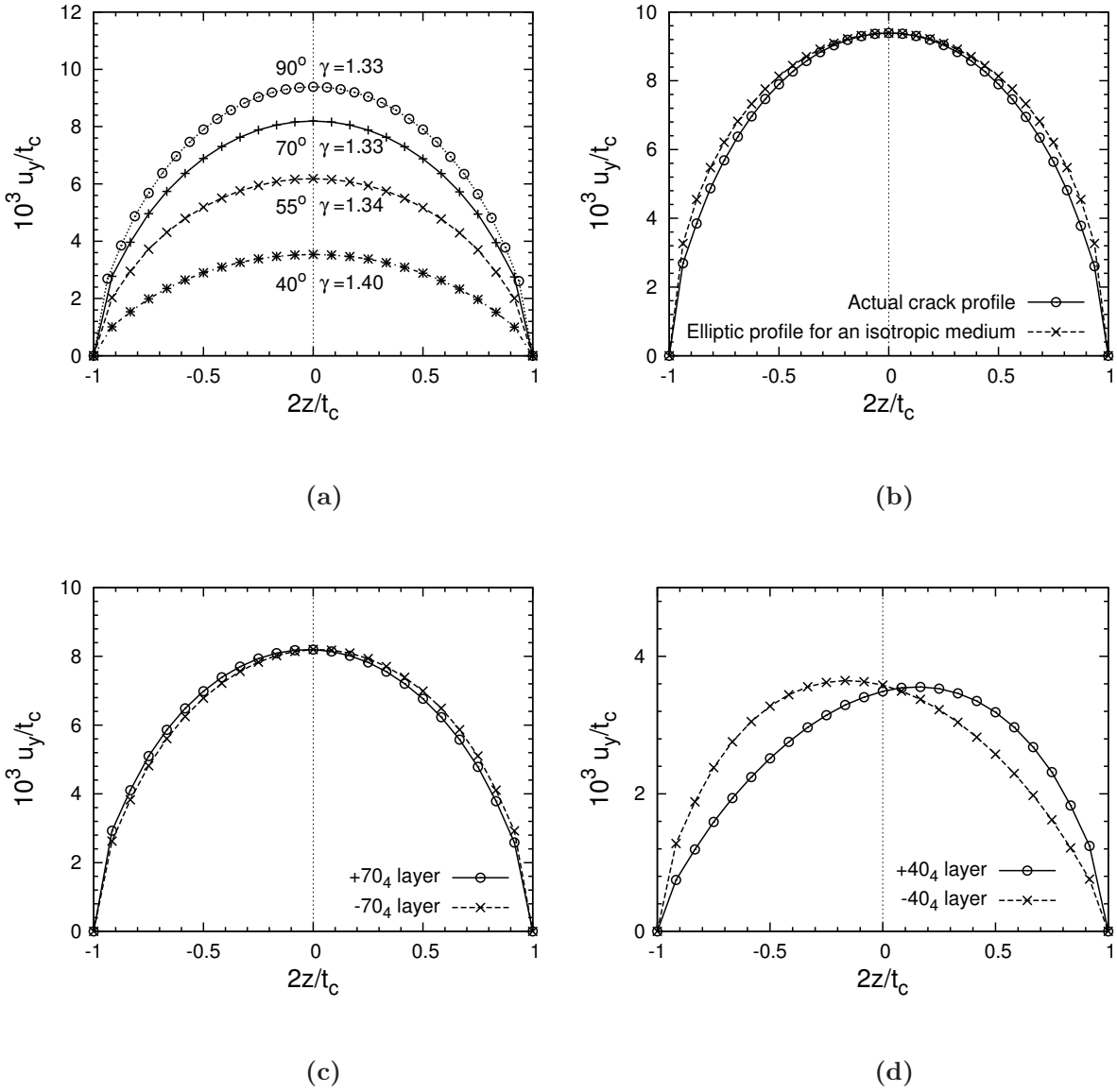

Fig. 31. COD profiles for cracked plies in $[0/\pm\theta_4/0_{1/2}]_s$ laminates. (a) CODs averaged over $-\theta$ and $+\theta$ plies; (b) Crack profile for 90° transverse crack compared with an elliptic profile for an isotropic medium; (c)-(d) COD profiles for $+\theta_4$ and $+\theta_4$ separately: (c) $\theta = 70°$,(d) $\theta = 40°$. The figures (c)-(d) depict the asymmetry of opening displacements for off-axis laminates, especially at a ply orientation farther from $\theta = 90°$.

from the surrounding material. Fig. 31(b) compares the actual COD profile (based on FE computations) and an elliptic profile with the same maximum COD. Thus, the magnitude of average COD for 90° crack is different from that for the elliptic crack. For other off axis laminates, the crack surface displacements are not symmetric about the mid-plane as shown in Fig. 31(b)-(d). This asymmetry increases as we go away from cross-ply laminates ($\theta = 90°$) and maximum COD does not occur midway through the thickness of the cracked $+\theta_4$ or $-\theta_4$ layers (e.g., for $\theta = 40°$, see Fig. 31(d)). The aspect ratio of COD profiles, $\gamma = \frac{(\Delta u_y)_{max}}{\overline{\Delta u_y}}$ varies from 1.33 for $\theta = 90°$ to 1.40 for $\theta = 40°$. This is different from the aspect ratio of $4/\pi \approx 1.273$ for an elliptic profile.

2. Prediction of Stiffness Degradation

In this section we will implement the SDM methodology described above for $[0/\pm\theta_4/0_{1/2}]_s$ laminates. Following the procedure sketched in Fig. 28, the constraint parameter κ_θ normalized by κ_{90} is taken as the average COD of the θ-cracks relative to the average COD of 90°-cracks. Thus,

$$\beta = \frac{\kappa_\theta}{\kappa_{90}} = \frac{\left(\overline{\Delta u_y}\right)_{\pm\theta_4}}{\left(\overline{\Delta u_y}\right)_{90_8}} \tag{4.47}$$

It is noted that the COD value in the numerator is the sum of CODs of the $+\theta_4$ and $-\theta_4$ cracks, while the COD in the denominator is of an 8-ply thick 90°-crack. All CODs are calculated at the same imposed displacement on the unit cells.

The procedure for stiffness prediction is now carried out in the following steps:

1. Determine the three material constants $\kappa_{90}a_1$, $\kappa_{90}a_2$ and $\kappa_{90}a_4$ by solving the three coupled equations (4.43)-(4.45). The data needed to solve these equations are the elastic moduli E_1, E_2 $(= E_2^0)$ and ν_{12} (ν_{21} is given by the reciprocal

relationship for orthotropic laminates) for a selected crack spacing $s = s_0$ in addition to the already known initial moduli and lamina thicknesses. This is the CDM procedure for cross ply laminates used in earlier works, e.g. [89, 143]. The prediction of the two moduli E_1 and ν_{12} normalized with corresponding values for a virgin laminate are shown in Fig. 32 where they are compared with experimental data reported in [109].

2. Determine β by using calculated COD values in equation (4.47). Find $\kappa_\theta a_1$, $\kappa_\theta a_2$ and $\kappa_\theta a_4$ by multiplying with β the constants $\kappa_{90} a_1$,$\kappa_{90} a_2$ and $\kappa_{90} a_4$ determined in Step 1. Calculate E_1, E_2 and ν_{12} from equations (4.37)-(4.40) by substituting these constants, using the assumption that a_1, a_2 and a_4 are independent of θ, as noted above.

The elastic moduli E_1 and ν_{12} predicted by SDM approach are shown in Fig. 33 for $[0/\pm 70_4/0_{1/2}]_s$ laminate. Experimental data reported by [109] are also shown for comparison. The agreement with data is about the same as that obtained by using experimentally measured COD values in equation (4.47).

For the $[0/\pm 55_4/0_{1/2}]_s$ laminate the stiffness reduction is caused by matrix cracking as well as shear induced damage in off-axis plies, as discussed in [109], where a procedure for calculating stiffness reduction due to shear damage was described. Fig. 34 shows the predictions of E_1 and ν_{12} by the SDM procedure. Experimental data from [109] are also shown for comparison. The total reduction in the elastic moduli is taken as the sum of the two effects, as in [109], and the final values are shown in Fig. 34 along with experimental data. Once again, the agreement of predictions with the experimental data is nearly the same as that reported in [109] by using measured COD values.

It would be of interest to note that the stiffness predictions using experimentally

measured COD values in equation (4.47) are subject to scatter, which is inherent in testing. Furthermore, the experimental procedure requires a specialized test set-up [109, 162], which is costly and takes a certain amount of training to operate. The 3-D FE computations on a unit cell, on the other hand, are easy to perform and can provide accurate values of CODs.

3. Parametric Study of Constraint Effects

In the preceding section we have illustrated the SDM procedure for stiffness prediction of $[0/\pm\theta_4/0_{1/2}]_s$ laminates using computed average COD results, which provide the relative constraint parameter β (equation (4.47)). It is of interest to know how the constraint parameter depends on the laminate configuration parameters within the broader class of laminates given by $[0_m/\pm\theta_n/0_{m/2}]_s$. This laminate configuration is restricted by the assumption that the cracks are present only in the $+\theta$ and$-\theta$ plies, which have nearly the same constraint. Thus, the parameters to vary are the crack orientation θ and ply thicknesses m and n. Furthermore, variation of the ply material itself can be accounted for through relative ply moduli, as suggested by previous studies [104, 161].

The FE model described above was used to calculate COD values for various cases by systematically varying the parameters involved. First, the effect of relative stiffness of the plies was studied by fixing the ply thicknesses at $m = 1$ and $n = 4$ and varying θ in the range $40^\circ \leq \theta \leq 90^\circ$. Lower θ values were not used since the experimental observations suggest that cracks do not form at those ply orientations under axial tensile loading. The computed average COD values are plotted against a ply stiffness ratio in the laminate axial direction (X_1 direction) given by $r = \left(\frac{E_A^{\pm\theta}}{E_A^{90}}\right)$ in Fig. 35(a) for different θ-values. Here, $E_A^{\pm\theta}$ and E_A^{90} represent the axial stiffness of $\pm\theta$-plies and the 90°-plies, respectively.

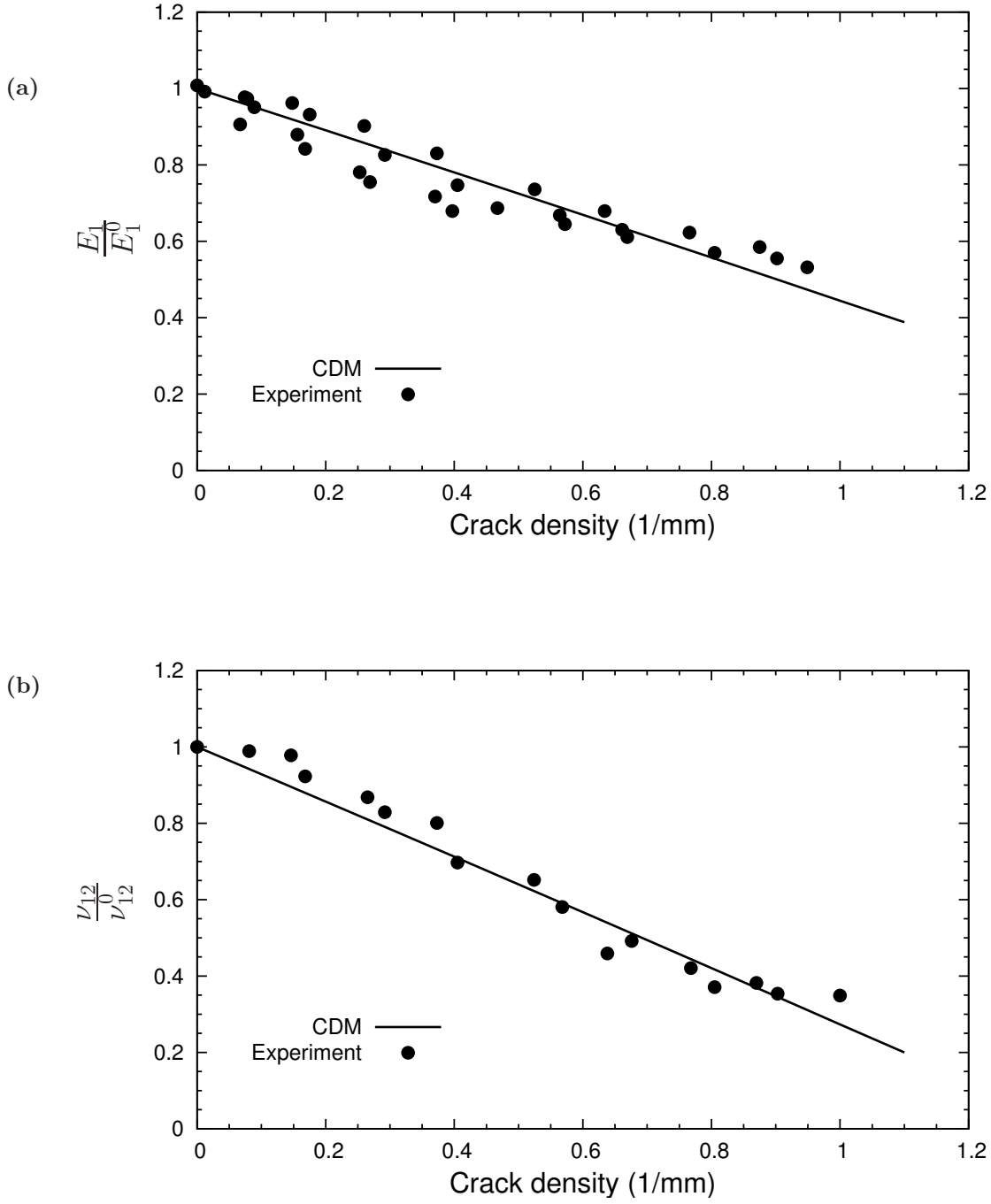

Fig. 32. Stiffness reduction for $[0/90_8/0_{1/2}]_s$ laminate compared with experimental results [109]. These results form the basis for computation of CDM constants.

(a)

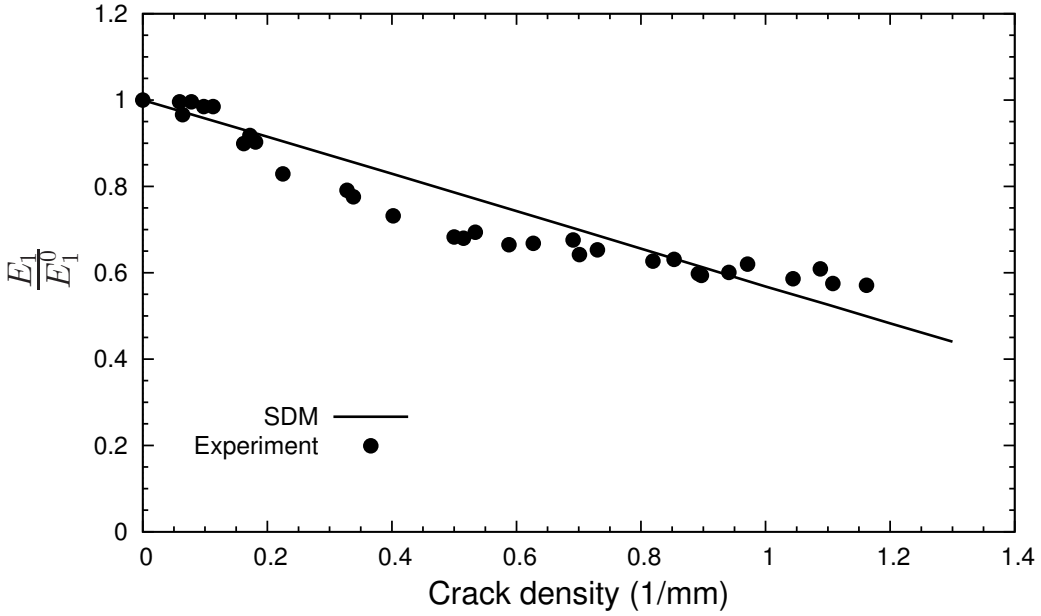

(b)

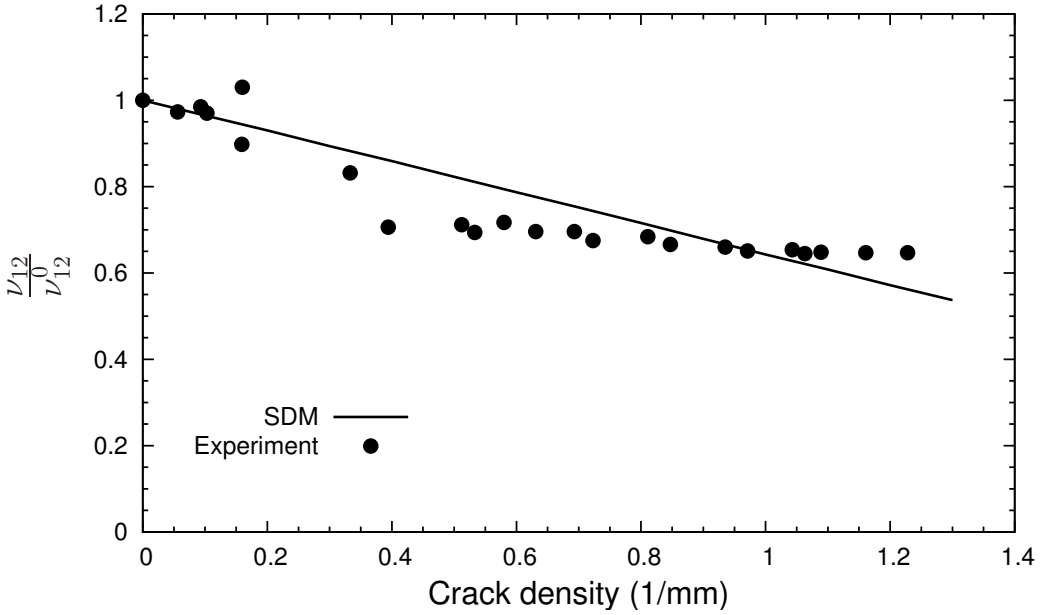

Fig. 33. Stiffness reduction for $[0/\pm 70_4/0_{1/2}]_s$ laminate compared with experimental results [109].

(a)

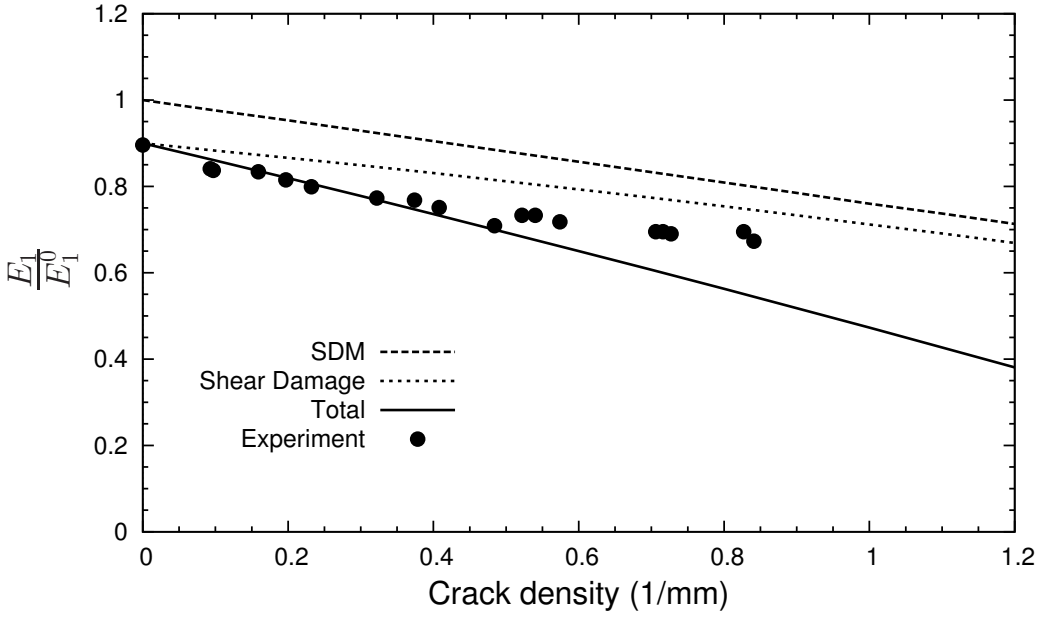

(b)

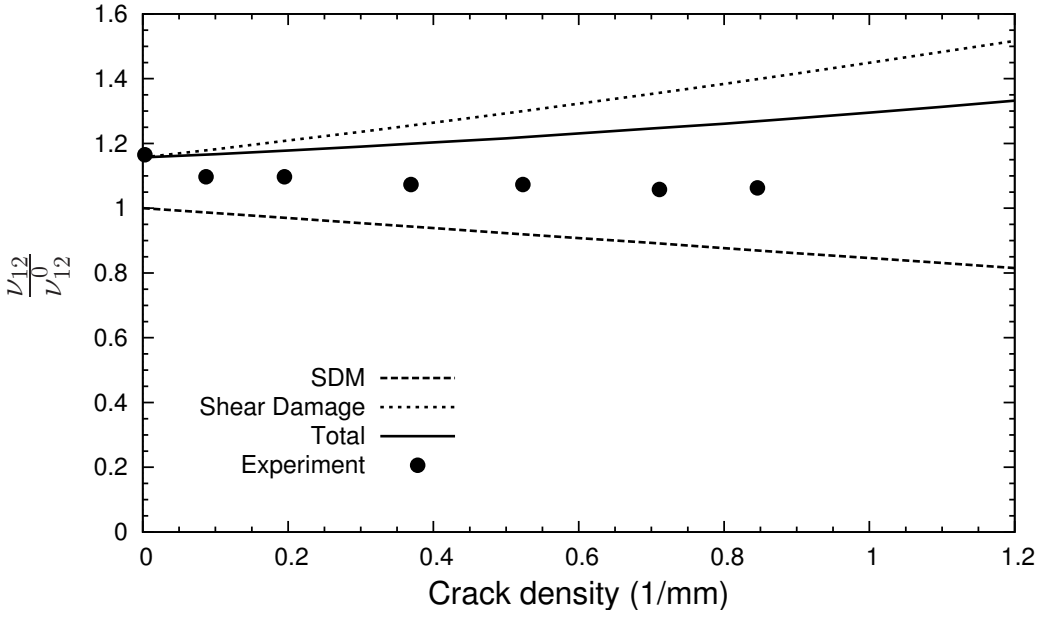

Fig. 34. Stiffness reduction for $[0/\pm 55_4/0_{1/2}]_s$ laminate compared with experimental results [109].

Next the effect of cracked ply thickness, or equivalently, the number 'n' of adjacent cracked plies is studied by fixing $m = 1$. The average COD is plotted against n for different θ in Fig 35(b). Finally, the effect of the thickness of the constraining plies is studied by fixing $n = 4$ and varying m. The COD variation for this case is shown in Fig 35(c). All variations of average COD described above are captured in a master equation assuming that the individual effects are independent, i.e., non-interactive. Thus, the following equation results

$$\left(\overline{\Delta u_y}\right)_{\pm\theta_n} = U.f_1(\theta).f_2(r).f_3(m).f_4(n) \tag{4.48}$$

where, U is the average COD for the reference laminate $[0/90_8/0_{1/2}]_s$.

The parametric functions f_i are obtained by curve-fitting the computed data and are given by

$$f_1(\theta) = sin^2\theta \tag{4.49}$$

$$f_2(r) = r^{-c_1} \tag{4.50}$$

$$f_3(m) = \frac{c_2}{m} + c_3 \tag{4.51}$$

$$f_4(n) = c_4 n^{c_5} \tag{4.52}$$

The values of the constants appearing in these relations are found to be: $c_1 = 0.0871; c_2 = 0.1038; c_3 = 0.8949; c_4 = 0.247; c_5 = 0.99$. It is noted that these constants are laminate material specific.

4. Stiffness Predictions for Other Laminates

The parametric study described above enables us to predict stiffness degradation in off-axis laminates with different geometry and stiffness values. For example, one can consider a laminate with stiffer outer plies. The average COD used in equation

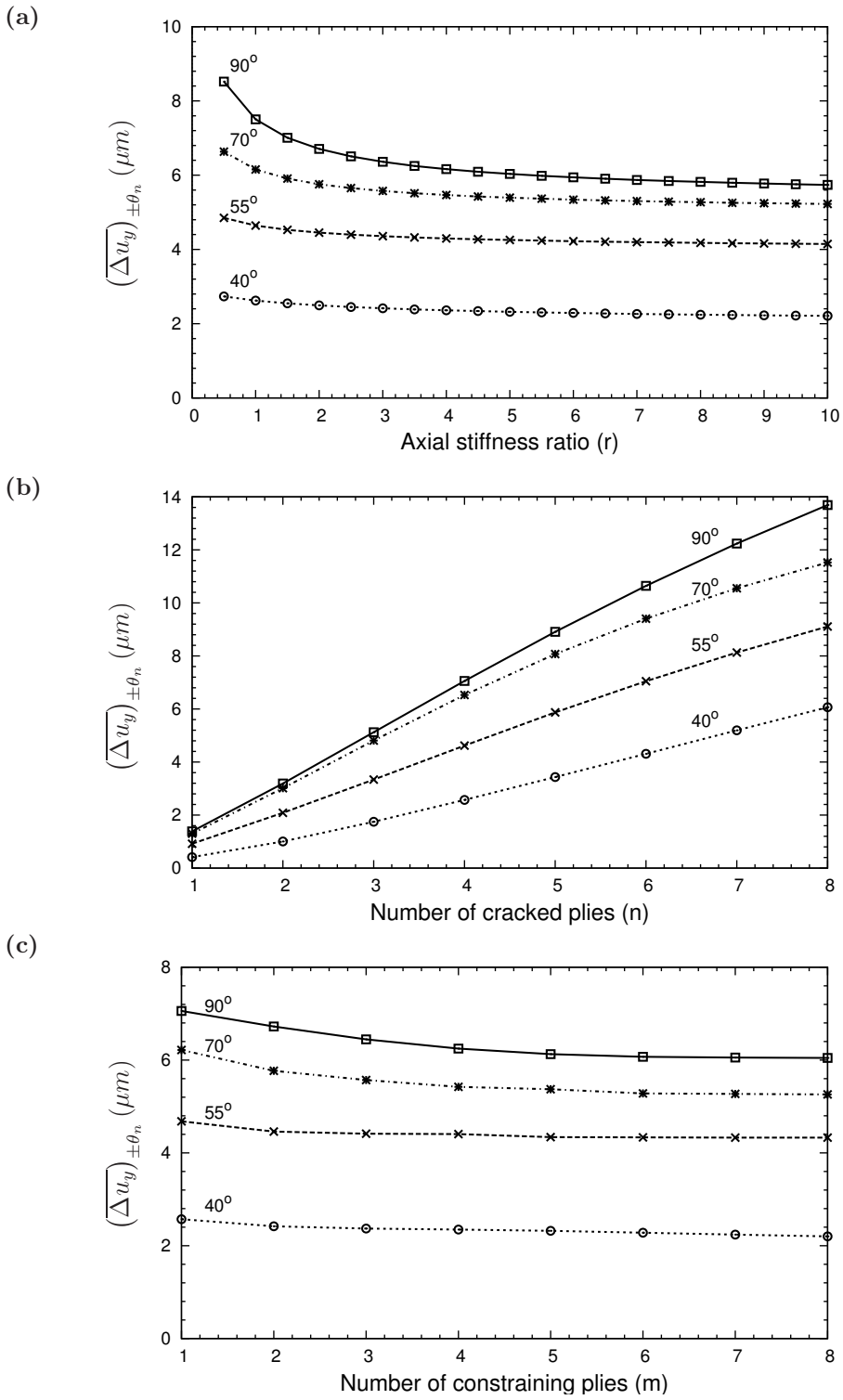

Fig. 35. Variation of average COD for $[0_m/\pm\theta_n/0_{m/2}]_s$ laminate with (a) axial stiffness ratio, r (for $m = 1, n = 4$); (b) number of cracked plies, n; and (c) number of constraining plies, m.

(4.47) for different values of stiffness ratio can be computed using equation (4.48). The variation of engineering moduli E_1 and ν_{12} for different stiffness ratios (r) for $[0/\pm 70_4/0_{1/2}]_s$ laminate is shown in Fig. 36. As expected, stiffer outer plies cause less sever degradation in the moduli. In contrast to changing the stiffness of outer plies, one can vary the number of constraining (m) or cracked plies (n). The effect of number of supporting plies over change in stiffness moduli E_1 and ν_{12} of the $[0_m/\pm 70_4/0_{m/2}]_s$ laminate is shown in Fig. 37. The effect of number of cracked plies over change in stiffness moduli E_1 and ν_{12} of the $[0/\pm 70_n/0_{1/2}]_s$ laminate is shown in Fig. 38. Fig. 36-38 indicate that the cracking ply thickness, i.e., crack size, has significant effect on stiffness degradation, while the thickness of the constraining plies as well as the change in axial stiffness ratio r have small effect.

E. Summary

One major goal of damage mechanics is to provide methodologies for predicting changes in the mechanical response of composite laminates undergoing damage. It appears unrealistic at this point that this goal can be achieved for general laminates by a single method or approach. To make progress, however, it is necessary that the approach taken is capable of treating laminates of more complex configuration than the cross ply laminate, at the least. In the work reported here, we have made effort in this direction by considering a class of laminates given by $[0_m/\pm\theta_n/0_{m/2}]_s$. The approach taken has been to use the CDM framework that has the capabilities to treat general laminates with wide range of damage modes. To make the CDM framework versatile and practical, a methodology has been developed that utilizes computational micromechanics in sufficient measure to provide synergism with CDM, producing what we have called synergistic damage mechanics (SDM). Specifically, a

(a)

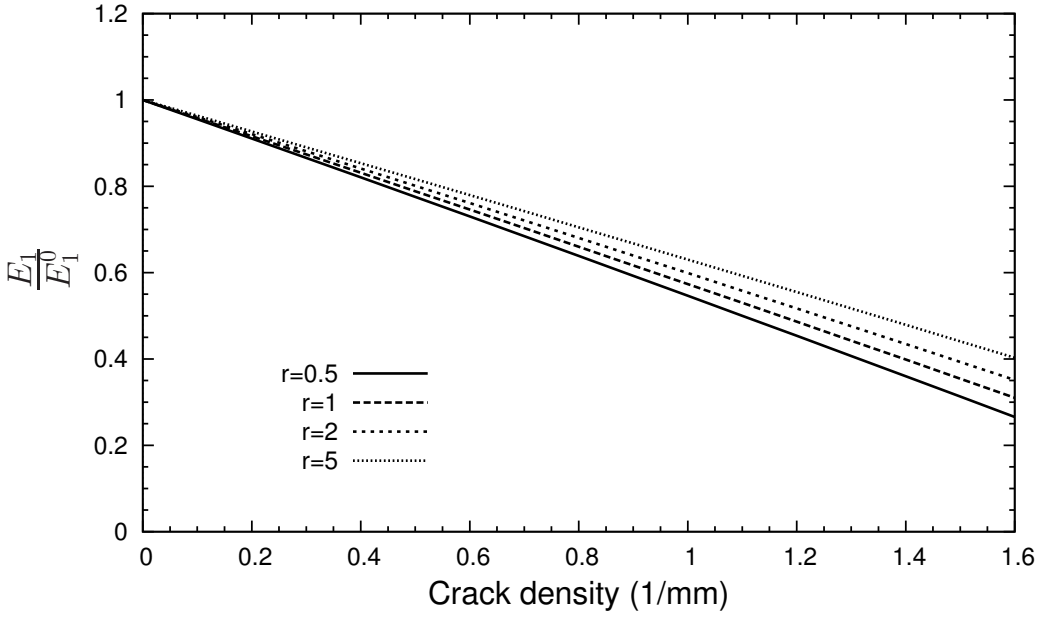

(b)

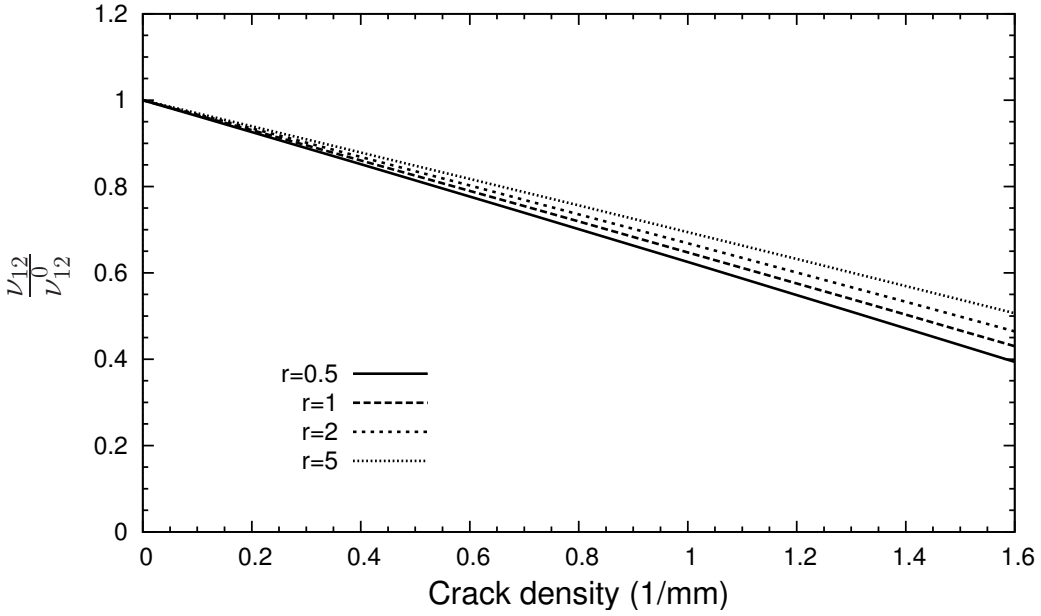

Fig. 36. Stiffness reduction for $[0/\pm 70_4/0_{1/2}]_s$ laminate for different axial stiffness ratio, r.

(a)

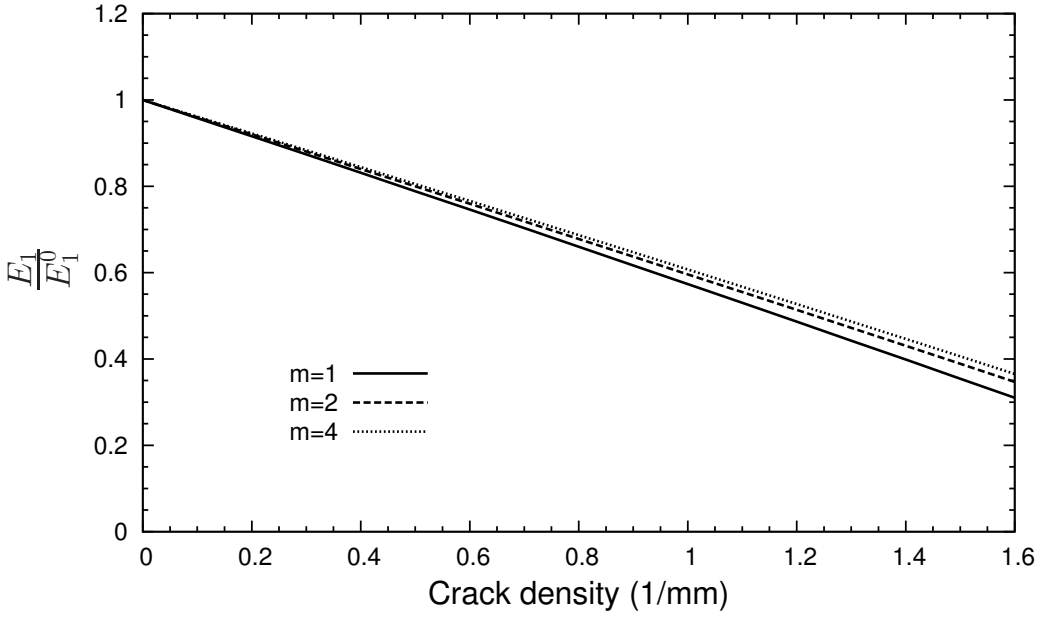

(b)

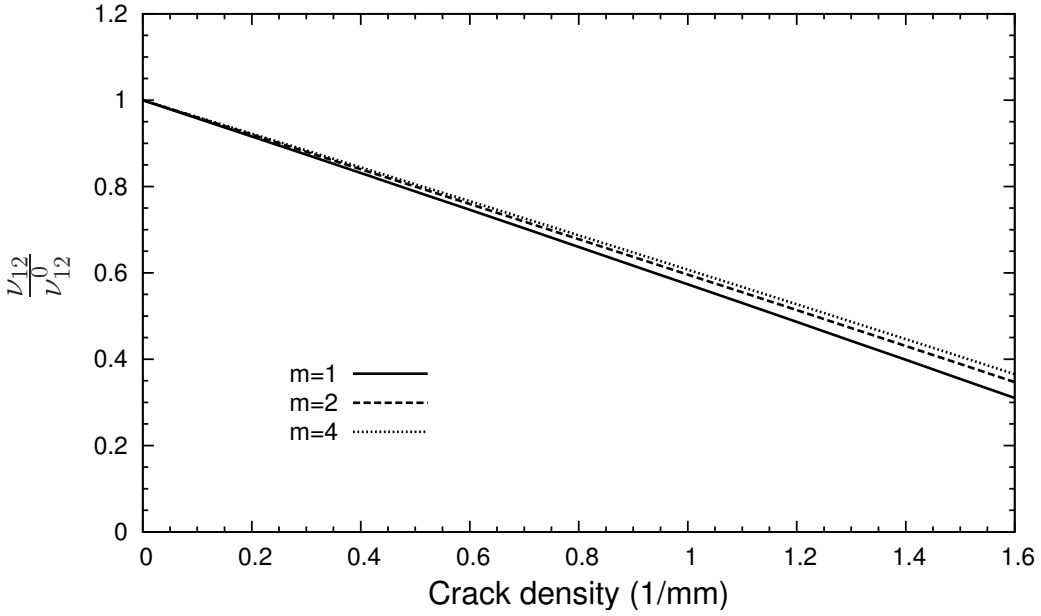

Fig. 37. Stiffness reduction for $[0_m/\pm 70_4/0_{m/2}]_s$ laminate for different number of constraining plies, m.

(a)

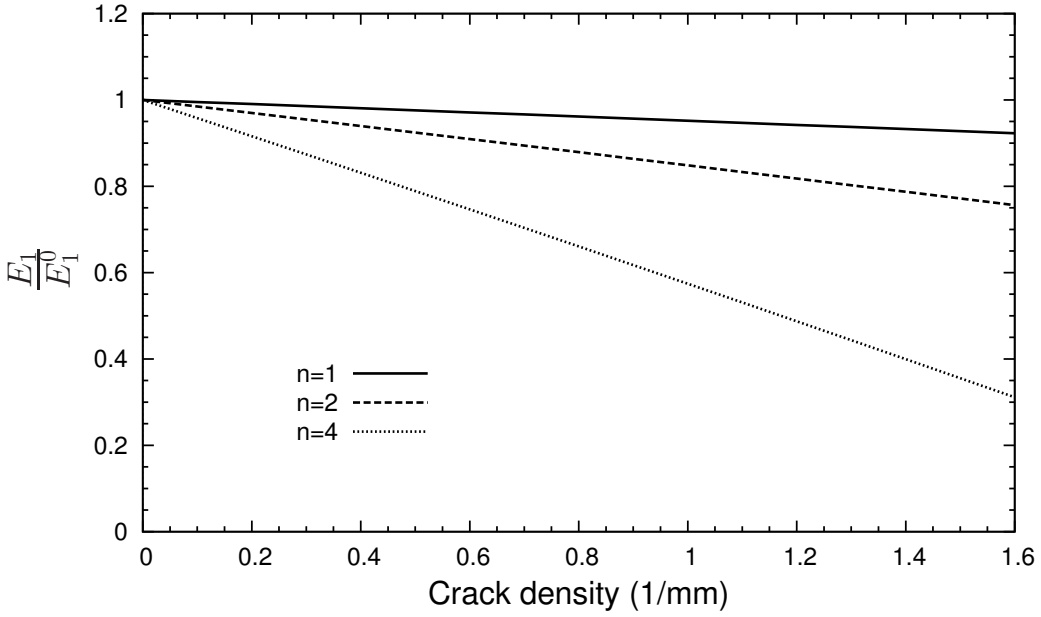

(b)

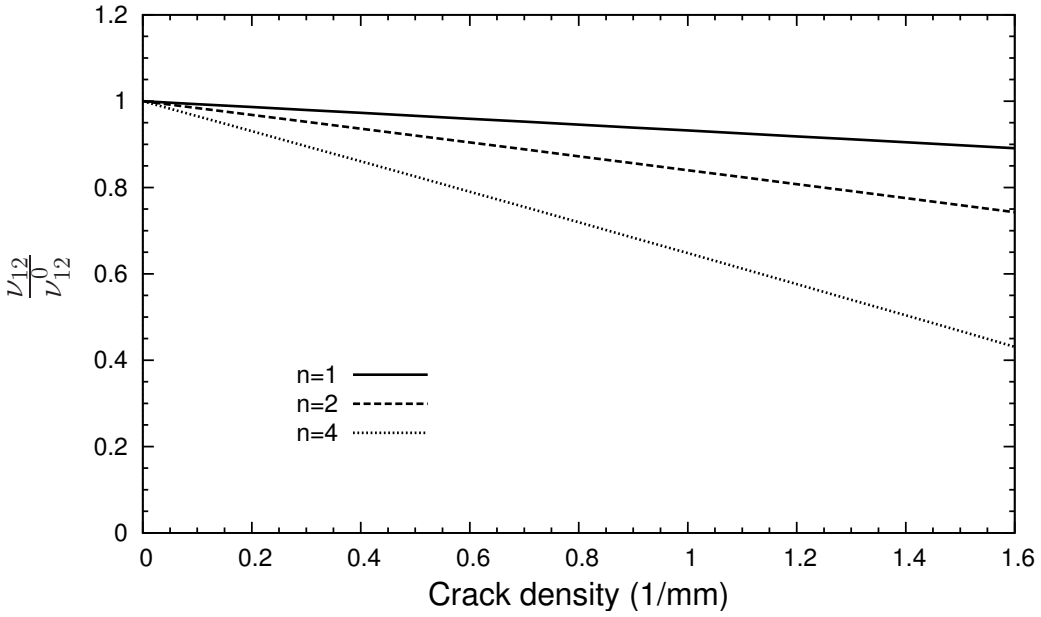

Fig. 38. Stiffness reduction for $[0/\pm 70_n/0_{1/2}]_s$ laminate for different number of cracked plies, n.

constraint parameter (or function) is computed from a FE analysis of CODs in a unit cell and entered into the CDM stiffness-damage relationships. This provides a methodology for prediction of stiffness changes due to cracking in the off-axis plies when those changes for a selected reference laminate ($[0/90_8/0_{1/2}]_s$) are known.

Although the SDM approach was described in earlier works [109, 142], it was illustrated only for one specific subclass of the general laminate configuration stated above, i.e. $[0/\pm\theta_4/0_{1/2}]_s$. Also, the CODs needed in the approach were measured on the edges of test coupons using a specialized set-up developed for the purpose. In the present work we have used those experimental CODs to verify the computed values by a 3-D FE analysis of appropriate unit cells. We have then performed a parametric study of CODs to cover the general $[0_m/\pm\theta_n/0_{m/2}]_s$ laminate over useful ranges of the parameters m, n and θ. A master equation is developed by curve-fitting the computed data that can provide the basis for stiffness prediction at a given damage state in the laminate at hand.

A successful completion of the task of treating two off-axis cracking modes ($+\theta$ and $+\theta$) points to proceeding further to treat three damage modes in $[0_m/\pm\theta_n/90_p]_s$. This will be the subject of our next chapter.

CHAPTER V

STIFFNESS CHANGES WITH THREE DAMAGE MODES

A. Introduction

Efficient use of composite laminates in a wide range of applications requires placing plies in multiple orientations. A common example is a class of laminates called quasi-isotropic that have ply orientations of 0, 45 and 90 degrees, exemplified by the $[0/\pm 45/90]_s$ configuration. In spite of such laminates already in use, there is no rigorous and comprehensive analysis available to assess their response in the presence of cracking in more than one set of plies. The need for such analysis in the context of durability and life prediction has been emphasized in a committee report [11]. Lacking such analysis, the current design procedures are conservative, often relying on criteria that allow no cracking at all. To remedy this situation we require an approach that is capable of incorporating effects of ply level (microscopic) failure events into a laminate level (mesoscopic) constitutive framework suited for structural analysis under general loading. One approach of this nature is Synergistic Damage Mechanics (SDM) that retains the Continuum Damage Mechanics (CDM) framework at the mesoscopic level of a representative volume element (RVE) while incorporating microscopic cracking through tensor-valued internal damage variables. Previous chapter focused on ply cracks in two symmetrically placed orientations in $[0_m/\pm\theta_n/0_{m/2}]_s$ laminates; the present work treats the more general case of $[0_m/\pm\theta_n/90_r]_s$ and $[0_m/90_r/\pm\theta_n]_s$ configurations where cracks are additionally present in the 90°-plies.

The literature in damage mechanics of composite materials is extensive, as covered in the first two chapters. Rather than cite all approaches, we shall outline those developments that are of direct relevance to treating ply cracking in multi-

ple off-axis orientations. The complexity of cracking in general off-axis orientations has been documented in several experimental studies, e.g. [60, 107–109]. Analytical methods for estimating elastic properties of laminates with distributed off-axis cracks are mostly accurate for transverse cracks in cross ply laminates. More general laminates with cracks require a three-dimensional stress analysis, and efforts to address these situations have typically resorted to either computational methods, e.g. the finite element method [94], or to different approximate methods, e.g., the equivalent constraint method [114] and its combination with modified shear lag theory [116] or the first-order shear deformation laminate plate theory [113]. More recently, a modified two-dimensional shear lag approach has also been attempted [168] for analysis of obliquely crossed cracks. Semi-analytical methods, such as based on Fourier series expansion to represent the displacement and stress fields, have also been suggested [141, 169]. The accuracy of such approximate solutions is difficult to assess in all cases, and most of studies compare their predictions with cross-ply laminates or similar variations (e.g.,$[\pm\theta/90]_s$) with cracks only in 90° plies, which is just a limiting case of general off-axis ply cracking. Besides, their incorporation in a structural analysis scheme has not been addressed.

The CDM framework, although quite general and well suited for structural analysis, needs, in its conventional form determination of material coefficients for each laminate configuration. The SDM methodology was proposed [142] to alleviate this problem by determining these coefficients for a reference configuration (typically a cross ply laminate) and deriving the coefficients for other cases via a "constraint" parameter that is given by relative crack surface displacements evaluated numerically by a finite element model of an appropriate representative volume. The micro-level evaluation of the constraint parameter, which carries the effect of the plies neighboring the cracking plies on the crack surface displacements, provides a convenient way

of incorporating the essential effect of cracks on changing the laminate response.

The previous work [170] on $[0_m/\pm\theta_n/0_{m/2}]_s$ laminates with cracks in $+\theta$ and $-\theta$ plies showed successful prediction of stiffness coefficients by the SDM methodology (see the previous chapter for further details). The crack density and the constraint to crack surface displacements in the two orientations were the same in that laminate configuration. Thus, taken together the two sets of cracks acted effectively as one mode of damage. In the current work, the $[0_m/\pm\theta_n/90_r]_s$ and $[0_m/90_r/\pm\theta_n]_s$ configurations analyzed contain cracks additionally in the 90°-plies, providing a truly multimode damage scenario and rendering the generalization of the previous work nontrivial. In the following sections, we shall first present the formulation of stiffness-damage relationships for multimode damage and specialize it to the case of $\pm\theta$-ply damage and 90°-ply damage as the two damage modes in the selected configurations. The constraint parameters appearing in these relationships will be defined in terms of the crack opening displacements (CODs) in a given damage mode. A 3-D finite element (FE) based procedure for calculating the CODs in a representative unit cell will be described next. The SDM methodology will be described and its predictions of elastic moduli for increasing crack densities will be compared with the moduli computed independently by the FE model. The experimental data for the case of a quasi-isotropic $[0/90/\mp 45]_s$ laminate will be compared with the SDM predictions. Finally, the effect of ply thickness in cracked versus uncracked plies will be illustrated by a limited parametric study.

B. Experimental Observations of Damage in Quasi-isotropic Laminates

An interesting layup sequence utilized in the design of composite laminates is so called "quasi-isotropic" laminates. They usually have a mix of plies in $0°, 90°, +45°$

and -45° orientations with respect to the laminate longitude, e.g., $[0/\pm 45/90]_s$, $[0/90/\pm 45]_s$ etc. such that the extensional stiffness matrix (A-matrix according to the CLPT) is directionally uniform, thereby approximating an in-plane isotropic material behavior. Hence, the extensional-twisting coupling terms are zero, and the Young's modulus measured in all in-plane directions is same. Because of this interesting property, these laminates are commonly used in structures to provide a good mix of longitudinal, transverse and shear properties.

For the case of multidirectional composites with damage in multiple orientations, the experimental data is limited to $[0/\pm 45]_s$ [37], $[0/\pm\theta_4/0_{1/2}]_s$ [109], and quasi-isotropic laminates [41, 60, 108]. The damage in $[0/\mp\theta_4/0_{1/2}]_s$ laminates has been dealt in the previous chapter. Here, we concentrate on the $[0_m/\pm\theta_n/90_r]_s$ and $[0_m/90_r/\pm\theta_n]_s$ laminates. The special case with $\theta = 45^\circ$ will give us predictions for a quasi-isotropic laminate.

The experimental observations cited above have shown some details regarding the damage development in quasi-isotropic laminates. Some of these studies concentrated on quasi-static loading while others focused on fatigue loading. Some interesting observations are summarized below:

1. As expected, the matrix cracking pattern in the quasi-isotropic laminates is more complex than in the cross-ply laminates. Microscopic observations [108] suggest that the $\pm 45^\circ$ cracks may be irregularly spaced, erratic or curved in shape, small in size, and partially grown through lamina thickness.

2. Almost always the matrix cracking initiates first in the 90° plies (see Fig. 39(a)). These cracks quickly traverse thickness and width of the lamina. They multiply somewhat stably upon increase in applied loading. Thus, the 90°-cracks are usually straight, fully grown and periodic. The $\pm 45^\circ$-cracks, in contrast, may

grow slowly through lamina thickness and width, as suggested in experimental observations by Tong et al. [108]. However, the data suggested that they multiplied very quickly. Thus, they become numerous while remaining small in size. The laminates failed by delamination before $\pm 45°$-cracks could grow through lamina thickness and width, or become periodic.

3. The cracks in an off-axis ply grow from the point of intersection of these plies with the $90°$ ply. For example, in $[0/90/\mp 45]_s$ laminates [108], cracks are observed to initiate in the $-45°$ ply at the point of intersection at the $90°/-45°$ interface and extend slowly both across the ply thickness and parallel to the fiber direction (Fig. 39(b)). On further increase in applied loading, the $-45°$-cracks may become numerous while remaining small and may never grow completely across the width of the specimen. Eventually $+45°$ cracks can form at some locations where the $-45°$ cracks meet the $-45°/+45°$ interface (Fig. 39(c)). These then can grow relatively rapidly across the (double thickness) $+45°$ ply and then grow slowly across the width of the specimen in the $+45°$ fiber direction.

4. The microscopical observations in the cited experimental program showed that the cracks in $90°$ plies spanned the thickness of the ply and were arrested by the fibers in the adjacent plies. On the contrary, the $-45°$ cracks usually initiated at the edge of $90°$ cracks along the $90°/-45°$ interface and tended to grow slowly across the thickness, such that some of them did not extend across the thickness of the ply by the end of the test. Cracking appeared to follow the fiber/matrix interface with signs of crack blunting and resin flow. There were also some indications of limited local delamination in the vicinity of $-45°$ cracks at the $90°/-45°$ interface.

5. The initiation strain for transverse cracks in 90° ply was observed to be more less the same in both $[0/90]_s$ and $[0/90/\mp 45]_s$ laminates [108]. However, the evolution of crack density was much faster initially in the cross-ply laminate. Also, the crack densities for 90°-cracks for both laminate sequences seemed to reach a saturation level, but with a higher value at saturation in the quasi-isotropic laminate than in the cross-ply laminate.

6. In terms of the stiffness property changes, a larger reduction and an even more pronounced reduction in Poissons ratio were observed for the cross-ply laminates than for the quasi-isotropic laminates. For quasi-isotropic laminates, the 90° damage mode causes more sever degradation in the stiffness properties than the ±45° damage modes. Thus, 90° is more dominating than other damage modes.

It is important to keep these things in mind while modeling stiffness degradation and predicting damage evolution in multidirectional laminates. For example, the initiation of off-axis ply cracks from the points of intersection between off-axis and 90° plies can be attributed to the higher stress concentration at the interface, and hence interaction between different cracking modes is an important consideration while modeling a multiple damage mode scenario. The interaction between stress perturbations due to cracks of different orientations not only affects the crack initiation strain in other off-axis plies, but also the overall stiffness changes in the damaged laminates. Generalized plane strain FE modeling by Tong et al. [94] seems to support this inference. These aspects will be discussed in detail in the discussion section of this chapter.

C. Stiffness Relations for $[0_m/\pm\theta_n/90_r]_s$ and $[0_m/90_r/\pm\theta_n]_s$ Laminates

Consider a laminate with a mix of on-axis and off-axis plies loaded axially, i.e. along the direction of fibers in the on-axis plies. Such a laminate is illustrated in Fig. 9 on

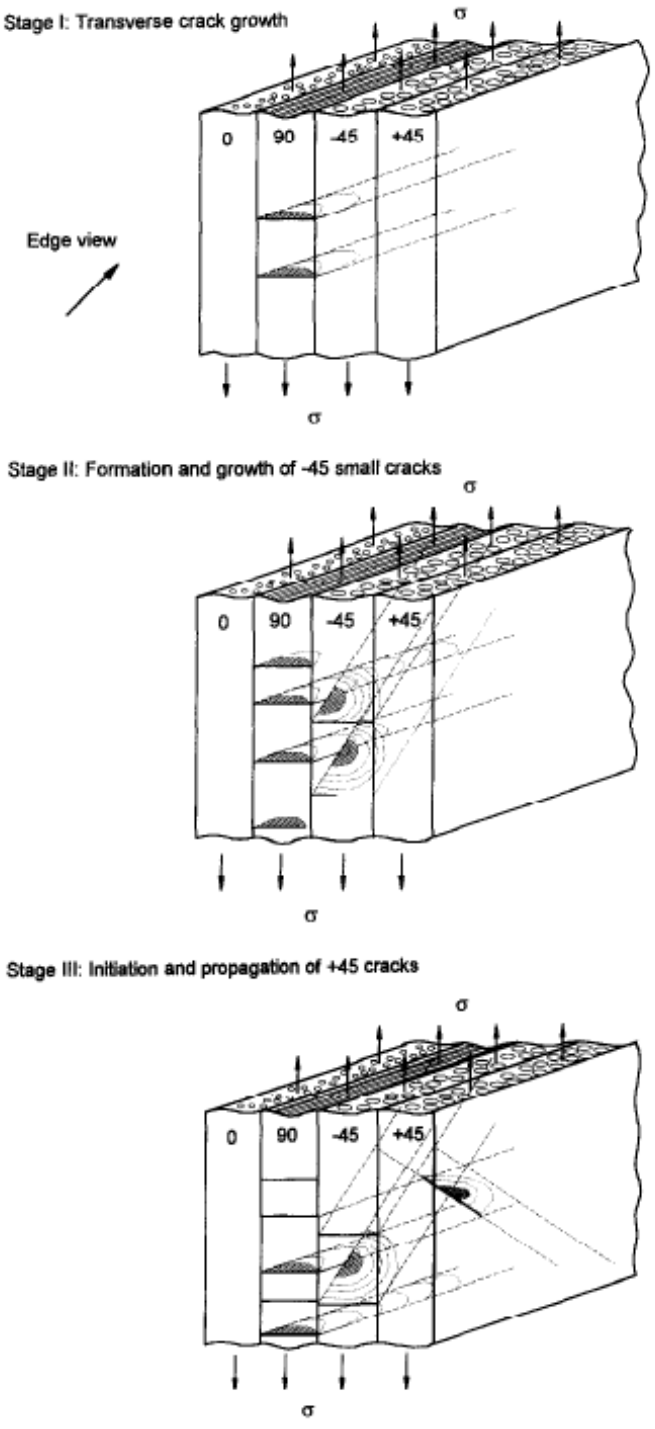

Fig. 39. Schematic representation of the matrix cracking sequence in quasi-isotropic $[0/90/\mp 45]_s$ laminate. Stage I: ply cracking in 90° ply, Stage II: Initiation and progression of small cracks in $-45°$ ply, Stage III: Initiation and Progression of cracks in $+45°$ ply. The figure is reproduced from [108].

page 9. Let the off-axis ply orientations be denoted by θ_1, θ_2, etc. The in-plane stress state in each of these plies with respect to the principal (material) axes is displayed in the figure. This stress state can attain a critical value for matrix cracking in one of the off-axis plies at an applied load, and with further increase of the load, multiple matrix cracking can ensue by the so-called shear-lag process. Similarly, the crack initiation and multiplication process in other off-axis plies can occur at different applied load values. Defining the set of intralaminar multiple cracks of a given orientation (θ_1, θ_2, etc.) as a damage mode, a load-induced multi-mode damage scenario can develop. To be sure, such a scenario is also possible under thermal loading (e.g. cooldown from curing temperature) or under a combined thermal and mechanical loading.

Since laminates are often designed to have plies aligned with the anticipated major load direction in order to sustain that load, while the off-axis plies are placed to provide the needed shear and transverse stiffness, the choice of $[0_m/\pm\theta_n/90_r]_s$ and $[0_m/90_r/\pm\theta_n]_s$ laminates for damage analysis presented here is intended to address many practical situations. Figure 40 illustrates the development of multiple damage modes in these laminate configurations under an axial tensile load. As indicated there, cracking initiates first in the 90-plies at an overall strain ϵ_0^{90}, and on increasing the load, this cracking multiplies. At the strain $\epsilon_0^{\theta_1}$ the θ_1-plies begin cracking and with further increase in the imposed load, an interactive cracking process continues in both ply orientations. Eventually, all off-axis plies can conduct the multiple cracking process. In the special case where two ply orientations have the same, or nearly the same, conditions (constraints) for cracking, two cracking modes can occur simultaneously. In earlier works [109, 170] it was found that in $[0_m/\pm\theta_n/0_{m/2}]_s$ laminates the crack densities in the $+\theta$ and $-\theta$ orientations could be assumed to be the same and their combined effect could be represented by a single equivalent damage mode. For the $[0_m/\pm\theta_n/90_r]_s$ and $[0_m/90_r/\pm\theta_n]_s$ laminates, we shall show later that the

cracking of the $\pm\theta$-plies also here with good approximation can be represented by one damage mode. Thus the total damage description in these laminates would require adding the 90°-ply cracking as a separate damage mode. Assuming that there are N damage entities of a given damage mode α in the RVE, the normal part of damage tensor is taken as [87, 89]

$$D_{ij}^{(\alpha)} = \frac{1}{V} \sum_{k_\alpha} \left[\int_S a n_i n_j \, \mathrm{d}S \right]_{k_\alpha} \tag{5.1}$$

where $n_i = (\sin\theta, \cos\theta, 0)$ are components of the unit vector normal to a matrix crack plane in the off-axis ply of orientation θ with respect to laminate longitudinal axis, V is volume of RVE and $k_\alpha = 1, 2, ..., N$. The surface area of a crack, S, and the influence vector magnitude, a, are specified as

$$S = \frac{t_c.W}{|\sin\theta|} \tag{5.2}$$

$$a = \kappa.t_c \tag{5.3}$$

where κ, called the constraint parameter, is an unspecified constant of (assumed) proportionality between a and the crack size t_c (also cracked-ply thickness), and W is the laminate width (Fig. 9). Assuming a to be constant over the crack surface, one gets from Eq. (5.1)

$$D_{ij}^{(\alpha)} = \frac{\kappa t_c^2}{s_\theta t \sin\theta} n_i n_j \tag{5.4}$$

where s_θ is the axial crack spacing in the cracked ply. The elastic stiffness tensor of the damaged laminate for in-plane response can be expressed as (see the derivation in previous chapter)

$$C_{pq} = C_{pq}^0 + \sum_\alpha C_{pq}^{(\alpha)} \tag{5.5}$$

where $p, q = 1, 2, 6$, C_{pq}^0 is the stiffness coefficient matrix of the virgin laminate and

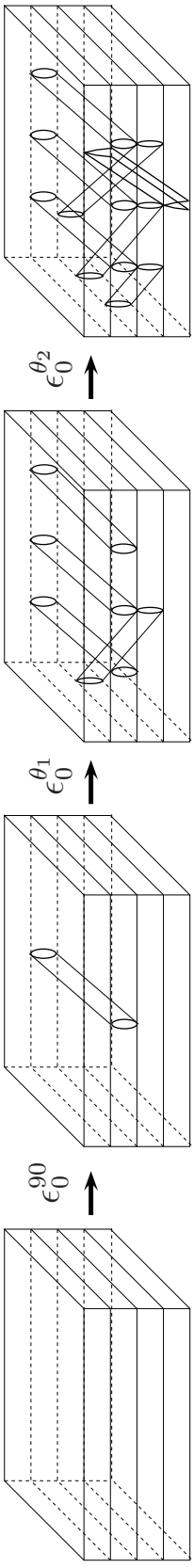

Fig. 40. Cracking process in $[0/90/\theta_1/\theta_2]_s$ half-laminate.

$\sum_{\alpha} C_{pq}^{(\alpha)}$ represents the total stiffness change due to all modes of matrix cracking averaged over the RVE.

The above relations have already been derived in the previous chapter, wherein $[0_m/\pm\theta_n/0_{m/2}]_s$ laminates were considered. There were two damage modes: $+\theta$ and $-\theta$ cracking modes. In the present scenario, we have the following three damage modes,

$$\text{Damage Mode 1} \Rightarrow \alpha = 1, \text{ cracks in } +\theta \text{ plies}$$
$$\text{Damage Mode 2} \Rightarrow \alpha = 2, \text{ cracks in } -\theta \text{ plies}$$
$$\text{Damage Mode 3} \Rightarrow \alpha = 3, \text{ cracks in } 90^\circ \text{ plies}$$

For two symmetric damage modes ($\pm\theta$), it was established in the previous chapter that the stiffness matrix of a thin laminates loaded in its plane can be written as

$$C_{pq}^{(1)} + C_{pq}^{(2)} = D_\theta \begin{bmatrix} 2a_1 & a_4 & 0 \\ & 2a_2 & 0 \\ Symm & & 2a_3 \end{bmatrix} \tag{5.6}$$

where

$$D_\theta = \frac{\kappa_\theta t_c^2}{s_n^\theta t} \tag{5.7}$$

where s_n^θ is the normal crack density, and t_c and t are thickness of the cracked ply and of the whole laminate, respectively.

Considering now that additionally, we have cracks in the 90°-plies for which the damage mode $\alpha = 3$ has the following components

$$D_1^{(3)} = \frac{\kappa_{90} t_{90}^2}{s^{90} t}, D_2^{(3)} = D_6^{(3)} = 0 \tag{5.8}$$

where $a_i^{'}, i = 1, 2, 3, 4$ are material constants. The integrity bases, Eq. (4.15), has an additional term $D_1^{(3)}$, and the free energy function gets the following additional

terms,

$$\rho\psi\,(\alpha=3) = a_1^{'}\epsilon_1^2 D_1^{(3)} + a_2^{'}\epsilon_2^2 D_1^{(3)} + a_3^{'}\epsilon_6^2 D_1^{(3)} + a_4^{'}\epsilon_1\epsilon_2 D_1^{(3)} \tag{5.9}$$

Following the steps taken above, we get

$$\begin{gathered} C_{11}^{(3)} = 2a_1^{'}D_1^{(3)}, \qquad C_{22}^{(3)} = 2a_2^{'}D_1^{(3)} \\ C_{12}^{(3)} = a_4^{'}D_1^{(3)}, \qquad C_{66}^{(3)} = 2a_3^{'}D_1^{(3)} \\ C_{16}^{(3)} = C_{26}^{(3)} = 0 \end{gathered} \tag{5.10}$$

It is noted here that for $[0_m/\pm\theta_n/90_r]_s$ laminate, $\pm\theta$-modes occur twice (below and above the laminate mid-plane) whereas the central 90°-mode occurs only once. Thus, the total stiffness change ΔC_{pq} with all the three modes active is given by

$$\begin{aligned} \Delta C_{pq} &= 2\left\{C_{pq}^{(1)} + C_{pq}^{(2)}\right\} + C_{pq}^{(3)} \\ &= 2D_\theta \begin{bmatrix} 2a_1 & a_4 & 0 \\ a_4 & 2a_2 & 0 \\ 0 & 0 & 2a_3 \end{bmatrix} + D_{90} \begin{bmatrix} 2a_1^{'} & a_4^{'} & 0 \\ a_4^{'} & 2a_2^{'} & 0 \\ 0 & 0 & 2a_3^{'} \end{bmatrix} \end{aligned} \tag{5.11}$$

where

$$D_{90} = D_1^{(3)} = \frac{\kappa_{90}t_{90}^2}{s^{90}t} \tag{5.12}$$

Now consider $\theta = 90^\circ$ in the $[0_m/\pm\theta_n/90_r]_s$ laminate. Let the normal crack spacing be the same in all cracked plies, i.e., $s_n^{\theta^+} = s_n^{\theta^-} = s^{90}$. Then, the terms of ΔC_{pq} matrix become, as illustrated by ΔC_{11} as

$$\begin{aligned} \Delta C_{11} &= 2\left\{C_{11}^{(1)} + C_{11}^{(2)}\right\} + C_{11}^{(3)} = 4D_\theta|_{\theta=90}a_1(90) + 2D_{90}a_1^{'} \\ &= \frac{4\kappa_{\theta=90}(t_0.2n)^2}{s^{90}t}a_1(90) + \frac{2\kappa_{90}(t_0.2r)^2}{s^{90}t}a_1^{'} \qquad (5.13) \\ &= \frac{8t_0^2}{s^{90}t}\left[2n^2\kappa_{\theta=90}a_1(90) + r^2\kappa_{90}a_1^{'}\right] \qquad (5.14) \end{aligned}$$

where t_0 is a single ply thickness. We can consider this stiffness change to be the

same as that for a $[0_m/90_{2n+r}]_s$ laminate with a single mode of damage given by

$$D_1 = \frac{\kappa_{90_{4n+2r}} t_0^2 . \{(4n+2r)\}^2}{s^{90} t} \tag{5.15}$$

where the sub-subscript on κ_{90} denotes the crack size. The stiffness change ΔC_{11} will then be

$$\Delta C_{11} = 2a_1^{'} D_1 = \frac{8t_0^2}{s^{90} t}(2n+r)^2 \kappa_{90_{4n+2r}} a_1^{'} \tag{5.16}$$

Equating ΔC_{11} from Eq. (5.13) and Eq.(5.16), we have

$$2n^2 \kappa_\theta|_{\theta=90} a_1(90) + r^2 \kappa_{90} a_1^{'} = (2n+r)^2 \kappa_{90_{4n+2r}} a_1^{'} \tag{5.17}$$

Solving the above equation, we obtain

$$a_1(90) = \left[\frac{(2n+r)^2 \kappa_{90_{4n+2r}} - r^2 \kappa_{90}}{2n^2 \kappa_\theta|_{\theta=90}}\right] a_1^{'} \tag{5.18}$$

Thus, the inter-relation between a_i and $a_i^{'}$ constants is given by

$$a_i = \left[\frac{(2n+r)^2 \kappa_{90_{4n+2r}} - r^2 \kappa_{90}}{2n^2 \kappa_\theta|_{\theta=90}}\right] a_i^{'} \tag{5.19}$$

Substituting (5.19) into (5.11), we obtain ΔC_{pq} for damaged $[0_m/\pm\theta_n/90_r]_s$ laminate as

$$\begin{aligned} \Delta C_{pq} &= 2\left\{C_{pq}^{(1)} + C_{pq}^{(2)}\right\} + C_{pq}^{(3)} = \frac{4t_0^2}{t}\left[2n^2 \frac{\kappa_\theta}{s_n^\theta}[a_i] + r^2 \frac{\kappa_{90}}{s^{90}}[a_i^{'}]\right] \\ &= \frac{4t_0^2}{t}\left[\frac{1}{s_n^\theta}\frac{\kappa_\theta}{\kappa_\theta|_{\theta=90}}\left\{(2n+r)^2 \kappa_{90_{4n+2r}} - r^2 \kappa_{90}\right\} + r^2 \frac{\kappa_{90}}{s^{90}}\right][a_i^{'}] \end{aligned} \tag{5.20}$$

where $[a_i]$ and $[a_i^{'}]$ represent the coefficient matrices, appearing as multiplying factors to $2D_\theta$ and D_{90}, respectively, in Eq. (5.11).

Thus, the entire stiffness matrix is given by

$$C_{pq} = \begin{bmatrix} \frac{E_1^0}{1-\nu_{12}^0\nu_{21}^0} & \frac{\nu_{12}^0 E_2^0}{1-\nu_{12}^0\nu_{21}^0} & 0 \\ & \frac{E_2^0}{1-\nu_{12}^0\nu_{21}^0} & 0 \\ Symm & & G_{12}^0 \end{bmatrix} + \bar{D} \begin{bmatrix} 2a_1^{'} & a_4^{'} & 0 \\ & 2a_2^{'} & 0 \\ Symm & & 2a_3^{'} \end{bmatrix} \tag{5.21}$$

where

$$\bar{D} = \frac{4t_0^2}{t} \left[\frac{1}{s_n^\theta} \frac{\kappa_\theta}{\kappa_\theta\big|_{\theta=90}} \left\{ (2n+r)^2 \kappa_{90_{4n+2r}} - r^2 \kappa_{90} \right\} + r^2 \frac{\kappa_{90}}{s^{90}} \right] \tag{5.22}$$

where t_0 is the thickness of a single ply, s_n^θ and s^{90} are the normal crack spacings in $\pm\theta$ and 90°-plies, respectively, and the constraint parameters are defined as

$$\kappa_\theta = \frac{\left(\overline{\Delta u_y}\right)_{\pm\theta_{2n}}}{2nt_0}; \qquad \kappa_{90_{4n+2r}} = \frac{\left(\overline{\Delta u_y}\right)_{90_{4n+2r}}}{(4n+2r)t_0}; \qquad \kappa_{90} = \frac{\left(\overline{\Delta u_y}\right)_{90_{2r}}}{2rt_0} \tag{5.23}$$

where subscript denotes a particular damage mode (orientation of cracked plies) and sub-subscript represents the number of cracked plies corresponding to that damage mode. $\overline{\Delta u_y}$ is the crack opening displacement (COD) averaged over thickness of the cracked ply, and is defined as

$$\overline{\Delta u_y} = \frac{1}{t_c} \int_{-t_c/2}^{t_c/2} \Delta u_y(z)\ \mathrm{d}z \tag{5.24}$$

where Δu_y represents the separation of crack planes in the direction normal to the crack face with the local coordinate system (x, y, z) placed on the crack as shown in Fig. 21. Since the 90° cracks are centrally placed along the laminate thickness, the crack size for 90° damage mode is $2nt_0$. The corresponding crack size for the $\pm\theta$ damage mode is $2nt_0$. The central mode occurs once in the damaged laminate, while the non-central mode occurs twice (on either side of the laminate mid-plane).

The stiffness-damage relationships for $[0_m/90_r/\pm\theta_n]_s$ laminates can be obtained by following the same steps as described above. It must be noted that unlike $[0_m/\pm\theta_n/90_r]_s$ laminates, $\pm\theta$ damage mode in this case is centrally placed, thereby the

corresponding equivalent crack size is $4nt_0$. On the other hand, the crack size for the 90° damage mode is rt_0. Analogous to the Eq. (5.11), for this case ΔC_{pq} is given by

$$\begin{aligned}\Delta C_{pq} &= \left\{C_{pq}^{(1)} + C_{pq}^{(2)}\right\} + 2C_{pq}^{(3)} \\ &= 2D_\theta \begin{bmatrix} 2a_1 & a_4 & 0 \\ a_4 & 2a_2 & 0 \\ 0 & 0 & 2a_3 \end{bmatrix} + D_{90} \begin{bmatrix} 2a_1' & a_4' & 0 \\ a_4' & 2a_2' & 0 \\ 0 & 0 & 2a_3' \end{bmatrix}\end{aligned} \tag{5.25}$$

and ΔC_{11} is given as

$$\Delta C_{11}(90) = \frac{8t_0^2}{s^{90}t}\left[n^2\kappa_{\theta=90}a_1(90) + 2r^2\kappa_{90}a_1'\right] \tag{5.26}$$

Equating this to ΔC_{11} for reference laminate $[0_m/90_{2n+r}]_s$ laminate, Eq. (5.16), we obtain the following inter-relationships between a_i and a_i' constants for $[0_m/90_r/\pm\theta_n]_s$ laminates,

$$a_i = \left[\frac{(2n+r)^2\kappa_{90_{4n+2r}} - 2r^2\kappa_{90}}{n^2\kappa_\theta|_{\theta=90}}\right]a_i' \tag{5.27}$$

Substituting (5.27) into (5.25), the entire stiffness matrix for damaged $[0_m/90_r/\pm\theta_n]_s$ laminate is given by

$$C_{pq} = \begin{bmatrix} \frac{E_1^0}{1-\nu_{12}^0\nu_{21}^0} & \frac{\nu_{12}^0E_2^0}{1-\nu_{12}^0\nu_{21}^0} & 0 \\ & \frac{E_2^0}{1-\nu_{12}^0\nu_{21}^0} & 0 \\ Symm & & G_{12}^0 \end{bmatrix} + \bar{D}\begin{bmatrix} 2a_1' & a_4' & 0 \\ & 2a_2' & 0 \\ Symm & & 2a_3' \end{bmatrix} \tag{5.28}$$

Clearly, the derived stiffness-damage relationships retain the form of equation (5.21). However $\bar{D}$ in this case is given by

$$\bar{D} = \frac{2t_0^2}{t}\left[\frac{1}{s_n^\theta}\frac{\kappa_\theta}{\kappa_\theta|_{\theta=90}}\left\{2(2n+r)^2\kappa_{90_{4n+2r}} - r^2\kappa_{90}\right\} + r^2\frac{\kappa_{90}}{s^{90}}\right] \tag{5.29}$$

with the corresponding constraint parameters given as

$$\kappa_\theta = \frac{\left(\overline{\Delta u_y}\right)_{\pm\theta_{4n}}}{4nt_0}; \qquad \kappa_{90_{4n+2r}} = \frac{\left(\overline{\Delta u_y}\right)_{90_{4n+2r}}}{(4n+2r)t_0}; \qquad \kappa_{90} = \frac{\left(\overline{\Delta u_y}\right)_{90_r}}{rt_0} \tag{5.30}$$

From stiffness-damage relationships (Eq. (5.21)), the engineering moduli for the damaged laminate can now be derived using the following relationships

$$E_1 = \frac{C_{11}C_{22} - C_{12}^2}{C_{22}}; \quad E_2 = \frac{C_{11}C_{22} - C_{12}^2}{C_{11}}; \quad \nu_{12} = \frac{C_{12}}{C_{22}}; \quad G_{12} = C_{66} \tag{5.31}$$

Thus,

$$E_1 = \frac{E_1^0}{1-\nu_{12}^0\nu_{21}^0} + 2\bar{D}a_1^{'} - \frac{\left[\frac{\nu_{12}^0 E_2^0}{1-\nu_{12}^0\nu_{21}^0} + \bar{D}a_4^{'}\right]^2}{\frac{E_2^0}{1-\nu_{12}^0\nu_{21}^0} + 2\bar{D}a_2^{'}} \tag{5.32}$$

$$E_2 = \frac{E_2^0}{1-\nu_{12}^0\nu_{21}^0} + 2\bar{D}a_2^{'} - \frac{\left[\frac{\nu_{12}^0 E_2^0}{1-\nu_{12}^0\nu_{21}^0} + \bar{D}a_4^{'}\right]^2}{\frac{E_1^0}{1-\nu_{12}^0\nu_{21}^0} + 2\bar{D}a_1^{'}} \tag{5.33}$$

$$\nu_{12} = \frac{\frac{\nu_{12}^0 E_2^0}{1-\nu_{12}^0\nu_{21}^0} + \bar{D}a_4^{'}}{\frac{E_2^0}{1-\nu_{12}^0\nu_{21}^0} + 2\bar{D}a_2^{'}} \tag{5.34}$$

$$G_{12} = G_{12}^0 + 2\bar{D}a_3^{'} \tag{5.35}$$

In the above expressions, the constants $a_i^{'}$, $i = 1, 2, 3, 4$ are material constants representing the effect of cracking on laminate stiffness properties. The usual way to obtain them is through experimental data for a selected reference laminate, e.g. a cross ply laminate ($\theta = 90°$), at a certain crack density. However, an alternative and more general way is by numerical simulation, which will be discussed later.

The flow chart in Fig. 41 describes the procedure for multiscale synergistic methodology for multimode damage assessment. Computational micromechanics involves analysis of a representative unit cell to determine the COD values and the constraint parameters. In a separate step, the material constants $a_i^{'}$ appearing in Eq. (5.32)-(5.35) are determined from experiments or numerical simulations carried for a

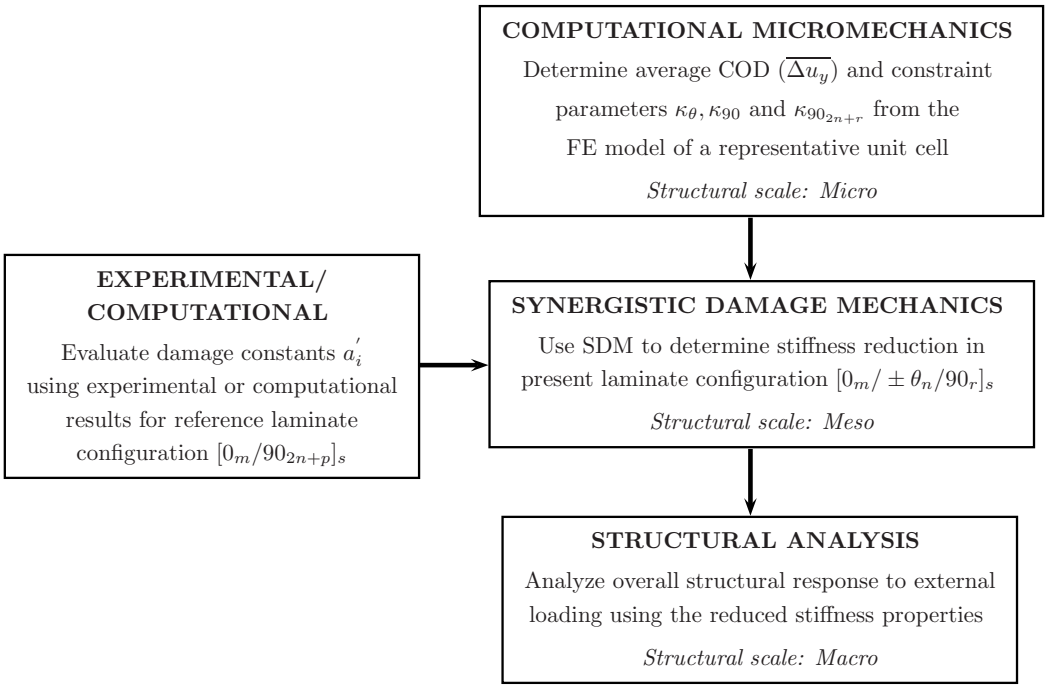

Fig. 41. Multi-scale synergistic methodology for analyzing damage behavior in a general symmetric laminate $[0_m/\pm\theta_n/90_r]_s$ with matrix cracks in $+\theta$, $-\theta$, and 90° layers.

reference laminate, specifically, $[0/90_3]_s$. These relations are then employed to predict stiffness degradation with constraint parameters and material constants obtained from experiments (or FE simulations) as inputs. In the final step, the overall structural behavior in response to external loading can be analyzed based on the degraded stiffness properties for the damaged laminate.

D. FE Modeling

As described in Section 2, SDM uses micromechanics modeling to evaluate the constraint effects of undamaged plies over cracked plies. Three-dimensional FE analysis is performed here as a micromechanical tool to calculate the constraint parameters. A representative unit cell of the RVE for $[0_m/\pm\theta_n/90_r]_s$ laminate configuration with

imposed symmetry boundary conditions is shown in Fig. 21 on page 57. In FE analyses, the cell size is taken sufficiently large so as to avoid significant interaction between adjacent cracks in an individual ply. Each ply in the laminate is 0.125 mm thick. The ply material is glass- epoxy (HyE 9082Af, Fiberite) with in-plane properties E_{11}=44.7 GPa, E_{22}=12.7 GPa, G_{12}=5.8 GPa and ν_{12}=0.297. To obtain the remaining properties for use in the 3-D model, the unidirectional ply is assumed transversely isotropic in the cross-sectional plane. Thus, $E_{33} = E_{22} = 12.7$ GPa; $G_{13} = G_{12} = 5.8$ GPa; $\nu_{13} = \nu_{12}$=0.297; $G_{23} = \frac{E_{22}}{2(1+\nu_{23})}$=4.885 GPa. The Poisson's ratio ν_{23} in the isotropic cross-sectional plane is taken as 0.3.

Separate 3-D FE models were constructed for ply orientations, θ = 25, 40, 55, 70, 80 and 90°, accounting for the mid-plane symmetry. As noted earlier, the matrix cracks were taken to have grown across the entire width of the specimen. ANSYS SOLID45 (eight-noded isoparametric) elements were used. Each FE model contained 10,000-50,000 elements to ensure sufficient accuracy of FE computations. A smooth flow of mesh through the thickness was obtained using mapped meshing. Aspect ratio of elements near the crack surfaces was kept close to 1.0 for better accuracy. Linear Elastic FE analyses were carried out on unit cells using ANSYS 10.0 at 0.5 % axial strain. More details on the 3-D FE methodology can be found in chapter III.

Due to presence of cracked surfaces in three directions ($+\theta, -\theta$ and 90°), it is not possible to construct a fully periodic unit cell for the cracked laminate. Since there is no periodicity in the width direction, the width of the unit cell is chosen large enough such that the errors due to effects from the free edges are negligible. Thus the cell used is not a unit cell, but a "representative" unit cell.

In a real scenario (experiments), the crack spacing may be different in different plies. To account for this, two extreme situations are modeled here. The first case refers to the scenario when cracks in all cracked layers intersect at the same X_1

location and hence there is maximum interaction between cracks. The other extreme is when the cracks in different cracked layers are far apart and do not interact. The real behavior will be between the two extremes. The unit cell shown in Fig. 21 on page 57 actually refers to the first scenario.

E. Results and Discussion

1. FE Simulations Methodology

As can be seen from the flowchart in Fig. 41, SDM requires determination of material constants $a_i^{'}$ from the results for a reference laminate. For the present case of $[0_m/\pm\theta_n/90_r]_s$ laminates, we choose $[0/90_3]_s$, i.e., $\theta = 90^\circ$ and $m = n = r = 1$, as the reference laminate. The stiffness-damage results for this cross-ply laminate can be obtained in a variety of ways. The most obvious way would be by using experimental data. However, although experiments reflect the real material behavior, they can be performed for limited cases. An alternative and more general way is to use a numerical tool such as an FE model to simulate stiffness degradation. FE simulations are in fact easier to carry out and have no scatter other than the accuracy of computations that may depend on mesh density and implementation of boundary conditions. Moreover, they can also be used to predict stiffness changes in other laminate layups. Thus, in what follows next, we will compare SDM predictions with independent FE simulations.

To gain confidence in the above approach for cracked off-axis laminates, we first validated the FE simulations methodology with the experimental data. Using an FE model, stiffness degradation in $[0/\pm\theta_4/0_{1/2}]_s$ glass-epoxy laminates was simulated. The crack density along X_1 direction (or equivalently, the crack spacing) was varied by changing the length of the unit cell considered. Linear FE analyses using ANSYS

10.0 were conducted for crack spacing, $s_\theta = 16, 8, 4, 3, 2, 1.5, 1.25, 1, 0.75, 0.6$ and 0.5 mm. The FE simulations compared well with the published experimental data [109] for $[0/90_8/0_{1/2}]_s$ and $[0/\pm 70_4/0_{1/2}]_s$ laminate configurations. The details have already been covered in chapter III.

2. SDM Predictions

Following the SDM flowchart (Fig. 41), stiffness prediction entails three main steps:

1. Using FE computations, evaluate constraint parameters for each damage mode and the effective damage parameter $\bar{D}$, given by Eq. (5.22) and (5.23).

2. Determinate damage constants $a_i^{'}$ appearing in Eq. (5.21) using the stiffness degradation data for a pre-selected reference laminate, viz. $[0/90_3]_s$.

3. Predict stiffness changes for $[0_m/\pm\theta_n/90_r]_s$ laminates using the stiffness-damage relations (Eq. (5.32)-(5.35)).

We will describe these steps in the following paragraphs.

a. CODs and interaction between damage modes

As seen from Eq. (5.23), the constraint parameters are given as average COD ($\overline{\Delta u_y}$) normalized by crack size (or thickness of the cracked layer). To estimate $\overline{\Delta u_y}$ numerically (Eq. (5.24)), Δu_y is determined from nodal y-direction (normal to the crack plane) displacements averaged over the entire crack surface. CODs in two symmetric modes ($+\theta$ and $-\theta$-cracks) are added together to get $\overline{\Delta\left(u_y\right)_{\pm\theta}}$ based on an observation in our previous paper [170] that these two symmetric damage modes can be added together to yield one equivalent damage mode.

For $[0_m/\pm\theta_n/90_r]_s$ laminates, three cracking modes are present in the damaged material. Due to similarity in the constraining nature and the influence on material

response of the cracks in $+\theta$ and $-\theta$ layers, these cracking modes can be coupled together to yield one effective $\pm\theta$-damage mode (see Appendix). However, $\pm\theta$ and 90° cracking modes can interact and influence the stress pattern around cracks in cracked as well as in un-cracked layers, thereby affecting the overall stiffness properties of the cracked laminate. Thus, one needs to incorporate this interaction between different cracking modes into the damage model.

The stiffness-damage relations derived in the present work do not explicitly account for the interaction between different damage modes because the polynomial used for Helmholtz free energy function does not contain terms involving product of $D_{ij}^{(\alpha)}$ terms, e.g., $D_1^{(1)}D_1^{(2)}, D_2^{(1)}D_2^{(2)}$, etc. However, the SDM approach provides an indirect means of dealing with intra-mode interaction through calculation of COD using FE model with multi-mode cracks. Let us consider the following two cases

1. No interaction between damage modes: This scenario will exist when the cracks in different damage modes are far apart and thus their mutual interaction is not significant. This can be simulated in the FE model by considering two damage modes separately and then adding (superposing) their effects. Thus, for $[0_m/\pm\theta_n/90_r]_s$ laminate, we carry out COD calculations in two different cracking conditions. In the first case, cracks are present only in $\pm\theta_n$ layers, while in the second case cracks are present only in the 90_r layers.

2. Maximum interaction between damage modes: This scenario will occur when the cracks in different damage modes are sufficiently close to cause additional perturbation in the stress fields on top of that due to individual damage modes. The total perturbation effect can be captured in the SDM technique indirectly in the calculated COD when both $\pm\theta_n$ and 90_r layers are cracked. The interaction effect is actually observed in experiments, e.g., for $[0/90/-45/45]_s$

laminates, Tong et al. [108] observed that -45° cracks grew from the points of intersection of the 90° cracks at the $90^\circ/-45^\circ$ interface, and $+45^\circ$ cracks initiated at the locations where -45° cracks met the $-45^\circ/+45^\circ$ interface. Hence, while modeling multi-mode damage scenario, one should consider these interaction effects.

It is noteworthy here that the two cases represent extremes and the real material behavior is expected to be somewhere in between.

The normalized average CODs for various laminate layups are given in Table II. The average CODs are nondimensionalized by the cracked-ply thickness ($10^3\frac{\overline{\Delta u_y}}{t_c}$) to give the constraint parameters. The first and the second halves in the table refer to the two cases described above. The columns in the table give the normalized average CODs for layers in this order: $+\theta$, $-\theta$, their average (i.e., for the combined $\pm\theta$ damage mode), and then 90°. $[0/\pm 90/90]_s$ is just a hypothetical case where cracks are in ± 90 layers. This is done in order to get $\kappa_\theta|_{\theta=90}$ (see Eq. (5.22)-(5.23)). From the table, it can be observed that the influence of crack interaction is the least for $+\theta$-cracking mode, and the highest for 90° mode. As θ in $[0_m/\pm\theta_n/90_r]_s$ laminates increases, this interaction becomes increasingly significant. It can also be observed that the interaction is not influential for ply orientations away from 90°. Figure 42 depicts the variation of average normalized COD ($\left(\hat{u} = 10^3\frac{\overline{\Delta u_y}}{t_c}\right)$) for $\pm\theta$ and 90° cracking with increase in θ. It can be seen that the interaction between stress perturbations due to different damage modes affects the average COD significantly. It should, however, be pointed out that the FE analysis performed here assumes same crack density in 90° and $\pm\theta$ plies, which is more severe situation than in reality. Experiments on quasi-isotropic laminates show that $\pm 45^\circ$ cracks initiate much after 90° cracks, and their crack density will be lower. Moreover, unlike cracks in 90° layers, $\pm 45^\circ$ cracks do

Table II. Normalized average COD $\left(10^3 \frac{\overline{\Delta u_y}}{t_c}\right)$.

Laminate	Non-interacting Modes				Interacting Modes			
Configuration	$+\theta$ layer	$-\theta$ layer	$\pm\theta$ layer	90° layer	$+\theta$ layer	$-\theta$ layer	$\pm\theta$ layer	90° layer
$[0/\pm 25/90]_s$	0.92	1.08	1.00	5.30	0.93	1.09	1.01	5.31
$[0/\pm 40/90]_s$	2.00	2.21	2.11	5.68	2.03	2.23	2.13	5.70
$[0/\pm 55/90]_s$	4.38	4.66	4.52	6.31	4.83	6.05	5.44	7.50
$[0/\pm 70/90]_s$	6.13	6.64	6.38	6.72	7.09	9.86	8.48	9.06
$[0/\pm 80/90]_s$	7.37	8.09	7.74	6.84	8.53	12.02	10.27	9.22
$[0/\pm 90/90]_s$	–	–	–	–	–	–	11.44	–
$[0/90_3]_s$	–	–	–	–	–	–	–	7.11
$[0_2/\pm 55/90]_s$	4.30	4.60	4.45	6.25	4.70	5.91	5.31	7.39
$[0/\pm 55_2/90]_s$	4.78	5.14	4.96	6.27	5.07	6.13	5.60	9.72
$[0/\pm 55/90_2]_s$	4.47	4.71	4.59	6.83	5.58	7.68	6.63	7.71

not grow fully. Hence, the intra-mode crack interaction will be lower than predicted here. The influence of crack interaction on stiffness changes will be discussed in the following sub-sections.

b. Calculation of damage constants $a_i^{'}$

In the second step, we obtain damage constants $a_i^{'}$ using the degradation results for the reference laminate configuration $[0/90_3]_s$. Although these results can be taken from experimental data or an analytical model, we use FE for calculation of stiffness changes for this reference laminate configuration as per the discussion above. Using Eq. (5.21) with $\theta = 90$ and a preselected $s_n^{\theta} = s^{90} = s_0$, we obtain

$$\begin{bmatrix} \frac{E_1^0}{1-\nu_{12}^0\nu_{21}^0} & \frac{\nu_{12}^0 E_2^0}{1-\nu_{12}^0\nu_{21}^0} & 0 \\ & \frac{E_2^0}{1-\nu_{12}^0\nu_{21}^0} & 0 \\ Symm & & G_{12}^0 \end{bmatrix} + \bar{D}_0 \begin{bmatrix} 2a_1^{'} & a_4{'} & 0 \\ & 2a_2^{'} & 0 \\ Symm & & 2a_3^{'} \end{bmatrix} = \begin{bmatrix} \frac{E_1}{1-\nu_{12}\nu_{21}} & \frac{\nu_{12}E_2}{1-\nu_{12}\nu_{21}} & 0 \\ & \frac{E_2}{1-\nu_{12}\nu_{21}} & 0 \\ Symm & & G_{12} \end{bmatrix} \tag{5.36}$$

where $\bar{D}_0 = \bar{D}|_{s_n^{\theta}=s^{90}=s_0,\theta=90^{\circ}}$, and the right-hand side of the equation represents the stiffness matrix of the damaged laminate expressed in terms of $E_1, E_2, G_{12}, \nu_{12}$ and ν_{21} evaluated at crack density $s_n^{\theta} = s^{90} = s_0$. Solving this equation the material constants of interest can be written as

$$\begin{aligned} a_1^{'} &= \frac{1}{2\bar{D}_0}\left[\frac{E_1}{1-\nu_{12}\nu_{21}} - \frac{E_1^0}{1-\nu_{12}^0\nu_{21}^0}\right] \\ a_2^{'} &= \frac{1}{2\bar{D}_0}\left[\frac{E_2}{1-\nu_{12}\nu_{21}} - \frac{E_2^0}{1-\nu_{12}^0\nu_{21}^0}\right] \\ a_4^{'} &= \frac{1}{\bar{D}_0}\left[\frac{\nu_{12}E_1}{1-\nu_{12}\nu_{21}} - \frac{\nu_{12}^0E_1^0}{1-\nu_{12}^0\nu_{21}^0}\right] \end{aligned} \tag{5.37}$$

For the present study, we have calculated the constants $a_i^{'}$ with FE data for the reference $[0/90_3]_s$ laminate with $s_0 = 1$ mm, given as: $E_1 = 0.675\ E_1^0, E_2 = E_2^0, \nu_{12} = 0.464\ \nu_{12}^0$. Fig. 43 shows the variation of longitudinal Young's modulus and the

(a)

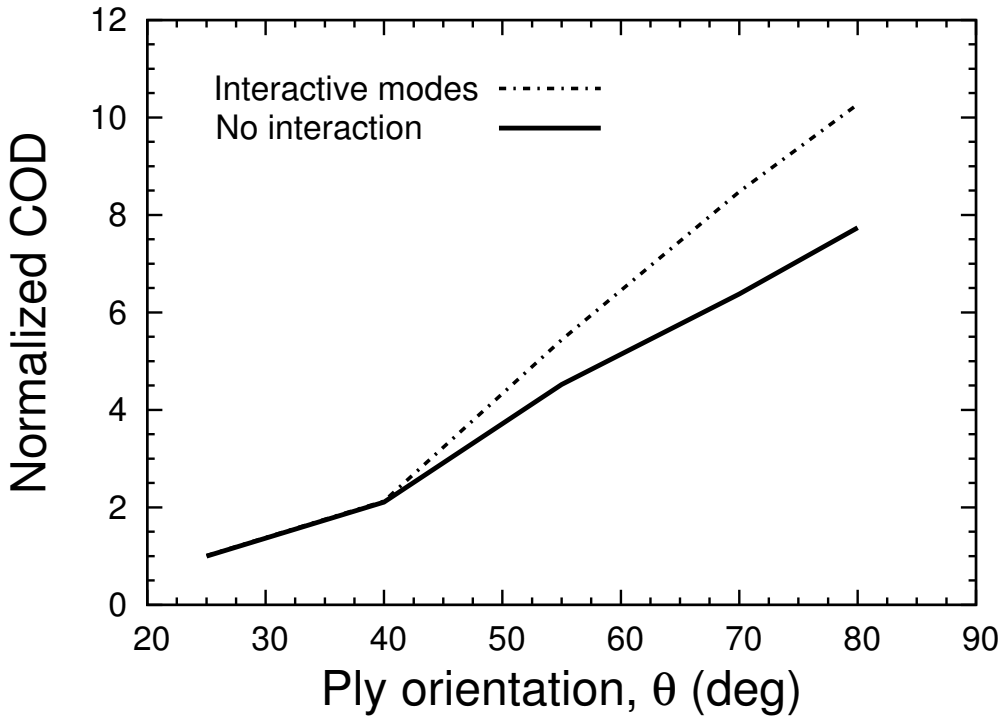

(b)

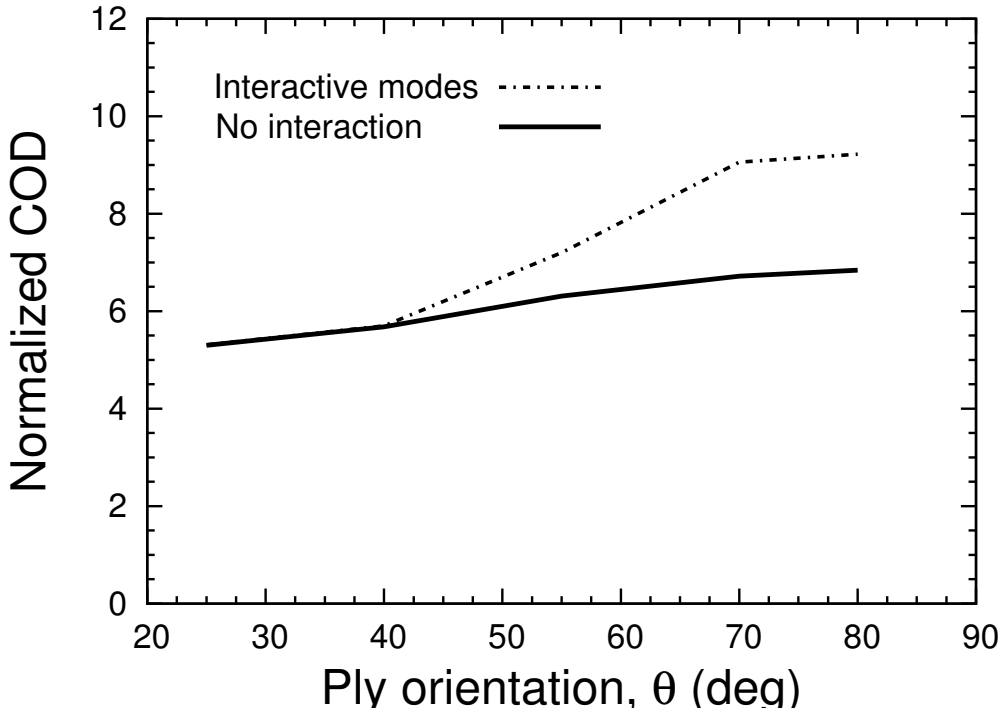

Fig. 42. Variation of normalized average COD $\left(\hat{u} = 10^3 \frac{\overline{\Delta u_y}}{t_c}\right)$ with ply orientation: (a) for $\pm\theta$ cracking mode, (b) for 90° cracking mode.

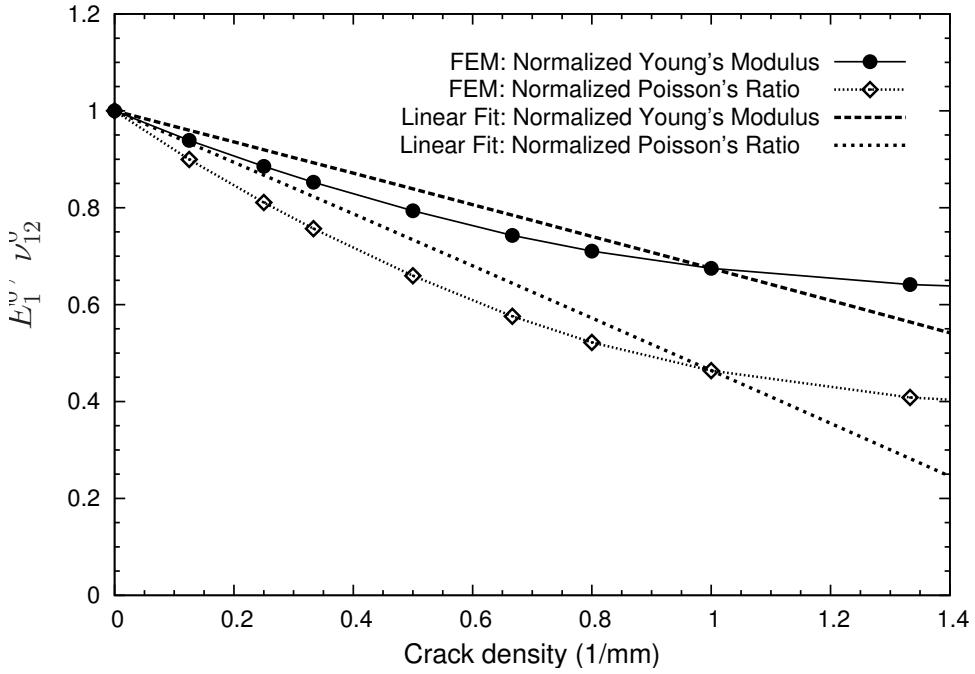

Fig. 43. Stiffness reduction for $[0/90_3]_s$ laminate by FE simulations. These results form the basis for computation of CDM constants.

Poisson's ratio with respect to the crack density for the reference $[0/90_3]_s$ laminate. The moduli values shown in the figure are normalized with the corresponding virgin state values. These FE results form the basis for computation of CDM constants, $a_i^{'}$. It is noted that the shear modulus for the cracked laminate can in principle be treated using Eq. (5.35) independent of the other moduli. But it needs evaluation of constant $a_3^{'}$, which would require setting up a boundary value problem different from that needed to determine the other moduli. Hence, we shall not treat the shear modulus here.

c. Predicted stiffness changes for $[0/\pm\theta/90]_s$ laminates

Finally, Eq. (5.32)-(5.34) are used to predict the stiffness degradation in $[0/\pm\theta/90]_s$ laminates for different ply orientations. The comparison of SDM predictions and FE

simulations for $\theta = 70, 55$ and 40° are shown in Figs. 44-46. SDM predictions are made using CODs determined for interacting damage modes (i.e., both $\pm\theta$ and 90° cracks present) as well as non-interacting damage modes. For $\theta = 70^\circ$ and 55°, SDM predictions agree reasonably well with FE simulations. However, for $\theta = 40^\circ$, SDM procedure predicts less severe degradation in axial modulus and in-plane Poisson's ratio than FE computations. This appears to be because the assumption in Eq. (4.34) is expected to limit the accuracy of the procedure to θ-angles greater than 60°. However, the experimental studies (e.g., [108, 109]) have also shown that for axially loaded laminates, transverse cracks do not grow fully for ply orientations below $\theta = 55^\circ$ and the failure in laminates is actually induced by delamination.

It is important to note that in the present study, we have not considered the degradation of shear modulus due to shear deformation in off-axis plies. This is still a less-understood topic. However, one can include shear deformation effects indirectly into SDM by using shear modulus variation with respect to applied loading as shown by Varna et al. [109].

d. Predictions for quasi-isotropic laminates

The experimental data available for stiffness degradation in off-axis laminates involving cracks in multiple ply orientations under quasi-static loading are limited to quasi-isotropic laminates. Here we compare our predictions with the work by Tong et al. [108], who carried extensive measurements of stiffness degradation in $[0/90/\mp 45]_s$ glass-epoxy laminate. They observed partially initiated cracks in $\mp 45^\circ$-layers and plotted stiffness changes of the whole laminate as a function of 90°-cracking density.

For stiffness predictions using the SDM approach, the corresponding material constants $a_i^{'}$ are evaluated from experimental data for $[0/90]_s$ laminate, shown in Fig. 47. The individual ply thickness for this laminate is 0.5 mm. This laminate

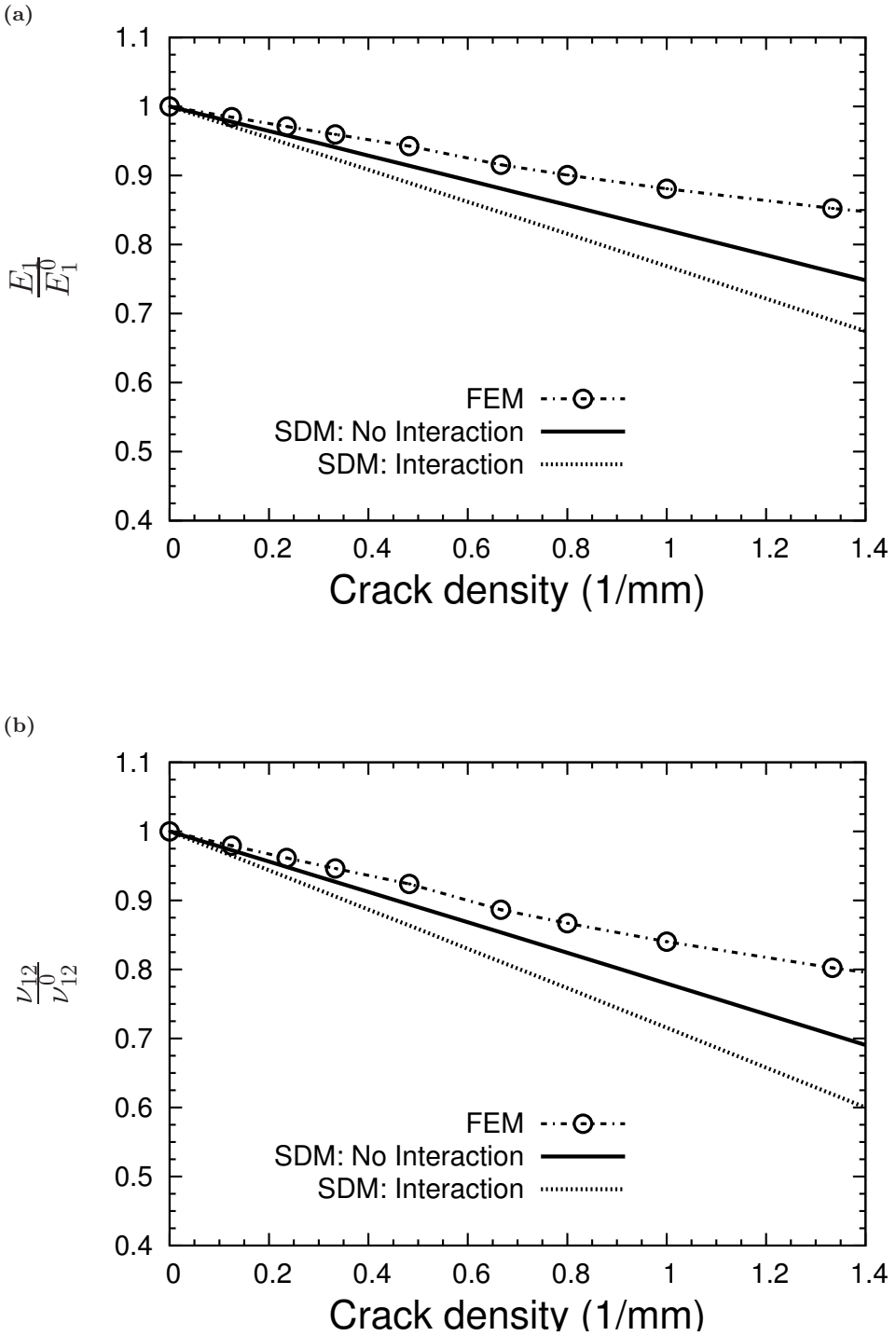

Fig. 44. Stiffness reduction for $[0/\pm 70/90]_s$ laminate compared with FE simulations. The crack density is along X_1 direction.

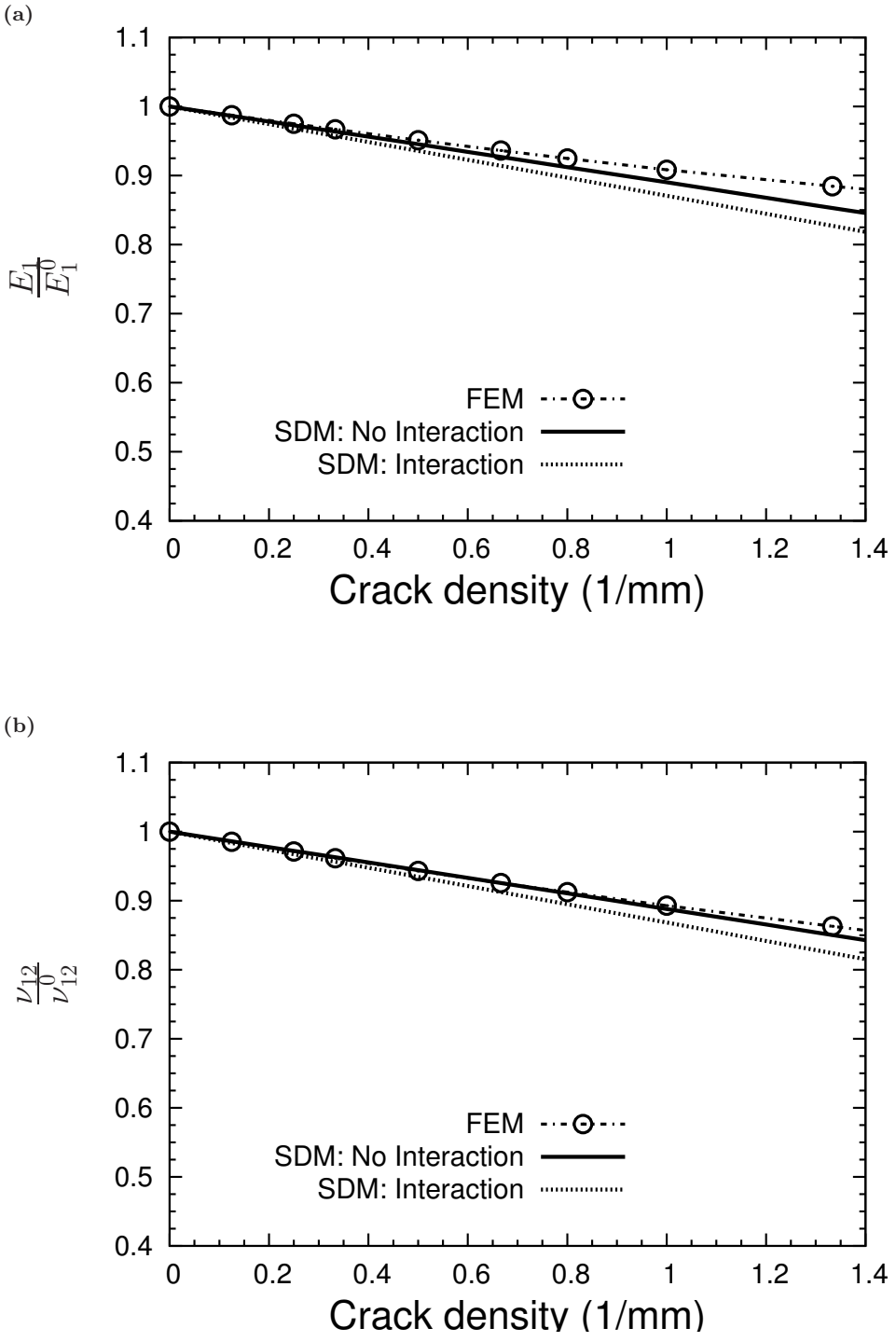

Fig. 45. Stiffness reduction for $[0/\pm 55/90]_s$ laminate compared with FE simulations.. The crack density is along X_1 direction.

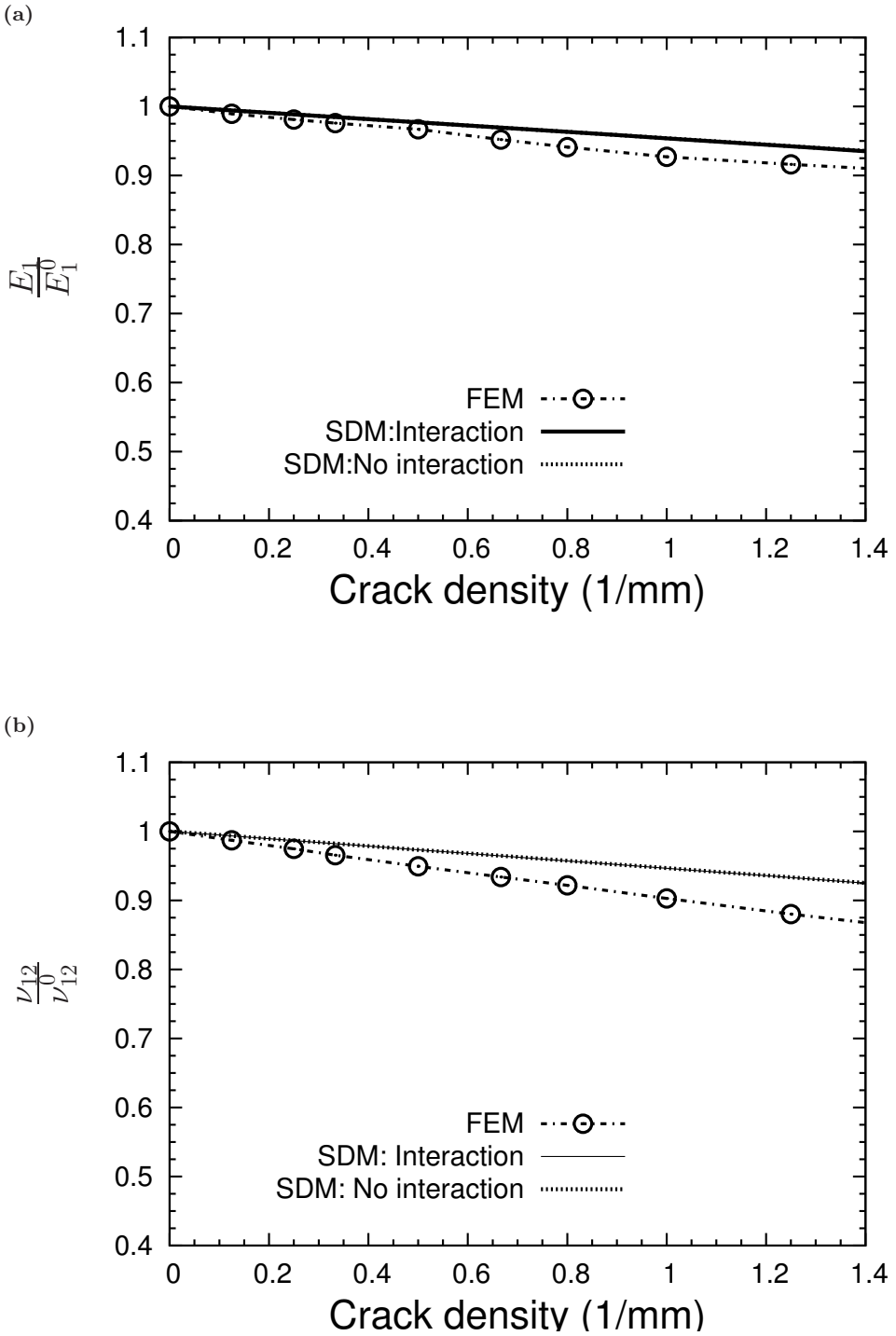

Fig. 46. Stiffness reduction for $[0/\pm 40/90]_s$ laminate compared with FE simulations. . The crack density is along X_1 direction.

corresponds to the $[0_m/90_r/\pm\theta_n]_s$ configuration for which the stiffness-damage relations are given in Eq. (5.32)-(5.34), $\bar{D}$ is given in Eq. (5.29), and the constraint parameters are defined in Eq. (5.30). The normalized average CODs were again determined using FE analysis. The corresponding constraint parameters are calculated as: $\kappa_{90_{4n+2r}} = 6.1\text{e-}3, \kappa_\theta|_{\theta=90} \approx \kappa_{90} = 5.4\text{e-}3, \kappa_{\theta^+} = 3.97\text{e-}3, \kappa_{\theta^-} = 3.35\text{e-}3, \kappa_\theta = \frac{1}{2}(\kappa_{\theta^+} + \kappa_{\theta^-}) = 3.66\text{e-}3$.

In experiments [108] $\mp 45°$-cracks did not grow fully and laminates failed by delamination. However, in FE analysis, we have assumed all cracks to be fully grown through laminate width. Now, the degradation effects due to cracks in a given layer (i.e., given crack size) should be directly proportional to the surface area of all the existing cracks. Thus, to account for partially grown cracks, we can reduce the crack density for that layer by a "relative density factor", defined as

$$\rho_r = \frac{\text{Actual surface area for partial cracks}}{\text{Surface area for full cracks}} \tag{5.38}$$

To find the actual surface area of partial cracks, the information regarding their actual length (along lamina width) is necessary. Since such data was not reported in the above experimental study [108], we consider two cases. We assume that the ∓ 45 cracks grow to half the laminate width in the first case and to $1/4^{th}$ in the latter, i.e., $\rho_r = 0.5, 0.25$, respectively.

SDM predictions for these cases using the FE computed CODs are shown against cracks density in 90°-ply in Fig. 47. The cracks in $-45°$-ply initiate at a cracks density of about 0.7 $cracks/mm$ in 90°-ply, whereas the cracks in $+45°$-ply initiate about 0.8 $cracks/mm$. The dotted line for $[0/90/\mp 45]_s$ laminate represents damage in 90°-ply only. The SDM predictions for the two cases of partial cracks are shown for $\rho_r = 0.5$ and $\rho_r = 0.25$ by dashed and solid lines, respectively. The results for both axial modulus and Poisson's ratio are in very good agreement with the test data.

The prediction with reduced crack density approaches a more realistic magnitude of stiffness degradation. The exact evaluation will, however, require the knowledge of crack length, their densities and evolution in each cracked layer with applied strain.

3. Comparison of Stiffness Degradation in $[0_m/\pm\theta_n/90_r]_s$ and $[0_m/90_r/\mp\theta_n]_s$ Laminates

It will be quite interesting to know how the layup sequence affects the stiffness degradation. This can be very useful while designing structures made of composite laminates. Property tailoring through optimization of layup sequence is an important design activity to make stronger and more durable structures. For example, the in-plane extensional stiffness properties of $[0_m/\pm\theta_n/90_r]_s$ and $[0_m/90_r/\mp\theta_n]_s$ laminates will be very similar. In fact, CLPT will result into identical properties, for the order of ply orientation does not matter for in-plane stiffness (A-matrix). However, when it comes to transverse cracking induced damage effects, the behavior of the structure could be different. This is because, in $[0_m/\pm\theta_n/90_r]_s$ laminates, 90° plies are centrally placed, i.e., they have double the thickness of 90° plies in $[0_m/90_r/\mp\theta_n]_s$ laminates. SDM provides an appropriate way to account for this ply layup. As an example, predictions for stiffness changes due to transverse cracking in quasi-isotropic laminates in these two cases is shown in Fig. 48. As expected, $[0/\pm45/90]_s$ laminates depict more severe stiffness reductions for both the longitudinal Young's modulus and Poisson's ratio than those for $[0/90/\mp45]_s$ laminates. The difference is mainly due to nearly double stiffness reduction due to 90° ply cracking in $[0/\pm45/90]_s$ than in $[0/90/\mp45]_s$ laminates. The laminate theory, when applied to virgin laminates, suggests identical in-plane stresses ($\sigma_{XX}, \sigma_{YY}, \sigma_{XY}$) for both of above laminate sequences. The through-the-thickness normal stress (σ_{ZZ}), however, is quite different for these two laminates.

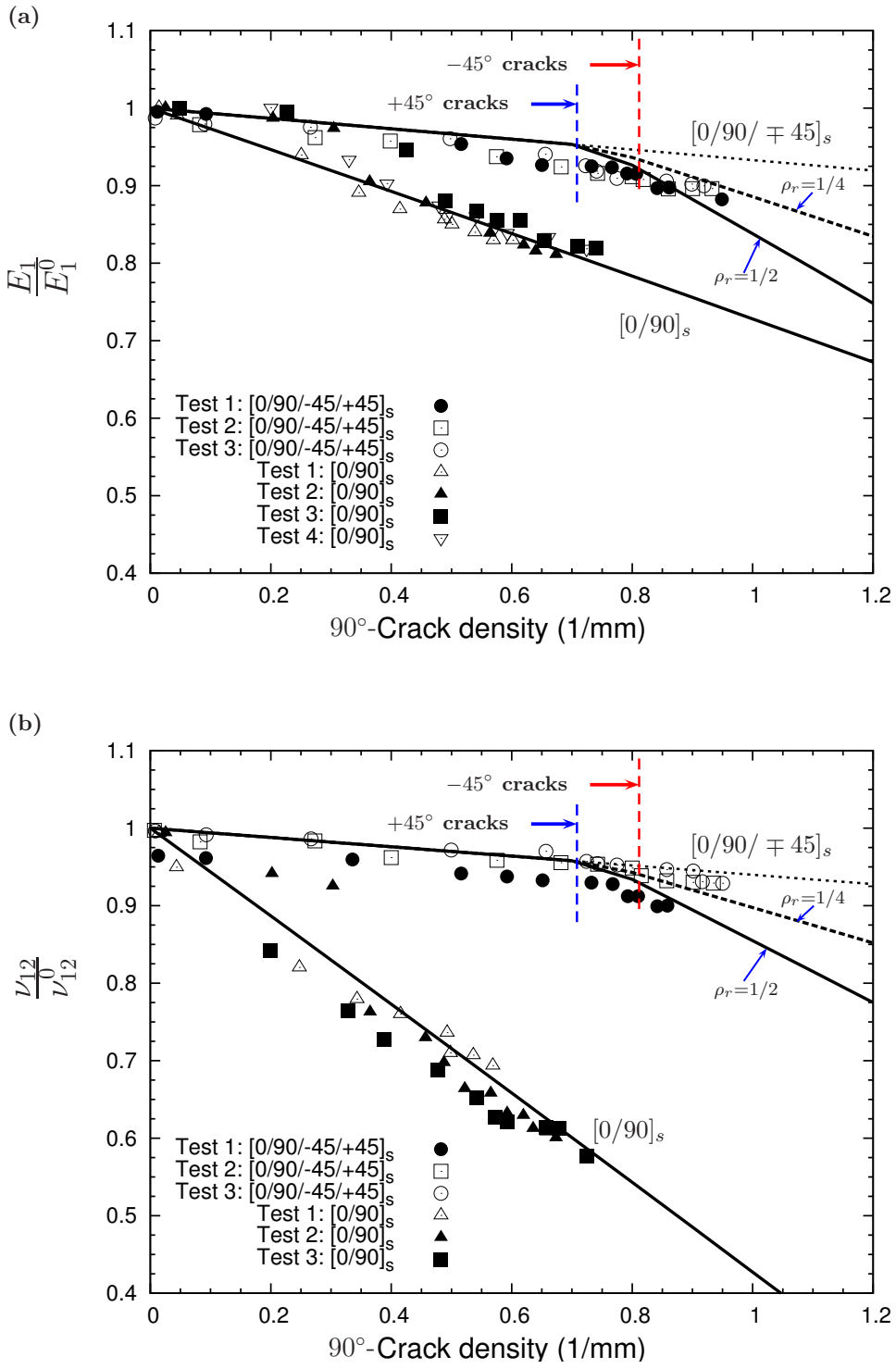

Fig. 47. Stiffness reduction for quasi-isotropic ($[0/90/\mp 45]_s$) laminate compared with experimental data [108]. The damage constants are calculated using CDM for $[0/90]_s$ laminate. The crack density is along X_1 direction.

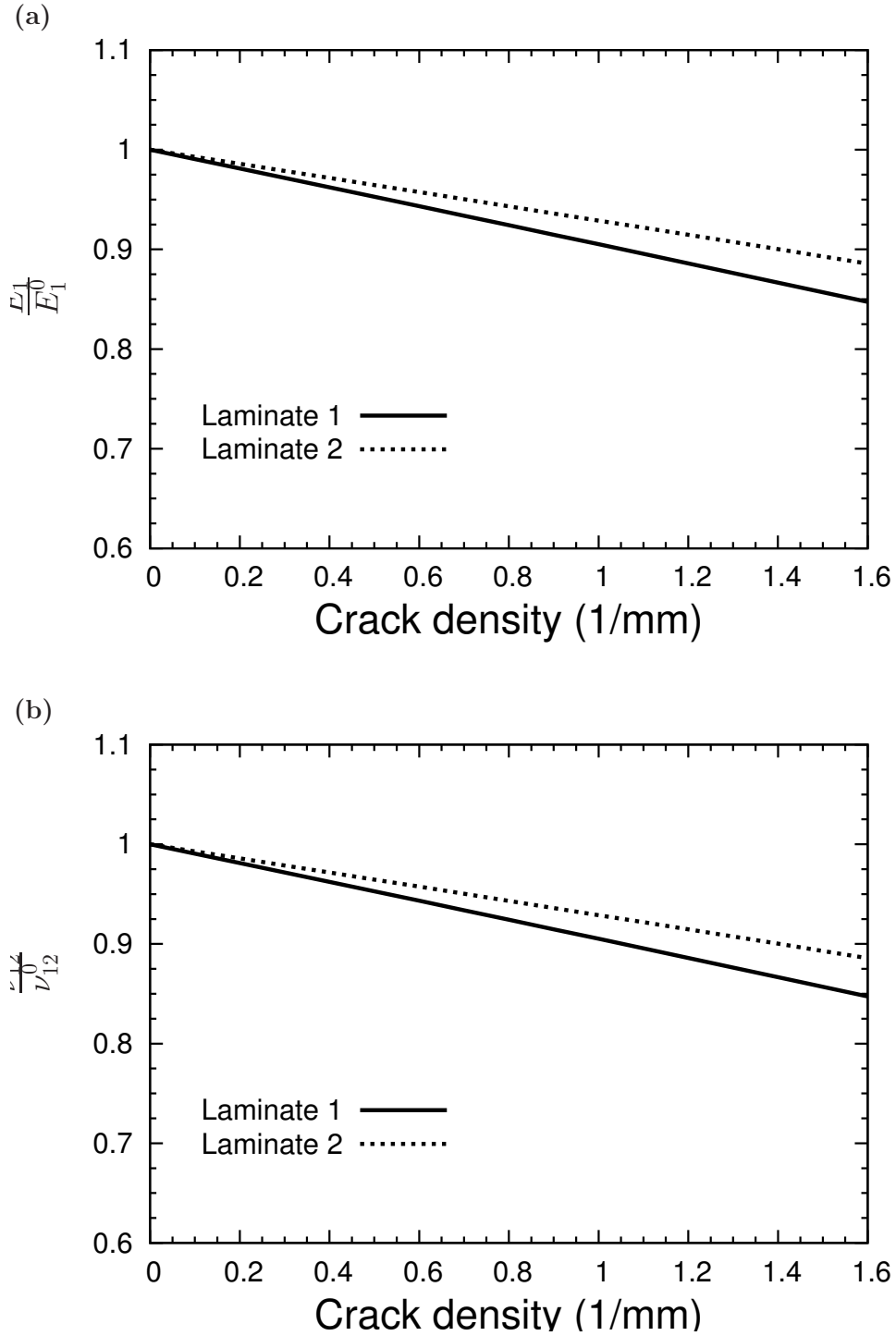

Fig. 48. Stiffness reduction for $[0/\pm 45/90]_s$ (Laminate 1) compared with quasi-isotropic $[0/90/\pm 45]_s$ (Laminate 2).

The effect of ply cracking in these laminates is quite different. In fact, some experimental data [60] indicate that $[0/\pm 45/90]_s$ and $[0/90/\pm 45]_s$ laminates developed two distinctly different cracks patterns, and the saturation crack density in two laminates were found to be different. Of course, due to the difference in 90° ply thickness in two cases, the crack initiation strain and rates of increase in crack density in that ply are very different in the two cases. These damage evolution aspects will be discussed in the next chapter.

4. Parametric Study

To seek further validation of the SDM procedure and to gain insight into the effects of relative thickness and stiffness of cracked vs. uncracked plies, we conduct a parametric study. The key again is numerical computation of constraint parameters. This can be attained by performing a suitable study of COD changes due to variation in material and geometry parameters of the laminate. Here, we carried out the study by varying the relative thickness of cracked and un-cracked layers for laminates in the class of $[0_m/\pm\theta_n/90_r]_s$ layup. The constants $a_i^{'}$ are taken from previous analysis for the reference $[0/90_3]_s$ laminate. The comparison of SDM predictions for $m = 2, n = 2$ and $p = 2$ with numerical computations for a representative ply orientation, $\theta = 55°$, are shown respectively in Fig. 49-51. Except for the axial Poisson's ratio for $[0/\pm 55_2/90]_s$, the results show good agreement with FE simulations. Obviously, stiffness changes are most severe for $p = 2$ and least severe for $m = 2$. In fact, there is negligible difference in results for $m = 1$ and $m = 2$. Also, the interaction between damage modes increases as the thickness of cracked layer(s) increases. The general observation is that the thickness of cracked layer(s) has a significant impact on stiffness changes whereas increasing thickness of supporting plies has small effect on overall properties of the cracked laminate. The same observation was made for $[0_m/\pm\theta_n/0_{m/2}]_s$ laminates

in [170]. Similar parametric studies can also be used to evaluate stiffness changes with varying degree of relative material stiffnesses of un-cracked and cracked layers, e.g., if 0°-layer is made of different material than off-axis plies. These parametric studies enable efficient computations during design of laminated structures.

5. Discussion and Assessment of the SDM Approach for Multi-mode Damage

The stiffness-damage relationships (5.21), or equivalently, in engineering moduli form, Eqs. (5.32)-(5.35), provide the basis for predicting RVE-averaged stiffness properties for $[0_m/\pm\theta_n/90_r]_s$ laminates with simultaneous cracks in $+\theta$ and $-\theta$-plies, as well as in 90°-plies. These relationships, which are for an initially orthotropic laminate, state that the laminate is orthotropic also with ply cracks present. The procedures for calculating the damage parameter $\bar{D}$ and the damage-material constants $a_i^{'}$ appearing in these equations have been described above. As noted above, we have treated the three coupled equations (5.32)-(5.34), while Eq. (5.35), which involves shear response has been left for future work.

While the predictions by the SDM approach can be viewed as satisfactory for changes in E_1 and ν_{12} for the class of laminates considered, as evidenced by comparisons in Figs. 44-51, it must be noted that the prediction of damage induced stiffness for multi-mode damage in general laminates is still a challenge. The previous work for $[0_m/\pm\theta_n/0_{m/2}]_s$ laminates [170], and the current effort for $[0_m/\pm\theta_n/90_r]_s$ and $[0_m/90_r/\pm\theta_n]_s$ laminates, taken together, show a path forward to meeting that challenge. However, to proceed further, we must note the limitations in what has been accomplished in the present work. Firstly, the evaluation of the constraint parameters, as discussed in Section 4.2.1, requires calculating the average CODs from an FE model of the representative unit cell. The FE model shown in Fig. 21, page 57 is for an imposed uniform displacement in the axial direction. The CODs from this model

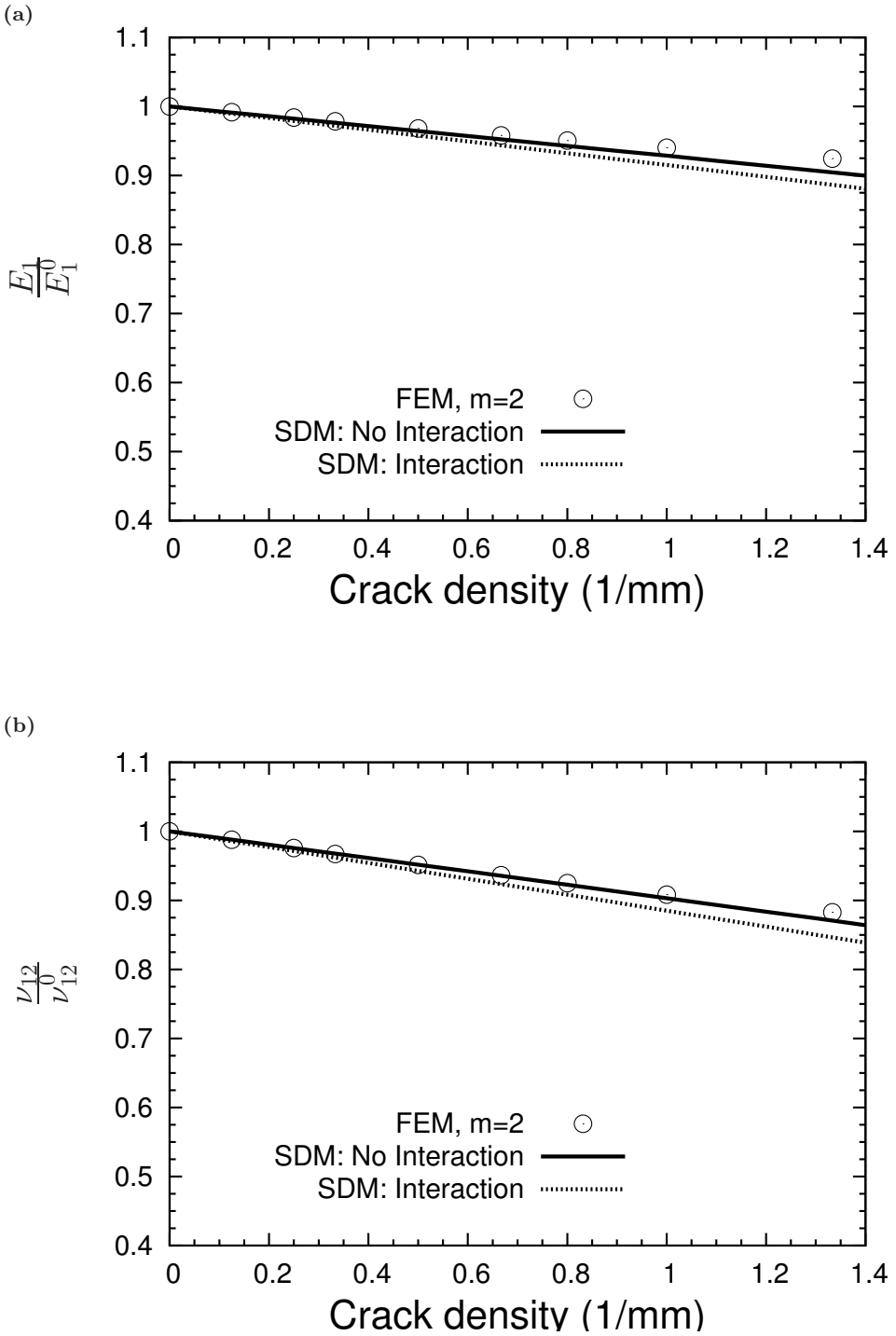

Fig. 49. Stiffness reduction for $[0_2/\pm 55/90]_s$ laminate compared with FE simulations. The crack density is along X_1 direction.

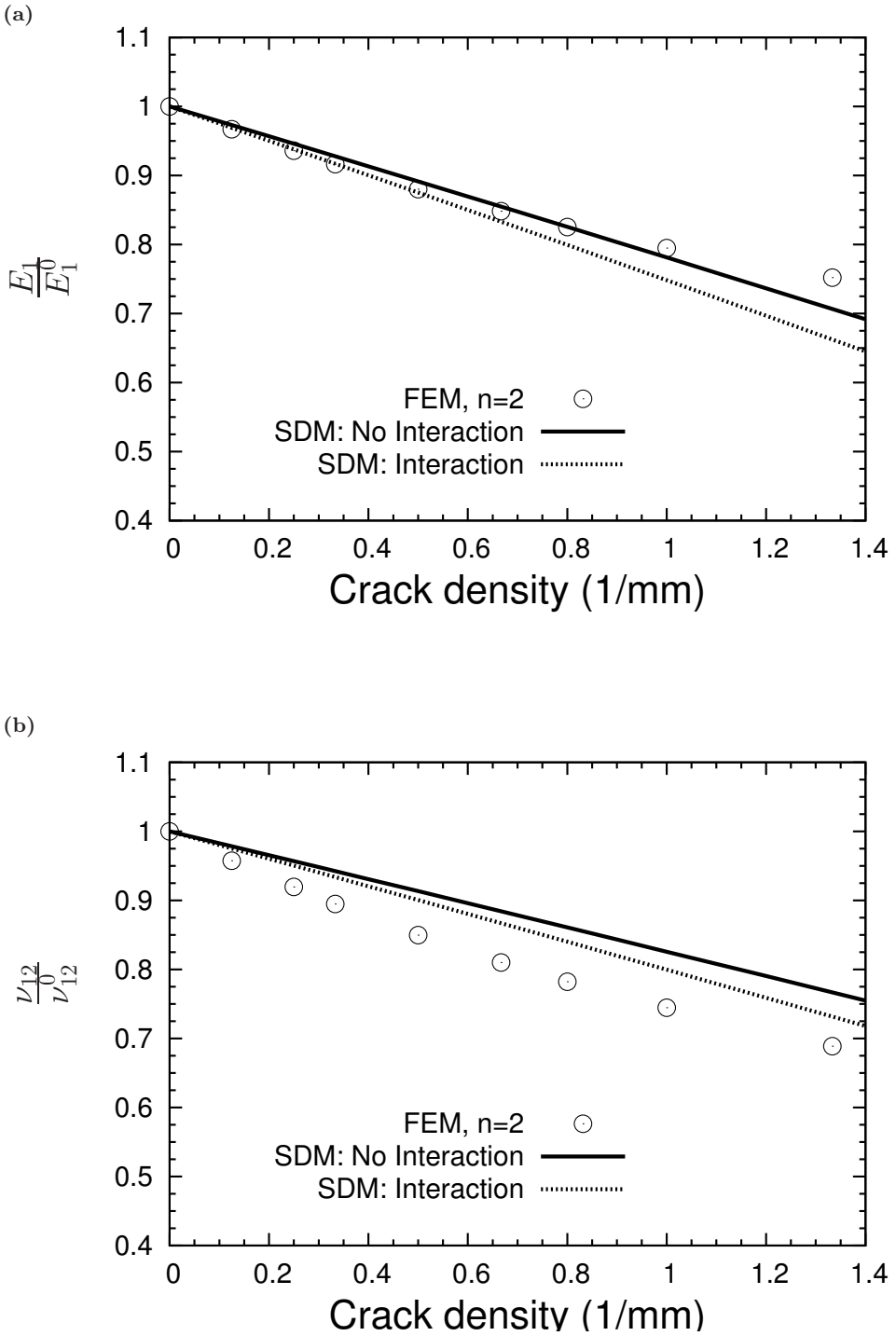

Fig. 50. Stiffness reduction for $[0/\pm 55_2/90]_s$ laminate compared with FE simulations. The crack density is along X_1 direction.

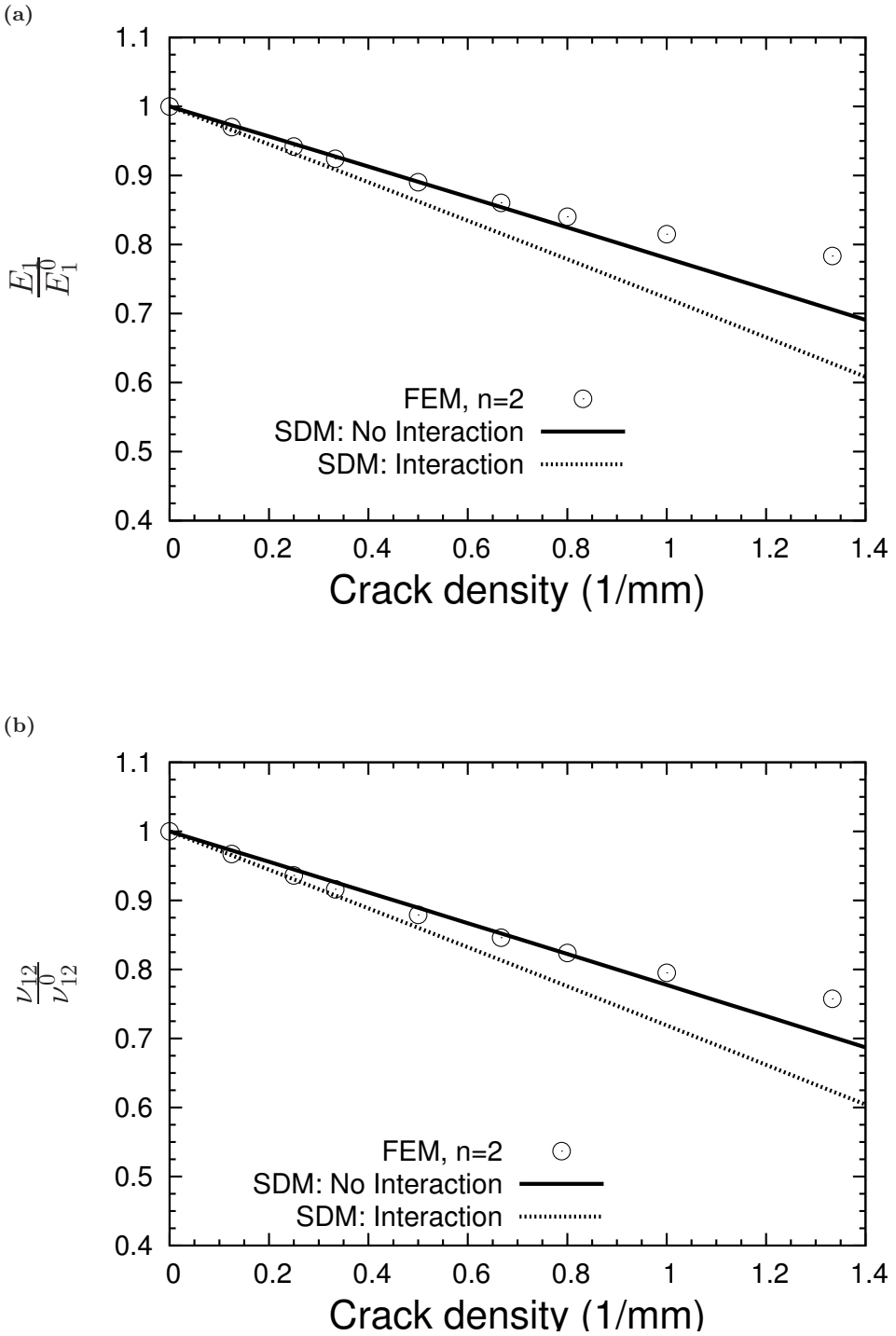

Fig. 51. Stiffness reduction for $[0/\pm 55/90_2]_s$ laminate compared with FE simulations. The crack density is along X_1 direction.

allow evaluation of the constraint parameters that successfully lead to predictions of axial properties E_1 and ν_{12}. Note that the assumption made in deriving Eq. (4.33), namely, $a_i \geq b_i$, is likely valid only for the case of axial loading of the laminate with damage. More work is needed to investigate the lateral loading case and to examine the associated prediction procedure for E_2 and ν_{21}.

On the limitations side of the current SDM approach, we also note that the stiffness-damage relationships (Eq. (5.21)) are linear in the damage parameter as a consequence of restricting the polynomial expansionto linear terms in damage. This restriction can be easily relaxed at the cost of requiring more data for prediction of stiffness changes. It turns out, however, that the predictions by the linearized equations is quite satisfactory in most cases for crack densities of up to 1.0 cracks/mm, as seen in Figs. 44-51. In practical design one would seldom exceed such high crack densities, particularly when most cases examined experimentally show that delamination sets in when plies are cracked extensively. One more implication of the linearization is in evaluating the damage-material constants $a_i^{'}$. As seen from Eq. (5.37), evaluation of these constants requires knowing changes in E_1, E_2 and ν_{12} for a selected cross ply laminate (here $[0/90_3]_s$), at one fixed crack density, as described in Section 4.2.2. Because of the linearization, while the actual stiffness dependence on damage is approximately linear, at least until reasonably high crack densities, the choice of the fixed crack density would affect the values of the $a_i^{'}$ constants. It turns out however, that a prudent choice of 1.0 cracks/mm gives fairly accurate stiffness predictions, except perhaps for $\theta = 70^{\circ}$ as seen in Fig. 44.

F. Summary

The previously developed synergistic damage mechanics approach for $[0_m/\pm\theta_n/0_{m/2}]_s$ laminates in [170] has been extended here for $[0_m/\pm\theta_n/90_r]_s$ and $[0_m/90_r/\pm\theta_n]_s$ laminates with cracks in 90°-plies in addition to the cracks in $+\theta$- and $-\theta$-plies. The extension is far from trivial, as the new case considered here has two distinct damage modes while in the previous case the two θ crack arrays could be treated equivalently as a single damage mode.

The stiffness-damage relationships derived for the current case for simultaneous presence of two damage modes show orthotropic symmetry for in-plane loading, leading to four new damage related constants. A procedure for determining three of the constants, corresponding to axial loading, has been presented. Evaluation of these constants can be done from known stiffness changes of a cross ply laminate at a fixed crack density. These known stiffness values can be obtained experimentally, or, as demonstrated here, from a finite element model. A damage parameter representing the two simultaneous damage modes has been evaluated from a finite element model of the representative unit cell of the laminate containing damage by calculating the crack-surface averaged opening displacements. The stiffness predictions of independent cases using the evaluated material constants and the damage parameter show good agreement with directly calculated values by finite element models. Further validation of the prediction procedure comes from a parametric study of cracked and uncracked ply thicknesses.

Although the methodology developed here is still not fully general, the limitations being in linearization of the stiffness-damage relationships and in not considering shear loading, it is the first such treatment for multi-mode damage. Further work in the direction pursued is thought to provide further advance in treating damage of general

laminates.

CHAPTER VI

DAMAGE EVOLUTION

A. Introduction

Multidirectional composites, which contain multiple plies with different orientations, are useful for applications requiring shear, multi axial and other complex loading scenarios. When subjected to tensile loading, they can develop ply cracks in multiple orientations. Although the approaches to analyze damage in single orientation, e.g., for cross-ply ($[0/90]_s$) laminates, have gained maturity, there has been little success in developing analysis methods which can work well for multidirectional composites. The usual analysis methods fail for multidirectional composites due to complexity of stress state, multiplicity of damage orientations and their interactions. Experimental investigations [108, 109, 127] have shown that cracking in off-axis plies may involve mixed mode of fracture and interactions between cracks of multiple orientations.

Damage analysis of composite laminates entails solving two inter-dependent problems. In the first problem the effect of transverse cracks on material stiffness is analyzed and stiffness properties as a function of crack density are predicted. The second problem caters to the prediction of increase in crack density as a function of applied load. Combining the two, the overall stress-strain response is obtained. For off-axis laminates, the first problem is dealt in detail by the authors in the previous chapters, published in [170, 171]. The present study aims at predicting the evolution of off-axis ply crack density as a function of applied loading.

To analyze the damage progression, two different approaches are commonly utilized. The first one, known as "strength-based" approach uses the solution to stress analysis problem to form a cracking criterion. According to these models, ply cracks

form when the stress reaches the transverse strength or of the ply material or some multi-axial stress state criterion is met [22]. On the other hand, the second approach known as "energy based" approach [22] predicts formation of new crack based on energy considerations. A comprehensive study by Nairn et al. [43] on cross-ply laminates has shown that none of the strength models gives consistent results and an energy-based failure criterion is the only acceptable option. Variational method coupled with a probabilistic energy criterion is found to match well with experimental results for cross-ply laminates [102].

For off-axis laminates, the only available approach is the modified shear lag analysis, used for predicting crack initiation in angle-ply laminates [119] and for obliquely crossed cracks [125]. However, all shear models involve approximate stress analysis rendering inaccurate predictions for multidirectional laminates.

In the present work, an energy based approach to predict evolution of ply cracks in multidirectional laminates is developed following the notions of fracture mechanics. The cracks in a given off-axis ply initiate and propagate when mixed mode fracture criterion is met. The critical energy release rate in normal mode (G_I) is determined by fitting the damage model with the experimental data for a reference cross-ply laminate. On the other hand, G_{II} (shear mode) is assumed to be 1500 J/m^2. The approach needs determination of average *crack opening displacement* (COD) and *crack sliding displacement* (CSD) as a function of crack spacing. This task is performed through a suitable 3-D *finite element* (FE) analysis. Then the proposed damage model is used to predict the evolution of crack density with applied loading for other laminate layups with the same material properties. The predictions are compared with experimental data for $[0/\pm\theta_4/0_{1/2}]_s$ and $[0/90/\mp 45]_s$ laminates [108, 109]. A parametric study coupled with suitable FE computations is carried out to predict damage evolution in $[0_m/90_n/\mp\theta_p]_s$ laminates with varying layer thicknesses.

B. Experimental Observations

The experimental studies on initiation and growth of intralaminar cracking in composite laminates has been extensive in the literature. Most of the work has focused on 90° ply cracking in cross-ply laminates, and quasi-isotropic laminates. An excellent book chapter by Nairn [22] provides a good overview of essentials and effects of ply cracking damage. Some interesting observations are as follows:

1. Crack initiation: Crack initiate from the sites of material defects, such as voids, inclusions, etc., and preferably from the free edges of the laminate. For multidirectional laminates containing 90° plies, the cracking often begins in those plies. The crack initiation strain for 90° plies is about 0.4 -1.0 %, depending upon the material, laminate sequence, and ply thickness, and it increases as ply orientation decreases. For 45° plies, for example, it could easily be more than 1.0%.

2. Tunneling cracks: Most experimental studies point out that once the ply cracks have grown through the lamina width, they often grow unstably along the fiber direction through the laminate width, and are thus called "tunneling cracks". Some studies [94, 125, 126], however, also show that for multidirectional laminates, cracks in plies other than 90° may not grow fully before laminate fails by delamination.

3. Damage evolution curve: Once the ply cracking has initiated, more and more ply cracks start appearing in between existing cracks, and the crack density rises quickly. As the crack spacing between adjacent cracks keeps decreasing, the cracks start interacting and the rate of cracking slows down and finally reaches a saturation asymptotically. Thus a typical damage growth curve consists of

three stages: initial rapid rise, slowing down, and saturation. The initial rapid rise and saturation crack density depend on the material type, the laminate sequence, and also the laminate fabrication process. For example, well-made carbon/epoxy laminates typically have a rapid rise in ply crack density.

4. Effect of ply thickness: The thickness of the cracked ply plays a significant role in changing the start of the multiple matrix cracking, as well as the rate of increase in crack density [14–21, 26]. As thickness of 90° ply, in a $[0_m/90_n]_s$ laminate, is decreased, required strain to induce initiation of matrix cracking increases (see Fig. 6). For very thin plies (e.g., less than 0.1 mm thick), the ply cracks may be suppressed entirely and the laminate may fail before initiation of cracking.

5. Effect of stacking sequence: The layup sequence may affect the cracking process appreciably. For example, the experiments overwhelmingly show that the strain to initiate ply cracking is lower for laminates with surface 90° plies than for laminates with the central 90° plies [22, 43]. For [0/90] laminates, the outer 0° plies provide support and constrain the development and opening of cracks in 90° plies, whereas no such constraint is available for surface 90° plies from the outer-side. The damage evolution curves for $[0_m/90_n]_s$ and $[90_n/0_m]_s$ laminates are compared in Fig. 52, reproduced from [22]. $[90_n/0_m]_s$ laminates clearly show a higher stiffness degradation than the $[0_m/90_n]_s$ laminates. For multidirectional laminates, the situation is more complex and has to be studied on a case to case basis.

6. Laminate material matters: For instance, the laminates made from carbon/epoxy show a higher resistance to multiple matrix cracking than those made from

glass/epoxy. Correspondingly, the stiffness degradation in carbon/epoxy laminates is much less severe than the glass/epoxy laminates.

7. Complexities of off-axis ply cracking: Off-axis ply cracks may initiate at much higher strains than 90° plies, may not grow fully and may sometimes show curved patterns (see, e.g., [172,173]). A 3D stress analysis study [103] on $[0/\mp\theta]_s$ laminates showed that the principal stress trajectories in the off-axis, θ plies may not be straight and may account for the development of curved matrix cracks.

8. Contiguous ply cracking: As mentioned above, an off-axis ply adjacent to a 90° ply shows numerous partial cracks, which may or may not join to form through cracks on increase in applied loading. The cracks in the contiguous ply almost always start from its interface with the 90° ply. A picture shown in Fig. 16 on page 42 shows numerous partial cracks in 60° ply of a $[0/60_2/90]_s$ laminate, growing from the 90/60 ply interface. Experiments by Yokozeki [125, 126] on $[0/\theta_2/90]_s$ laminates also point out that the angle of intersection between 90° and θ plies, and thickness of the θ ply may have a significant impact on the initiation and growth of ply cracking in that ply.

9. Loading and environmental affects: Most experiments are performed using uniaxial tension, but ply cracks will also form under other loading conditions, such as fatigue, biaxial or shear loading. In the case of bending, ply cracks will form on the tension side [41, 174], and analysis for such loading situation analyses need to account for the different stress state in laminates undergoing bending than undergoing tension [41,73,135,136]. Biaxial loading of $[0_m/90_n]_s$ laminates may show cracks in both 0° and 90° plies. On thermal loading, the differential shrinkage between the 0° and 90° plies may also induce biaxial loading [175–180]. The residual stresses due to thermal effects or moisture etc. may also affect the

cracking process [181, 182].

C. Energy Based Criterion for Transverse Cracking

Consider a generally symmetric composite laminate loaded in axial tension (Fig. 26). The in-plane stress state in off-axis plies with respect to material axes is displayed in the figure. When this stress state in a particular ply reaches a critical value, matrix cracking initiates in that ply. On further increase in loading, multiple cracking ensues by the so-called shear lag process. In a similar way, other off-axis plies may also develop multiple cracks at different load values. Experimental studies have shown that for plies transverse to the loading axis, the ply cracks grow instantly through the laminate width. However, for lower off-axis angles, cracks may not fully develop. At angles lower than 45°, ply cracks may not even initiate before material fails due to delamination.

Now assume that on some applied load, one off-axis ply has developed a periodic array of N fully grown cracks (Fig. 53). On further increase in load to σ_0, a new crack appears midway between two existing cracks, increasing the total number of cracks in the layer to $2N$. During this process, the spacing between two adjacent cracks decreases from 's' to '$s/2$'. The released energy due to these N new cracks is equal to the work needed to close them [104]. If we denote this work by $W_{2N\to N}$, and the work to close all cracks at once by $W_{2N\to 0}$, we have, by energy balance

$$W_{2N\to 0} = W_{2N\to N} + W_{N\to 0} \tag{6.1}$$

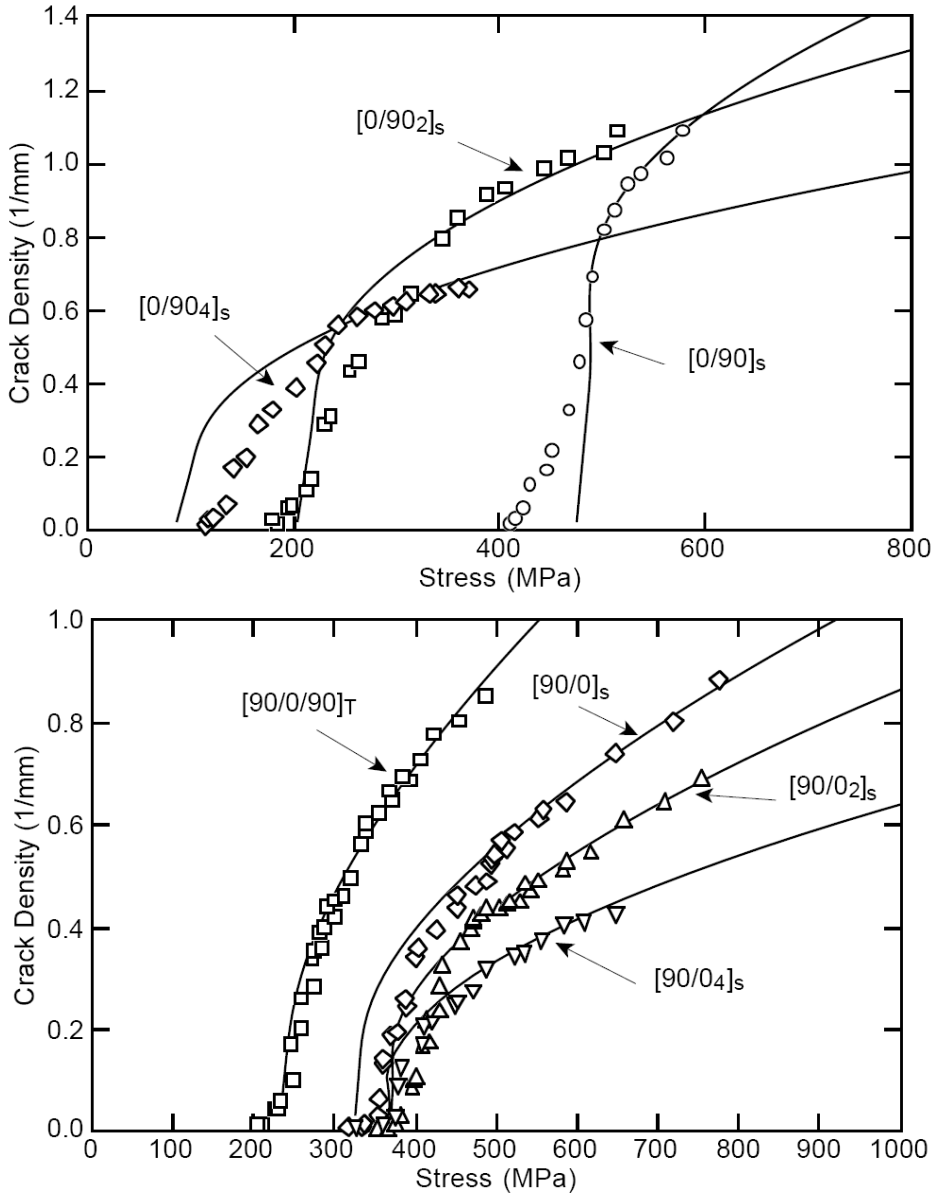

Fig. 52. Comparison of ply cracking in $[0_m/90_n]_s$ and $[90_n/0_m]_s$ laminates (source: [22]).

Using the crack closure technique, $W_{N\to 0}$ can be determined as

$$\begin{aligned} W_{N\to 0} &= \mathbf{F.u} = F_n.u_n + F_t.u_t \\ &= 2.N.\tfrac{1}{\sin\theta}.\tfrac{1}{2}\int_{-t_\theta/2}^{t_\theta/2}\sigma_{20}^{\theta}u_n(z)dz + 2.N.\tfrac{1}{\sin\theta}.\tfrac{1}{2}\int_{-t_\theta/2}^{t_\theta/2}\sigma_{120}^{\theta}u_t(z)dz \qquad (6.2) \\ &= N.\tfrac{1}{\sin\theta}.t_\theta.\left[\sigma_{20}^{\theta}.\bar{u}_n^{\theta}(s) + \sigma_{120}^{\theta}.\bar{u}_t^{\theta}(s)\right] \end{aligned}$$

where t_θ is the thickness of the cracked ply, and $\bar{u}_n^{\theta}(s)$ and $\bar{u}_t^{\theta}(s)$ represent average COD and CSD for the cracked layer with crack spacing equal to s, and σ_{20}^{θ} and σ_{120}^{θ} represent the far away normal and shear stresses in the lamina coordinate system for undamaged material. Therefore, σ_{20}^{θ} and σ_{120}^{θ} are responsible for opening and sliding of the cracked surfaces, respectively. Since the average COD and CSD depend on the applied stress (strain) level and the crack size (or equivalently the thickness of the cracked layer), we normalize these quantities with respect to the applied load and the thickness of the cracked layer as

$$\begin{aligned} \tilde{u}_n^{\theta} &= \frac{\bar{u}_n^{\theta}}{t_\theta\left(\sigma_{20}^{\theta}/E_2\right)} = \frac{1}{t_\theta^2\left(\sigma_{20}^{\theta}/E_2\right)}\int_{-t_\theta/2}^{t_\theta/2}u_n(z)dz \\ \tilde{u}_t^{\theta} &= \frac{\bar{u}_t^{\theta}}{t_\theta\left(\sigma_{120}^{\theta}/E_2\right)} = \frac{1}{t_\theta^2\left(\sigma_{120}^{\theta}/E_2\right)}\int_{-t_\theta/2}^{t_\theta/2}u_t(z)dz \end{aligned} \qquad (6.3)$$

where E_2 is transverse modulus for virgin unidirectional lamina, $u_n = \delta u_y = u_y^+ - u_y^-$, and $u_t = \delta u_x = u_x^+ - u_x^-$, respectively represent the normal (opening) and tangential (sliding) displacement of the crack surfaces. They are determined using FE calculations for nodal displacements in the local crack plane coordinate system (x, y, z), as shown in Figs. 20, and 21 shown on pages 56 and 57 for two and three damage modes, respectively. Using the normalization in Eq. 6.3, the work required to close

N-cracks with spacing s is given by

$$W_{N\to 0} = N\frac{1}{\sin\theta}\left(t_\theta\right)^2.\frac{1}{E_2}\left[\left(\sigma_{20}^{\theta}\right)^2.\tilde{u}_n^{\theta}\left(s\right)+\left(\sigma_{120}^{\theta}\right)^2.\tilde{u}_t^{\theta}\left(s\right)\right] \tag{6.4}$$

Similarly, the work required to close $2N$ cracks with spacing $s/2$ is given by

$$W_{2N\to 0} = 2N\frac{1}{\sin\theta}\left(t_\theta\right)^2.\frac{1}{E_2}\left[\left(\sigma_{20}^{\theta}\right)^2.\tilde{u}_n^{\theta}\left(\frac{s}{2}\right)+\left(\sigma_{120}^{\theta}\right)^2.\tilde{u}_t^{\theta}\left(\frac{s}{2}\right)\right] \tag{6.5}$$

Using Eqs. (6.1), (6.4) and (6.5), $W_{2N\to N}$ can be written as

$$W_{2N\to N} = N\frac{1}{\sin\theta}\left(t_\theta\right)^2.\frac{1}{E_2}\left[\left(\sigma_{20}^{\theta}\right)^2\left\{2\tilde{u}_n^{\theta}\left(\frac{s}{2}\right)-\tilde{u}_n^{\theta}\left(s\right)\right\}+\left(\sigma_{120}^{\theta}\right)^2\left\{2\tilde{u}_t^{\theta}\left(\frac{s}{2}\right)-\tilde{u}_t^{\theta}\left(s\right)\right\}\right] \tag{6.6}$$

Following fracture mechanics, the transverse cracks will form in the matrix if the energy released is greater than the critical energy release rate of the matrix for the given laminate layup and material, i.e., if

$$W_{2N\to N} \geq N.G_c.\frac{1}{\sin\theta}t_\theta \tag{6.7}$$

where, $G_c = 2\gamma$, with γ representing the energy required to form a unit area of new material surface [183]. The factor 2 refers to the two new material surfaces formed during crack multiplication. The equation (6.7) represents the mode I fracture criterion for multiple matrix cracking in a given off-axis ply. However, if the critical energy release rate for the matrix for the given laminate system is different in the normal and shear modes, the above criterion needs to be modified. Separating the Mode I and Mode II work in Eq. (6.6), the fracture criterion (6.7) can be rewritten as

$$\left(\frac{W_I}{G_I}\right)^a+\left(\frac{W_{II}}{G_{II}}\right)^b \geq 1 \tag{6.8}$$

where W_I and W_{II} represent the energy released per unit surface area in the opening (Mode I) and sliding (Mode II) of the crack surfaces, respectively, G_I and G_{II} are

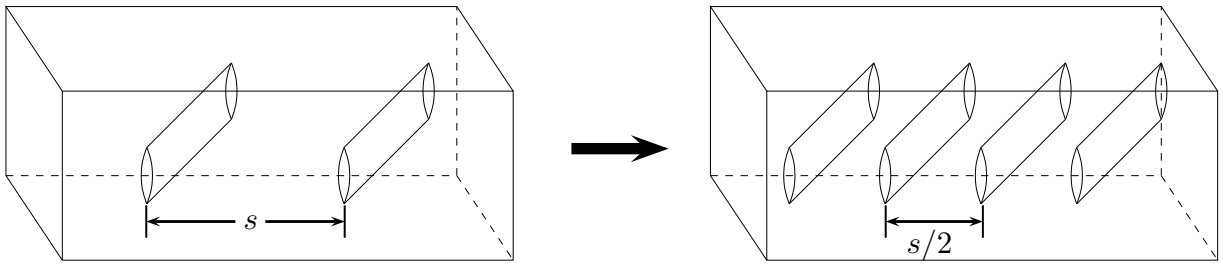

State 1: N cracks, crack spacing $=s$ State 2: 2N cracks, crack spacing $=s/2$

Fig. 53. Progressive multiplication of transverse cracks.

the critical energy release rate in these modes, and the exponents a and b depend on the material system, for example, for glass/epoxy system, $a = 1$, $b = 2$ [119,184]. W_I and W_{II} are given by

$$W_I = \frac{\left(\sigma_{20}^{\theta}\right)^2 t_\theta}{E_2}\left[2\tilde{u}_n^{\theta}\left(\frac{s}{2}\right) - \tilde{u}_n^{\theta}(s)\right], \qquad W_{II} = \frac{\left(\sigma_{120}^{\theta}\right)^2 t_\theta}{E_2}\left[2\tilde{u}_t^{\theta}\left(\frac{s}{2}\right) - \tilde{u}_t^{\theta}(s)\right] \quad (6.9)$$

It is important to note here that Mode I refers to the opening of crack surfaces whereas Mode II refers to an out-of-plane displacement and is actually referred to as Mode III in the conventional fracture mechanics.

To simulate the randomness in crack spacing and material resistance to cracking, the whole laminate specimen along the longitudinal direction is divided into small intervals of length δX such that only one transverse crack appears in a given length interval. Here X represents the global (laminate) axial direction. δX is chosen to be equal to length scale at the initiation of ply cracking, i.e., the fiber diameter. In the present paper it is assumed to be $\delta X = t_\theta/10$. During simulation of progressive cracking, the first ply crack appears in a random length interval. Once the transverse crack appears in a given length interval, it is taken out of consideration for further ply cracking.

The lamina stresses in an initially orthotropic laminate are found using the lam-

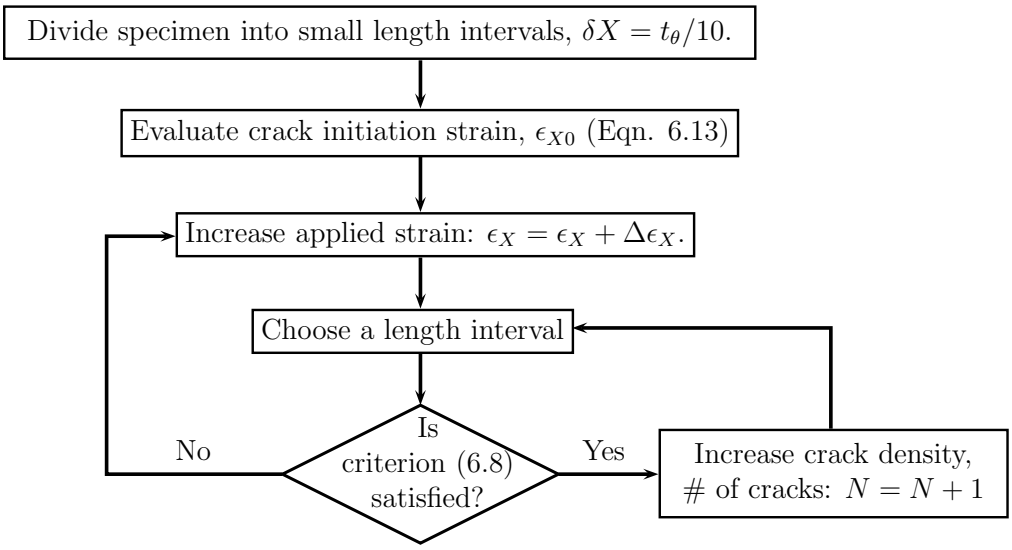

Fig. 54. Flowchart for implementation of transverse cracking simulation using *fracture-mechanics* based energy method.

inate theory as follows

$$\left\{ \begin{array}{c} \sigma^\theta_{10} \\ \sigma^\theta_{20} \\ \sigma^\theta_{120} \end{array} \right\} = \left[\begin{array}{ccc} Q_{11} & Q_{12} & 0 \\ Q_{12} & Q_{22} & 0 \\ 0 & 0 & Q_{66} \end{array} \right] \left\{ \begin{array}{c} \epsilon^\theta_{10} \\ \epsilon^\theta_{20} \\ \epsilon^\theta_{120} \end{array} \right\} \tag{6.10}$$

where the strains in the off-axis ply resolved in the material directions, are given in terms of applied strains, as

$$\left\{ \begin{array}{c} \epsilon^\theta_{10} \\ \epsilon^\theta_{20} \\ \epsilon^\theta_{120} \end{array} \right\} = \left[\begin{array}{ccc} m^2 & n^2 & 2mn \\ n^2 & m^2 & -2mn \\ -mn & mn & m^2 - n^2 \end{array} \right] \left\{ \begin{array}{c} \epsilon_X \\ \epsilon_Y \\ \epsilon_{XY} \end{array} \right\} \tag{6.11}$$

where $m = \cos\theta; n = \sin\theta$, and the elements of the stiffness matrix are given in terms of engineering moduli as

$$Q_{11} = \frac{E^0_1}{1 - \nu^0_{12}\nu^0_{21}}; \quad Q_{22} = \frac{E^0_2}{1 - \nu^0_{12}\nu^0_{21}}; \quad Q_{11} = \frac{\nu^0_{12}E^0_2}{1 - \nu^0_{12}\nu^0_{21}}; \quad Q_{66} = G^0_{12} \tag{6.12}$$

Using equations (6.2)-(6.8), with $N = 1$ and $a = 1, b = 2$, we obtain

$$A^2\epsilon_{X0}^4 + B\epsilon_{X0}^2 = 1 \tag{6.13}$$

with

$$\begin{aligned} A &= \frac{\tilde{u}_t^\theta|_{s\to\infty}\, t_\theta}{E_2 G_{II}} \left[Q_{66}.2mn.\,(1+\nu_{120})\right]^2 \\ B &= \frac{\tilde{u}_n^\theta|_{s\to\infty}\, t_\theta}{E_2 G_I} \left[Q_{12}\left(m^2 - \nu_{120}n^2\right) + Q_{22}\left(n^2 - \nu_{120}m^2\right)\right]^2 \end{aligned} \tag{6.14}$$

The solution of equation (6.13) provides us the strain at ply crack initiation in an off-axis ply.

The complete procedure to implement the described energy model for the ply crack initiation and evolution in an off-axis ply of a general symmetric laminate is outlined below (also see Fig. 54).

1. Determine/Assume G_I, G_{II} by fitting experimental data for reference laminate. For example, for predicting damage evolution in $[0/\pm\theta_4/0_{1/2}]_s$ laminates, we have chosen $[0/90_8/0_{1/2}]$ as the reference laminate.

2. From FE simulations, determine COD and CSD variation with crack spacing.

3. Predict damage evolution in other off-axis laminates:

   (a) Divide specimen length in small intervals of length $\delta X = t_\theta/10$.

   (b) Find strain at crack initiation using Eq.(6.13). What we need for this step is geometry and material properties for the laminate configuration, and normalized COD/CSD at a sufficiently large crack spacing (corresponding to nearly no cracks).

   (c) Assume a very small initial crack density.

(d) Choose a random length interval and check for cracking. A new crack forms when criterion set in Eq.(6.8) is satisfied. Increase crack density and eliminate the cracked length interval from further consideration for transverse cracking.

(e) Choose another length interval and repeat previous step till fracture criterion is satisfied.

(f) Increase applied strain. Repeat (c)-(d) at this strain value.

D. FE Modeling

As would be clear from the previous section, the prediction of transverse cracking using Eq.(6.8) requires normalized average COD ($\tilde{u}_t^\theta$) and CSD ($\tilde{u}_t^\theta$) as a function of crack spacing s. To evaluate average COD and CSD for various laminate configurations and crack densities, separate 3-D FE models were constructed for $[0/\pm\theta_4/0_{1/2}]_s$, $[0_m/\pm\theta_n/90_p]_s$ and $[0_m/90_p/\mp\theta_n]_s$ laminates. Representative geometric models (RVE) for the two laminate configurations along with symmetry boundary conditions are shown in Figs. 20 and 21 on pages 56, and 57, respectively. In FE analysis, the RVE size is varied to determine CODs and CSDs at varying crack density. More details on FE modeling are given in chapter III.

The ply material properties are shown in Table III. To obtain the remaining properties for use in the 3-D model, the unidirectional ply is assumed transversely isotropic in the cross-sectional plane. The Poisson's ratio in the isotropic cross-sectional plane ν_{23} is taken as 0.42. The mid-plane symmetry of the laminate was accounted for in the FE models.

Table III. Ply properties

	Material 1: Fiberite [109]	Material 2: glass/epoxy [108]
Laminate layup	$[0/\pm\theta_4/0_{1/2}]_s$	$[0/90]_s$, $[0_m/\pm\theta_p/90_n]_s$ & $[0_m/90_n/\mp\theta_p]_s$
Ply thickness	0.125 mm	0.50 mm
E_1	44.7 GPa	46.0 GPa
E_2	12.7 GPa	13.0 GPa
G_{12}	5.8 GPa	5.0 GPa
ν_{12}	0.297	0.3

E. Analysis Results

To illustrate the *fracture mechanics* based energy model for transverse cracking in off-axis laminates developed in the section 2, we compare our predictions with the available experimental data. Two laminate configurations are considered here: $[0/\pm\theta_4/0_{1/2}]_s$ and and quasi-isotropic ($[0/90/\mp 45]_s$) laminates. The experimental data for the two configurations were published by Varna et al. [109], and Tong. et al. [108]. We, then, will predict damage evolution for more general case of $[0_m/\pm\theta_n/90_p]_s$ and $[0_m/90_p/\mp\theta_n]_s$ laminates and finish with a limited parametric study of changes in layer thicknesses.

From FE simulations at a fixed crack spacing, the average COD and CSD are calculated as

$$\bar{u}_t^\theta = \frac{1}{t_\theta}\int_{-t_\theta/2}^{t_\theta/2} \Delta u_x(z)\ \mathrm{d}z; \quad \bar{u}_n^\theta = \frac{1}{t_\theta}\int_{-t_\theta/2}^{t_\theta/2} \Delta u_y(z)\ \mathrm{d}z \tag{6.15}$$

where Δu_x and Δu_y represents the separation of crack planes in the direction normal and parallel, respectively, to the crack face. The coordinate x, and y are along the

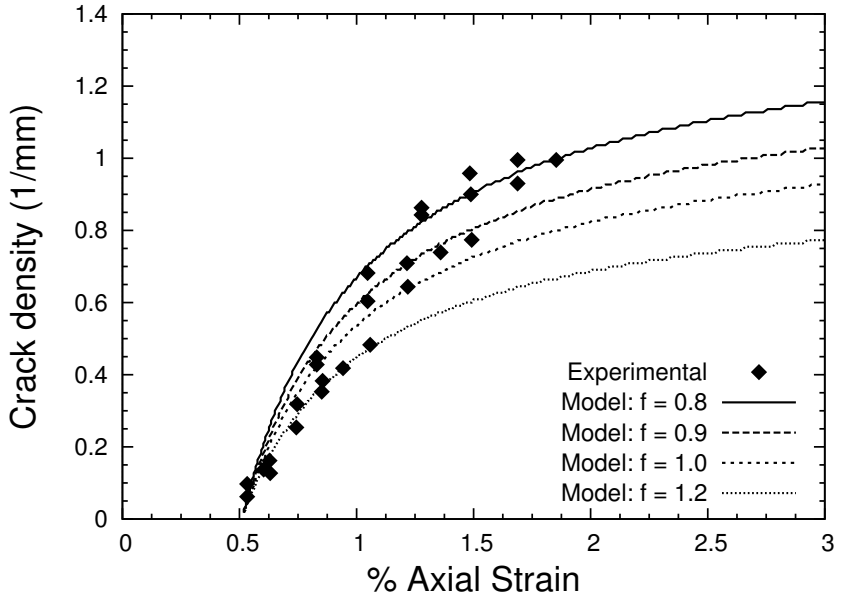

Fig. 55. Determination of fitting parameter f and critical energy release rate G_i using experimental data for $[0/90_8/0_{1/2}]_s$ laminate [109].

fiber and transverse to the fiber, respectively, in the local lamina coordinate system. Numerically, Δu_x and Δu_y are determined from nodal x and y-direction displacements averaged over the entire crack surface.

1. $[0/\pm\theta_4/0_{1/2}]_s$ Laminates

Each ply in the laminate is 0.125 mm thick. The ply material is glass- epoxy (HyE 9082Af, Fiberite).

Normalized COD and CSD values calculated using FE analysis are shown in Table IV for different laminate layups. As the crack spacing decreases, COD and CSD decrease due to interaction between nearby cracks in a given layer. The values shown in the table are at discrete values of crack spacing s. To enable representation of COD and CSD as a continuous function of s, polynomial fits were used in numerical simulations while predicting damage evolution.

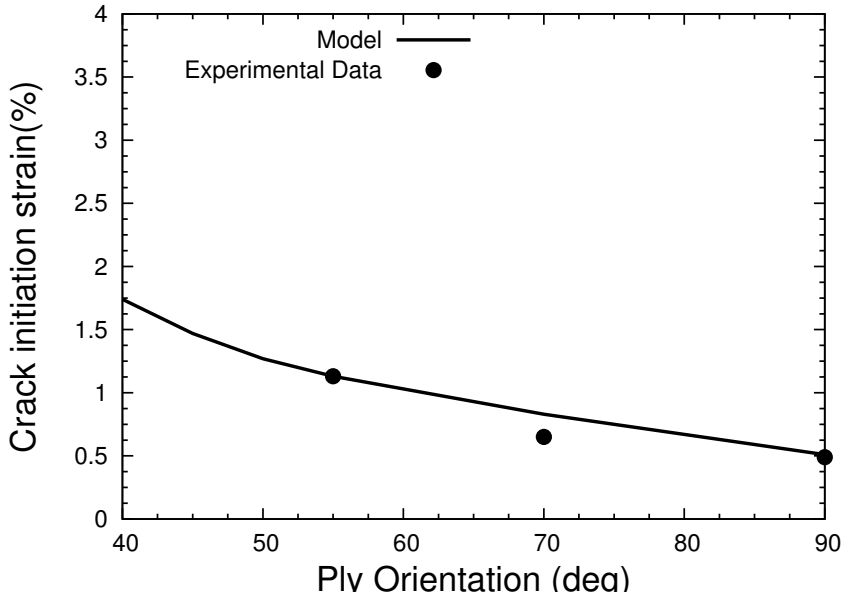

Fig. 56. Comparison of crack initiation strains with experimental data reported in [109].

It is important to note that at low crack densities, the energy release rate is almost constant. However, on development of sufficient cracks with a distribution in inter-crack spacing, it will be a function of this spacing. To account for this behavior, Liu and Nairn [44] suggested that Eq. (6.9) be modified, by introducing the concept of an effective crack spacing, as follows

$$W_I = \frac{\left(\sigma_{20}^{\theta}\right)^2 t_\theta}{E_2}\left[2\tilde{u}_n^{\theta}\left(\frac{fs}{2}\right) - \tilde{u}_n^{\theta}\left(fs\right)\right]; \qquad W_{II} = \frac{\left(\sigma_{120}^{\theta}\right)^2 t_\theta}{E_2}\left[2\tilde{u}_t^{\theta}\left(\frac{fs}{2}\right) - \tilde{u}_t^{\theta}\left(fs\right)\right] \tag{6.16}$$

where f is the average ratio of the size of the crack interval in which a ply crack forms to the average crack spacing. For cross-ply laminates, they found that $1.2 < f < 1.5$ fits well with experimental data. However, for $[0/\pm\theta_4/0_{1/2}]_s$ laminate we find that $f = 0.8$ predicts damage evolution plot closest to the experimental data. Fig. 55 forms the basis for calculation of G_I. In literature, different investigators have used different values of critical energy release rate even for the same material. This is because for

predictions of transverse cracking phenomenon, G_I is not a material constant and not equal to the fracture toughness of the matrix material, especially when the laminate layup changes. Another reason is that fracture toughness predicts the crack path and rate of progression for a single crack and not evolution of crack density. Hence, transverse cracking is a quite different phenomenon than crack propagation, although the basic concepts hold true. As a pragmatic solution, we propose that use G_I as a calibration parameter and determine it based on experimental data for a specific reference laminate. This reference laminate could be a cross-ply laminate with the same material properties. We determine $G_I = 212\ J/m^2$ by calibrating crack density evolution for $[0/90_8/0_{1/2}]_s$ laminate. Also, we assume $G_{II} = 1500\ J/m^2$ based on the literature [119].

Fig. 56 shows the comparison of crack initiation from experimental data [109] and predicted by the energy model. The figure depicts that for ply orientations close to 90°, the strain to initiate crack increases almost linearly as θ decreases. However, for $\theta < 55°$, this strain increases almost exponentially and below 40°, there are no cracks in the laminate system, because the strain to initiate crack is more than 1.5%. Moreover, below 55° transverse cracks usually do not cover the laminate width, i.e., they are non-tunneling cracks. These predictions are consistent with the experimental results on off-axis laminates [108, 109, 127].

Once we have determined G_i, we can now predict damage progression in other off-axis laminates following the procedure described in the Section 2. Using $f = 0.8$, the plots of crack density evolution for $[0/\pm 70_4/0_{1/2}]_s$ and $[0/\pm 55_4/0_{1/2}]_s$ laminates, are shown in Fig. 57 and 58, respectively. The predictions agree very well with the experimental data. In case of $\theta = 70°$, the damage model does not match with experimental measurements at high crack densities because the experimental data could be spurious due to initiation of delamination in the laminate specimen. For

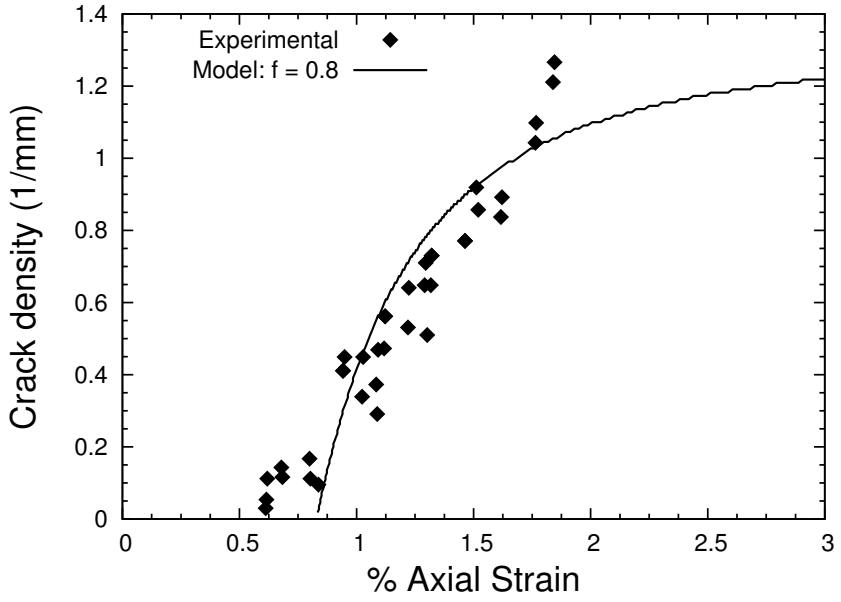

Fig. 57. Damage evolution in $[0/\pm 70_4/0_{1/2}]_s$ laminates. The experimental data is from [109].

$\theta = 55°$, the experimental data showed huge coupon-to-coupon variation [109], and thus two sets of experimental data are shown.

2. Quasi-isotropic ($[0/90/\mp 45]_s$) Laminates

The ply properties for this case are: ply thickness = 0.5 mm, E_{11}=46 GPa, E_{22}=13 GPa, G_{12}=5 GPa and ν_{12}=0.3. The CODs and CSDs for $[0/90]_s$ and $[0/90/\mp 45]_s$ laminates are shown in Table IV. The corresponding G_I value, determined by calibrating the experimental data for $[0/90]_s$ laminate, is 232 J/m^2.

The damage progression plots for $[0/90]_s$ and $[0/90/\mp 45]_s$ glass-epoxy laminates are shown in Fig. 59. In general, the model predictions are in good agreement with the experimental data. The important point to consider is the transverse cracking process in quasi-isotropic laminates in comparison to cross-ply laminates. The cracks initiate always first in 90° layer at about 0.4 % applied strain for both cross-ply and

Table IV. Normalized average COD and CSD for $[0/\pm\theta_4/0_{1/2}]_s$, $[0/90]_s$ and $[0/90/\mp 45]_s$ laminates.

$[0/\pm\theta_4/0_{1/2}]_s$ laminates								$[0/90]_s$, $[0/90/\mp 45]_s$ laminates			
$\theta = 90°$		$\theta = 70°$			$\theta = 55°$			$[0/90]_s$		$[0/90/\mp 45]_s$ (no $\mp 45°$-cracks)	
s (mm)	$\tilde{u}_n^\theta$	s (mm)	$\tilde{u}_n^\theta$	$\tilde{u}_t^\theta$	s (mm)	$\tilde{u}_n^\theta$	$\tilde{u}_t^\theta$	s (mm)	$\tilde{u}_n^\theta$	s (mm)	$\tilde{u}_n^\theta$
16.00	1.502	16.00	1.475	1.625	16.00	1.416	1.489	8.00	2.614	8.00	1.859
8.00	1.423	7.93	1.437	1.583	10.24	1.397	1.470	4.00	2.530	4.00	1.822
4.00	1.287	5.43	1.403	1.546	7.28	1.377	1.449	2.00	2.265	3.00	1.790
2.80	1.190	4.44	1.380	1.521	5.13	1.351	1.421	1.50	2.015	2.00	1.688
2.00	1.078	3.60	1.351	1.488	4.04	1.327	1.396	1.25	1.822	1.60	1.586
1.60	0.988	2.87	1.312	1.446	3.58	1.310	1.378	1.00	1.569	1.20	1.404
1.20	0.852	2.26	1.256	1.384	3.16	1.288	1.355	0.75	1.255		
0.80	0.642	1.98	1.215	1.338	2.79	1.247	1.312	0.583	1.012		
		1.73	1.159	1.276				0.50	0.882		

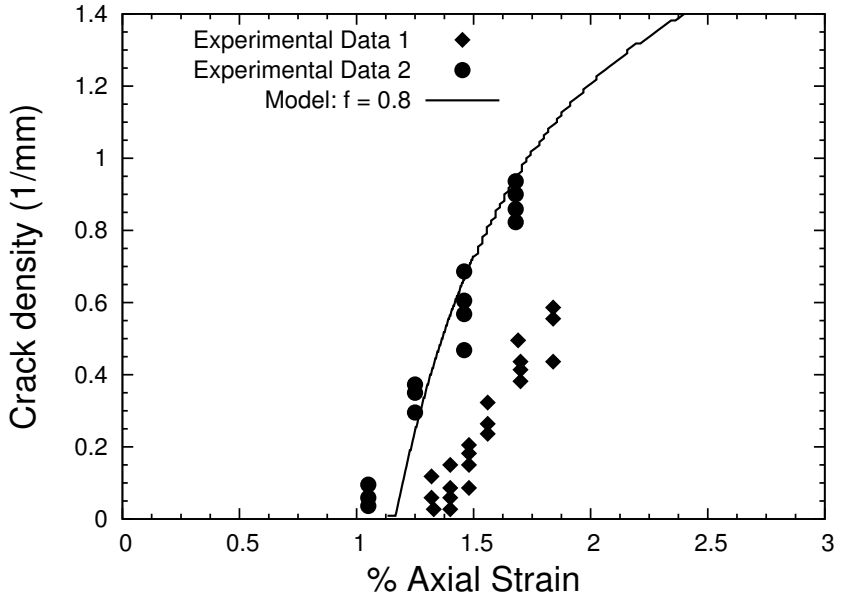

Fig. 58. Damage evolution in $[0/\pm 55_4/0_{1/2}]_s$ laminates. The experimental data is from [109].

quasi-isotropic layups. However, the crack density at saturation is higher in the quasi-isotropic laminate than in the cross-ply laminate. The dotted line in the figure shows the evolution of ply cracks in 90° layer when there are no transverse cracks in −45° and +45° layers. This is true initially during the loading process. However, on high levels of loading, cracks appear in −45° and +45° layers also. During experiments, Tong et al. [108] observed that the transverse cracks initiate in −45° layer at the interface where 90° cracks meet the −45° layer. Later, cracks develop in +45° layer at the intersection of developed −45°-cracks and -45/+45 interface. These cracks, however, do not progress fully in the laminate width before other damage modes (delaminations etc.) appear. As reported in our previous paper [171], cracks in −45° and +45° layers cause only a small degradation in the stiffness of the whole laminate.

In order to further understand the cracking behavior in $[0/90/\mp 45]_s$ laminates, a detailed 3-D stress analysis was performed with and without −45° and +45°-cracks.

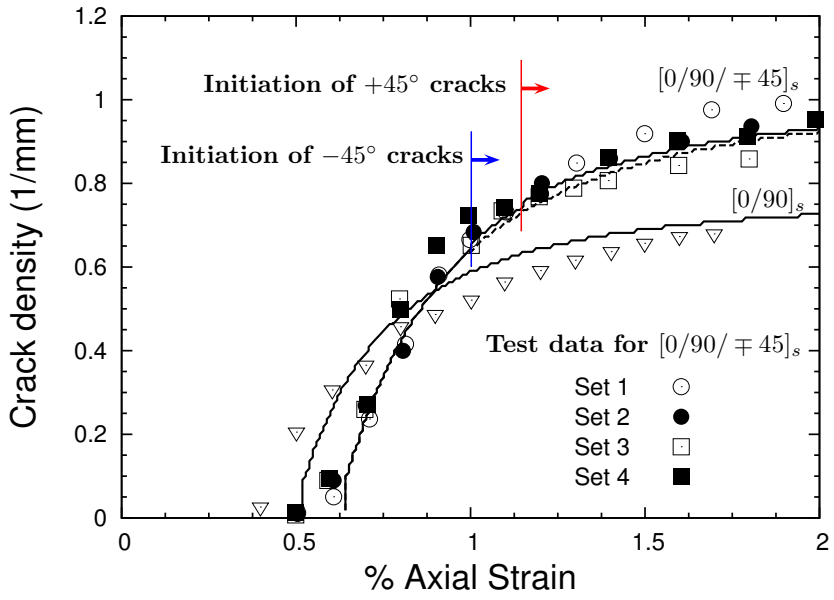

Fig. 59. Damage evolution in $[0/90]_s$ and $[0/90/\mp 45]_s$ laminates. The experimental data is from [108].

As can be seen in Fig. 60, these cracks perturb the stress state around 90° cracks also and the maximum principal stress in the laminate increases from 265 MPa to 392 MPa (a 48% increase). The maximum stress in the case without ∓45-cracks occurs at the edge interface of 90°-ply, whereas in the other case, it occurs at the intersection of 90° and −45° cracks. As a result of this stress concentration, the normalized average COD for 90° cracks increases by 10%. The resulting evolution curve is shown by a solid line in Fig. 59. There is an instantaneous increase in density of 90°-cracks on development of −45° as well as of +45°-cracks. In reality, however, this increase would not be so rapid because FE modeling did not assume growth of −45° and +45°-cracks through the laminate width. The huge scatter in experimental data after formation of −45°-cracks is due to non-uniform size and propagation of these cracks and interactions with 90°-cracks.

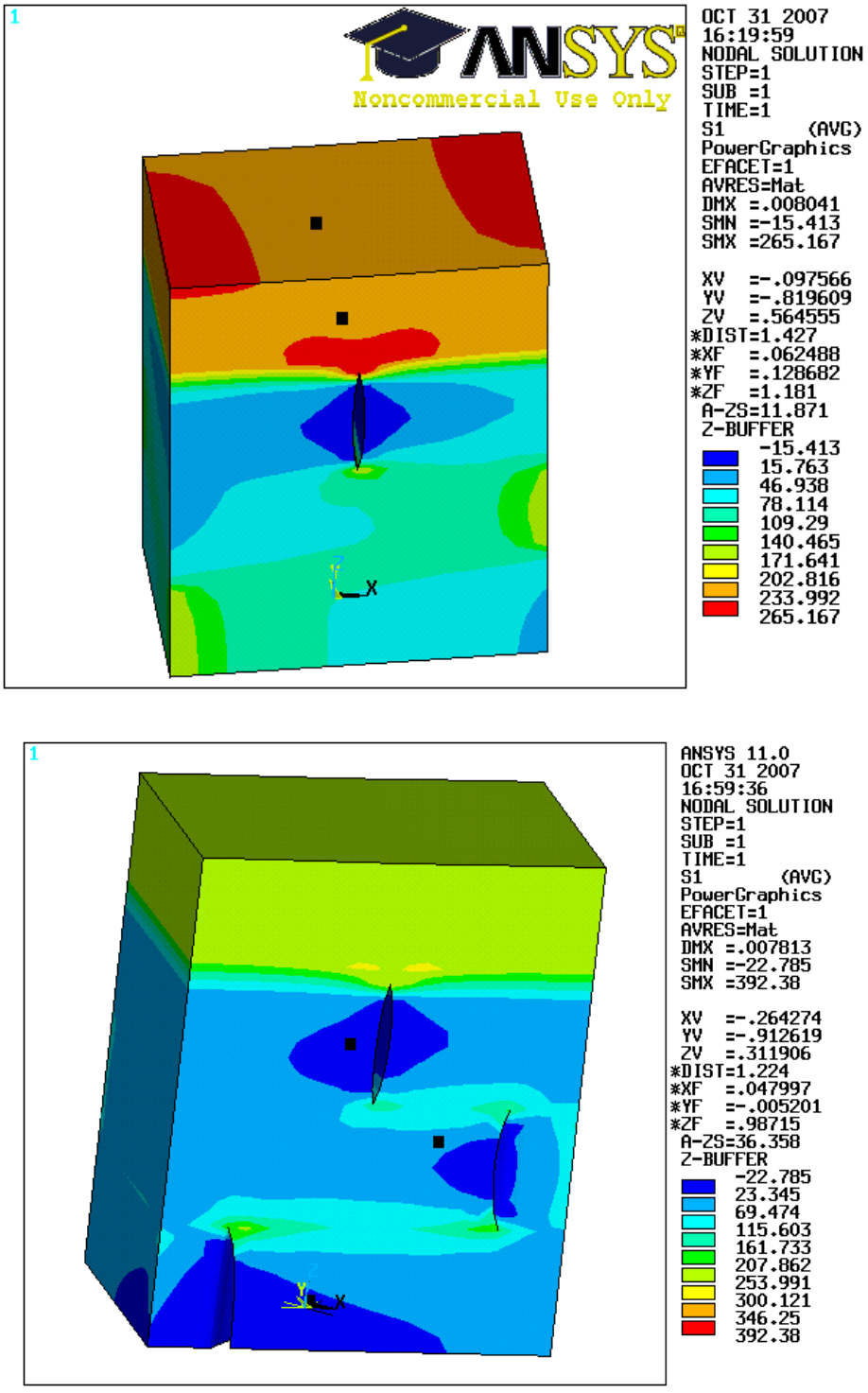

Fig. 60. Principal stress profiles for $[0/90/\mp 45]_s$ laminates: (a) without $\mp$45-cracks, (b) with $\mp$45-cracks.

3. $[0_m/90_n/\mp\theta_p]_s$ Laminates

As discussed in the previous sub-section, the damage in the case of quasi-isotropic laminates is primarily due to 90°-cracking mode. However, for $[0_m/90_n/\mp\theta_p]_s$ laminates with θ close to 90°, $\mp\theta$-modes could also be significant and consequently there could be important interactions between the two damage modes. Please note that this interaction between damage modes is appreciable only when θ is close to 90° as then the cracked surfaces for $\mp\theta$ and 90°-plies are closer to each other.

The initiation and progression of cracking in these damage modes can be predicted by computing CODs and CSDs when both form of crack systems are present in the laminate FE analysis. The applied axial strain to initiate cracking in different plies of $[0/90/\mp 60]_s$ and $[0/90/\mp 75]_s$ laminates are tabulated in Table V. The corresponding damage progression predictions with applied axial strain for these laminates are shown in Figs. 61-62. For $\theta = 60°$, 90°-cracks were predicted to form first. 90°-cracks then help in initiation and progression of $\mp 60°$-cracks from the interface between $\mp 60°$ and 90°-layers. Hence, initially in the simulation only 90°-mode is active till $\mp 60°$-cracks form. However, for $\theta = 75°$, both damage modes are found to initiate at almost the same applied strain; hence all modes are active initially in the FE simulation.

Table V. Crack initiation strains (%) in $[0_m/90_n/\mp\theta_p]_s$ laminates.

Case	$\theta = 45°$	$\theta = 60°$			$\theta = 75°$		
	90° ply	90° ply	−60° ply	+60° ply	90° ply	−75° ply	+75° ply
m=n=p=1	0.665	0.773	0.964	0.898	0.781	0.796	0.752
m=2, n=p=1	0.667	0.776	0.967	0.9006	0.785	0.796	0.755
n=2, m=p=1	0.472	0.520	0.952	0.886	0.522	0.793	0.750
p=2, m=n=1	0.673	0.778	0.650	0.643	0.821	0.535	0.533

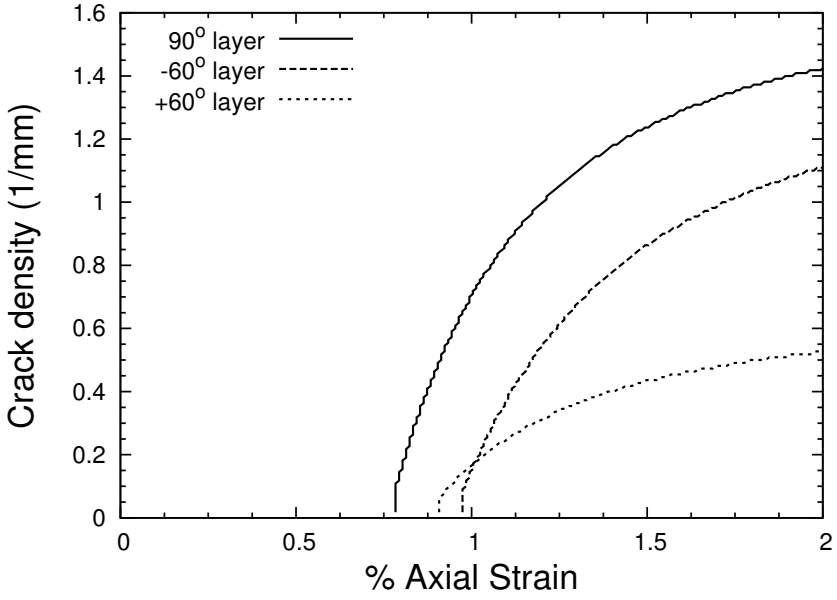

Fig. 61. Damage evolution in $[0/90/\mp 60]_s$ laminates.

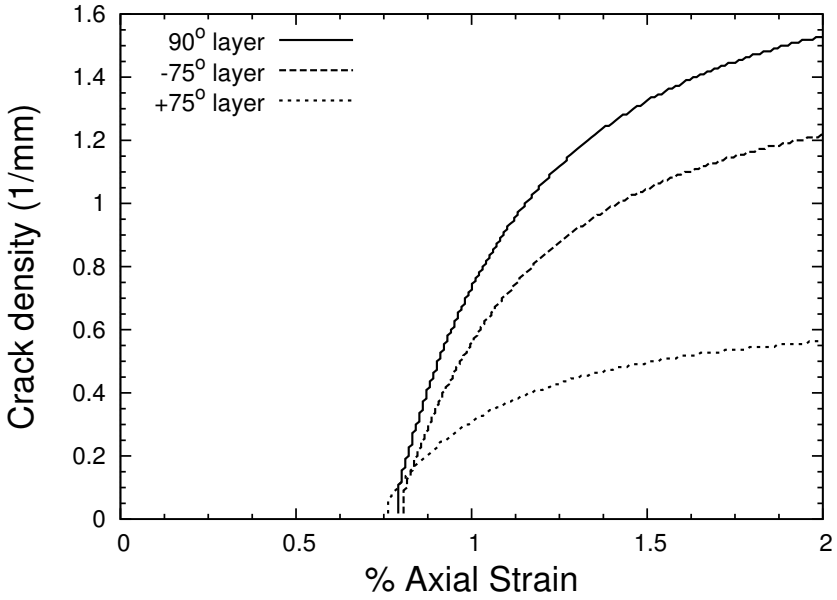

Fig. 62. Damage evolution in $[0/90/\mp 75]_s$ laminates.

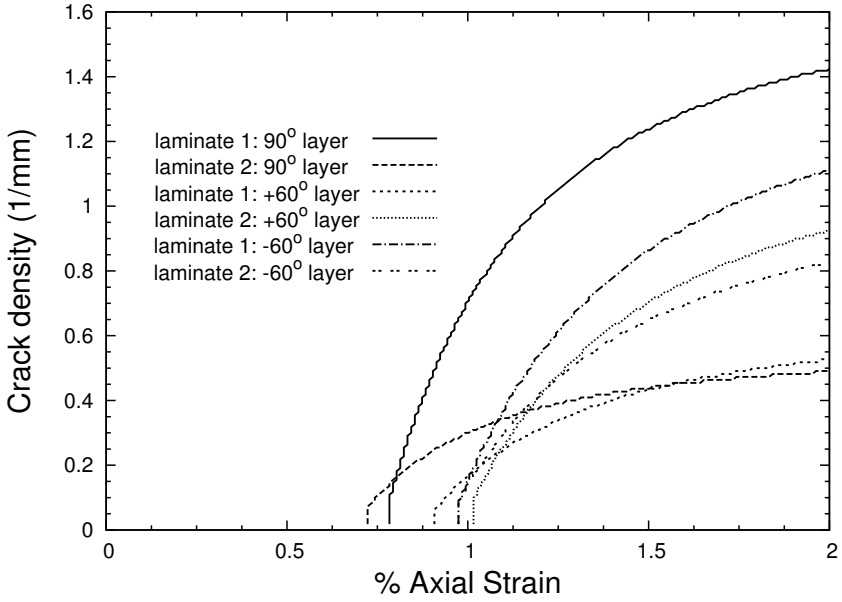

Fig. 63. Damage evolution in $[0/90/\mp 60]_s$ (laminate 1) and $[0/\pm 60/90]_s$ (laminate 2) layup configurations.

4. $[0_m/\pm\theta_p/90_n]_s$ vs. $[0_m/90_n/\mp\theta_p]_s$ Laminates

It is interesting to observe that the actual layup may matter for transverse crack initiation and progression. Fig. 63 illustrates this aspect by comparing damage evolution in $[0/90/\mp 60]_s$ and $[0/\pm 60/90]_s$ laminates. It is notable here that most of the present techniques have no clear way of differentiating the damage progression in these two laminates. The present approach, however can model this aspect through determination of CODs and CSDs, which are different for the two sets of laminates. Although the difference in the overall stiffness behavior for these laminates may turn out to be small, the crack initiation strains and the rate of progression are different in some plies, e.g., internal ply at the laminate mid-plane (being of a larger size) develops cracks much earlier than other plies of same orientation.

5. Shape of Damage Evolution Curve

Fig. 64 depicts the actual and predicted shape of the damage evolution curve. The transverse cracking phenomenon usually comprises three distinct stages. The first stage corresponds to the formation of initial ply cracks and their propagation though the specimen thickness and width. In most cases, transverse ply cracks initiate at the surface of the specimen and quickly traverse the thickness direction. However, depending upon the ply orientations, these cracks may or may not propagate instantaneously through the whole laminate width. For cross-ply laminates, this through-width propagation is facilitated by the fact that propagation direction is normal to the loading direction and as a result, they do propagate almost instantaneously (at the experimental time scale), and are called *tunneling cracks*. This instant propagation of cracks in the laminate width direction may not occur for other ply configurations and material. It also depends upon how well made the coupons are. If specimens are well prepared, they will have less variability in flaws and show a more rapid rise in crack density just after first ply crack formation [22]. The stage II and III in the plot refer to increase in density of transverse cracks. In the beginning of stage II, these cracks are not equally spaced due to randomness of the material resistance to fracture. However, in the later part of stage II, these cracks form roughly periodic arrays. The stage III represents higher crack densities and there is a *shielding effect* due to adjacent cracks, resulting in slowing down leading to saturation of cracking process. Since the damage model discussed here does not account for crack propagation through laminate width, it does not predict the stage I of the curve correctly. Also, the damage model will predict axial strain at first crack formation close to starting of stage II. Thus, the damage model predicts *crack propagation strain* instead of *crack initiation strain*. However, Stage II and Stage III are predicted well by the damage

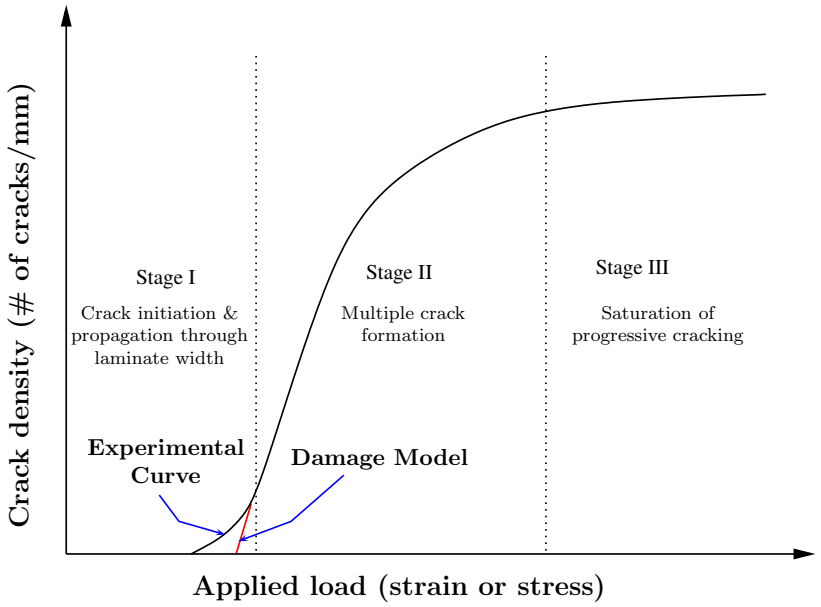

Fig. 64. A typical damage evolution curve for transverse ply cracking in composite laminates.

model.

6. Parametric Study of Layer Thickness

The same procedure can be handy in predicting damage progression of other laminates of the class $[0_m/90_n/\mp\theta_p]_s$. With change in cracked/uncracked ply thicknesses, CODs and CSDs computed from FE simulation also change and they affect the damage initiation and progression accordingly. As the thickness of a cracked layer is increased, the applied strain to initiate cracking in that layer, as well as other cracking layers, decreases. On the other hand, increase in thickness of uncracked supporting plies increases the crack initiation strain. Table V lists the predicted crack initiation strains for different m, n and p values for $[0_m/90_n/\mp\theta_p]_s$ laminates. It can be observed that the change in thickness of a cracked layer have the maximum influence in crack initiation in that ply; whereas the influence of change in thickness of other layers

fairly small.

The first case considered here is $[0_m/90_n/\mp 45_p]_s$ laminate. For this laminate configuration, fully grown cracks are assumed only in 90° layer. Predicted damage evolution curves for 90°-cracking for different values of m, n and p are shown in Fig. 65. It is clearly seen that the crack initiation strain are almost same for $m = n = p = 1, m = 2$, and $p = 2$, whereas for $n = 2$, crack initiation strain decreases to below 0.5% as compared to 0.66% for $m = n = p = 1$. Also, the shape of evolution curve is influenced by the relative no. of plies in a specific orientation. As the thickness of 90°-layer is doubled, the saturation crack density decreases to almost half. However, change in thickness of other layers does not change crack density at saturation much.

The second case refers to $[0_m/90_n/\mp 60_p]_s$ laminates. In this situation, cracks usually initiate in 90° first and then in $\mp 60°$ layers. Thus, initial simulation assumes only 90° cracks; whereas after the initiation of $\mp 60°$ cracks, a multi mode scenario is used in FE modeling. As described earlier, $\mp 60°$ cracks influence the damage progression in 90° layer. The predictions for different m, n, p values are shown in Fig. 66 (a)-(c) for $90°, -60°$ and $+60°$ layers, respectively. For $p = 2$, the model predicts that cracks in $\mp 60°$ layers will initiate earlier than 90° layer.

The final case caters to damage progression in $[0_m/90_n/\mp 75_p]_s$ laminates. In this scenario, cracks can initiate in all cracking layers almost at same applied strain. Hence, all modes of damage could be present simultaneously. The predictions for this laminate are shown in Fig. 67 (a)-(c) for $90°, -75°$ and $+75°$ layers, respectively. Observations similar to the above can be made with regards to crack initiation strain, shape of evolution curve and the saturation cracks density.

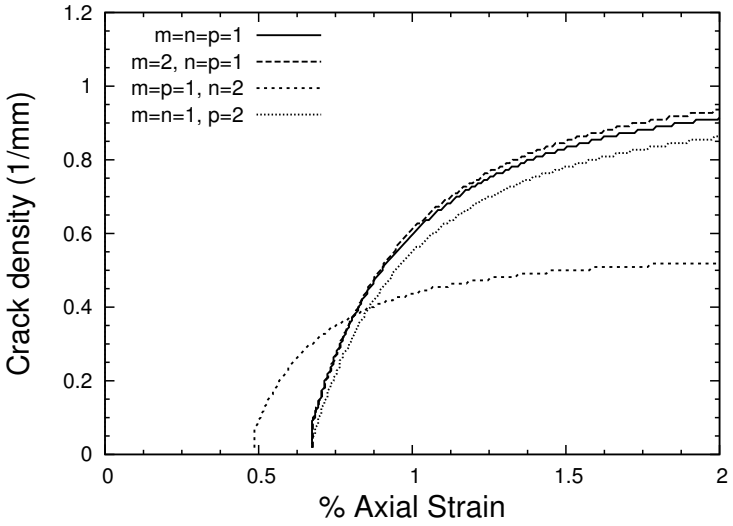

Fig. 65. Damage evolution for 90°-cracking in $[0_m/90_n/\mp 45_p]_s$ laminates.

F. Summary

In this chapter, an energy based approach was developed and implemented to predict initiation and progression of damage due to transverse cracking in a multidirectional laminate. The developed multimode criterion predicts formation of new cracks when the total energy supplied by loading exceeds the energy required to close these cracks. A reference laminate is selected to calibrate the energy release rates in the opening and sliding modes. Based on the cracking criterion, initiation of ply cracks in different off-axis plies, and increase in their densities as a function of applied loading are predicted for two classes of multidirectional laminates: $[0/\pm\theta_4/0_{1/2}]_s$ containing cracks in $+\theta$, and $-\theta$ plies, and $[0_m/\pm\theta_p/90_n]_s$ containing cracks in 90°, $+\theta$, and $-\theta$ plies. The predictions for selected laminate sequences show good agreement with the published experimental data.

In previous chapters, we predicted stiffness degradations for these laminate layups as a function of crack density, whereas this chapter focused on predicting increase in

(a)

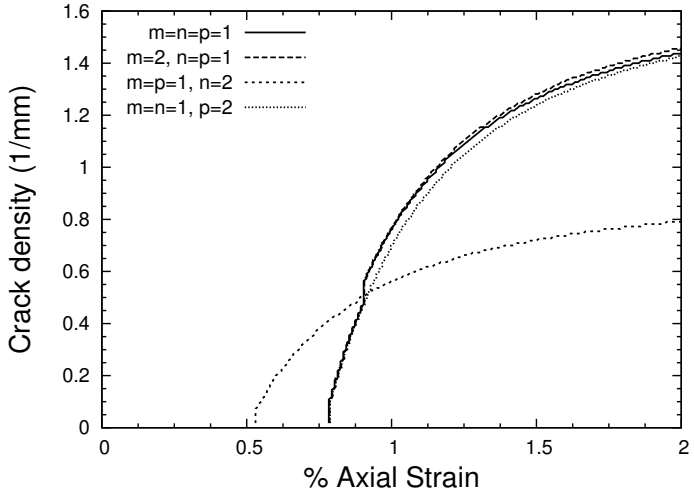

(b)

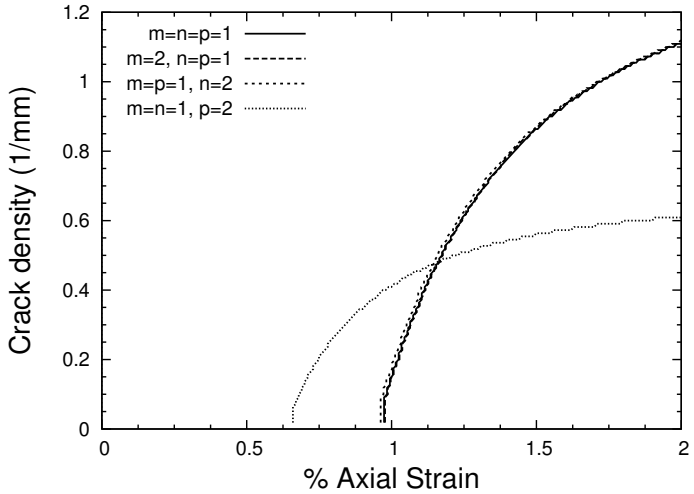

(c)

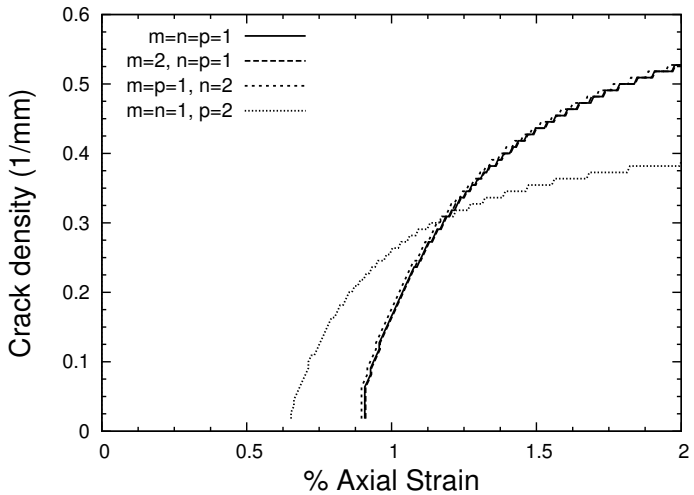

Fig. 66. Damage evolution in $[0_m/90_n/\mp 60_p]_s$ laminates: (a) 90° layer, (b) −60° layer, (c) +60° layer.

(a)

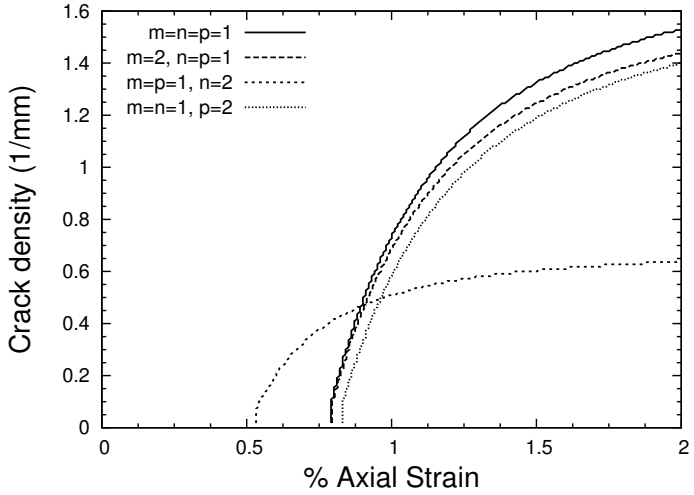

(b)

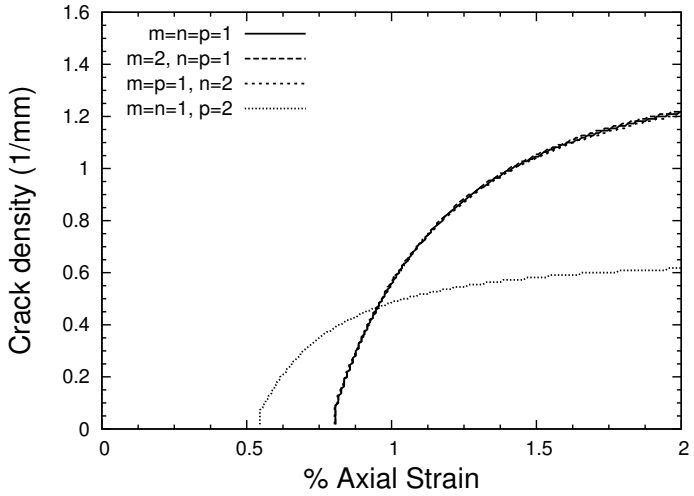

(c)

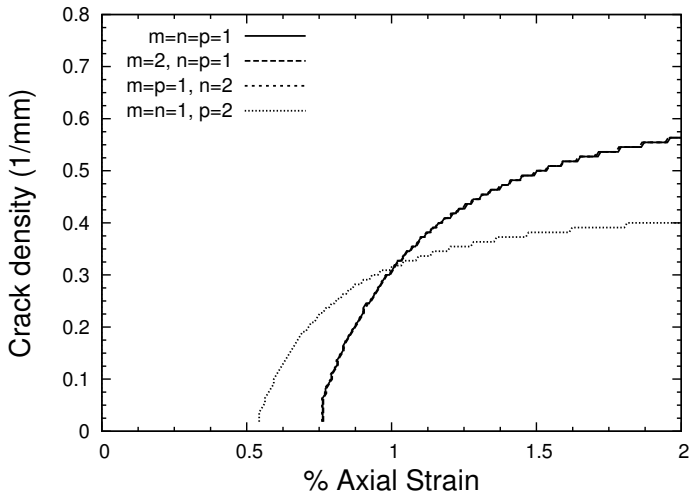

Fig. 67. Damage evolution in $[0_m/90_n/\mp 75_p]_s$ laminates: (a) 90° layer, (b) $-75°$ layer, (c) $+75°$ layer.

crack density as a function of applied load. Combining the two solutions, we obtain the effect of damage on structural performance as a function of loading, and this will be covered in the next chapter.

CHAPTER VII

OVERALL LAMINATE BEHAVIOR

A. Laminate Stress-Strain Response

From the mechanics view point, the most important characteristic of a structure is its stress-strain response. Considering the case of displacement controlled loading, i.e., the strain applied at the boundaries of the laminate, we are interested in

$$\sigma_{ij} = C_{ijkl}\left(\epsilon_{kl}\right)\epsilon_{kl} \tag{7.1}$$

where, C_{ijkl} represents the stiffness matrix of the damaged laminate. To get stress-strain response, we need to express C_{ijkl} in terms of applied loading ϵ_{ij}. In damage analysis of composite laminate there is no direct way of predicting the stiffness tensor C_{ijkl} as a function of the applied strain. Rather, the usual practice is to solve two interdependent sub-problems to arrive at the overall stress-strain behavior:

1. Describe stiffness changes as a function of crack density: In this step C_{ijkl} is expressed in terms of some damage characteristic, such as the ply crack density,

$$C_{ijkl} = C_{ijkl}\left(\rho^{(\alpha)}\right) \tag{7.2}$$

   where $\rho^{(\alpha)}$ is the crack density of damage mode α.

2. Describe the evolution of crack density as a function of applied loading: This step refers to the determination of damage initiation and its progression. Here, $\rho^{(\alpha)}$ is determined as a function of applied loading, i.e.,

$$\rho^{(\alpha)} = \rho^{(\alpha)}\left(\epsilon_{kl}\right) \tag{7.3}$$

Combining the solution to above two sub-problems, we obtain

$$C_{ijkl} = C_{ijkl}\left(\rho^{(\alpha)}\left(\epsilon_{kl}\right)\right) \tag{7.4}$$

The solution to first sub-problem was covered in chapters IV and V, for $[0_m/\pm\theta_n/0_{m/2}]_s$, and $[0_m/\pm\theta_n/90_r]_s$ and $[0_m/90_r/\pm\theta_n]_s$ laminates, respectively. Chapter VI concentrated on the second sub-problem for both layups.

1. $[0_m/\pm\theta_n/0_{m/2}]_s$ Laminates

This is the case with two damage modes referring to the cracks in $+\theta$ and $-\theta$ layers. The crack density in each of θ layers, and their effects on laminate response are assumed to be the same. Thus, they are lumped into a single effective damage mode. The predictions of stiffness changes for this laminate layup are shown in Figs. 32, 33, and 34 on pages 92, 93, and 94, for $\theta = 90°, 70°$, and $55°$, respectively. The evolution of crack density with applied strain for these laminates are correspondingly shown in Figs. 55, 57, and 58 on pages 158, 161, and 163. The ply material is Fiberite, for which the properties are given in Table III on page 157 (see properties for Material 1).

Combining the two solutions, according to Eq. (7.4), the stress-strain response for these laminates is determined, as shown in Fig. 68. The solid lines represent the actual non-linear response of the damaged laminate, whereas the dotted lines are shown to depict the assumed behavior if the laminate was not cracked arrived using the Young's moduli for the virgin laminates, which are: 18.995, 17.879, and 17.841 GPa for $\theta = 90°, 70°$, and $55°$, respectively. They are calculated by the classical laminated plate theory [147]. The laminates are assumed to be stress free initially, i.e., no residual stresses due to thermal cooldown, or chemical shrinkage, etc. are considered.

As expected, the off-axis ply in $[0/90_8/0_{1/2}]_s$ laminate starts cracking earlier than that for other ply angles, and its effect on the stress-strain response is also the highest. The nonlinearity in the stress-strain curve is thus depends on the laminate material as well as the off-axis ply orientation. The variations of effective longitudinal modulus and Poisson's ratio with applied longitudinal strain for $[0/\pm\theta_4/0_{1/2}]_s$ laminates are shown in Fig. 69. Although the longitudinal modulus in virgin state is practically same for $\theta = 90°$ and 70°, the reduction in its magnitude is much severe for 90°. At a longitudinal strain of 2.5%, the longitudinal modulus reduce to about $63\%, 48\%$, and 36% of their initial magnitude, for $\theta = 55°, 70°$, and 90°, respectively. Correspondingly, the Poisson's ratios decrease upto $77\%, 56\%$, and 17% of the initial values. These reductions are quite high from a practical view point. This is partially because the SDM model is linear with respect to crack density, and thus predicts a more severe degradation than what would be actually observed in experiments. From the figures, it is also evident that the degradation in the longitudinal modulus and Poisson's ratio is appreciable in the beginning of the cracking process, and both of them seem to attain asymptotic saturation values at high strain values.

2. $[0_m/\pm\theta_n/90_r]_s$ and $[0_m/90_r/\pm\theta_n]_s$ Laminates

These laminates can undergo cracking in three damage modes: $+\theta$, $-\theta$, and 90°. From the stiffness changes and damage evolution curves, covered in the previous chapters, it can be realized that the 90° cracking represents the most dominant damage mode for these laminate configurations. In a practical scenario it means that when subjected to tensile loading in the longitudinal direction, 90° plies will start cracking first and cause significant stiffness degradation before $\pm\theta$ cracks may even start to initiate. Also, as observed in several experimental studies (e.g., [108]), cracks in $\pm\theta$ plies may not even develop fully before the laminate fails by delamination. As a result, the degradation

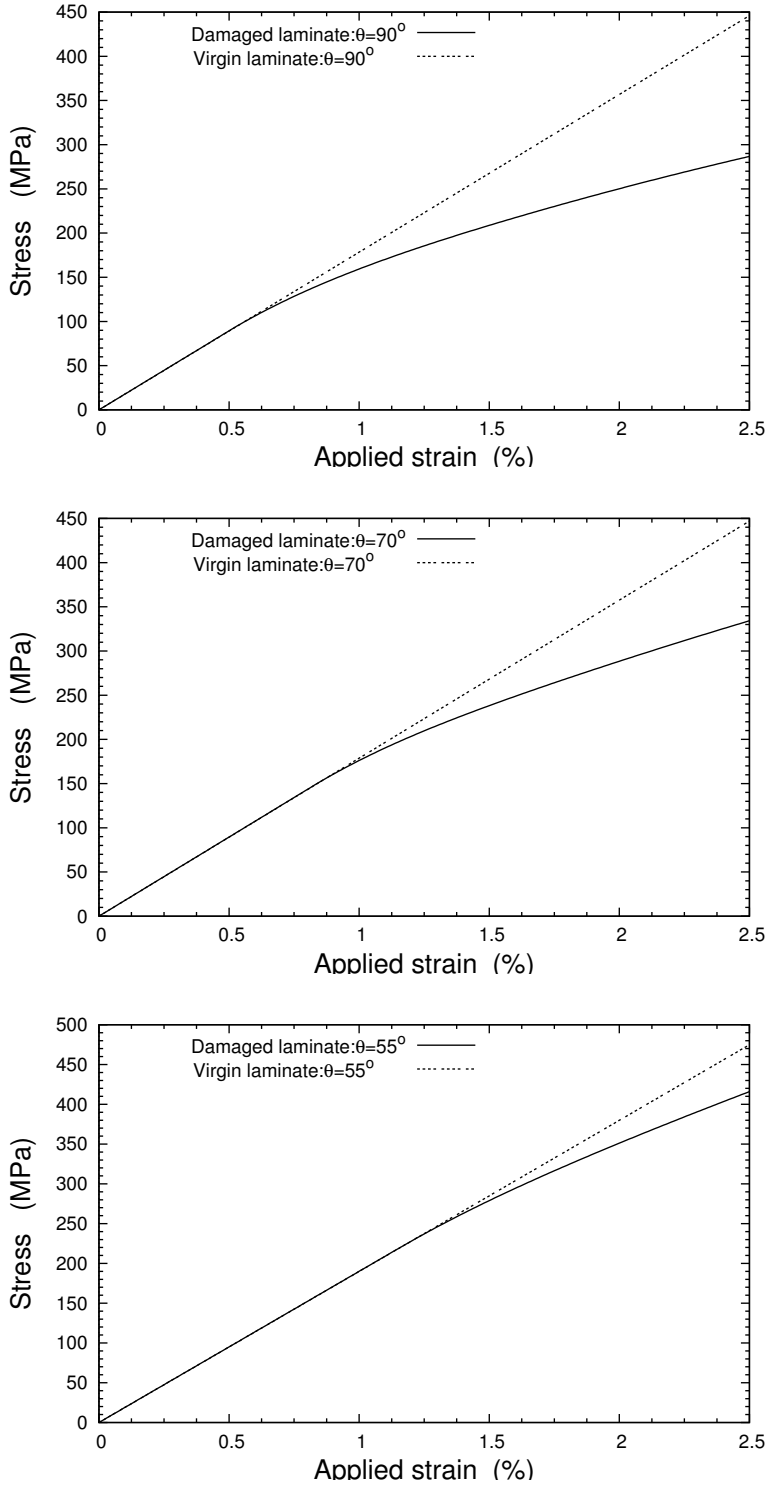

Fig. 68. Stress-strain response for $[0/\pm\theta_4/0_{1/2}]_s$ laminates: (a) $\theta = 90°$, (b) $\theta = 70°$, (c) $\theta = 55°$. For $\theta = 55°$, the damage due to shear deformation is not considered (see chapter IV for more details).

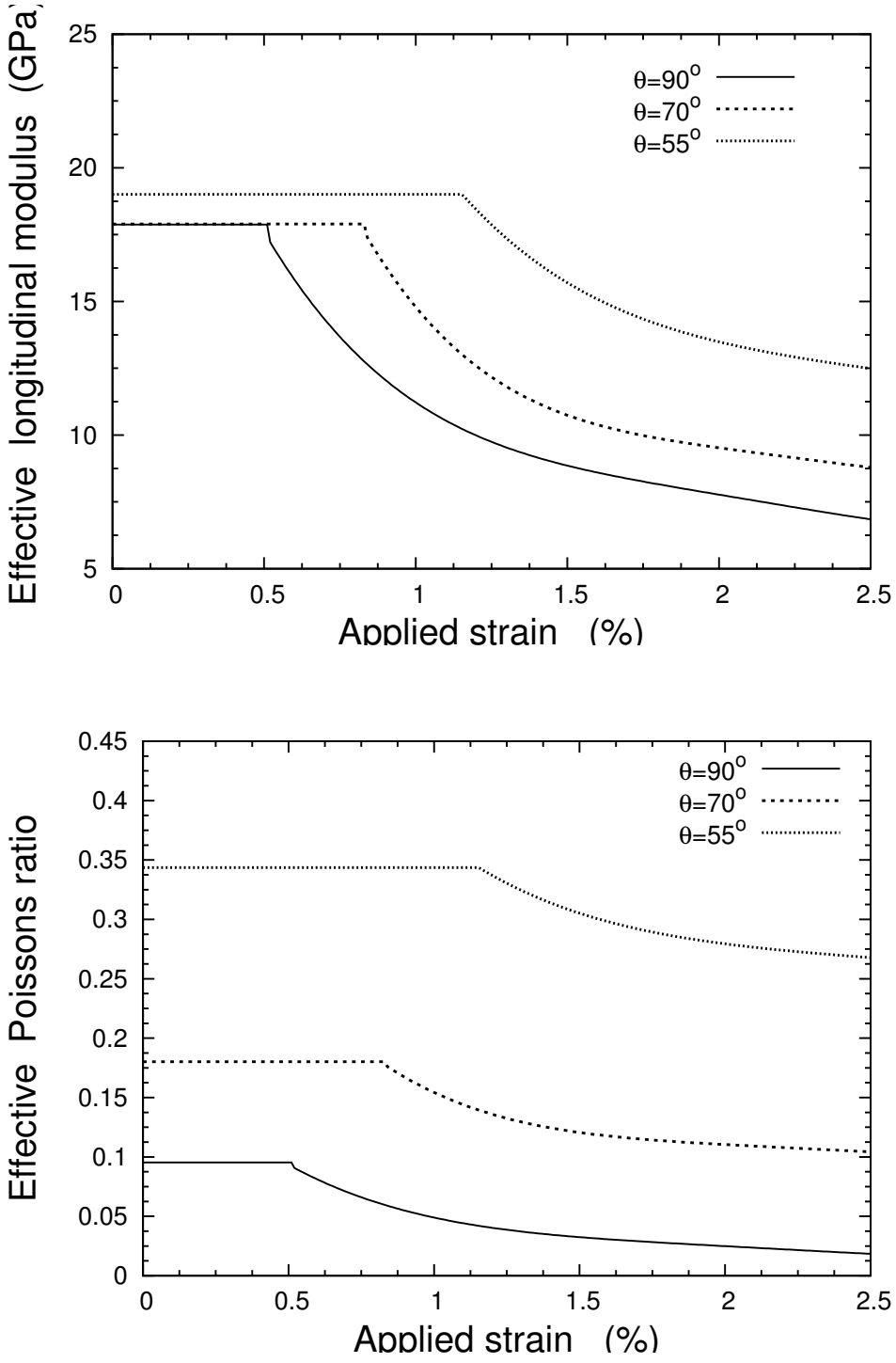

Fig. 69. Variation of effective longitudinal modulus and Poisson's ratio for $[0/\pm\theta_4/0_{1/2}]_s$ laminates: (a) Longitudinal modulus E_1, (b) Poisson's ratio. For $\theta = 55°$, the damage due to shear deformation is not considered (see chapter IV for more details).

in the overall stiffness properties of these laminates is mostly contributed from the 90° cracking. This is specially true for laminates with $\theta < 45°$. However, for laminates with $\theta \approx 90°$, $\pm\theta$ plies may also crack at lower loading levels, and thereby contribute significantly to the stiffness changes. The different cracks systems may even interact and cause further stress perturbations. To illustrate these two cases, we first consider a quasi-isotropic laminate with a dominant 90° cracking. Next, $[0/\pm 60/90]_s$ laminate will be considered to illustrate a truly multi-mode damage scenario. The ply material is glass/epoxy (Material 2 in Table III shown on page 157).

a. Quasi-isotropic laminate

Here, we consider the laminates experimentally studied in the reference [108]. The SDM predictions for the stress-strain response for the cross-ply and quasi-isotropic laminates considered in that study are shown in Fig. 70. Similar to what was observed in the experiments, SDM predicts 90° cracking to begin at about 0.4% applied strain in both the cross-ply and quasi-isotropic laminates. ±45° cracks appear in the quasi-isotropic laminate at about 1% applied strain, and do not grow fully through the laminate width. The nonlinearity due to a degradation in the longitudinal modulus is predicted to be of a larger magnitude in the cross-ply than that in the quasi-isotropic laminates. This is because in a quasi-isotropic laminate the constraint to 90° ply cracking from supporting plies is much higher than in a cross-ply laminate: the quasi isotropic laminate has three supporting plies (+45°, −45° and 0°) on each side of cracked 90° ply, whereas the constraint in a cross-ply laminate is available only from 0° ply.

For a quasi-isotropic laminate, three cases for stress-strain response are shown in Fig. 70. The first case considers that only 90° ply is cracked and the resulting predictions are shown by a solid line. Two dotted lines representing nonlinear responses

refer to the case in which $\pm 45^\circ$ cracks are also present in the laminate, with $a = 0.25$, and $a = 0.5$. Here, a refers to the assumed ratio between the surface area occupied by 90° and $\pm 45^\circ$ cracks at a given loading (it is the same as ρ_r in chapter V, Eq. (5.38) on page 132). In this way, we can model partially grown cracks. A more accurate determination of a would require observation of cracked laminates to see the extent of $\pm 45^\circ$ crack size and growth.

The changes in the longitudinal modulus and the Poisson's ratio for the cross-ply and quasi-isotropic laminates are shown in Figs. 71 and 72, respectively. As mentioned above, multiple lines in plots for quasi-isotropic case signify cases with 90° cracking only, 90° as well as $\pm 45^\circ$ cracking with $a = 0.25$, and $a = 0.5$.

b. $[0/90/\mp 60]_s$ laminate

To illustrate the capability of the SDM approach for interacting multimode damage scenario, $[0/90/\mp 60]_s$ glass/epoxy laminate is chosen here. As discussed in the previous chapter, 90° ply in this case begins cracking at about 0.77% applied strain, whereas $+60^\circ$, and -60° plies develop cracks at about 0.9, and 1.0 % strain, respectively. Although -60° plies are adjacent to 90° plies, and have more interaction effects from them, $+60^\circ$ ply cracking is predicted to occur before -60° cracking, probably because the $+60^\circ$ plies are centrally placed and their thickness is double of individual -60° plies on either side of the laminate mid-plane. For this laminate, the constraint parameters are calculated from FEM as: $\kappa_{90_{4n+2r}} = 7.11\text{e-}3, \kappa_\theta|_{\theta=90} = 11.44\text{e-}3, \kappa_\theta = 6.45\text{e-}3, \text{and} \kappa_{90_r} = 9.11\text{e-}3$. The stiffness changes are obtained using Eq. (5.28) on page 116. Initial value for the longitudinal modulus and the Poisson's ratio for the laminate using CLPT are calculated as $E_1^0 = 21.354$ GPa, and $\nu_{12}^0 = 0.2098$, respectively.

The predicted stress-strain response for the laminate is shown in Fig. 73. While

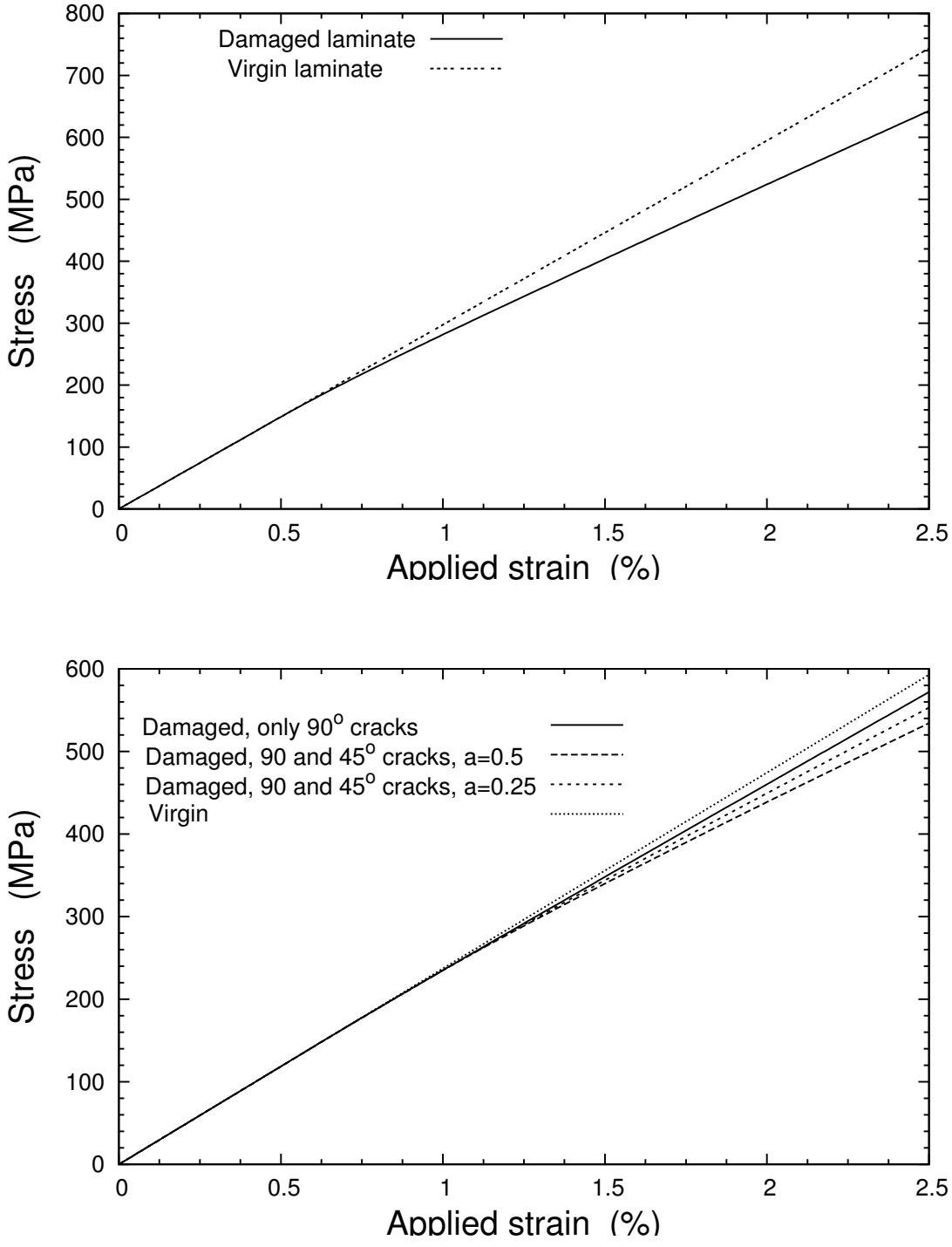

Fig. 70. Stress-strain response of cross-ply and quasi-isotropic laminates: (a) Longitudinal modulus E_1, (b) Poisson's ratio. The laminate properties are from [108].

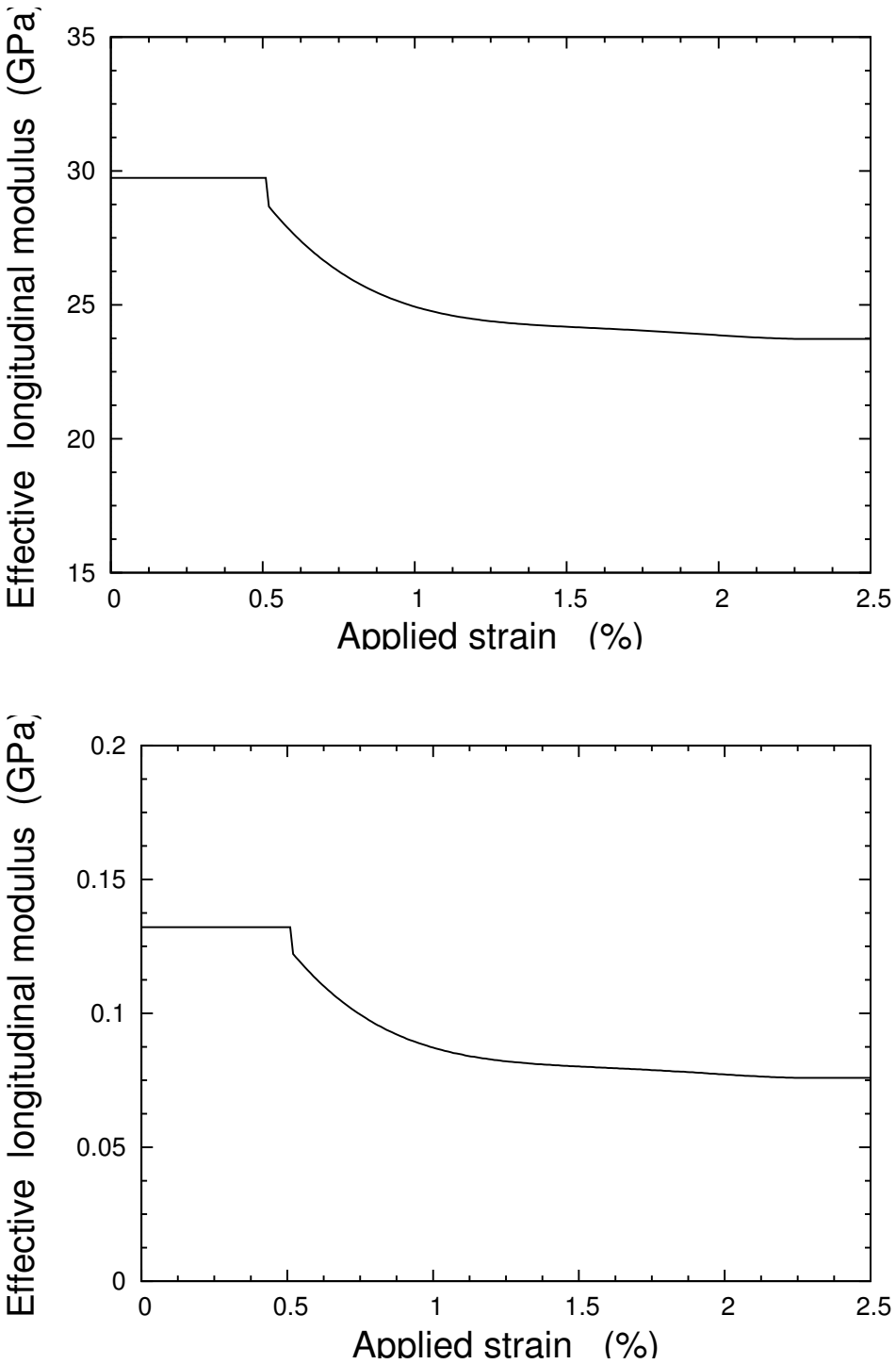

Fig. 71. Variation of effective Longitudinal modulus and Poisson's ratio for cross-ply laminate.

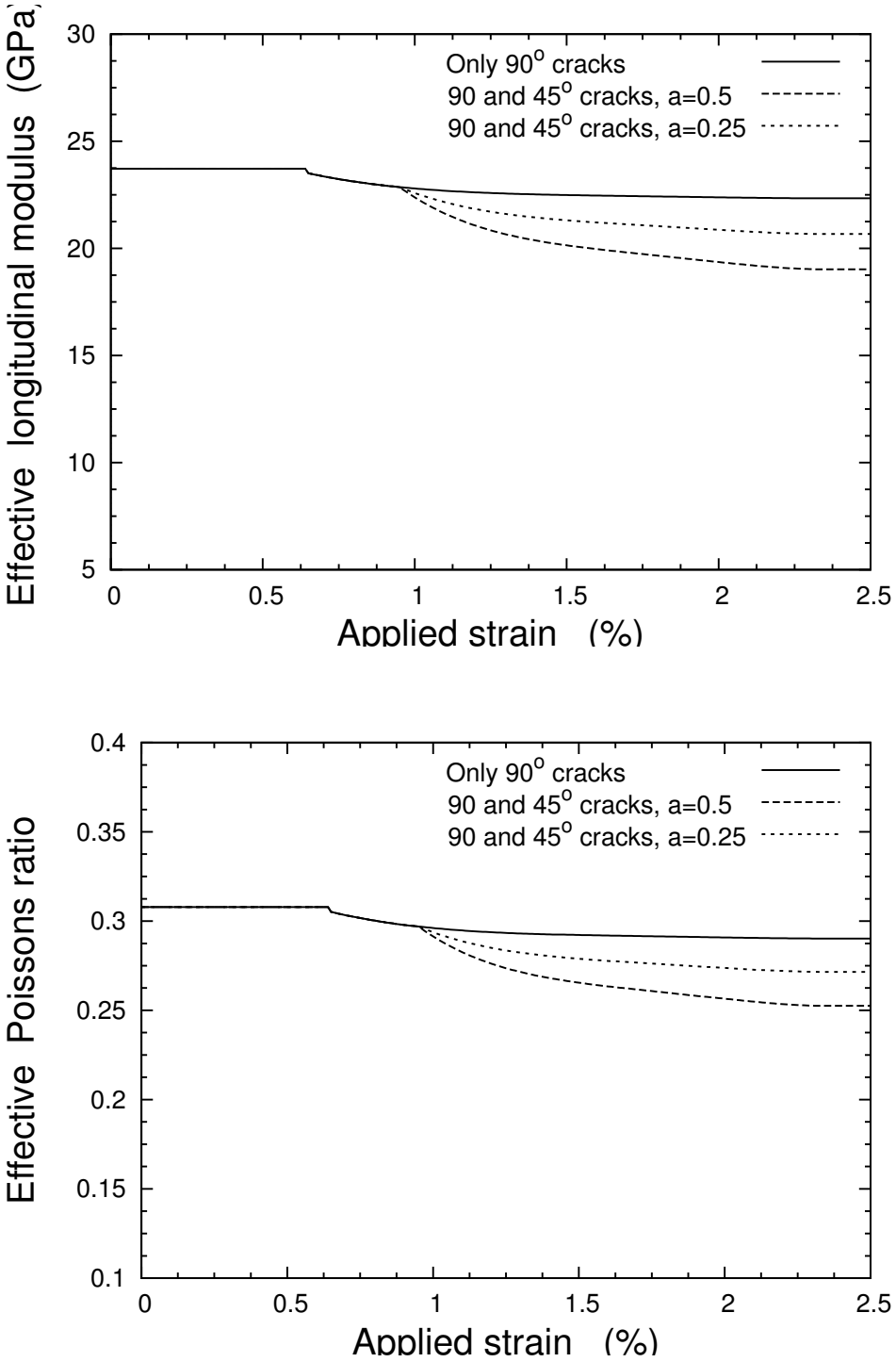

Fig. 72. Variation of effective Longitudinal modulus and Poisson's ratio for quasi-isotropic laminate.

calculating stiffness changes as a function of applied loading for a multimode scenario, one should add changes caused by the active modes only. For example, for this laminate, the stiffness changes as a function of applied longitudinal strain can be expressed as

$$\begin{aligned}
C_{ijkl} &= C^0_{ijkl}, && \epsilon_X < \epsilon^{90}_{X0} \\
C_{ijkl} &= C^0_{ijkl} + C^{(90)}_{ijkl}\left(\rho^{(90)}\right), && \epsilon^{90}_{X0} \le \epsilon_X < \epsilon^{+60}_{X0} \\
C_{ijkl} &= C^0_{ijkl} + C^{(90)}_{ijkl}\left(\rho^{(90)}\right) + C^{(+60)}_{ijkl}\left(\rho^{(+60)}\right), && \epsilon^{+60}_{X0} \le \epsilon_X < \epsilon^{-60}_{X0} \\
C_{ijkl} &= C^0_{ijkl} + C^{(90)}_{ijkl}\left(\rho^{(90)}\right) \\
&\quad + C^{(+60)}_{ijkl}\left(\rho^{(+60)}\right) + C^{(-60)}_{ijkl}\left(\rho^{(-60)}\right) && \epsilon_X \ge \epsilon^{-60}_{X0}
\end{aligned} \tag{7.5}$$

This is reflected in the stress-strain curve as well. For comparison, the stress-strain curve assuming only 90° cracking is also in the figure by a solid line. The nonlinearity in the stress-strain curve due to all cracking modes is much higher than that due to only 90° cracking. This is because of contribution from ±60° cracking modes, as well as due to the intra-mode interactions, which increase the rate of stiffness reduction. The plots for the longitudinal modulus, and the Poisson's ratio with respect to the applied loading are shown in Fig. 74. In these graphs also, the reduction due to all modes active is observed to be quite severe as compared to only 90° cracking. For $[0_m/\pm\theta_n/90_r]_s$ and $[0_m/90_r/\pm\theta_n]_s$ laminates, these intra-mode interaction effects will be quite extensive as θ is chosen closer to 90° as the region of interaction between cracked surfaces becomes larger. For $\theta < 45°$, however, they might not be as appreciable.

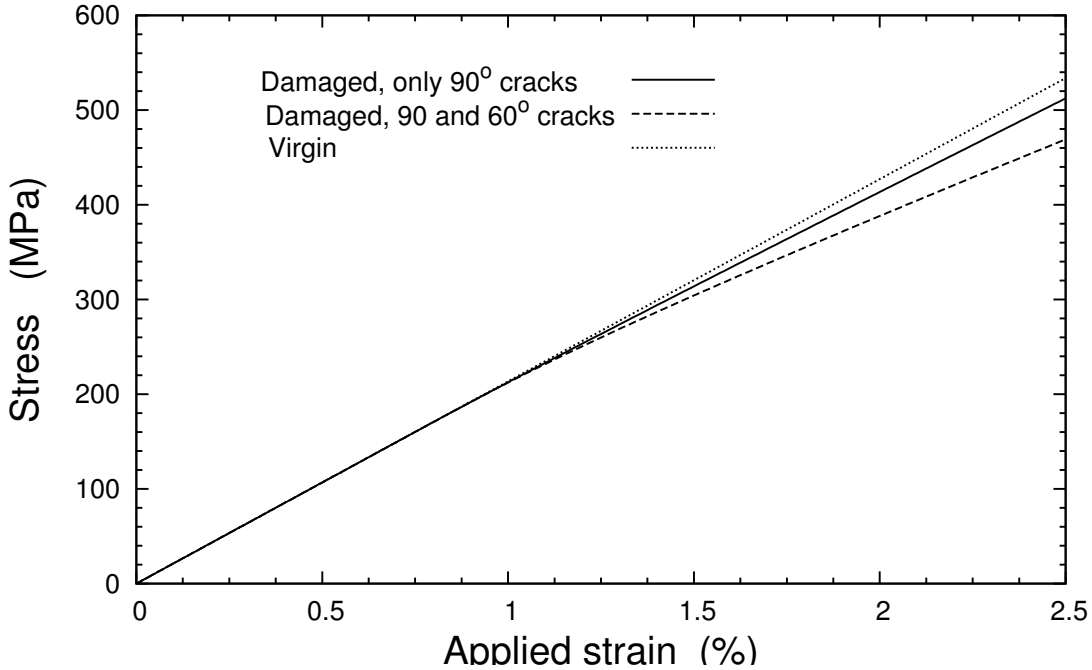

Fig. 73. Stress-strain response of $[0/90/\mp 60]_s$ laminate.

B. Multiscale Modeling

The damage in materials occurs due to dissipative mechanisms which usually occur at lower length scales, like microns or sometimes even sub-microns. To fully understand the underlying phenomena, and characterize its affect on material performance, it is essential to link the two scales: the length scale at which these processes take place (the *micro scale*), and the length scale at which we use the material (the 'structural' or 'macro' scale). These two scales, in reality may be orders of magnitude different from each other, and may require consideration of "in-between" scales (also known as 'meso' scale). The process of linking material behavior at these different scales is termed as the "multiscale modeling". The area of multiscale materials modeling is becoming manageable due to improvement in computational power, as well as advancement in understanding of material behavior at lower length scales.

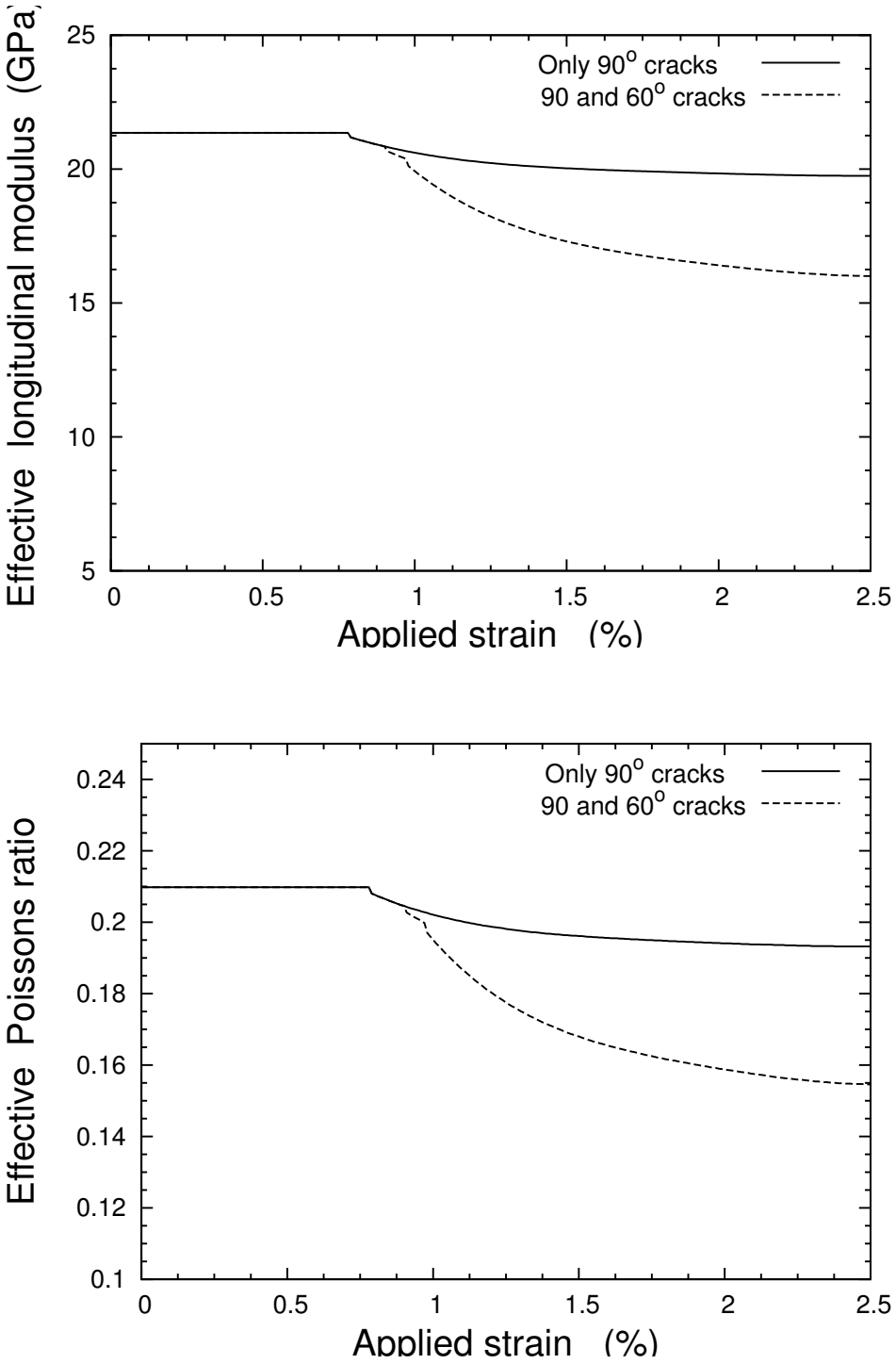

Fig. 74. Variation of effective Longitudinal modulus and Poisson's ratio for $[0/90/\mp 60]_s$ laminate.

The scale at which dissipative processes manifest themselves could be dependent on the size of the heterogeneities, or the manufacturing defects. For example, in a composite material, matrix cracking may initiate by debonding at the fiber/matrix interface. Hence for this phenomenon, the fiber diameter may be the characteristic length scale governing damage due to matrix cracking. From a theoretical view point, the most fundamental scale is the atomic scale. Multiscale modeling using atomistic descriptions, like "molecular modeling" or "atomistic modeling", choose to describe material behavior in the most fundamental way by modeling of inter-atomic forces and potential. This, however, is not only very difficult computationally, but sometimes even irrelevant and unwarranted. Therefore, from a practical consideration, the fundamental length scale depends upon our capacity to observe, i.e., the scale at which damage effects are seen, and thus it is more useful to define it as the first significant scale (manifesting behavior of lower scales, if any) that governs the property of interest, preferably, the scale of observable entities, e.g., for plasticity nano-meters is the length scale at which dislocations appear. The choice of length scale, thus, must depend upon the "purpose" at hand. For example, if we are modeling stiffness changes due to transverse cracking, the characteristic length scale is the crack size, i.e., the thickness of the cracked ply.

Figure 75 describes the hierarchy of all possible length scales involved in multiscale materials modeling. A careful observation of the figure deliniates two big issues that arise in developing an accurate and physics-based multiscale model:

1. The difference in "macro" and "atomistic" scale is extremely large, and

2. The difference in material behavior at different scales and difference in approaches required to model them. For example, at atomistic scale, quantum mechanics and molecular dynamics may be able to describe material behavior

accurately. However, on the macro-scale, we need continuum-mechanics type approaches.

Hence "bridging" of different length scales is the major consideration in multiscale modeling.

For damage modeling of composite materials, our basic purpose is to predict properties and performance of the material, or to design its properties for a selected performance. This requires that we account for the scale of inhomogeneities (fibers, particles, plies, etc.) because damage entities are often initiated by inhomogeneities, and evolve under their influence. Hence, the scales lower than micromechanical are un-necessary (except if the entities are of nano-size).

Another issue, particular to multiscale damage modeling, is that the total damage may be due to multiple damage mechanisms, whose length scales might be quite different from one another. Moreover, these length scales may "evolve" as loading is increased. Consider the example of matrix cracking. It may initiate from debonding of fibers, thereby making the 'fiber dia' as the length scale. But when matrix cracks have grown fully through the ply thickness and width, they start multiplying, and for this process the appropriate length scale is the 'ply thickness'. Hence, a "hierarchical" multiscale methodology, based on the notion that 'modeling of the basic laws at the lowest length scale, and then going up the length scales would ascertain accurate modeling' is not appropriate in damage modeling. As observed by Talreja [157], "the microstructural configuration and driving forces for damage initiation and progression determine the length scales of damage". Thus, the length scales of damage and their hierarchy are not fixed but are subject to evolution as a function of loading.

A more suitable approach for multiscale modeling of composite materials would rather be the synergistic damage mechanics (SDM). As illustrated in earlier chapters,

SDM combines CDM and MDM to characterize response function in terms of fields variables (stress, strain etc.) and internal variables representing the smeared-out field of evolving damage entities. Fig. 76 (adapted from [185]) illustrates the multiscale SDM approach considering the substructure to be region of potential criticality. This substructure is first analyzed to determine the loading on its boundary. In the next step, damage induced from this loading is characterized using the CDM in terms of internal variables. To characterize the microstructure using MDM, we zoom-in this region and perform micromechanics calculations over a representative unit cell to obtain constraint like parameters. Thus, unlike in the hierarchical approach, we move "top-down" upto the lowest length scale of interest to us. This ensures accurate representation of the processes at the lowest length scales, and also allows us to link it to the macro-scale in an easier way. For a more thorough discussion of multiscale damage analysis using synergistic approach, the reader is referred to [157, 185].

C. Multiple Damage Mechanisms

Although only intralaminar cracking is considered in this study, damage in composite materials can take place by a variety of damage mechanisms, such as delamination, fiber/matrix debonding, interfacial sliding, fiber fracture among others. The structural performance when the material is undergoing more than one of these mechanisms simultaneously is given by the total sum of individual effects, along with any interaction between them that may be important. This requires consideration of all active damage mechanisms in a common framework. Each of these requires a somewhat different treatment, but they can be appropriately described in the same SDM framework. Talreja [186] considered four distributed damage configurations (see Fig. 77) for ceramic matrix composites (CMCs), where the interfacial damage and debonding

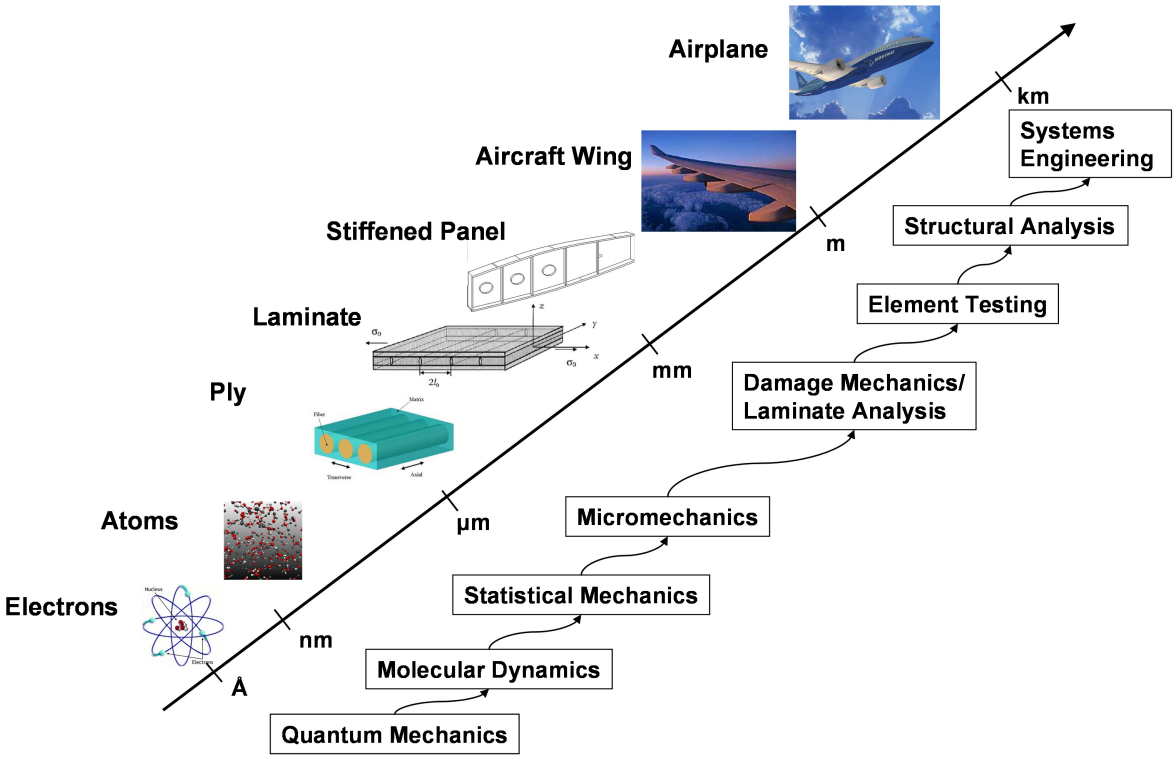

Fig. 75. Hierarchy of structural scales in damage modeling of composite materials.

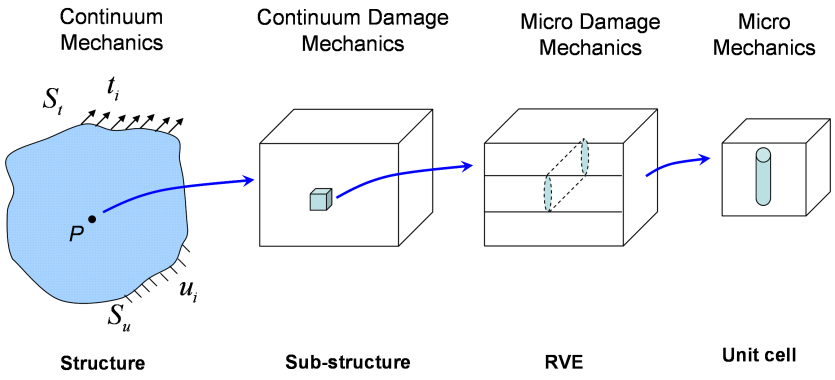

Fig. 76. Multiscale synergistic methodology (adapted from [185]).

can occur in conjunction with matrix cracking [187, 188]. Following the logical approach used in SDM with multiple damage modes, the free energy for a composite undergoing damage due to multiple mechanisms can be written as

$$\psi = \psi\left(\epsilon_{ij}, D_{ij}^{(\alpha)}, K_{mn}, \delta_{rs}^{(\beta)}\right) \tag{7.6}$$

where $\epsilon_{ij} = \frac{1}{2}\left(u_{i,j} + u_{j,i}\right)$ is the strain tensor, $D_{ij}^{(\alpha)}$ is the damage mode tensor for matrix cracking in orientation $\alpha = 1, 2, 3..$, K_{mn} is the slip damage tensor, and $\delta_{pq}^{(\beta)}, \beta = 1, 2, 3...$ is the damage tensor describing debonding. Consequently, the stiffness tensor of the damaged body is given by

$$\begin{aligned} C_{ijkl} &= \rho\frac{\partial^2\psi}{\partial\epsilon_{ij}\partial\epsilon_{kl}} \\ &= C_{ijkl}^0 + \sum_{\alpha} C_{ijkl}^{(\alpha)} + C_{ijkl}^K + \sum_{\beta} C_{ijkl}^{(\beta)} \end{aligned} \tag{7.7}$$

where C_{ijkl}^0 represents the stiffness tensor for the virgin laminate, $\sum_{\alpha} C_{pq}^{(\alpha)}$ represents the stiffness change brought about by matrix cracking in all orientations, C_{ijkl}^K is the stiffness change due to interfacial slip, and $\sum_{\beta} C_{ijkl}^{(\beta)}$ represents the stiffness change brought about by debonding in all directions. For more details, please see [186].

D. Failure Analysis and Design of Composite Materials

Although numerous failure models are available for predicting lamina failure, there is no consistent model for laminates. These failure criteria are more empirical in nature and can at the most describe the failure of a unidirectional lamina to a reasonable accuracy. For laminates, however, damage or failure of an individual lamina does not cause structural failure. Depending upon the application, a composite laminate may have developed significant amount of transverse cracking and still perform satisfactorily according to the design specifications. Although the final failure of a laminate

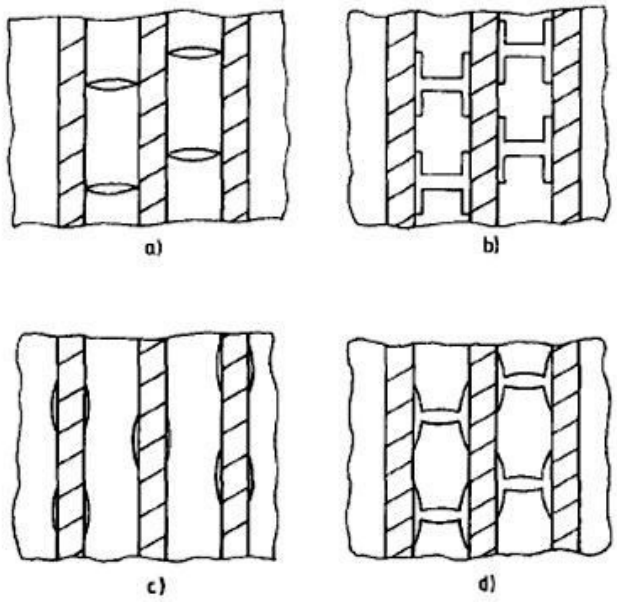

Fig. 77. Multiple damage mechanisms in CMCs (source: [186]).

may occur from fiber breakage, substantial delamination in the laminate may also be considered to signify its failure based on the design function. Hence, it is necessary to account for progressive sub-critical damage while predicting the failure of the laminate. For example, one can make use of the changes in stiffness properties and the nonlinearity in the stress-strain response due to transverse cracking while designing the component. Consideration of effects of other damage mechanisms will depend on the actual scenario and the design criteria.

E. Assessment of Structural Integrity and Durability

Based on the discussion above, the whole procedure for analyzing the integrity and the durability of the composite structure can be outlined as shown in Fig. 78 (source: [145]). The first step is to carry out stress analysis of the component under the prescribed service loading using initial deformation models. This step may ignore any consideration of damage, i.e., use initial constitutive relation for the material,

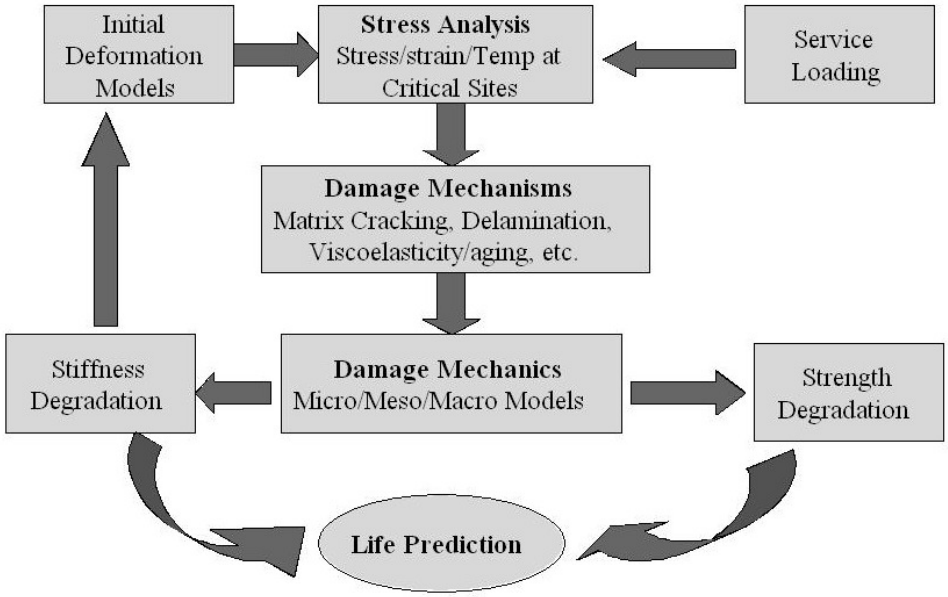

Fig. 78. Procedure to assess the integrity and durability of a composite structure, reproduced from [145].

while focusing on arriving at basic stress and temperature histories in the structure. This information then can be used to predict mechanisms and modes of damage which will be operative in the life cycle of the structure. Next, the damage mechanics concepts should be used to evaluate the growth and effects of progressive damage on the stiffness and strength properties of the structure. Finally, these effects will be used to modify the constitutive behavior and re-assess the stress and temperature fields, which can then form the basis for assessing the integrity and durability of the structure.

F. Summary

This chapter focused on providing an overall picture how the SDM methodology and the results developed in this dissertation can be used for composite structural design. The stress-strain responses of selected multidirectional laminates were predicted based

on the results of the previous chapters. The effect of cracking in multiple damage modes on the overall stress-strain response was discussed. In general, a multi-mode cracking involves interaction between different modes not only affects the stiffness properties detrimentally, but also increases the rate of damage progression. This typically results into increased nonlinearity in the stress-strain response.

To characterize the microstructural effects, the developed SDM approach can be easily incorporated in a multiscale modeling framework. Unlike the commonly used hierarchical approach, it follows a "top-down" approach, while focusing mainly on the macro-response and going down to the scale of damage entities as and when needed. The SDM approach can also be easily used for the comprehensive assessment of the structural integrity and its durability.

CHAPTER VIII

CONCLUSIONS AND FUTURE DIRECTIONS

The primary goals of damage analysis of composite materials are to determine the conditions for initiation of the first damage event, its evolution with increase in loading, and describe the resulting thermomechanical response. This information can then aid in determining the failure or criticality of damage and aid into overall structural analysis and design.

The significant developments in understanding of the basic damage processes and their effects on the material behavior have gained some maturity for simple cases of laminate layups, such as the cross-ply laminates. We are still far from being able to predict damage in a general multidirectional laminate under a complex loading situation. The resulting boundary value problem for multidirectional laminates is too complicated to achieve any reasonable elastic solution, and the common strategy has been to use computational tools. Hence, there has been a need to develop a simpler approach, which could be used for predicting the damage behavior of such laminates, and could also be integrated easily into a multiscale analysis model. The SDM approach developed in this study can fill this gap. It bypasses solution of a complex BVP and rather focuses on the overall constitutive behavior of the damaged laminate. In this study, we have developed and implemented a multiscale synergistic damage methodology to characterize the effects of intralaminar cracking in multidirectional laminates on their stiffness properties. The approach, termed as "synergistic damage mechanics" (SDM), combines the micro damage mechanics and the continuum damage mechanics. The approach has been verified in this work against experiments as well as independent computational simulations for two complex off-axis laminate configurations.

The main benefit of the SDM approach is that it does not need complex stress analysis calculations unlike many of other analytical and numerical tools. Moreover, evaluation of CODs is more accurate than the determination of stress state around matrix crack through FEM, as it is a displacement based approach. It is also shown that we do not always need experimental results for SDM to work. Accurate predictions from numerical simulations or through an applicable analytical method, e.g., variational method, for the reference cross-ply configuration can be used to determine damage constants, and feed into SDM for prediction of stiffness changes in other laminate configurations.

SDM equations are simple and easy to implement in a general FEM based multiscale analysis framework because it directly gives meso-level stiffness changes in the laminate in terms of a constitutive law, which are just like constitutive laws through the laminate theory. The consitutive law incorporates the microstructural changes brought about by damage processes through constraint-like parameters. SDM framework, thus, effectively treats the multiscale nature of damage processes.

The composites which are used in extreme environments may require additional considerations. For example, the polymers used in composites for high temperature applications such as in engines and launch vehicles for spacecraft can display time-dependent (visco-elastic) response. Damage due to ply cracking can further alter the material response. Using the correspondence principle, the visco-elastic boundary value problem can be converted to an equivalent elasticity problem in the Laplace domain and then inverting the solution to the time domain gives us the required solution for the viscoelastic problem. SDM approach can be easily extended to analyze viscoelastic composites in presence of damage, as shown in some earlier works [144, 189] for the case of cross-ply laminates.

Although the basic framework to analyze multidirectional laminates in presence

of intralaminar damage has been developed, there are some unresolved issues which should be focused in future research. For instance, the present work has focused only on a quasi-static loading. For fatigue loading, more comprehensive research is required to understand effects of damage in a multiple damage mode scenario. The usual approach in fatigue of composites is to use the theory of metal fatigue, although its relevance to composite materials such as glass or carbon fiber reinforced polymers is questionable. Thus, fatigue induced damage in composite laminates is still somewhat less understood, and the area needs to gain maturity before we can convincingly model fatigue damage in multidirectional laminates.

Any structure made of composites in a practical scenario can undergo complex loading, which may be truly three dimensional. Damage assessment in such cases is presently not possible. There have been some recent developments to account for triaxial loading for cross-ply configurations, e.g. [73,74], and the knowledge developed from these works can be incorporated in the SDM framework in the future.

While using SDM stiffness-damage relationships, the inherent damage constants were assumed to be independent on the ply orientation. This assumption is reasonably valid for the longitudinal loading case, where cracks will only form in off-axis plies which are placed in orientations close to the direction transverse to the loading direction. For the case of biaxial loading, generated due to actual mechanical loading or by a differential thermal shrinkage, this is not true, and even the plies in the longitudinal direction may develop cracks. The above assumption will be invalid in such complex loading scenarios. Further work is needed to understand the variation of damage constants in biaxial, and triaxial loading states.

The future research in the field should also concentrate on the implementation of the synergistic methodology in a multiscale procedure to enable solution to structural problems. Final goal should be to incorporate the constitutive and damage evolution

relationships developed in this work in a computational scheme, such as a finite element code, capable of carrying out a complete structural analysis and design.

REFERENCES

[1] A. Moropoulou, A. Bakolas, and S. Anagnostopoulou, "Composite materials in ancient structures," *Cement and Concrete Composites*, vol. 27, no. 2, pp. 295–300, 2005.

[2] L. A. Mignery, T. M. Tan, and C. T. Sun, "The use of stitching to suppress delamination in laminated composites," in *Delamination and Debonding of Materials*, W. S. Johnson, Ed., pp. 371–385. ASTM STP 876, Philadelphia, 1985.

[3] K. Dransfield, C. Baillie, and Y. W. Mai, "Improving the delamination resistance of cfrp by stitching - a review," *Compos. Sci. Tech.*, vol. 50, no. 3, pp. 305–317, 1994.

[4] A. P. Mouritz and B. N. Cox, "A mechanistic approach to the properties of stitched laminates," *Composites A: Appl Sci Mfg*, vol. 31, no. 1, pp. 1–27, 2000.

[5] Y. Iwahori, T. Ishikawa, N. Watanabe, A. Ito, Y. Hayashi, and S. Sugimoto, "Experimental investigation of interlaminar mechanical properties on carbon fiber stitched cfrp laminates," *Advanced Compos. Mater.*, vol. 16, no. 2, pp. 95–113, 2007.

[6] D. D. R. Cartie, M. Troulis, and I. K. Partridge, "Delamination of z-pinned carbon fibre reinforced laminates," *Compos. Sci. Tech.*, vol. 66, no. 6, pp. 855–861, 2006.

[7] S. Yamashita, H. Hatta, T. Takei, and T. Sugano, "Interlaminar reinforcement of laminated composites by addition of oriented whiskers in the matrix," *J. Compos. Mater.*, vol. 26, no. 9, pp. 1254–1268, 1992.

[8] W. X. Wang, Y. Takao, T. Matsubara, and H. S. Kim, "Improvement of the interlaminar fracture toughness of composite laminates by whisker reinforced interlamination," *Compos. Sci. Tech.*, vol. 62, no. 6, pp. 767–774, 2002.

[9] "Growth opportunities in carbon fiber market 2004-2010," e-Composites, Sept, 2004.

[10] "The research requirements of the transport sectors to facilitate an increased usage of composite materials. Part I: The composite material research requirements of the aerospace industry," Tech. Rep., EADS Deutschland GmbH, Corporate Research Center, June 2004.

[11] Committee on Durability and National Research Council Life Prediction of Polymer Matrix Composites in Extreme Environments, *Going to Extremes: Meeting the Emerging Demand for Durable Polymer Matrix Composites*, National Academies Press, Washington, D.C., 2005.

[12] A. Kelly, "The 1995 bakerian lecture: Composite materials," *Phil. Trans. Royal Soc. London A*, vol. 354, no. 1714, pp. 1841–1874, 1996.

[13] J. Aveston, G. A. Cooper, and A. Kelly, "Single and multiple fracture," in *The Properties of Fiber Composites*, National Physical Laboratory, 1971, pp. 15–26, IPC Science and Technology Press, Surrey, UK.

[14] K. W. Garrett and J. E. Bailey, "Multiple transverse fracture in 90-degrees cross-ply laminates of a glass fiber-reinforced polyester," *J. Mat. Sci.*, vol. 12, no. 1, pp. 157–168, 1977.

[15] K. W. Garrett and J. E. Bailey, "Effect of resin failure strain on tensile properties of glass fiber-reinforced polyester cross-ply laminates," *J. Mat. Sci.*, vol.

12, no. 11, pp. 2189–2194, 1977.

[16] A. Parvizi, K. W. Garrett, and J. E. Bailey, "Constrained cracking in glass fiber-reinforced epoxy cross-ply laminates," *J. Mat. Sci.*, vol. 13, no. 1, pp. 195–201, 1978.

[17] A. Parvizi and J. E. Bailey, "Multiple transverse cracking in glass-fiber epoxy cross-ply laminates," *J. Mat. Sci.*, vol. 13, no. 10, pp. 2131–2136, 1978.

[18] M. G. Bader, J. E. Bailey, P. T. Curtis, and A. Parvizi, "The mechanisms of initiation and development of damage in multi-axial fibre-reinforced plastic laminates," in *Proc. of Int. Conf. on Mechanical Behavior of Materials*, Cambridge, UK, 1979, pp. 227–239.

[19] J. E. Bailey, P. T. Curtis, and A. Parvizi, "On the transverse cracking and longitudinal splitting behavior of glass and carbon-fiber reinforced epoxy cross ply laminates and the effect of poisson and thermally generated strain," *Proc. Royal Soc. London A*, vol. 366, no. 1727, pp. 599–623, 1979.

[20] J. E. Bailey and A. Parvizi, "On fiber debonding effects and the mechanism of transverse-ply failure in cross-ply laminates of glass fiber-thermoset composites," *J. Mat. Sci.*, vol. 16, no. 3, pp. 649–659, 1981.

[21] F. R. Jones, A. R. Wheatley, and J. E. Bailey, "The effect of thermal strains on the microcracking and stress corrosion behaviour of grp," in *Composite structures 1st International Conference*, I.H. Marshall, Ed., pp. 415–429. Applied Science Publishers, Barking, UK, 1981.

[22] J. A. Nairn, "Matrix microcracking in composites," in *Polymer Matrix Composites*, R. Talreja and J. A. E. Manson, Eds., vol. 2, pp. 403–432. Elsevier

Science, Amsterdam, The Netherlands, 2000.

[23] R. Talreja, "Transverse cracking and stiffness reduction in composite laminates," *J. Compos. Mater.*, vol. 19, no. 4, pp. 355–375, 1985.

[24] H. T. Hahn and S. W. Tsai, "Behavior of composite laminates after initial failures," *J. Compos. Mater.*, vol. 8, pp. 288–305, 1974.

[25] S. W. Tsai and E. M. Wu, "General theory of strength for anisotropic materials," *J. Compos. Mater.*, vol. 5, pp. 58–80, 1971.

[26] D. L. Flaggs and M. H. Kural, "Experimental determination of the in-situ transverse lamina strength in graphite epoxy laminates," *J. Compos. Mater.*, vol. 16, pp. 103–116, Mar 1982.

[27] H. Fukunaga, T. W. Chou, P. W. M. Peters, and K. Schulte, "Probabilistic failure strength analyses of graphite epoxy cross-ply laminates," *J. Compos. Mater.*, vol. 18, no. 4, pp. 339–356, 1984.

[28] H. Fukunaga, T. W. Chou, K. Schulte, and P. W. M. Peters, "Probabilistic initial failure strength of hybrid and non-hybrid laminates," *J. Mat. Sci.*, vol. 19, no. 11, pp. 3546–3553, 1984.

[29] P. W. M. Peters, "The strength distribution of 90-deg plies in 0/90/0 graphite-epoxy laminates," *J. Compos. Mater.*, vol. 18, pp. 545–556, 1984.

[30] N. Takeda and S. Ogihara, "In-situ observation and probabilistic prediction of microscopic failure processes in cfrp cross-ply laminates," *Compos. Sci. Tech.*, vol. 52, no. 2, pp. 183–195, 1994.

[31] P. W. M. Peters, "The fiber/matrix bond strength of cfrp deduced from the strength transverse to the fibers," *J. Adhesion*, vol. 53, pp. 79–101, 1995.

[32] J. A. Nairn and S. Hu, "Micromechanics of damage: a case study of matrix microcracking," in *Damage Mechanics of Composite Materials*, Ramesh Talreja, Ed., pp. 187–243. Elsevier, Amsterdam, 1994.

[33] W. W. Stinchcomb, K. L. Reifsnider, P. Yeung, and J. M. Masters, "Effect of ply constraint on on fatigue damage development in composite material laminates," in *ASTM STP 723*, pp. 64–84. 1981.

[34] P. A. Smith, L. Boniface, and N. F. C. Glass, "A comparison of transverse cracking phenomena in (0/90)(s) and (90/0)(s) cfrp laminates," *Appl. Compos. Mater.*, vol. 5, no. 1, pp. 11–23, 1998.

[35] J. A. Nairn and S. F. Hu, "The formation and effect of outer-ply microcracks in cross-ply laminates - a variational approach," *Eng. Frac. Mech.*, vol. 41, no. 2, pp. 203–221, 1992.

[36] L. Boniface and S. L. Ogin, "Application of the paris equation to the fatigue growth of transverse ply cracks," *J. Compos. Mater.*, vol. 23, no. 7, 1989.

[37] A. L. Highsmith and K. L. Reifsnider, "Stiffness-reduction mechanisms in composite laminates," in *Damage in Composite Materials*, K.L. Reifsnider, Ed., pp. 103–117. ASTM STP, Philadelphia, 1982.

[38] M. Caslini, C. Zanotti, and T. K. O'Brien, "Fracture mechanics of matrix cracking and delamination in glass/epoxy laminates," *J. Compos. Tech. Research*, pp. 121–130, 1987.

[39] A. S. D. Wang, N. N. Kishore, and C. A. Li, "Crack development in graphite epoxy cross-ply laminates under uniaxial tension," *Compos. Sci. Tech.*, vol. 24, no. 1, pp. 1–31, 1985.

[40] S. Ogihara, N. Takeda, and A. Kobayashi, "Experimental characterization of microscopic failure process under quasi-static tension in interleaved and toughness-improved cfrp cross-ply laminates," *Compos. Sci. Tech.*, vol. 57, no. 3, pp. 267–275, 1997.

[41] E. Adolfsson and P. Gudmundson, "Matrix crack initiation and progression in composite laminates subjected to bending and extension," *Int. J. Solids Struct.*, vol. 36, no. 21, pp. 3131–3169, 1999.

[42] S. Yalvac, L. D. Yats, and D. G. Wetters, "Transverse ply cracking in toughened and untoughened graphite/epoxy and graphite/polycyanate crossply laminates," *J. Compos. Mater.*, vol. 25, pp. 1653–1667, 1991.

[43] J. A. Nairn, S. F. Hu, and J. S. Bark, "A critical-evaluation of theories for predicting microcracking in composite laminates," *J. Mat. Sci.*, vol. 28, no. 18, pp. 5099–5111, 1993.

[44] S. L. Liu and J. A. Nairn, "The formation and propagation of matrix microcracks in cross-ply laminates during static loading," *J. Reinforced Plast. Compos.*, vol. 11, no. 2, pp. 158–178, 1992.

[45] K. L. Reifsnider and A. Talug, "Analysis of fatigue damage in composite laminates," *Int. J. Fatigue*, vol. 2, no. 1, pp. 3–11, 1980.

[46] K. L. Reifsnider and R. Jamison, "Fracture of fatigue-loaded composite laminates," *Int. J. Fatigue*, vol. 4, no. 4, pp. 187–197, 1982.

[47] N. V. Akshantala and R. Talreja, "A micromechanics based model for predicting fatigue life of composite laminates," *Mater. Sci. Eng.*, vol. A285, no. 1-2, pp. 303–313, 2000.

[48] M. J. Hinton, P. D. Soden, and A. S. Kaddour, "Strength of composite laminates under biaxial loads," *Appl. Compos. Mater.*, vol. 3, no. 3, pp. 151–162, 1996.

[49] A. Puck and H. Schurmann, "Failure analysis of frp laminates by means of physically based phenomenological models," *Compos. Sci. Tech.*, vol. 62, no. 12-13, pp. 1633–1662, 2002.

[50] P. A. Zinoviev, O. V. Lebedeva, and L. P. Tairova, "A coupled analysis of experimental and theoretical results on the deformation and failure of composite laminates under a state of plane stress," *Compos. Sci. Tech.*, vol. 62, no. 12-13, pp. 1711–1723, 2002.

[51] A. Kuraishi, Stephen W. Tsai, and K. K. S. Liu, "A progressive quadratic failure criterion, part b," *Compos. Sci. Tech.*, vol. 62, no. 12-13, pp. 1683–1695, 2002.

[52] M. J. Hinton, A. S. Kaddour, and P. D. Soden, "A comparison of the predictive capabilities of current failure theories for composite laminates, judged against experimental evidence," *Compos. Sci. Tech.*, vol. 62, no. 12-13, pp. 1725–1797, 2002.

[53] R. Talreja and C. V. Singh, "Life cycle engineering and sustainability of composite materials," in *Int. Conf. on Trends in Product Life Cycle, Modeling, Simulation and Synthesis*, Bangalore, India, December 2006.

[54] J. M. Whitney, "On the 'ply discount method' for determining effective thermoelastic constants of laminates containing transverse cracks," *Composites A: Appl Sci Mfg*, vol. 36, no. 10 SPEC. ISS., pp. 1347–1354, 2005.

[55] Z. Hashin, "Analysis of damage in composite materials," in *Yielding, Damage, and Failure of Anisotropic Solids*, J. P. Boehler, Ed., pp. 3–31. Mechanical Engineering Publications, London, 1990.

[56] S. G. Lim and C. S. Hong, "Prediction of transverse cracking and stiffness reduction in cross-ply laminate composites," *J. Compos. Mater.*, vol. 23, no. 7, pp. 695–713, 1989.

[57] Y. M. Han and H. T. Hahn, "Ply cracking and property degradations of symmetric balanced laminates under general inplane loading," *Compos. Sci. Tech.*, vol. 35, no. 4, pp. 377–397, 1989.

[58] S. C. Tan and R. J. Nuismer, "A theory for progressive matrix cracking in composite laminates," *J. Compos. Mater.*, vol. 23, no. 10, pp. 1029–1047, 1989.

[59] P. W. Manders, T. W. Chou, F. R. Jones, and J. W. Rock, "Statistical analysis of multiple fracture in [0/90/0] glass fiber/epoxy resin laminates," *J. Mat. Sci.*, vol. 19, pp. 2876–2889, 1983.

[60] J. M. Masters and K. L. Reifsnider, "An investigation of cumulative damage development in quasi-isotropic graphite/epoxy laminates," in *Damage in Composite Materials*, K.L. Reifsnider, Ed., pp. 40–62. ASTM STP, Philadelphia, 1982.

[61] J. A. Nairn, "On the use of shear-lag methods for analysis of stress transfer unidirectional composites," *Mech. Mater.*, vol. 26, no. 2, pp. 63–80, 1997.

[62] J. A. Nairn and D. A. Mendels, "On the use of planar shear-lag methods for stress-transfer analysis of multilayered composites," *Mech. Mater.*, vol. 33, no. 6, pp. 335–362, 2001.

[63] J. M. Berthelot, "Transverse cracking and delamination in cross-ply glass-fiber and carbon-fiber reinforced plastic laminates: Static and fatigue loading," *Appl. Mech. Reviews*, vol. 56, no. 1, pp. 111–147, 2003.

[64] Z. Hashin, "Analysis of cracked laminates: a variational approach," *Mech. Mater.*, vol. 4, no. 2, pp. 121–136, 1985.

[65] Z. Hashin, "Thermal-expansion coefficients of cracked laminates," *Compos. Sci. Tech.*, vol. 31, no. 4, pp. 247–260, 1988.

[66] J. Varna and L. Berglund, "Multiple transverse cracking and stiffness reduction in cross-ply laminates," *J. Compos. Tech. Research*, vol. 13, no. 2, pp. 97–106, 1991.

[67] J. Varna and L. Berglund, "2-dimensional transverse cracking in [0(m)/90(n)](s) cross-ply laminates," *European J. Mechanics A-Solids*, vol. 12, no. 5, pp. 699–723, 1993.

[68] J. Varna and L. A. Berglund, "Thermoelastic properties of composite laminates with transverse cracks," *J. Compos. Tech. Research*, vol. 16, no. 1, pp. 77–87, 1994.

[69] J. A. Nairn, "The strain energy release rate of composite microcracking: A variational approach," *J. Compos. Mater.*, vol. 23, no. 11, pp. 1106–1129, 1989.

[70] Z. Hashin, "Analysis of orthogonally cracked laminates under tension," *J. Appl. Mech., Trans ASME*, vol. 54, no. 4, pp. 872–879, 1987.

[71] J. A. Nairn and S. Hu, "The initiation and growth of delaminations induced by matrix microcracks in laminated composites," *Int. J. Frac.*, vol. 57, no. 1, pp. 1–24, 1992.

[72] L. N. Mccartney, "Theory of stress transfer in a 0-degrees-90-degrees-0-degrees cross-ply laminate containing a parallel array of transverse cracks," *J. Mech. Phys. Solids*, vol. 40, no. 1, pp. 27–68, 1992.

[73] L. N. McCartney, "Physically based damage models for laminated composites," *Proc. Inst. Mech. Engr. Part L-J Mater. Design and Appl.*, vol. 217, no. L3, pp. 163–199, 2003.

[74] L. N. McCartney, "Model to predict effects of triaxial loading on ply cracking in general symmetric laminates," *Compos. Sci. Tech.*, vol. 60, no. 12-13, pp. 2255–2279, 2000.

[75] L. N. McCartney, "Energy-based prediction of failure in general symmetric laminates," *Eng. Frac. Mech.*, vol. 72, no. 6, pp. 909–930, 2005.

[76] N. Laws, G. J. Dvorak, and M. Hejazi, "Stiffness changes in unidirectional composites caused by crack systems," *Mech. Mater.*, vol. 2, no. 2, pp. 123–137, 1983.

[77] G. J. Dvorak, N. Laws, and M. Hejazi, "Analysis of progressive matrix cracking in composite laminates .1. thermoelastic properties of a ply with cracks," *J. Compos. Mater.*, vol. 19, no. 3, pp. 216–234, 1985.

[78] K. Hoiseth, "A micromechanics study of transverse matrix cracking in cross-ply composites," M.S. thesis, Georgia Institute of Technology, Atlanta, Georgia, May 1995.

[79] J. Qu and K. Hoiseth, "Evolution of transverse matrix cracking in cross-ply laminates," *Fatigue Fract. Eng. Mater. Struct.*, vol. 21, no. 4, pp. 451–464, 1998.

[80] P. Gudmundson and S. Ostlund, "First order analysis of stiffness reduction due to matrix cracking," *J. Compos. Mater.*, vol. 26, no. 7, pp. 1009–1030, 1992.

[81] P. Gudmundson and W. Zang, "Thermoelastic properties of microcracked composite laminates," *Mechanics of Compos. Mater.*, vol. 29, no. 2, pp. 107–114, 1993.

[82] E. Adolfsson and P. Gudmundson, "Matrix crack induced stiffness reductions in [(0(m)/90(n)/+theta(p)/-theta(q))(s)](m) composite laminates," *Composites Engineering*, vol. 5, no. 1, pp. 107–123, 1995.

[83] E. Adolfsson and P. Gudmundson, "Thermoelastic properties in combined bending and extension of thin composite laminates with transverse matrix cracks," *Int. J. Solids Struct.*, vol. 34, no. 16, pp. 2035–2060, 1997.

[84] P. Lundmark and J. Varna, "Constitutive relationships for laminates with ply cracks in in-plane loading," *Int. J. Dam. Mech.*, vol. 14, no. 3, pp. 235–259, 2005.

[85] P. Lundmark, "Damage mechanics analysis of inelastic behaviour of fiber composites," Ph.D. thesis, Lulea University of Technology, Lulea, Sweden, 2005.

[86] P. Lundmark and J. Varna, "Crack face sliding effect on stiffness of laminates with ply cracks," *Compos. Sci. Tech.*, vol. 66, no. 10, pp. 1444–1454, 2006.

[87] R. Talreja, "Internal variable damage mechanics of composite materials," in *Yielding, Damage, and Failure of Anisotropic Solids*, J. P. Boehler, Ed., pp. 509–533. Mechanical Engineering Publications, London, 1990.

[88] R. Talreja, "A continuum mechanics characterization of damage in composite materials," *Proc. Royal Soc. London A*, vol. 399, no. 1817, pp. 195–216, 1985.

[89] R. Talreja, "Damage characterization by internal variables," in *Damage Mechanics of Composite Materials*, R. Talreja, Ed., pp. 53–78. Elsevier, Amsterdam, 1994.

[90] D. H. Allen, C. E. Harris, and S. E. Groves, "A thermomechanical constitutive theory for elastic composites with distributed damage.1. theoretical development," *Int. J. Solids Struct.*, vol. 23, no. 9, pp. 1301–1318, 1987.

[91] D. H. Allen, C. E. Harris, and S. E. Groves, "A thermomechanical constitutive theory for elastic composites with distributed damage.2. application to matrix cracking in laminated composites," *Int. J. Solids Struct.*, vol. 23, no. 9, pp. 1319–1338, 1987.

[92] J. W. Lee, D. H. Allen, and C. E. Harris, "Internal state variable approach for predicting stiffness reductions in fibrous laminated composites with matrix cracks," *J. Compos. Mater.*, vol. 23, no. 12, pp. 1273–1291, 1989.

[93] A. Krasnikovs and J. Varna, "Transverse cracks in cross-ply laminates. i. stress analysis," *Mechanics of Compos. Mater.*, vol. 33, no. 6, pp. 565–582, 1997.

[94] J. Tong, F. J. Guild, S. L. Ogin, and P. A. Smith, "On matrix crack growth in quasi-isotropic laminates - ii. finite element analysis," *Compos. Sci. Tech.*, vol. 57, no. 11, pp. 1537–1545, 1997.

[95] P. Lundmark and J. Varna, "Modeling thermo-mechanical properties of damaged laminates," *Advances in Fracture and Damage Mechanics*, vol. 251-2, pp. 381–387, 2003.

[96] S. Li, S. R. Reid, and P. D. Soden, "A finite strip analysis of cracked laminates," *Mech. Mater.*, vol. 18, no. 4, pp. 289–311, 1994.

[97] D. Gamby and J. L. Rebiere, "A two-dimensional analysis of multiple matrix cracking in a laminated composite close to its characteristic damage state," *Composite Structures*, vol. 25, no. 1-4, pp. 325–337, 1993.

[98] G. N. Praveen and J. N. Reddy, "Transverse matrix cracks in cross-ply laminates: stress transfer, stiffness reduction and crack opening profiles," *Acta Mechanica*, , vol. 130, pp. 227–248, 1998.

[99] A. S. D. Wang, "Fracture mechanics of sublaminate cracks in composite materials," *Composites Technology Review*, vol. 6, no. 2, pp. 45–62, 1984.

[100] F. W. Crossman, W. J. Warren, A. S. D. Wang, and Jr. G. E. Law, "Initiation and growth of transverse cracks and edge delamination in composite laminates: Part 2. experimental correlation," *J. Compos. Mater. Suppl*, vol. 14, pp. 89–108, 1980.

[101] Z. Hashin, "Finite thermoelastic fracture criterion with application to laminate cracking analysis," *J. Mech. Phys. Solids*, vol. 44, no. 7, pp. 1129–1145, 1996.

[102] V. Vinogradov and Z. Hashin, "Probabilistic energy based model for prediction of transverse cracking in cross-ply laminates," *Int. J. Solids Struct.*, vol. 42, no. 2, pp. 365–392, 2005.

[103] S. A. Salpekar and T. K. Obrien, "Analysis of matrix cracking and local delamination in (o/theta/-theta)s graphite-epoxy laminates under tensile load," *J. Compos. Tech. Research*, vol. 15, no. 2, pp. 95–100, 1993.

[104] R. Joffe, A. Krasnikovs, and J. Varna, "COD-based simulation of transverse cracking and stiffness reduction in [S/90n]s laminates," *Compos. Sci. Tech.*, vol. 61, no. 5, pp. 637–656, 2001.

[105] J. Varna, R. Joffe, and R. Talreja, "Mixed micromechanics and continuum damage mechanics approach to transverse cracking in [S,90(n)](s) laminates," *Mechanics of Compos. Mater.*, vol. 37, no. 2, pp. 115–126, 2001.

[106] J. Varna, R. Joffe, and R. Talreja, "A synergistic damage-mechanics analysis of transverse cracking in [+/-theta/90(4)](s) laminates," *Compos. Sci. Tech.*, vol. 61, no. 5, pp. 657–665, 2001.

[107] T. K. O'Brien and S. J. Hooper, Eds., *Composite materials: fatigue and fracture*, ASTM STP, Philadelphia, 1993.

[108] J. Tong, F. J. Guild, S. L. Ogin, and P. A. Smith, "On matrix crack growth in quasi-isotropic laminates - i. experimental investigation," *Compos. Sci. Tech.*, vol. 57, no. 11, pp. 1527–1535, 1997.

[109] J. Varna, R. Joffe, N. V. Akshantala, and R. Talreja, "Damage in composite laminates with off-axis plies," *Compos. Sci. Tech.*, vol. 59, no. 14, pp. 2139–2147, 1999.

[110] W. M. Marsden, F. J. Guild, S. L. Ogin, and P. A. Smith, "Modelling stiffness-damage behaviour of (+/- 45/90)(s) and (90/+/- 45)(s) glass fibre reinforced polymer laminates," *Plast. Rubber. Compos.*, vol. 28, no. 1, pp. 30–39, 1999.

[111] P. Johnson and F. K. Chang, "Characterization of matrix crack-induced laminate failure - part i: Experiments," *J. Compos. Mater.*, vol. 35, no. 22, pp. 2009–2035, 2001.

[112] P. Johnson and F. K. Chang, "Characterization of matrix crack-induced laminate failure - part ii: Analysis and verifications," *J. Compos. Mater.*, vol. 35, no. 22, pp. 2037–2074, 2001.

[113] J. Zhang and K. P. Herrmann, "Stiffness degradation induced by multilayer intralaminar cracking in composite laminates," *Composites A: Appl. Sci. Mfg.*, vol. 30, no. 5, pp. 683–706, 1999.

[114] J. Zhang, J. Fan, and C. Soutis, "Analysis of multiple matrix cracking in [+/-theta(m)/90(n)]s composite laminates .1. in-plane stiffness properties," *Composites*, vol. 23, no. 5, pp. 291–298, 1992.

[115] Y. N. Lapusta and C. Henaff-Gardin, "An analytical model for periodic alpha(0) layer cracking in composite laminates," *Int. J. Frac.*, vol. 102, no. 3, pp. L73–L76, 2000.

[116] M. Kashtalyan and C. Soutis, "Modelling stiffness degradation due to matrix cracking in angleply composite laminates," *Plast. Rubber Compos.*, vol. 29, no. 9, pp. 482–488, 2000.

[117] M. Kashtalyan and C. Soutis, "Strain energy release rate for off-axis ply cracking in laminated composites," *Int. J. Frac.*, vol. 112, no. 2, pp. L3–L8, 2001.

[118] M. Kashtalyan and C. Soutis, "Analysis of composite laminates with intra- and interlaminar damage," *Progress in Aerospace Sciences*, vol. 41, no. 2, pp. 152–173, 2005.

[119] M. Kashtalyan and C. Soutis, "Modelling off-axis ply matrix cracking in continuous fibre-reinforced polymer matrix composite laminates," *J. Mat. Sci.*, vol. 41, no. 20, pp. 6789–6799, 2006.

[120] M. Kashtalyan and C. Soutis, "Stiffness and fracture analysis of laminated composites with off-axis ply matrix cracking," *Composites A: Appl Sci Mfg*, vol. 38, no. 4, pp. 1262–1269, 2007.

[121] K. Maslov, R. Y. Kim, V. K. Kinra, and N. J. Pagano, "A new technique for the ultrasonic detection of internal transverse cracks in carbon-fibre/bismaleimide composite laminates," *Compos. Sci. Tech.*, vol. 60, no. 12-13, pp. 2185–2190, 2000.

[122] V. K. Kinra, A. S. Ganpatye, and K. Maslov, "Ultrasonic ply-by-ply detection of matrix cracks in laminated composites," *Journal of Nondestructive Evaluation*, vol. 25, no. 1, pp. 39–51, 2006.

[123] H. Kumazawa, T. Aoki, and I. Susuki, "Analysis and experiment of gas leakage through composite laminates for propellant tanks," *AIAA Journal*, vol. 41, no. 10, pp. 2037–2044, 2003.

[124] J. A. Lavoie and E. Adolfsson, "Stitch cracks in constraint plies adjacent to a cracked ply," *J. Compos. Mater.*, vol. 35, no. 23, pp. 2077–2097, 2001.

[125] T. Yokozeki, T. Aoki, T. Ogasawara, and T. Ishikawa, "Effects of layup angle and ply thickness on matrix crack interaction in contiguous plies of composite laminates," *Composites A: Appl. Sci. Mfg.*, vol. 36, no. 9, pp. 1229–1235, 2005.

[126] T. Yokozeki, T. Aoki, and T. Ishikawa, "Consecutive matrix cracking in contiguous plies of composite laminates," *Int. J. Solids Struct.*, vol. 42, no. 9-10, pp. 2785–2802, 2005.

[127] L. E. Crocker, S. L. Ogin, P. A. Smith, and P. S. Hill, "Intra-laminar fracture in angle-ply laminates," *Composites A: Appl. Sci. Mfg.*, vol. 28, no. 9-10, pp. 839–846, 1997.

[128] L. N. McCartney, "Predicting transverse crack formation in cross-ply laminates," *Compos. Sci. Tech.*, vol. 58, no. 7, pp. 1069–1081, 1998.

[129] L. N. McCartney and G. A. Schoeppner, "Predicting the effect of non-uniform ply cracking on the thermoelastic properties of cross-ply laminates," *Compos. Sci. Tech.*, vol. 62, no. 14, pp. 1841–1856, 2002.

[130] D. G. Katerelos, L. N. McCartney, and C. Galiotis, "Local strain re-distribution and stiffness degradation in cross-ply polymer composites under tension," *Acta Materialia*, vol. 53, no. 12, pp. 3335–3343, 2005.

[131] D. G. Katerelos, P. Lundmark, J. Varna, and C. Galiotis, "Raman spectroscopy investigation of stiffness change and residual strains due to matrix cracking," *Mechanics of Compos. Mater.*, vol. 42, no. 6, pp. 535–546, 2006.

[132] D. G. Katerelos, L. N. McCartney, and C. Galiotis, "Effect of off-axis matrix cracking on stiffness of symmetric angle-ply composite laminates," *Int J Frac*, vol. 139, no. 3-4, pp. 529–536, 2006.

[133] D. T. G. Katerelos, P. Lundmark, J. Varna, and C. Galiotis, "Analysis of matrix cracking in gfrp laminates using raman spectroscopy," *Compos. Sci. Tech.*, vol. 67, no. 9, pp. 1946–1954, 2007.

[134] S. Kuriakose and R. Talreja, "Variational solutions to stresses in cracked cross-ply laminates under bending," *Int. J. Solids Struct.*, vol. 41, no. 9-10, pp. 2331–2347, 2004.

[135] S. R. Kim and J. A. Nairn, "Fracture mechanics analysis of coating/substrate systems: Part i: Analysis of tensile and bending experiments," *Eng. Frac. Mech.*, vol. 65, no. 5, pp. 573–593, 2000.

[136] S. R. Kim and J. A. Nairn, "Fracture mechanics analysis of coating/substrate systems: Part ii: Experiments in bending," *Eng. Frac. Mech.*, vol. 65, no. 5,

pp. 595–607, 2000.

[137] L. N. McCartney, "Energy-based prediction of progressive ply cracking and strength of general symmetric laminates using an homogenisation method," *Composites A: Appl. Sci. Mfg.*, vol. 36, no. 2, pp. 119–128, 2005.

[138] V. V. Silberschmidt, "Matrix cracking in cross-ply laminates: Effect of randomness," *Composites A: Appl. Sci. Mfg.*, vol. 36, no. 2 SPEC. ISS., pp. 129–135, 2005.

[139] V. V. Silberschmidt, "Effect of micro-randomness on macroscopic properties and fracture of laminates," *J. Mat. Sci.*, vol. 41, no. 20, pp. 6768–6776, 2006.

[140] B. F. Sorensen and R. Talreja, "Effects of nonuniformity of fiber distribution on thermally-induced residual-stresses and cracking in ceramic-matrix composites," *Mech. Mater.*, vol. 16, no. 4, pp. 351–363, 1993.

[141] D. Zhang, J. Ye, and D. Lam, "Properties degradation induced by transverse cracks in general symmetric laminates," *Int. J. Solids Struct.*, vol. 44, no. 17, pp. 5499–5517, 2007.

[142] R. Talreja, "A synergistic damage mechanics approach to durability of composite material systems," in *Progress in Durability Analysis of Composite Systems*, A. Cardon, H. Fukuda, and K. L. Reifsnider, Eds., pp. 117–129. A.A. Balkema, Rotterdam, 1996.

[143] R. Talreja, "Damage mechanics of composite materials based on thermodynamics with internal variables," in *Polymer Based Composite Systems for Structural Applications*, A. Cardon and G. Verchery, Eds., pp. 65–79. Elsevier, London, 1991.

[144] J. Varna, A. I. Krasnikovs, R. S. Kumar, and R. Talreja, "A synergistic damage mechanics approach to viscoelastic response of cracked cross-ply laminates," *Int. J. Dam. Mech.*, vol. 13, no. 4, pp. 301–334, 2004.

[145] R. Talreja, "Damage analysis for structural integrity and durability of composite materials," *Fatigue Fract. Eng. Mater. Struct.*, vol. 29, no. 7, pp. 481–506, 2006.

[146] B. W. Rosen, "Tensile failure of fibrous composites," *AIAA Journal*, vol. 2, pp. 1985–1991, 1964.

[147] R. M. Jones, *Mechanics of Composite Materials*, Taylor and Francis, Philadelphia, PA, 1999.

[148] A. Argon, "Fracture of composites," in *Treatise on Materials Science and Technology*, H. Herman, Ed., vol. 1, p. 79114. Academic Press, New York, 1972.

[149] S. L. Phoenix and I. J. Beyerlein, "Statistical strength theory for fibrous composite materials," in *Comprehensive Composite Materials*, T.W. Chou, Ed., vol. 1, pp. 559-639. Elsevier Science, Amsterdam, The Netherlands, 2000.

[150] F. G. Yuan and M. C. Selek, "Transverse cracking and stiffness reduction in composite laminates," *J. Reinforced Plast. Compos.*, vol. 12, no. 9, pp. 987–1015, 1993.

[151] L. E. Asp, L. A. Berglund, and R. Talreja, "Effects of fiber and interphase on matrix-initiated transverse failure in polymer composites," *Compos. Sci. Tech.*, vol. 56, no. 6, pp. 657–665, 1996.

[152] L. E. Asp, L. A. Berglund, and R. Talreja, "Prediction of matrix-initiated transverse failure in polymer composites," *Compos. Sci. Tech.*, vol. 56, no. 9, pp. 1089–1097, 1996.

[153] L. E. Asp, L. A. Berglund, and R. Talreja, "A criterion for crack initiation in glassy polymers subjected to a composite-like stress state," *Compos. Sci. Tech.*, vol. 56, no. 11, pp. 1291–1301, 1996.

[154] H. Huang and R. Talreja, "Numerical simulation of matrix micro-cracking in short fiber reinforced polymer composites: Initiation and propagation," *Compos. Sci. Tech.*, vol. 66, no. 15, pp. 2743–2757, 2006.

[155] K. A. Chowdhury, "Damage initiation, progression and failure of polymer based composites due to manufacturing induced defects," Ph.D. dissertation, Texas A&M University, 2007.

[156] K. A. Chowdhury, R. Talreja, and A. A. Benzerga, "Effects of manufacturing-induced voids on local failure in polymer-based composites," *J. Eng. Mater. Tech., Trans ASME*, vol. 130, no. 2, pp. 021010, 2008.

[157] R. Talreja, "Multi-scale modeling in damage mechanics of composite materials," *J. Mat. Sci.*, vol. 41, no. 20, pp. 6800–6812, 2006.

[158] B. D. Coleman and M. E. Gurtin, "Thermodynamics with internal state variables," *J. Chem. Phys.*, vol. 47, pp. 597–613, 1967.

[159] J. E. Adkins, "Symmetry relations for orthotropic and transversely isotropic materials," *Arch. Rational Mech. Anal.*, vol. 4, pp. 193–213, 1960.

[160] G. F. Smith, "On transversely isotropic functions of vectors, symmetric 2nd-order tensors and skew-symmetric 2nd-order tensors," *Quart. Appl. Math.*, vol.

39, no. 4, pp. 509–516, 1982.

[161] J. Varna, N. V. Akshantala, and R. Talreja, "Crack opening displacement and the associated response of laminates with varying constraints," *Int. J. Dam. Mech.*, vol. 8, no. 2, pp. 174–193, 1999.

[162] J. Varna, L. Berglund, R. Talreja, and A. Jakovics, "A study of crack opening displacement of transverse cracks in cross-ply laminates," *Int. J. Dam. Mech.*, vol. 2, no. 3, pp. 272–289, 1993.

[163] J. Varna, L. Berglund, A. Krasnikovs, and A. Chihalenko, "Crack opening geometry in cracked composite laminates," *Int. J. Dam. Mech.*, vol. 6, no. 1, pp. 96–118, 1997.

[164] P. Gudmundson and W. L. Zang, "An analytic model for thermoelastic properties of composite laminates containing transverse matrix cracks," *Int. J. Solids Struct.*, vol. 30, no. 23, pp. 3211–3231, 1993.

[165] S. Li, "Boundary conditions for unit cells from periodic microstructures and their implications," *Compos. Sci. Tech.*, vol. 68, no. 9, pp. 1962–1974, 2008.

[166] S. Li, C. V. Singh, and R. Talreja, "A representative volume element based on translational symmetries for fe analysis of cracked laminates with two arrays of cracks," *submitted to Int. J. Solids Struct.*, .

[167] T. Yokozeki and T. Aoki, "Stress analysis of symmetric laminates with obliquely-crossed matrix cracks," *Advanced Compos. Mater.*, vol. 13, no. 2, pp. 121–140, 2004.

[168] T. Yokozeki and T. Aoki, "Overall thermoelastic properties of symmetric laminates containing obliquely crossed matrix cracks," *Compos. Sci. Tech.*, vol. 65,

no. 11-12, pp. 1647–1654, 2005.

[169] D. Zhang, J. Ye, and D. Lam, "Ply cracking and stiffness degradation in cross-ply laminates under biaxial extension, bending and thermal loading," *Compos. Struct.*, vol. 75, no. 1-4, pp. 121–131, 2006.

[170] C. V. Singh and R. Talreja, "Analysis of multiple off-axis ply cracks in composite laminates," *Int. J. Solids Struct.*, vol. 45, no. 16, pp. 4574–4589, 2008.

[171] C. V. Singh and R. Talreja, "A synergistic damage mechanics approach for composite laminates with matrix cracks in multiple orientations," *submitted to Mechanics of Materials*.

[172] S. E. Groves, C. E. Harris, A. L. Highsmith, D. H. Allen, and R. G. Norvell, "An experimental and analytical treatment of matrix cracking in cross-ply laminates," *Experimental Mechanics*, vol. 27, no. 1, pp. 73–79, 1987.

[173] S. F. Hu, J. S. Bark, and J. A. Nairn, "On the phenomenon of curved microcracks in [(s)/90(n)](s) laminates - their shapes, initiation angles and locations," *Compos. Sci. Tech.*, vol. 47, no. 4, pp. 321–329, 1993.

[174] P. A. Smith and S. L. Ogin, "On transverse matrix cracking in cross-ply laminates loaded in simple bending," *Composites Part A: Appl. Sci. and Mfg.*, vol. 30, no. 8, pp. 1003–1008, 1999.

[175] H. L. McManus and J. R. Maddocks, "On microcracking in composite laminates under thermal and mechanical loading," *Polymers and Polymer Composites*, vol. 4, no. 5, pp. 305–314, 1996.

[176] C. T. Herakovich and M. W. Hyer, "Damage-induced property changes in composites subjected to cyclic thermal loading," *Eng. Frac. Mech.*, vol. 25, no.

5-6, pp. 779–791, 1986.

[177] R. G. Spain, "Thermal microcracking of carbon fibre/resin composites," *Composites*, vol. 2, no. 1, pp. 33–37, 1971.

[178] H. L. McManus, D. E. Bowles, and S. S. Tompkins, "Prediction of thermal cycling induced matrix cracking," *J. Reinforced Plast. Compos.*, vol. 15, no. 2, pp. 124–140, 1996.

[179] Daniel S. Adams, David E. Bowles, and Carl T. Herakovich, "Thermally induced transverse cracking in graphite-epoxy cross-ply laminates," *J. Reinforced Plast. Compos.*, vol. 5, no. 3, pp. 152–169, 1986.

[180] C. H. Park and H. L. McManus, "Thermally induced damage in composite laminates: Predictive methodology and experimental investigation," *Compos. Sci. Tech.*, vol. 56, no. 10, pp. 1209–1217, 1996.

[181] T. G. Reynolds and H. L. McManus, "Understanding and accelerating environmentally-induced degradation and microcracking," in *Collection of Technical Papers - AIAA/ASME/ASCE/AHS/ASC Structures, Structural Dynamics and Materials Conference*, 1998, vol. 3, pp. 2106–2113.

[182] M. H. Han and J. A. Nairn, "Hygrothermal aging of polyimide matrix composite laminates," *Composites A: Appl. Sci. Mfg.*, vol. 34, no. 10, pp. 979–986, 2003.

[183] E. E. Gdoutos, *Fracture Mechanics: An Introduction*, 2nd edition, Springer, Norwell, MA, 2005.

[184] R. Rikards, F. G. Buchholz, H. Wang, A. K. Bledzki, A. Korjakin, and H. A. Richard, "Investigation of mixed mode I/II interlaminar fracture toughness of

laminated composites by using a cts type specimen," *Eng. Frac. Mech.*, vol. 61, no. 3-4, pp. 325–342, 1998.

[185] R. Talreja and C. Singh, "Multiscale modeling for damage analysis," in *Multiscale Modeling and Simulation of Composite Materials and Structures*, Y. W. Kwon, D. H. Allen, and R. Talreja, Eds., pp. 529–578. Springer, New York, 2008.

[186] R. Talreja, "Continuum modeling of damage in ceramic matrix composites," *Mech. Mater.*, vol. 12, no. 2, pp. 165–180, 1991.

[187] D. B. Marshall, B. N. Cox, and A. G. Evans, "The mechanics of matrix cracking in brittle-matrix fiber composites," *Acta Metallurgica*, vol. 33, no. 11, pp. 2013–2021, 1985.

[188] D. B. Marshall and A. G. Evans, "Failure mechanisms in ceramic-fiber/ceramic-metrix composites," *J. American Ceramic Society*, vol. 68, no. 5, pp. 225–231, 1985.

[189] E. Ahci and R. Talreja, "Characterization of viscoelasticity and damage in high temperature polymer matrix composites," *Compos. Sci. Tech.*, vol. 66, no. 14, pp. 2506–2519, 2006.

VITA

Chandra Veer Singh was born in India. He received his B.Sc. (Engg.) in mechanical engineering from Dayalbagh Educational Institute, Agra, India, in 2001. Thereafter, he did his M.Tech. in Satellite Technology and Applications from the Indian Institute of Science, Bangalore, India in 2003. Then, he worked for two and half years as a design engineer in the life management devision of GE aircraft engines at John F. Welch Technology Center situated at Bangalore, India. In Fall 2005, he joined Texas A&M University for his Ph.D. education. He received his doctorate in December, 2008. His research interests include damage and failure of composite materials, multiscale modeling, computational mechanics and nanomechanics. Mr. Singh can be reached at his official address: Department of Aerospace Engineering, H.R. Bright Building, Rm. 701, Ross Street - TAMU 3141, College Station, TX 77843.